Phenotypic characterisation of the PLM3SA mouse expressing unphosphorylatable phospholemman

Aughton, Karen Louise

Awarding institution:
King's College London

Phenotypic characterisation of the PLM^{3SA} mouse expressing unphosphorylatable phospholemman.

Karen L Aughton

Thesis undertaken for the degree of

Doctor of Philosophy in Cardiovascular Medicine

Cardiovascular Division

The Rayne Institute

St Thomas' Hospital

London, SE1 7EH

Submitted May 2013

ABSTRACT

Cardiac Na^+/K^+ ATPase plays a pivotal role in maintaining the Na^+ transmembrane gradient which is essential for normal cardiac function. Elevation of intracellular Na^+ ($[Na^+]_i$) is a key contributor to contractile and electrical dysfunction in a variety of pathologies. Phospholemman (PLM), is the cardiac specific member of the FXYD family of small membrane spanning proteins, and forms a complex with Na^+/K^+ ATPase pump. PLM regulates the pump by exerting a tonic inhibition which is relieved by PKA or PKC phosphorylation at 3 serine (Ser)/threonine (Thr) residues in its cytoplasmic tail (Ser63, Ser68, Thr/Ser69). Phosphorylation at any of these sites results in disinhibition of the pump and even active stimulation. The work described in this thesis investigates the role of PLM in regulating the Na^+/K^+ ATPase and the subsequent effect on $[Na^+]_i$.

A new mouse model, PLM^{3SA}, has been created by mutating all 3 Ser residues to alanine (Ala) rendering the protein unphosphorylatable. This inability to phosphorylate PLM may cause $[Na^+]_i$ overload, contractile dysfunction and cardiac arrhythmias. The aim of this thesis was to investigate the effects of unphosphorylatable PLM on Na^+/K^+ ATPase regulation and $[Na^+]_i$ by characterising the PLM^{3SA} mouse phenotype using biochemical and Langendorff methodology under basal conditions and during β-receptor stimulation. The measurement of $[Na^+]_i$ using flame photometry and ^{23}Na NMR completed the work.

Biochemical studies confirmed the successful mutation of the PLM protein and absence of Ser63, Ser68 and Ser69 phosphorylation sites. Mutated PLM was found to remain co-localised with the Na^+/K^+ ATPase α1 subunit in the membrane. Expression of total PLM was decreased in PLM^{3SA} hearts, however all Na^+/K^+ ATPase subunit expression remained unchanged. Comparison of paced basal contractility in the PLM-WT and PLM^{3SA} hearts revealed that PLM^{3SA} hearts have significantly greater contractility, consistent with an inhibited pump and increased $[Na^+]_i$. Arrhythmia quantification revealed no differences in scores between genotypes suggesting $[Na^+]_i$ was not detrimental under these conditions. Force-frequency relationship (FFR) studies were consistent with a high $[Na^+]_i$ in both genotypes. However, the lack of difference between WT and PLM^{3SA} hearts suggests that changes in $[Na^+]_i$ in response to pacing do not substantially differ between genotypes.

β-receptor stimulation by isoprenaline (ISO) perfusion was investigated to highlight potential changes in cardiac function between unphosphorylatable PLM in PLM^{3SA} hearts compared with

WT. Contractile data however revealed no differences suggesting that PKA activation of other key excitation-contraction coupling proteins dominate the contractile response to ISO.

Direct measurement of $[Na^+]_i$ using flame photometry and ^{23}Na NMR showed no differences in intracellular Na^+ concentration in PLM^{3SA} hearts compared with WT under basal conditions. Quantification of $[Na^+]_i$ by ^{23}Na NMR using the shift reagent, $Tm(DOTP)^{5-}$, gave values for PLM^{3SA} hearts of 12.7±2.5mM, and 14.49±3.1mM for PLM-WT hearts. β-receptor stimulation, pacing and ouabain effects on $[Na^+]_i$ were also investigated and ouabain significantly increased $[Na^+]_i$ compared to baseline in both PLM^{3SA} and WT hearts to a similar extent.

The work described in this thesis investigates the role of unphosphorylatable PLM on $[Na^+]_i$ in PLM^{3SA} hearts revealing findings that show:

- No effect on $[Na^+]_i$ under basal conditions
- No evidence for differences in basal Na^+/K^+ ATPase activity - based on rubidium (Rb^+) uptake flame photometry studies
- No evidence for a role of PLM phosphorylation in control of Na^+ at high pacing rates or in the presence of ISO.

However, these conclusions may reflect technical limitations of the experimental approaches used.

ACKNOWLEDGEMENTS

Firstly, I would like to thank my supervisor, Professor Michael Shattock, for his continual support, guidance and encouragement throughout my PhD. His limitless knowledge, enthusiasm and advanced DIY skills were invaluable and I will truly miss working in the Phospholemman lab.

Thank you also to the Phospholemman team, past and present, for your time, advice and many laughs. Davor, Andrii, Jason, Andy, Olena and Erika, I will miss the lively debates and banter and I wish you all well in your future adventures. To the Dundee Phospholemman contingent, especially Dr Will Fuller, thank you for all the technical advice and support from afar, it is much appreciated. To all those at the Rayne who have offered advice, experimental teaching and guidance, thank you too.

I would especially like to thank Dr Thomas Eykyn, "the NMR guru" for his expertise in the field and help and support in completing the NMR studies. It wasn't an easy challenge that was set and there were many times of frustration, head scratching and tiredness which I would not have got through without Tom's resilience, wise words and encouragement.

I have thoroughly enjoyed my time at the Rayne Institute and have made many good friends with whom I have shared many wonderful experiences with from marathon running to Wine Wednesdays, to weddings and the arrival of little ones, themed Christmas parties and cream teas. To Alex, Becky, Sonya, Denise, Dina, Elizabeth, Tasha, Ike, Rekha, Abi and Ellen – it has been a pleasure to have met you all and look forward to many more outings soon.

A great thank you to all my family - the Fenny family (Jo, Col, Beth and Jack), the Shears family (Jan and Ken), the Dundavans (Grandma, Nancie and Lynn), my late grandparents and especially my mum and dad - for supporting me throughout this PhD (and my lifetime) with endless love and encouragement. I would not have achieved so much without you and hope I have made you proud.

And finally to my wonderful boys, my husband Dan and baby boy Edward, without you to make me laugh and give me cuddles at the end of a long day, I would have not got through this. Your complete belief in me and constant love and support have made the past few years truly magical. It is to you both that I dedicate this thesis.

LIST OF PUBLICATIONS

Karen L Aughton, Andrew R Hall, William Fuller, Michael J Shattock
Reduced Na/K pump current, enhanced contractility and negative force-frequency relationship in cardiomyocytes and hearts isolated from mice expressing unphosphorylatable phospholemman.
Circulation 2010; 122: A15890

Davor Pavlovic, Andrew R Hall, Erika J Kennington, **Karen L Aughton**, Andrii Boguslavskyi, William Fuller, Sanda Despa, Donald M Bers and Michael J Shattock
Nitric oxide regulates cardiac intracellular Na^+ and Ca^{2+} by modulating Na^+/K^+ ATPase via PKCε and phospholemman-dependent mechanism.
Journal of Molecular and Cellular Cardiology 2013; S0022-2828(13)00144-2 (in print)

Krzysztof J Wypijewski, Jacqueline Howie, Louise Reilly, **Karen Aughton**, Michael J Shattock, Sarah Calaghan and William Fuller
A separate pool of cardiac phospholemman that does not regulate the sodium pump: multimers of phospholemman in ventricular muscle
Journal of Biochemical Chemistry 2013; 288: 13808-13820

CONTENTS

LIST OF FIGURES

LIST OF TABLES

ABBREVIATIONS

AAS	atomic absorption spectroscopy
AC	adenylyl cyclase
ADP	adenosine dipohosphate
ANOVA	analysis of variance
Ala	alanine residue
Arg	arginine residue
Asp	aspartic residue
ATP	adenosine triphosphate
ATPase	adenosine triphosphatase
AU	arbitrary units
AV	atrio-ventricular
β-receptor	β adrenergic receptor
bp	base pairs
bpm	beats per minute
β-stimulation	β adrenergic stimulation
Ca^{2+}	Ca ion
$[Ca^{2+}]_e$	extracellular Ca^{2+} concentration
$[Ca^{2+}]_{free}$	free Ca^{2+} concentration
CaMKII	calcium-calmodulin dependent protein kinase II
cAMP	cyclic adenosine monophosphate
cGMP	cyclic guanosine monophosphate
CHIF	corticosteroid hormone inducing factor
CICR	calcium induced calcium release
CNS	central nervous system
CP	creatine phosphate
Co-IP	co-immunoprecipitation
C-terminal	carboxy terminal
DAG	diacylglycerol
DQ	double quantum
DQF	double quantum filtering
E_1	Na^+/K^+ ATPase conformation where the cation binding site is open to the intracellular side of the membrane
E_2	Na^+/K^+ ATPase conformation where the cation binding site is open to the extracellular side of the membrane
E-C	excitation-contraction
EC_{50}	half maximal effective concentration
ECHO	echocardiogram
ECL	enhanced chemiluminescent
EDTA	ethylenediaminetetraaectic acid
EGTA	ethylene glycol tetraacetic acid
E_K	potassium ion equilibrium potential
E_m	membrane equilibrium potential
E_{Na}	sodium ion equilibrium potential
E_{NCX}	sodium calcium exchanger equilibrium potential
eNOS	endothelial nitric oxide synthase
ES cell	embryonic stem cell
FFR	force-frequency relationship
FRET	fluorescence energy transfer

FXYD	family of proteins expressing consensus motif Proline-Phenylalanine–X–Tyrosine–Aspartic acid
GPCR	G protein coupled receptor
HEK	human embryonic kidney cell line
HEPES	(4-(2-hydroxyethyl)-1-piperazineethanesulfonic acid)
HR	heart rate
HCN	hyperpolarising cAMP nucleotide channel
HRP	horse radish peroxidase
HRV	heart rate variability
I1	inhibitor 1
IB	immunoblot
I.D.	inner diameter
I_{NCX}	Na^+/Ca^{2+} exchanger current
$I_{Ca,L}$	L-type Ca^{2+} channel current
I_{Pump}	Na^+/K^+ ATPase current
IP_3	inositol 1,4,5-triphosphate
I_{to}	transient channel current
ISE	iso-sensitive electrode
K^+	potassium ion
$[K^+]_i$	intracellular K^+ concentration
kDa	kilodalton
kg	kilogram
KHB	Krebs Henseleit bicarbonate buffer
K_m	Michaelis-Menten constant
Leu	leucine residue
LV	left ventricular
LVDP	left ventricular developed pressure
LVEDP	left ventricular end diastolic pressure
LVP	left ventricular pressure
MAT-8	mammary tumour marker 8
Mg^{2+}	magnesium ion
mM	millimolar
mmHg	millimetres mercury
Mn^{2+}	manganese ion
µH	micro Henry
MQF	multiple quantum filtering
ms	millisecond
mV	millivolt
Na^+	sodium ion
^{23}Na	sodium isotope
$[Na^+]_e$	extracellular sodium concentration
$[Na^+]_i$	intracellular sodium concentration
Na_{ref}	reference capillary sodium
NBE	Na^+/HCO_3^- cotransporter
NCX	sodium calcium exchanger
NHE	Na^+/H^+ exchanger
Na^+/K^+ATPase	sodium potassium ATPase
NIMA	‘never in mitosis’ kinase
NKCC	$Na^+/K^+/2Cl^-$ co-transporter
nM	nanomolar
NMgX	Na^+/Mg^{2+} exchanger
NMR	nuclear magnetic resonance

NMDG	n-methyl d-glucamine
nNOS	neuronal nitric oxide synthase
NO	nitric oxide
NOS	nitric oxide synthase
N-terminal	amino terminal
O.D.	outer diameter
^{31}P	phosphorus isotope
PAGE	polyacrylamide gel electrophoresis
PCR	polymerase chain reaction
Phe	phenylalanine residue
PKA	protein kinase A
PKC	protein kinase C
PLB	phospholamban
PLC	phospholipase C
PLM	phospholemman
PLM^{3SA}	phospholemman knock-in mouse with 3 Ser residues mutated to Ala
PLM-KO	phospholemman knock-out
PLMS	phospholemman-like shark protein
PLM-WT	phospholemman wild type
PP1	protein phosphatase 1
PP2A	protein phosphatase 2A
Pro	proline residue
PVDF	polyvinyl difluoride
Rb^+	rubidium ion
RIC	related to ion channel
rpm	revolutions per minute
RF	radio frequency
RyR	ryanodine receptor
SA	sino-atrial
SBFI	sodium-binding benzofuran isophthalate
SDS	sodium dodecyl sulphate
sec	second
sem	standard error of the mean
Ser	serine residue
Ser63	standard notation of amino acid (Ser) and residue number (63)
SERCA	sarco/endoplasmic reticulum calcium ATPase
SQ	single quantum
SR	sarcoplasmic reticulum
T	tesla
T-PBS	phosphate buffered saline with Tween
TAE	tris acetate EDTA
TFA	trifluoroacetic acid
Thr	threonine residue
t-tubule	transverse tubule
TQ	triple quantum
TQF	triple quantum filtering
Tyr	tyrosine residue
V	volt
Val	valine residue
VPB	ventricular premature beats
VF	ventricular fibrillation
V_{max}	maximal rate of activity

1 CHAPTER 1 - INTRODUCTION

1.1 Overview of Na^+ transport, Na^+/K^+ ATPase and PLM

Intracellular Na^+ concentration is a key modulator of cardiac cell function.[1] At steady state, intracellular Na^+ concentration ($[Na^+]_i$) is between 4-16mM[2-10] depending on species whilst the extracellular Na^+ concentration ($[Na^+]_e$) is approximately 140mM. This creates an electrochemical gradient that favours Na^+ entry into the cell providing energy for action potential propagation and the transport of many energetically unfavourable ions, amino acids and neurotransmitters into the cell. $[Na^+]_i$ is important for the control of intracellular Ca^{2+} via the NCX and consequently determines sarcoplasmic reticulum (SR) Ca^{2+} content. Ca^{2+} overload can cause contractile dysfunction and arrhythmias. Therefore maintenance of the Na^+ gradient is important in normal physiology and is critically important in cardiac hypertrophy and heart failure where the elevation of $[Na^+]_i$ contributes to contractile and electrical dysfunction.[11, 12]

The steady state $[Na^+]_i$ is carefully maintained by a fine balance of influx and efflux pathways. Na^+ influx occurs predominantly by voltage-gated Na^+ channels during the action potential upstroke[1, 3] but there are other co-transporters and exchangers that also contribute to Na^+ influx: Na^+/Ca^{2+} exchanger (NCX), Na^+/H^+ exchanger (NHE), Na^+/HCO_3^- co-transporter (NBE), $Na^+/K^+/2Cl^-$ co-transporter (NKCC) and Na^+/Mg^{2+} exchanger (NMgX).

The major pathway of Na^+ efflux is via the Na^+/K^+ ATPase, a member of the P-type ATPase family, which extrudes $3Na^+$ in exchange for $2K^+$ using the energy derived from ATP hydrolysis to drive the reaction.[3, 13] This pump plays an important role in maintaining ion gradients and hence the resting membrane potential of the cell and in excitable cells enables subsequent action potentials and processes to occur. Therefore regulation of the Na^+/K^+ ATPase is crucial to maintain normal cardiac function.

The FXYD family of small-membrane proteins have been recognised as tissue-specific regulators of Na^+/K^+ ATPase.[14-19] FXYD1 or phospholemman (PLM) is the cardiac specific regulator of the Na^+/K^+ ATPase and is unique in that it contains the consensus sequences for PKA and PKC in its cytoplasmic tail.[20-25] The function of PLM is analogous to phospholamban (PLB) regulation of sarcoplasmic reticulum Ca^{2+} ATPase (SERCA) and phosphorylation by PKA/PKC relieves pump inhibition[26-29] and increases Na^+ affinity of the pump. Indeed in myocytes it has been shown that β-adrenergic stimulation and subsequent increase in cAMP and

PKA, phosphorylate PLM Ser68 residue and result in activation and stimulation of the Na^+/K^+ ATPase with increases in both V_{max} and Na^+ sensitivity reported.[30, 31] This effect is absent in PLM-knockout (PLM-KO) myocytes and points to the importance of PLM in helping to regulate $[Na^+]_i$ during "fight or flight" induced increases in heart rate.[32] It is proposed in PLM-KO mice that the Na^+/K^+ ATPase is unregulated and can freely act to remove Na^+, however recent studies have shown that resting $[Na^+]_i$ are similar to those from wild-type (WT) myocytes.[32] Evidence of decreased pump expression in these mice may help explain this and potentially compensates in order to maintain a normal $[Na^+]_i$.[33, 34]

A new genetically modified mouse has been created, PLM^{3SA}, which carries an unphosphorylatable PLM protein. It is hypothesised that resting $[Na^+]_i$ may be higher than in WT mice due to the permanent inhibition of Na^+/K^+ ATPase under basal conditions and that this may be exaggerated during β-adrenergic stimulation, frequency stress and ouabain inhibition. The inability to phosphorylate PLM in these mice may cause $[Na^+]_i$ overload, contractile dysfunction and arrhythmias. The overall aim of these studies is to compare PLM^{3SA} mice with their littermate controls, to measure $[Na^+]_i$ and to use this mutant mouse to increase understanding of the role of PLM phosphorylation in the response of the heart to stress.

1.2 Excitation-contraction coupling and the action potential

Cardiac excitation-contraction coupling is the process by which electrical excitation of the myocyte leads to contraction of the heart.[35] Excitation, in the form of action potentials, propagates from myocyte to myocyte via gap junctions located at the intercalated discs[36] resulting in synchronised contraction of the heart. This process involves the movement of ions down concentration gradients through voltage-gated ion channels that are activated in response to changes in the membrane potential. The cation channels involved are Na^+, K^+ and Ca^{2+} channels and it is Ca^{2+} that activates cross-bridge cycling which subsequently drives myofilament contraction. Following the movement of ions during the action potential the resting ionic state is restored by Na^+/K^+ ATPase, SERCA and NCX ion transporters.

1.2.1 The action potential

Action potentials are generated in the sino-atrial (SA) node by pacemaker cells, a group of modified myocytes, which discharge spontaneously at regular intervals (automaticity).[37] The

action potential is the result of rapid changes in membrane permeability that allows the movement of ions through specific ion channels in accordance to their concentration and electrochemical gradients. These gradients are set by intracellular and extracellular ion concentrations and the membrane potential, E_m. In the cardiac myocyte the resting membrane potential is stable at ~ -80mV and is predominantly set by K^+, which has high membrane permeability and large outward concentration gradient at rest,[38, 39] with a small contribution from the less membrane permeable Na^+ ion. The Nernst equation predicts the equilibrium potential for each ion, E_K and E_{Na}, at which there is no net ion movement. Since the resting cell membrane is not solely permeable to K^+ (the ratio of K^+ permeability to Na^+ permeability is estimated to be around 100:1), then the resting membrane potential of ~-80mV is more accurately predicted by the Goldman-Hodgkin-Katz equation. The Na^+/K^+ ATPase helps maintain a stable E_m by balancing the constant trickle of outward K^+ and inward Na^+ which results from the differences between E_m and E_K or E_{Na}.

The action potential itself comprises of depolarisation followed by a subsequent repolarisation over 5 phases. In intact tissues, the action potential is initiated when a neighbouring cell depolarises and the electrogenic coupling to its neighbour results in a local membrane depolarisation. When the membrane potential reaches around -65mV, the action potential threshold, Na^+ channels open allowing a sudden influx of Na^+ ions into the myocyte[40] (Phase 0). This rapid Na^+ influx causes the cell to depolarise and reach positive membrane potentials of +20 to +30mV termed the overshoot. At this point most myocytes start to repolarise by activation of a transient current, I_{to}, that allows mainly K^+ to exit the cell until the membrane potential reaches 0 to -20mV (Phase 1). The opening of L-type Ca^{2+} channels at this membrane potential triggers a plateau phase that lasts 200 to 400ms in humans (Phase 2). The myocyte then starts to repolarise due to K^+ efflux through the delayed rectifier channels until the cell reaches resting membrane potential (Phase 3). Ionic balance of Na^+, K^+ and Ca^{2+} is restored by Na^+/K^+ ATPase, NCX, SERCA and a small amount by the sarcolemmal Ca^{2+} ATPase[35] (Phase 4).

The overall shape of the action potential is influenced by the distribution and timings of the ion channels and can differ between species.[41] The mouse action potential does not have the prolonged plateau phase which is present in the human action potential (see Figure 1.1). This is due an increased population of K^+ channels that contribute to I_{to} current in Phase 1 masking the L-type Ca^{2+} channel current (i.e. K^+ efflux is greater than Ca^{2+} influx) and shortening the plateau

phase significantly. The delayed rectifier currents are also different in rat and mouse compared to human, however both bring about final repolarisation.

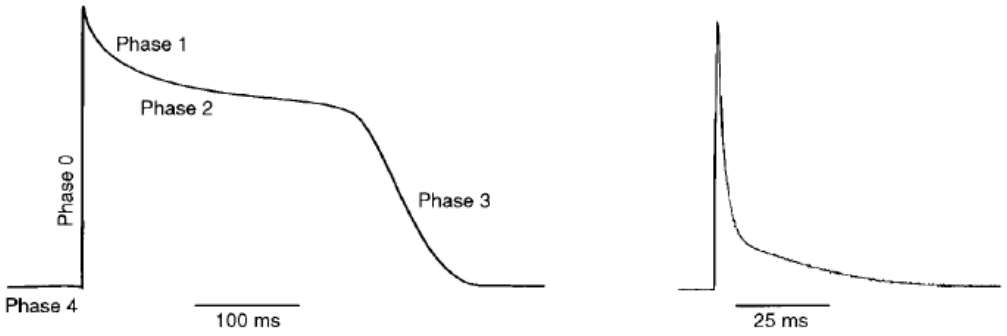

Figure 1.1: Schematic of human (*left*) and murine (*right*) action potentials.
The phases of the adult human action potential (0-4) are defined. Phase 2 shows a prolonged plateau phase which is absent in the mouse ventricular myocyte action potential shown on the right. Taken from Nerbonne *et al*.[41]

1.2.2 Excitation-contraction coupling

It is during the plateau phase of the action potential that contraction of the myocyte occurs. Ca^{2+} influx through the L-type Ca^{2+} channels during this phase of the action potential is not sufficient to evoke a full-size contraction on its own. It does however trigger the opening of the ryanodine receptors (RyR) in the sarcoplasmic reticulum (SR) membrane resulting in the release of SR Ca^{2+} into the cytosol through a process known as Ca^{2+}-induced Ca^{2+} release (CICR).[35, 42] The cytosolic Ca^{2+} concentration increases 10-fold peaking at ~1µM and activates the contractile machinery of the cell culminating in myocyte contraction.[43, 44] Cytosolic Ca^{2+} binds to troponin C causing a conformational change in troponin releasing the tropomyosin-troponin complex from blocking the actin binding site. Myosin heads now bind and pull the actin filament to the centre of the sarcomere using ATP hydrolysis and causing myofilament shortening and cell contraction, known as crossbridge cycling.[42] Figure 1.2 shows a schematic diagram of excitation-contraction coupling as it occurs in the rabbit/human myocyte.[35]

Once systole is complete, excess cytosolic Ca^{2+} must be removed in order to allow the heart to relax (diastole) and refill with blood. If excess Ca^{2+} remains then it can give rise to diastolic dysfunction, a prominent feature in heart failure and hypertrophy.[45] The majority of Ca^{2+} is removed by SERCA[35] into the SR, which is regulated by PLB[46] in much the same way that Na^+/K^+ ATPase is regulated by PLM. PLB phosphorylation by PKA[47] or Ca^{2+}/calmodulin-dependent kinase II (CaMKII)[48] causes SERCA to be disinhibited and pump affinity for Ca^{2+} is

increased.[49] Remaining Ca^{2+} is removed by the NCX, sarcolemma Ca^{2+} ATPase and Ca^{2+} uniporter.[35]

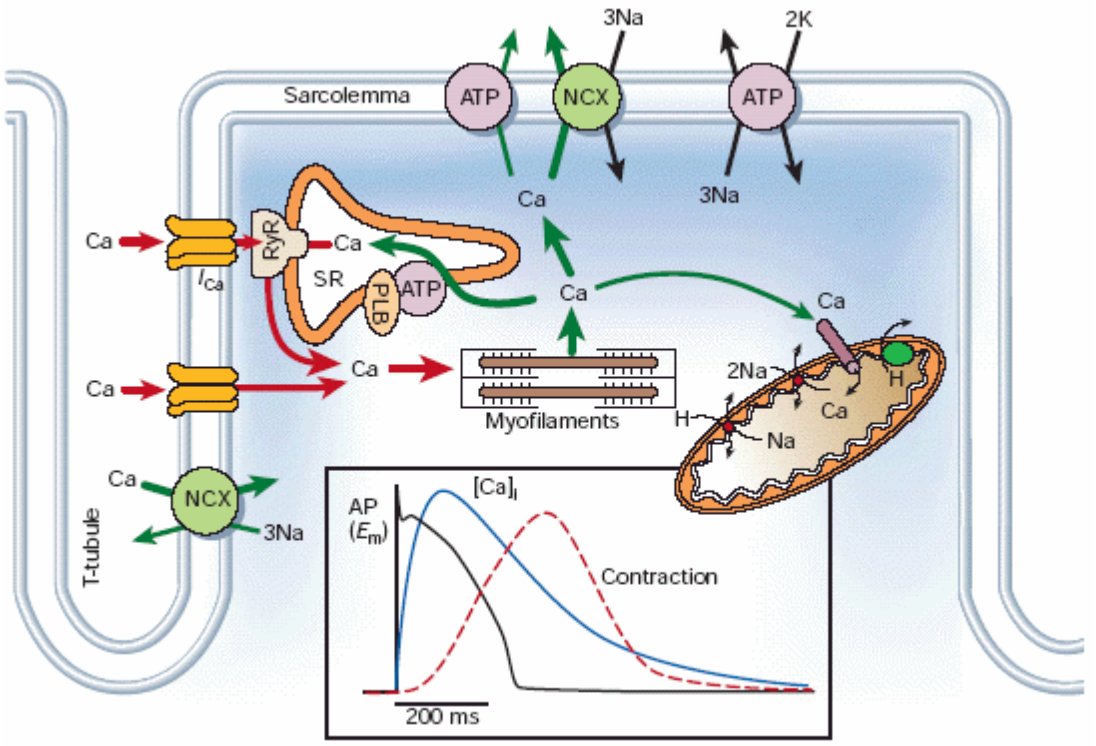

Figure 1.2: Schematic diagram of excitation-coupling in the rabbit/human ventricular myocyte.
Pre-contraction Ca^{2+} influx is shown in red, with post-contraction Ca^{2+} efflux shown in green. Inset is shown the time course of the action potential with the Ca^{2+} transient and contraction. As described by Bers, 2002.[35]

1.2.3 The influence of $[Na^+]_i$ on E-C coupling

SERCA is responsible for the majority of Ca^{2+} removal from the cytosol; however Ca^{2+} is also removed by the NCX. Na^+/Ca^{2+} exchanger is a bidirectional electrogenic transporter with a stoichiometry of one Ca^{2+} ion for 3 Na^+ ions.[35] The NCX can work in two modes: (1) forward mode in which 1 Ca^{2+} ion is extruded in exchange for 3 Na^+ ions in and (2) reverse mode in which 3 Na^+ ions are extruded for 1 Ca^{2+} ion in. The NCX normally works in the forward mode producing an inward ionic current ($I_{Na/Ca}$) that results in the net inward movement of one positive charge. The reversal potential for the exchanger can be calculated by using equilibrium potentials for Na^+ and Ca^{2+} ($E_{Na/Ca} = 3E_{Na} - 2E_{Ca}$).[35] There are four factors that determine the direction of net transport including transport cycle stoichiometry, the transmembrane electrical potential, transmembrane $[Ca^{2+}]$ and transmembrane $[Na^+]$.[50] NCX activity is highly influenced

by $[Na^+]_i$ and consequently $[Na^+]_i$ helps regulates cellular Ca^{2+} load and consequently contraction.[1] Low $[Na^+]_i$ will cause NCX to work in the forward mode resulting in Ca^{2+} efflux and increasing relaxation rates. High $[Na^+]_i$ will do the opposite and either limit forward mode exchange or, possible in extremes, may promote reverse mode NCX[51] thereby increasing $[Ca^{2+}]_i$ and contributing to stronger contraction but associated with elevated diastolic Ca^{2+}. Ca^{2+} overload can lead to cardiac dysfunction and the potential of arrhythmias which can be fatal.[52] Therefore the maintenance of a normal $[Na^+]_i$ by Na^+/K^+ ATPase is vital for cardiac function. In essence it can be said that Na^+/K^+ ATPase indirectly controls myocardial contraction[45] and any alterations in Na^+ pump expression, or regulation may have profound effects.

1.3 β-adrenergic stimulation

Stimulation of the sympathetic nervous system is a necessary physiological response that increases cardiac output and contractility as part of the "fight or flight" stress response.[53] It is mediated mainly by activation of β-adrenergic receptors present in the sarcolemma and results in increased chronotropy, inotropy and lusitropy. β-adrenergic receptors are G-protein coupled receptors that increase adenylyl cyclase (AC) activity and this leads to an increase in cyclic adenosine monophosphate (cAMP) which in turn increases protein kinase A (PKA) activity.[54]

PKA phosphorylates major proteins involved in E-C coupling such as L-type Ca^{2+} channels (increasing Ca^{2+} current),[55] PLB (increasing SERCA activity),[49, 56] RyR (modifying channel gating),[57] troponin I[58, 59] and myosin binding protein C (decreasing Ca^{2+} affinity of myofilaments and enhancing crossbridge cycling). PKA substrate phosphorylation increases cardiac inotropy by altering the amount and rate of Ca^{2+} handling in the cell. Increases in heart rate and PKA phosphorylation of L-type Ca^{2+} channels allows a greater and more prolonged Ca^{2+} influx which in turn activates CICR from RyR which is again enhanced by PKA phosphorylation causing a quicker and greater Ca^{2+} release from SR stores. This additional cytosolic Ca^{2+} can activate the cells contractile machinery binding to troponin C allowing faster and stronger cross-bridge cycling, generating a powerful cardiac contraction.[60]

The strength and rate of contraction must be matched equally by relaxation. Again due to PKA phosphorylation, TnI exhibits reduced myofilament Ca^{2+} sensitivity which aids relaxation by promoting quicker myofilament dissociation.[60, 61] However, the main driver of cardiac relaxation is PLB phosphorylation which disinhibits SERCA increasing its affinity for Ca^{2+} and

rate of Ca^{2+} uptake. PLB phosphorylation has a dual effect and as well as enhancing cytosolic Ca^{2+} removal it loads the SR stores with Ca^{2+} such, that at the next action potential, there is more Ca^{2+} available for release and hence increased inotropy.[60]

Additionally, with increased frequency of contraction (chronotropy) there will be increased Na^+ influx[1] which will need to be removed if intracellular Na^+ is not to rise. As the major pathway of Na^+ extrusion is via the Na^+/K^+ ATPase then the rate at which it works must be increased to match the influx rate. As resting $[Na^+]$ is close to the K_m for activation of Na^+/K^+ pump and the Na^+ activation curve is steep, intracellular Na^+ itself is a major contributor to enhanced Na^+ efflux if cytosolic Na^+ rises. In addition, the activity of Na^+/K^+ ATPase is modified by PLM which under normal conditions acts to inhibit the pump. PLM phosphorylation by PKA[28, 30] leads to disinhibition of the pump and pump rate increases (V_{max}) and affinity of the pump for Na^+ (K_m) is enhanced.[62, 63]

1.4 Na^+/K^+ ATPase

1.4.1 Role

The Na^+/K^+ ATPase is the major route for Na^+ extrusion and is found in plasma membrane of all animal cells.[64, 65] It is responsible for maintaining the trans-sarcolemmal Na^+ gradient which is important for ion exchange and transport processes in the cardiac myocyte.[66] Transport is stochiometrically coupled to ATP hydrolysis and the pump extrudes $3Na^+$ from the cell in exchange for $2K^+$ for every one terminal phosphate group of ATP hydrolysed.[67] It is able to maintain this stoichiometry over a wide range of $[Na^+]_i$, extracellular K^+ concentrations ($[K^+]_e$) and E_m.[65] Regulation of $[Na^+]_i$ is important as it in turn influences intracellular Ca^{2+} and contractility via the NCX.[68] Changes in Na^+/K^+ ATPase activity can profoundly affect contractility.[35]

Na^+/K^+ ATPase was first discovered in 1957 by Jens Christian Skou in crab neurons[69] but it has been the target of pharmacological agents such as digoxin (*digitalis lanata*) and ouabain since the 1800's for treatment of heart failure. It is now known that the target for these cardiac glycosides is the Na^+/K^+ ATPase. Cardiac glycosides have a positive inotropic effect on cardiac contractility and work by effectively decreasing the amount of Na^+ efflux which changes the Na^+ trans-sarcolemmal gradient and helps limit Ca^{2+} extrusion via the NCX.[76] By inhibiting the outward Na^+/K^+ pump current, they prolong the action potential plateau allowing more time for

Ca^{2+} to enter the cell and, if heart rate (HR) remains constant, reduces the diastolic interval and hence time for Ca^{2+} extrusion. Following the plateau phase this increased cytosolic Ca^{2+} is taken up into the SR by SERCA which loads to allow more Ca^{2+} for release on the next action potential, creating larger Ca^{2+} transients and stronger contractions. Cardiac glycosides are used in the treatment of congestive heart failure and cardiac arrhythmias.[70, 71]

The maintenance of the Na^+ gradient by the pump is essential to prevent long term cardiac pathophysiologies, such as heart failure and hypertrophy, occurring in the first place. $[Na^+]_i$ can be dysregulated in cardiac disease[52] and high intracellular Na^+ has been implicated in hypertrophy,[72, 73] ischemia-reperfusion injury[74, 75] and heart failure.[11, 76, 77] As an indirect regulator of $[Ca^{2+}]_{i,}$ it is essential to balance Na^+ influx with Na^+ efflux by the pump in order to prevent the risk of arrhythmias and cardiac diseases.

Maintenance of K^+ gradient by the Na^+/K^+ ATPase is also important to help establish the resting membrane potential which allows future action potentials to be generated. K^+ influx helps maintain $[K^+]_i$ during activity and hence helps set the resting membrane potential to -80mV.

1.4.2 Structure

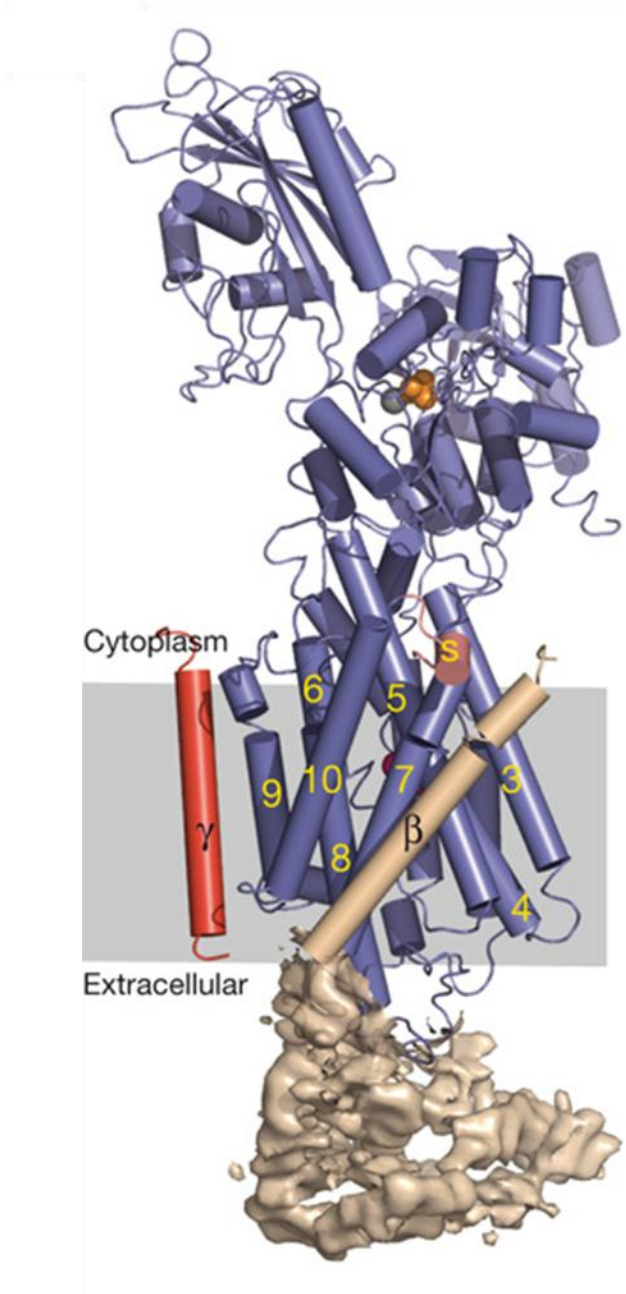

Figure 1.3: Structure of the Na^+/K^+ ATPase as determined by X-ray crystallography. The α subunit is coloured in blue, with the β subunit coloured in white and the γ subunit coloured in red. The transmembrane helices of the α subunit are numbered in ascending order starting with the most N-terminal. The S denotes the switch domain (C-terminal helix) which has been suggested to alter conformation with Na^+ binding. The red balls represent the K^+ binding sites whilst the yellow balls denote the Na^+ binding sites. Taken from Morth *et al*, 2007.[78]

The Na^+/K^+ ATPase is a multi-subunit enzyme belonging to the P-type ATPase family. In order to form a functional pump there is a minimum requirement for one α and one β subunit[66] of which there are various isoforms. The α subunit contains the catalytic domain of the enzyme and is responsible for transport and pharmacological characteristics of the pump but must be associated with a β subunit in order to navigate the secretory pathway to the membrane.[79, 80] Each α subunit has a molecular mass of 110kDa[81] and contains the binding sites for ATP, Na^+, K^+, cardiac glycosides and a phosphorylation site.[82] The β subunit is under half the size at 35kDa but usually exists in a highly glycosylated form with a molecular weight of 50kDa.[81] It is essential for enzyme maturation and membrane insertion.[83, 84]

As mentioned, there are several isoforms of both the α and the β subunits. The α subunit exists in 4 isoforms (α1- α4) of which α1- α3 are expressed in human heart[85] and only α1 and α2 are expressed at significant levels.[86, 87] α1 and α2 subunits are also the only isoforms expressed in the mouse heart[47] with 40% of functional α1 and 70% of functional α2 found in the t-tubules.[66] In the sarcolemma α1 is the dominant isoform whilst it is α2 in the t-tubules.[82] It has been concluded that both subunits are involved in E-C coupling but the difference each isoform has on downstream biochemical pathways is undetermined.[66]

There are 3 isoforms of the β subunit with the human heart expressing mainly the β1 subunit with a small amount of β2 subunit.[86] It has only one transmembrane domain in comparison to the 10 transmembrane domains of the α subunit.[88] The affinity of the Na^+/K^+ ATPase for potassium ions has been shown to be β isozyme-dependant.[89]

Often described with the pump is a third sub-unit, referred to as the γ subunit,[18, 90, 91] which is a tissue specific member of the FXYD small family of proteins. It is proposed that the FXYD families are regulators of the Na^+/K^+ ATPase and will be discussed in more detail in Section 1.5.

1.4.3 Function

The basic function of the Na^+/K^+ ATPase pump is to move 3 Na^+ ions from the cytosol and replace it with 2 K^+ ions. The Na^+/K^+ ATPase is the major route of Na^+ efflux from the cell and helps to re-establish the correct ionic gradients that drive many cellular processes. The pump is responsible for 40% of the resting heart's ATP turnover which indicates its importance in cellular homeostasis.[92]

The molecular mechanism of ion transport in P-type ATPases was first described by Post-Albers[84, 93] which considers 2 conformations of the enzyme E_1 and E_2 which can either be in a phosphorylated or unphosphorylated state.[94] In Figure 1.4 a basic representation of the way the pump works is shown. In the E_1 conformation, in which the enzyme is open to the cytosol, the enzyme has a high affinity for Na^+ and ATP and binds 3 Na^+ ions and 1 ATP molecule. ATP then phosphorylates the α subunit causing the dissociation of ADP and a conformational change in the enzyme, E_2. In this state the enzyme opens to the extracellular space where it releases the Na^+ ions, due to its affinity for Na^+ having decreased and its affinity for K^+ having increased. K^+ ions now bind and cause a spontaneous dephosphorylation and the phosphate molecule is released prompting another conformational change on the enzyme back to the original state, E_1. The enzyme opens again to the cytosol and now that its affinity for Na^+ over K^+ is restored, the K^+ ions are released and the cycle starts again.

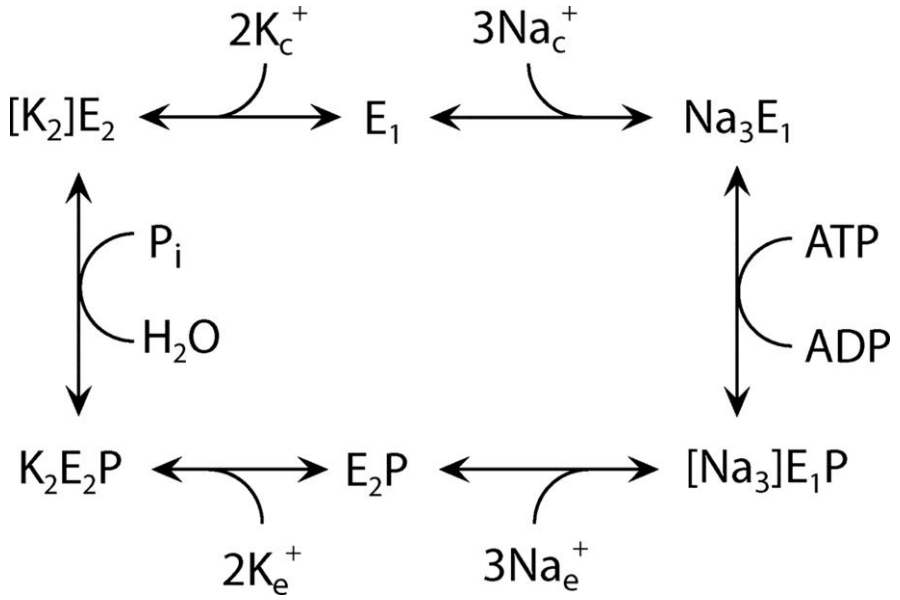

Figure 1.4: Post-Albers model for the reaction cycle of Na^+/K^+ ATPase.
Cytoplasmic and extracellular ions represented by c and e respectively. E_1P and E_2P are the phosphorylation intermediates sensitive to ADP and K^+. E_1P phosphorylation is activated by binding of $3Na^+$ from cytoplasm and whilst E_2P dephosphorylation is activated by binding of $2K^+$ from extracellular space. However, $2Na^+$ ions may replace K^+ at this site, resulting in a slower dephosphorylation than with K^+. Taken from Einholm *et al*, 2010.[95]

1.4.4 Regulation

Regulation of the Na^+/K^+ ATPase is important for normal cellular function as the Na^+ gradient it helps maintain, in turn helps regulate many other ions by driving ion exchange and transport processes. The Na^+ gradient is important for the NCX, NHE, NBE, NKCC and NMgX

transporters.[3, 45] (For a comprehensive list of Na^+ affected transporters, exchangers and co-transporters see Shattock PLM review, 2009[45]). Changes to Na^+ gradient will therefore affect H^+, HCO_3^-, Cl^-, Mg^{2+} and most importantly Ca^{2+}. It is the indirect effect of the pump on $[Ca^{2+}]_i$ via the NCX which sets SR Ca^{2+} load and determines cardiac contractility.[96-98]

1.4.4.1 Pump regulation by substrate availability

ATP

In normal physiological conditions the concentration of myocyte intracellular ATP, ~7mM,[99-104] is far in excess of the concentration required for pump activation. Some studies in giant patches from guinea pig, rabbit and mouse myocytes have a half maximal pump activation, K_m, of 94μM[105] whilst other studies report pump K_m between 0.1 and 0.8mM.[98, 100, 105, 106] Therefore ATP is considered to be saturating and non-limiting for pump activity under most physiological conditions.

Even in situations of ATP depletion such as hypoxia, for example at high altitude, the pump has adaptive mechanisms which affectively lower the V_{max} and K_m for ATP allowing the pump to function relatively normally.[107] However, in extreme cases of ATP reduction such as complete ischemia an immediate increase in $[Na^+]_i$ has been widely suggested to contribute to the loss of the Na^+ gradient by depression of pump function.[63] However, Fuller *et al*, in a paper first suggesting the existence of a phosphorylatable cardiac 'γ' subunit, reported Na^+/K^+ pump inhibition in ischemia through accumulation of a labile cytosolic inhibitor long before ATP falls to levels that would limit pump function.[63] Whatever the mechanism of the impairments of Na^+ extrusion in ischemia, it is clear this leads to a secondary acidosis[3, 108] and impaired cardiac function.

Intracellular Na^+ and K^+

The main physiological regulators of the pump are internal Na^+ and external K^+. $[Na^+]_i$ displays a sigmoidal relationship with Na^+/K^+ ATPase activity and $[Na^+]_i$ for half maximal pump activation is dependent on the internal and external ionic conditions. K_m is usually in the range of 8-22mM Na^+ which is very similar to the resting $[Na^+]_i$ in most cells.[109, 110] Therefore any small changes in $[Na^+]_i$ will result in large changes in pump activity.[66] This allows the pump to

react quickly to maintain intracellular Na^+ regulation during normal E-C coupling and during times of increased heart rate (β-adrenergic stimulation) as $[Na^+]_i$ increases during stimulation in a frequency-dependent manner.[3] Successful regulation of Na^+ will limit the rise of $[Na^+]_i$ and hence $[Ca^{2+}]_i$[111] helping to prevent Ca^{2+} overload and contractile dysfunction.[45]

There is a further consideration when looking at Na^+ activation of the Na^+/K^+ ATPase concerning the available pool of Na^+ that can activate the pump. Many studies provide evidence that there is a sub-sarcolemmal (fuzzy-space) pool of Na^+ that can transiently activate Na^+/K^+ ATPase[65] that differs from the bulk cytosolic Na^+ pool by a diffusional barrier.[2, 112-115] This would suggest that the activity of co-localised Na^+ influx pathways which charge this subsarcolemmal pool are important in controlling Na^+/K^+ ATPase activity.[66] A transient increase in subsarcolemmal Na^+ following I_{Na} action potential upstroke may activate NCX, which has been shown by some to be functionally coupled to Na^+/K^+ ATPase,[87, 116] to act in reverse mode to bring Ca^{2+} into the cell[117-120] and should also activate Na^+/K^+ ATPase at this point aiding early repolarisation by removing Na^+.[65] In addition, in forward mode the coupled NCX may influence Na^+/K^+ ATPase activity by influencing subsarcolemmal $[Na^+]$ especially in heart failure where NCX expression is upregulated.[121, 122] However, Silverman *et al*, suggested that the subsarcolemmal steady state $[Na^+]$ returns to normal in under 10ms[65] suggesting no transient effect on NCX or Na^+/K^+ ATPase.

$[K^+]_e$ displays a hyperbolic relationship with Na^+/K^+ ATPase activation. Half-maximal activation of the pump by external K^+ is in the range of 1-2mM[65, 109, 123] when external Na^+ is at its physiological concentration. Considering that $[K^+]_e$ in normal conditions is 4mM, the pump is approximately 70% saturated with regard to external K^+.[124] This will buffer the activation of the pump with respect to K^+, depending on the extent that $[K^+]_e$ changes physiologically. Small $[K^+]_e$ physiological changes, <5mM, will have little effect on pump current; however during intense exercise if $[K^+]_e$ rises to approximately 9mM it can be estimated from Bers *et al*, that there may be an increase in pump current by almost 30%.[124]

In summary, under physiological conditions, large changes in pump activity occur with small changes in $[Na^+]_i$ and relatively little changes in pump activity occur with changes in $[K^+]_e$.

1.4.4.2 Pump regulation by kinase phosphorylation

Kinase activation of the cardiac pump by PKA and PKC during adrenergic stimulation of the heart is widely accepted,[19] although several outcomes on pump activity have been reported and the mechanism of action has been debated.

PKA

β-adrenergic stimulation activates the G_s-protein coupled receptor (GPCR) causing AC activation which in turn increases the amount of cAMP and consequently PKA which phosphorylates its downstream substrates. Currently most groups report Na^+/K^+ ATPase stimulation by PKA,[28, 30, 62, 63, 109, 125-131] however some report inhibition,[111, 132] others report no change[133] and one reports both inhibition and no change.[134] This in itself is confusing and additionally in early studies it was also unclear as to whether these effects were due to direct or indirect activation of the pump.[128]

The differing opinions of the functional effect of β-adrenergic stimulation on the pump are difficult to reconcile due to the many varied techniques, laboratories and species used for each study. One confounding factor appears to be the concentration of intracellular Ca^{2+} in these studies. It would appear that where studies have used sub-physiological concentrations of Ca^{2+}, below 100nM, they report an inhibition or no change in pump activity.[132, 134] Indeed the presence of Ca^{2+} is required for ISO stimulation of the pump[111, 131, 135] which may have caused the differing findings in some of the variety of models investigated.

In studies describing a β-receptor mediated stimulation of the pump, the effects of PKA on pump activity are accepted to be either a change of the pump affinity for Na^+ (K_m effects[28, 29, 129, 135]) or to increase the maximal pump rate (V_{max}[111]) or both.[62, 63] Pump activity has been shown to increase by as much as 40%.[128] In the heart, the phosphorylation target of PKA has been debated to be the pump itself[136, 137] or its accessory protein, phospholemman, which co-localises with the pump. However direct phosphorylation of the pump has only been seen when detergents have been added[138, 139] suggesting previous studies have perhaps not been measuring direct I_{Pump}. To further support this argument, the Na^+/K^+ ATPase phosphorylation site for PKA, Ser938, is not accessible when the protein is fully folded.[140]

PKC

As with PKA, PKC has been shown to both activate[29, 141, 142] and inhibit pump function.[143-145] Increases in PKC can arise from α1 adrenergic receptor stimulation which activates phospholipase C (PLC) causing cleavage of phosphatidylinositol 4,5-diphosphate into inositol 1,4,5-triposphate (IP_3) and diacylglycerol (DAG). IP_3 increases intracellular Ca^{2+} release which combined with DAG activates PKC.[146-148] Again Na^+/K^+ ATPase activation is linked to intracellular Ca^{2+} levels and could again explain the differences in the various studies.[142] PKC isoforms expression, PKCα, δ and ε, in the heart may also add to the complexity of the published results.[66]

PKC also appears to have different effects depending on the subunit of Na^+/K^+ ATPase investigated. Han *et al*, 2010[149] show PKC in cardiac myocytes has no effect on pump V_{max} when α1 isoform is present; but shows an effect on V_{max} with the α2 isoform. Other studies are in agreement with this finding and also show effects on mainly the α2 isoform.[29, 135, 141] One study showed a K_m effect as well.[150]

The end phosphorylation target of PKC is again most likely to be the PLM accessory protein although direct phosphorylation by PKC of the α subunit has been seen both *in vitro*[136, 139, 151] and *in vivo*.[152-154] PKC-mediated phosphorylation of the α subunit has been shown to occur at Ser16 and Ser23 in rat,[154, 155] whereas the sequence for Ser23 is absent in other mammals and phosphorylation only occurs at Ser16.[139] Chibalin *et al*, have shown that in some tissues phosphorylation of the α subunit by PKC is involved in signalling pump internalisation and degradation,[156-158] however this does not appear to be the case in cardiac tissue.[66]

PKC has been shown to phosphorylate 3 sites on PLM, Ser63, Ser68 and Ser/Thr69[21, 22, 130, 159] and it is through these sites that pump function is most likely to be modulated. In support of this idea PKC stimulation of the pump has been shown to be absent in PLM-KO mice.[29]

1.4.4.3 Pump regulation by other mechanisms

Oxidation

Although regulation of the pump is usually deemed to be the result of phosphorylation either of the pump or an accessory subunit, it is widely accepted that the Na^+/K^+ ATPase is also regulated by oxidant stress. Free radical induced stress was shown to reduce Na^+ pump current in voltage-

clamped rabbit ventricular myocytes by up to 50%[160] and subsequent work showed pump activity was significantly decreased by glutathione depletion.[161] White *et al*, showed PKC epsilon (PKCε) induced angiotensin II-mediated inhibition of the pump in rabbit myocytes which could not be attributed to phosphorylation[145] but was deduced to be via signalling of Ang II through NADPH oxidase and superoxide.[29]

It has now been shown that the cardiac Na^+ pump is regulated by glutathionylation of β1 subunit at Cys46 which reduces pump turnover.[162] Glutathionylation can occur during normal physiology as well as during oxidative stress and the β1 subunit is found glutathionylated in unstimulated myocytes with additional glutathionylation promoted by peroxynitrite or hydrogen peroxide.[162] The result of glutathionylation is to destabilise the α and β subunit interaction and decrease V_{max} of the pump. This could have important consequences during pathophysiological diseases with neurohormonal dysregulation, oxidative stress and increased $[Na^+]_i$.[162]

Interestingly, PKA has been proposed to inhibit the cardiac pump through similar mechanisms. In rabbit myocytes PKA stimulation via forskolin has been reported to activate NADPH oxidase via PKCε resulting in glutathionylation of the β1 subunit and inhibition of the pump.[163] This opposes previously discussed PKA stimulation of the pump and may again relate to the use of inappropriate and unphysiological intracellular pipette Ca^{2+} concentrations in these studies. It may be that the presence of PLM, which has been shown to relieve pump inhibition by glutathionylation of the β1 subunit, may protect the pump from oxidative inhibition whilst allowing stimulatory phosphorylation.[164]

Nitric oxide

Nitric oxide (NO) has been reported to have conflicting effects upon the Na^+/K^+ ATPase pump. Some studies report NO mediates inhibition of the pump,[165-170] with others reporting stimulation.[171-176] It appears that stimulatory effects have been seen in cardiac/vascular tissues expressing phosphorylatable PLM, whereas inhibition has been shown mainly in renal and nervous system tissue. The exact pathways are still to be resolved but it has been suggested that NO is generated by an increase in heart rate[165, 177, 178] or synthesised by atrial naturetic receptor stimulation.[171] NO has been shown to activate PKCε[179] which has been shown to stimulate the Na^+/K^+ ATPase most probably via phosphorylation of the accessory protein, PLM. Indeed work by our group, Pavlovic *et al*, 2012 supports this finding and has shown pacing induced phosphorylation of PLM at PKCε Ser63 site by NO in rat ventricular myocytes.[177]

Additional factors

Several other factors can regulate pump activity for example in skeletal muscle exercise training can upregulate pump expression.[180] Cardiac pump activity can be affected by pH[181] with deviations from pH 7.5 in either direction decreasing pump function.[182-184] Changes to phosphatase activity can indirectly alter pump function,[185] and temperature, gene expression[186] and hormones[106, 187] e.g. insulin, all play a role. Insulin has been shown to increase activity of Na^+/K^+ ATPase in fibroblasts[188-190] and stimulates transport of potassium.[191] All these regulators either have a short term immediate effect or can alter expression patterns of the pump subunits. For example high fat diets can down regulate α2 subunit of the pump which will have long term ramifications on activity.[192]

Accessory proteins – FXYD family

As previously mentioned, there is a third subunit associated with the αβ-complex of the Na^+/K^+ ATPase which regulates the pumping activity in a tissue- and isoform- specific way.[19, 193] The third component, the gamma (γ) subunit,[17, 194-199] of the renal Na^+/K^+ ATPase was first discovered in the 1970's but little was known about its functional role or influence on the pump. Coincidentally a family of FXYD proteins had also been discovered but it was not known that they interacted with Na^+/K^+ ATPase. It is now known that the FXYD protein family is a small group of tissue specific membrane spanning proteins that interact with the Na^+/K^+ ATPase and help to regulate activity by influencing V_{max} and/or K_m (for review see Garty *et al*, 2006[193]).

The FXYD family are type 1, single membrane spanning proteins[22] which have a COOH terminus in the cytosol and that share a common 35 amino acid signature sequence that includes the short motif PFXYD (proline-phenylalanine-X-tyrosine-aspartate).[90] Most commonly X is tyrosine but can also be histidine, threonine or glutamate. There are 7 mammalian FXYD proteins with FXYD10 or PLMS found in shark rectal gland and Figure 1.5 shows the common mammalian amino acid sequence. There is close sequence homology between human, rat and mouse for most family members. Figure 1.6 shows the basic features of the individual family members and Table 1.1 details where each FXYD is found and the interacting isoform.

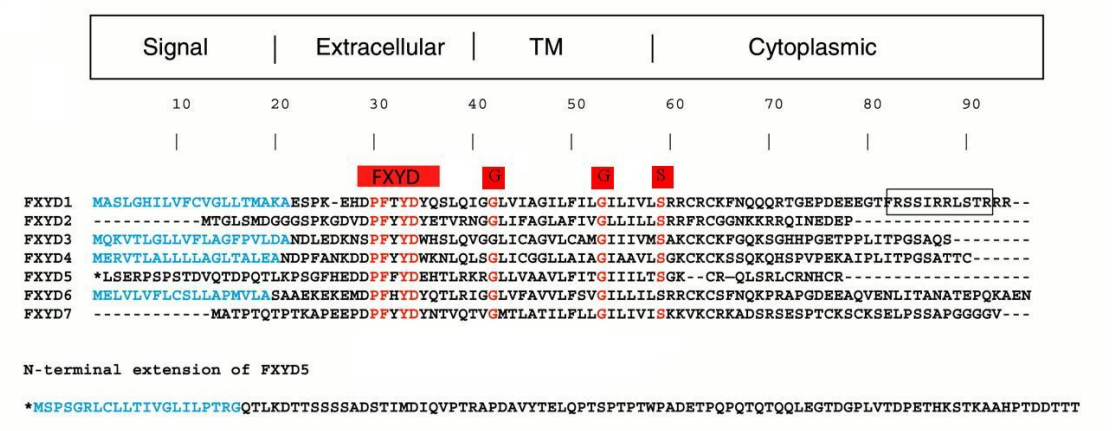

Figure 1.5: Amino acid sequence alignment of FXYD 1-7.
The amino acid sequence of the FXYD proteins (excluding PLMS) showing commonly shared residues including FXYD motif in red. Cleaved amino terminal residues are shown in blue. The box in the cytoplasmic region of FXYD1 surrounds the amino acids containing putative phosphorylation sites. Adapted from Cornelius *et al*.[83]

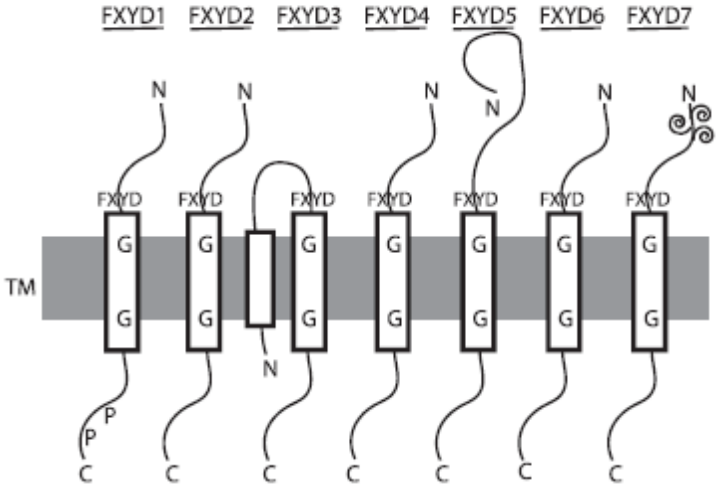

Figure 1.6: Structural characteristics of mammalian FXYD proteins.
All FXYD proteins are type 1 single membrane spanning proteins with an extracellular N-terminus (N) and cytoplasmic-C terminus (C) with the exception of FXYD3. The FXYD motif and conserved glycine residue (G) position are highlighted. FXYD1 phosphorylation sites (P) are shown on the cytoplasmic tail. FXYD7 O-glycosylation sites are represented as spirals. Adapted from Geering Review, 2006.[14]

FXYD Family Member	Alternative Name	Interacting Isoform	Tissue Distribution	References
FXYD 1	Phospholemman	α1 and α2	Cardiac, Skeletal Muscle, Smooth Muscle, Brain	26, 200-202
FXYD2	γ	α1	Kidney	18, 203-208
FXYD3	MAT-8	α1	Stomach	209
FXYD4	CHIF	α1	Kidney, Colon	15, 208, 210, 211
FXYD5	RIC/dysadherin	ND	Kidney, Intestine, Lung, Heart, Spleen	212
FXYD6	Phosphohippolin	ND	CNS	213
FXYD7		α1	Brain	16
FXYD10	PLMS	α3	Shark rectal gland	27, 204, 214

Table 1.1: FXYD family of proteins.
Table detailing each family member with alternative name, the interacting isoform, the tissue distribution and references. ND –not determined.

FXYD1 or phospholemman (PLM) is the cardiac specific FXYD protein and the only member of the FXYD family that can be phosphorylated.[26] It is through phosphorylation that FXYD1 regulates the Na^+ pump whilst other FXYD members appear to regulate the pump activity via simple association/disassociation kinetics. Therefore phosphorylation of FXYD1 plays an important role in regulation of the cardiac pump and consequently $[Na^+]_i$ and cardiac function control.[14]

1.5 FXYD1- Phospholemman

In 1985, Presti *et al*,[20] first described a cardiac sarcolemmal protein with a molecular weight of 15kDa and which was a substrate for β-adrenergic stimulation. In the same year, the group also discovered that the unidentified protein was also a major substrate for protein kinase C (PKC) phosphorylation.[21] In 1991, this 15kDa protein was named as phospholemman, reflecting its position in the membrane with its characteristic multisite phosphorylation.[22]

Phospholemman (PLM) is a 72 amino acid phosphoprotein expressed in the plasma membrane of cardiac, skeletal and smooth muscle cells as well as in the liver.[22] PLM can also be found in the choroid plexus of the brain[26, 200] and in the kidney.[215, 216] It is synthesised as a 92 amino acid protein but during protein maturation it is truncated to 72 amino acids. It consists of an extracellular acidic amino-terminal end which carries the FXYD motif (17 amino acids), an alpha helical[217, 218] membrane spanning region (20 amino acids) and a cytoplasmic carboxyl tail (35 amino acids) which carries the phosphorylation sites for PKA and PKC[219] (see Figure 1.7). In the human genome the PLM gene resides on chromosome 19q13.1.[22, 220, 221]

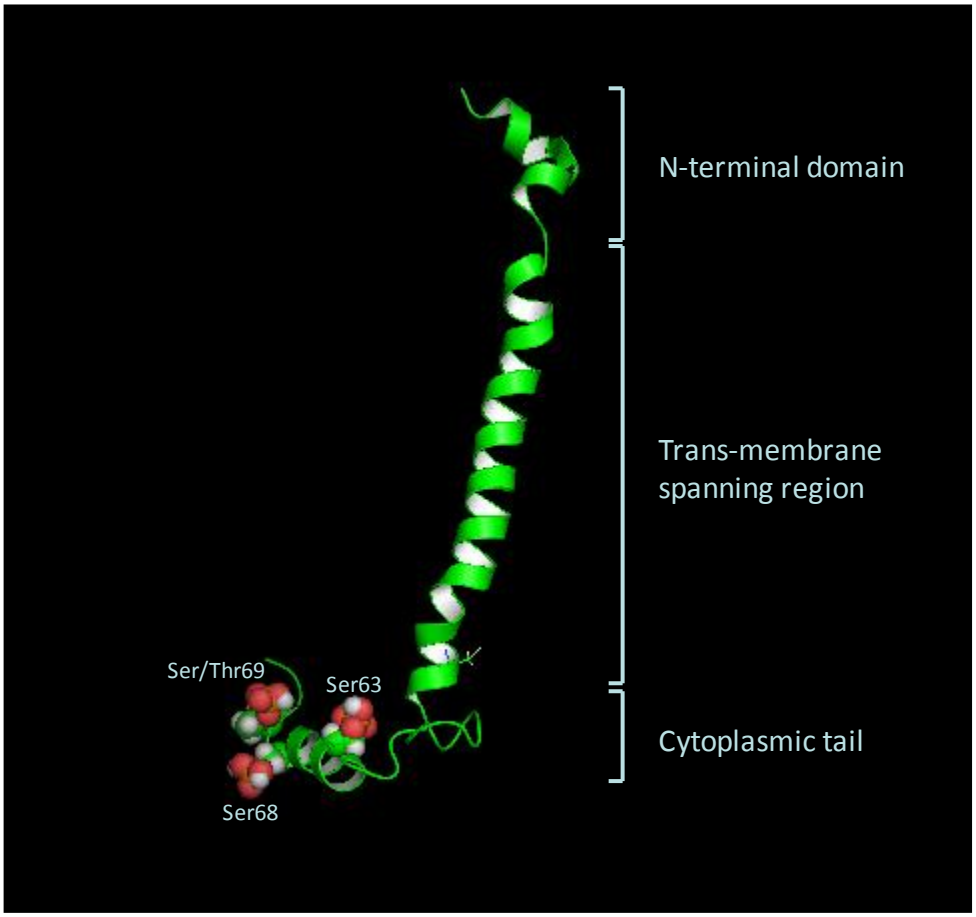

Figure 1.7: Ribbon diagram of phospholemman.
Ribbon diagram of human recombinant PLM highlighting the key sections of the protein and the phosphorylated serine/threonine residues in the cytoplasmic tail. N-terminal domain consists of 17 amino acids, trans-membrane single spanning region consists of 20 amino acids and 35 amino acid C-terminal cytoplasmic tail carrying the 3 phosphorylation sites. In the human Ser63, Ser68 and Thr69 phosphorylation sites are present; however in the mouse Ser63, Ser68 and Ser69 are present. Both have been represented in the above diagram. Adapted from Marassi *et al*.[222]

1.5.1 Role

At first the function of PLM was widely speculated with *in vitro* evidence in Xenopus oocytes overexpressing PLM suggested it played a role as a chloride[219] or taurine channel[223, 224] thereby suggesting a role in cell volume regulation. Taurine is a non-essential amino acid which can be extruded from the cell to reduce swelling. However, later studies by Bell *et al*, 2008, showed no significant osmoregulatory role of PLM in intact hearts and cardiomyocytes from WT and PLM-KO mice and suggested previous findings were possibly artefacts of overexpression.[225]

It is now well accepted that the major role of PLM is as a tissue-specific regulator of the Na^+/K^+ ATPase.[22] PLM has been shown to associate with both α1 and α2 subunit isoforms[193] in a 1:1 stoichiometry, potentially in the membrane pocket formed by M2, M4, M6 and M9 α subunit transmembrane segments as determined by work on the renal Na^+/K^+ ATPase and γ subunit (FXYD2).[13, 226-229] The mode of regulation is via a change in PLM association with the pump due to phosphorylation of serine/threonine (Ser/Thr) residues in the cytoplasmic tail.[230]

More recently there has been growing speculation that PLM may act to regulate NCX as they have been shown to co-localise.[231-233] HEK293 expression systems of PLM and NCX[231] and overexpression of PLM in rat cardiomyocytes[28, 30] support this. However, there are conflicting views as although there is evidence of NCX and PLM co-immunoprecipitation there is no evidence of FRET between the 2 suggesting that interaction is limited.[230] NCX and PLM interaction will be discussed in more length later (see Section 1.5.3).

1.5.2 Regulation of cardiac Na^+/K^+ ATPase by PLM

PLM lies adjacent to the Na^+/K^+ ATPase enzyme in the membrane, confirmed by FRET analysis,[230] and acts to modulate the catalytic properties of the Na^+/K^+ ATPase by interacting with specific domains.[83] It has been shown that PLM associates with both α1 and α2 subunit isoforms.[26, 193] The proposed mechanism through which PLM exerts its effect on Na^+/K^+ ATPase is that unphosphorylated PLM applies a tonic inhibition on the pump that is relieved by phosphorylation or genetic absence.[28, 234] Crambert *et al*, 2002, first proposed this by studying co-expression of PLM with Na^+/K^+ ATPase in Xenopus oocytes and concluded that the presence of PLM decreased K_m of the pump for Na^+ in both isozymes.[26] Other groups have since produced supporting evidence that unphosphorylated PLM decreases Na^+ affinity (K_m),[28,

[29, 129] decreases K^+ affinity [29] or reduces V_{max}.[62] However, pump inhibition is relieved by PLM phosphorylation.[27, 230, 235]

Amino acid sequence determination revealed there are 4 potential sites of phosphorylation on the PLM cytoplasmic tail: Serine62, Serine63, Serine68 and Threonine69 (Serine69 in mouse[22]), however it is believed that Ser62 is too close to the membrane to be phosphorylated. PKC has been shown to phosphorylate all 3 sites Ser63, Ser68 and Ser/Thr69.[30, 130, 159, 236] Whilst Ser68 is the only site activated by PKA and critical in the maintenance of cardiac contractility.[23, 28, 30, 232, 237]

It is believed that PLM and the pump remain associated even during phosphorylation and that there is a realignment of the structures resulting in the α subunit cross linked less efficiently to phosphorylated PLM.[66] FRET studies have also confirmed this with the FRET signal being abolished by PLM phosphorylation.[230] It is hypothesised that upon phosphorylation, the additional negative charge now on the cytoplasmic tail changes its orientation with respect to the α subunit, thus relieving inhibition.

1.5.2.1 Signalling pathways leading to the phosphorylation of PLM

PLM has been shown to be one of the major membrane target substrates for PKA and PKC phosphorylation. The action of each kinase is discussed in more detail below and Figure 1.8 shows a diagram highlighting PKA and PKC phosphorylation of PLM.

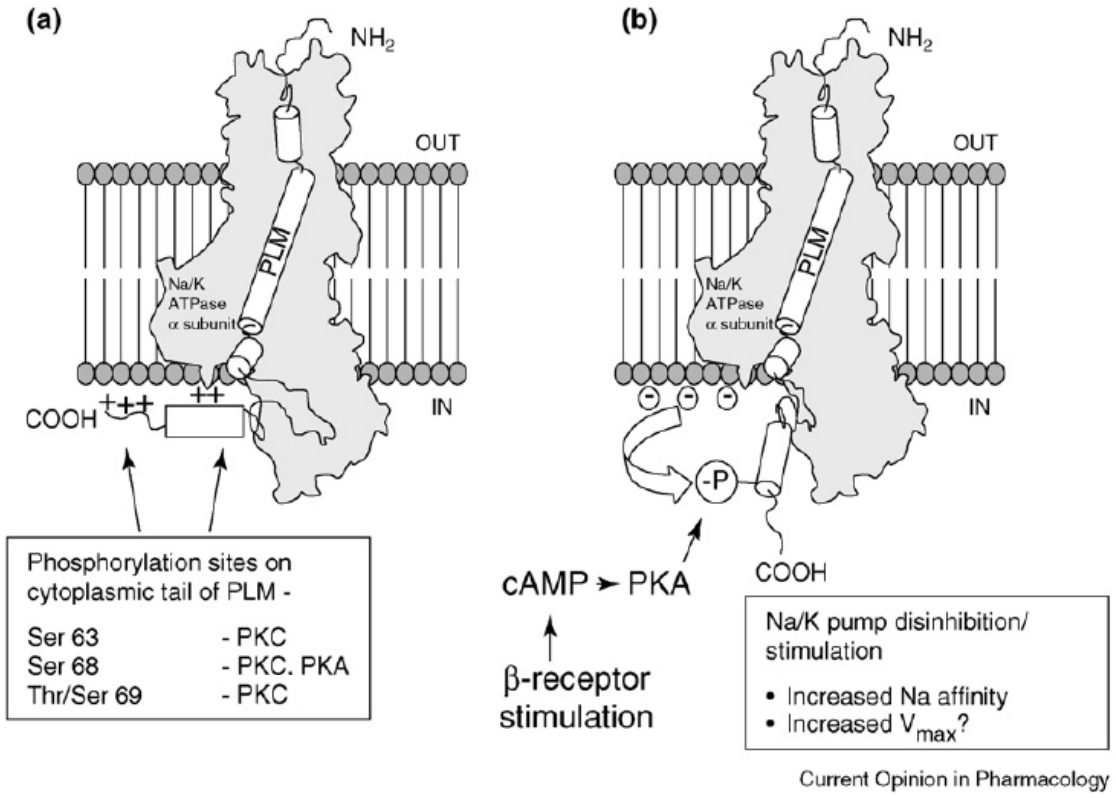

Figure 1.8: Hypothetical kinase regulation of PLM and its interaction with Na^+/K^+ ATPase α subunit.
a) Unphosphorylated PLM (taken from Franzin *et al*,[222]) interacts with the α subunit and the cytoplasmic tail orientates close to the membrane due to its positive charge; b) Phosphorylated PLM changes the charge on the cytoplasmic tail becoming more negative which repels the tail away from the membrane altering PLM interaction with the α subunit and potentially disinhibiting/stimulating Na^+/K^+ ATPase. Diagram adapted from Shattock *et al*, 2009.[45]

PKA

Activation of PKA by β-adrenergic signalling pathway has previously been discussed in Section 1.4.4.2. In early studies, it was unclear whether the effect of β-adrenergic signalling directly targeted the Na^+/K^+ ATPase or whether it was via phosphorylation of other regulatory proteins (such as the more recently identified PLM). It is now clear that PKA phosphorylates PLM at Ser68 and there is no evidence for direct phosphorylation of the α subunit in the intact protein in situ. Work by Despa *et al*, 2005, in PLM-KO mice provides evidence for this by showing that pump affinity for Na^+ in PLM-KO myocytes is higher than that in WT myocytes due to the lack of PLM inhibition.[28] With the addition of ISO, WT myocyte pump activity is increased; an effect which is absent in PLM-KO myocytes.[28] This finding has been supported by work by the Shattock group, however they also report an increase in maximal pump turnover rate, V_{max}.[62, 234]

It is now widely accepted that PLM phosphorylation at Ser68 stimulates the pump by increasing its Na^+ affinity, however there are conflicting opinions as to whether this K_m effect is accompanied by an increase in total maximal pump turnover rate, V_{max}.[28, 32, 62, 129, 149, 234]

The differing findings may be simply down to the way measurements were taken in each study. For example in Despa *et al*, 2005[28] and Pavlovic *et al*, 2007[62] both results were reported from studies using myocytes from PLM-KO mice but differed in their reported V_{max} effects. This could be due to one study being performed at room temp (Despa) and the other at 35-37^{o}C (Pavlovic) resulting in differing enzymatic kinetics being measured.

Other differences could be due to the influence of myocyte manipulation by different groups. It has been shown in rat ventricular myocytes that PLM under basal conditions is at least 30% phosphorylated at Ser68[62] (as much as 46% in some studies[232]) and a more recent study suggests that in addition to this Ser63 is basally phosphorylated by 50%. This potentially leaves only 40% of PLM not basally phosphorylated.[130] Myocyte isolation is accepted to cause a high level of stress to the cells and could potentially cause levels of basal phosphorylation to be different from day to day and lab to lab which could result in differing starting points for future enzyme kinetics measurements. Basal phosphorylation is highly sensitive to resting cellular Ca^{2+} load and hence responses to agonists can vary greatly.[66]

Finally, it has been suggested by some laboratories that different findings are due to specific Na^+/K^+ ATPase isozymes selectively being activated by PLM. It has previously been discussed that although the α1 subunit is the predominant isoform in mammalian myocytes[86] located mainly in the sarcolemmal membrane, it is the α2 subunit that has greater functional density in the t-tubules in both rats and mouse.[30] James *et al*, deduced that α2 was the isoform involved in regulation of NCX activity, intracellular Ca^{2+} concentrations and hence cardiac contractility but not α1 isoform,[87] and this was supported by other groups.[238] However, other reports contested these findings and showed α1 subunit was also involved in inotropic effects.[239] Co-immunoprecipitation (co-IP) experiments also proved controversial with some groups reporting PLM co-immunoprecipitating with both α1 and α2 subunits[240] and others showing only α1 interaction,[30, 63] however the latter group do recognise that there may be an issue with the quality of the α2 antibody used for the co-IP experiments. Bossuyt *et al*, 2009[129] have attempted to address this once and for all using SWAP mice, in which the ouabain affinities of the α subunits have been "swapped" and have shown that PLM regulates the apparent affinities for Na^+ of both α1 and α2 subunits equally. Therefore it is likely that PLM regulates both isozymes of Na^+/K^+ ATPase α subunit.

PLM phosphorylation by PKA has been compared to the relationship PLB has with SERCA. Phosphorylation by PKA or CaMKII cause the dissociation of PLB from SERCA and results in pump activation however, with no change in V_{max}.[56]

PKC

PKC activation of the Na^+ pump requires PLM[29] and phosphorylates all 3 Ser residues available Ser63, Ser68 and Ser69.[130, 149] Bibert *et al*,[241] showed that PKC phosphorylation has a V_{max} effect on α2 subunit but not α1 which is in agreement with the Bossuyt *et al*, SWAP mice data.[129] However, Bossuyt *et al*, showed a K_m effect with both isozymes in contrast to a publication by the same group showing PKC pump V_{max} effect only with no change to K_m.[29] To clarify, it has been proposed that PKA and PKC have additive effects and that whilst PKA lowers K_m for Na^+, PKC can additionally stimulate V_{max}. This may open more questions as to why there is a difference between V_{max} effects of α1 and α2 isozymes and needs further investigation. It is unlikely that all the V_{max} effects can come from α2 subunit interaction because the mouse myocyte expresses mainly α1 subunit (90%).[66] One possible explanation is that while PKA phosphorylation of PLM at Ser68 can stimulate both α1 and α2 subunits, the additional phosphorylation of Ser63 by PKC preferentially affects the α2 subunit.

Dephosphorylation

Relatively little is known about PLM dephosphorylation which is an important aspect of PLM regulation of pump activity. However, in recent years there has been more interest in this area. It is known that Ser68 is a substrate for phosphatase 1 (PP1) dephosphorylation whilst Ser63 is most like to be dephosphorylated by phosphatase 2A (PP2A).[130] PP1 is under the control of Inhibitor 1 (I1) which can be phosphorylated by PKA at Thr35 and acts in a feedback loop.[185] Our group recently showed that when I1 is phosphorylated by PKA it inhibits PP1 preventing it from dephosphorylating PLM which will also have been phosphorylated at Ser68 by PKA.[185]

We have also recently shown that PP2A is structurally associated with the α subunit and dephosphorylates PLM at Ser63 such that PLM associated with the pump is never phosphorylated at Ser63.[242] It is unclear whether dephosphorylation of Ser63 is necessary for α subunit association or α subunit binding is necessary for dephosphorylation of this residue.

These very recent observations open up the possibility that there are pools of PLM that may not be associated with the pump and pools of α subunit that may not be associated with PLM. This study[242] also reports the existence of PLM-PLM multimers under physiological conditions (previously only described in artificial overexpression systems). This raises the possibility that dephosphorylation of Ser63 may be important, either as a regulator of or a marker for, the dynamic trafficking of PLM between different subcellular pools and hence adding another regulatory mechanism.

1.5.2.2 Additional post-translational modes of PLM regulation

Palmitoylation

A further mechanism of PLM regulation has been revealed recently which is palmitoylation of PLM cysteine residues.[243] Palmitoylation is a post-translational modification of cysteine (Cys) residues which is catalysed by palmitoyl acetyltransferases and reversed by protein thioesterases. It can occur in a number of tissues and is a dynamic and reversible modification. With respect to PLM, palmitoylation occurs at Cys 40 and 42 in the cytoplasmic tail, at the border with the transmembrane domain[243] and the functional effect is to inhibit pump activity, a reverse of phosphorylation. Paradoxically, the phosphorylation status of PLM influences the palmitoylation status. If PLM is phosphorylated at Ser68, then there is more palmitoylation. The functional consequence of this is yet to be determined.

NO stimulation

Rasmussen *et al*, show nitric oxide stimulation of the cardiac pump[173] which has since been shown to be dependent on PLM.[244] Indeed in endothelial nitric oxide synthase (eNOS) knock-out mice, neuronal nitric oxide synthase (nNOS) knock-out mice and a dual nitric oxide synthase (e/nNOS) knock-out mouse they show a reduced pump activity by 25-40%[245] indicating that endogenous NO stimulates the Na^+/K^+ ATPase. Other groups have reported similar findings.[171-176] The exact pathways have yet to be resolved but increases in heart rate have been suggested to be responsible for NO generation.[165, 177-178] In addition, increases in heart rate in the absence of β-adrenergic stimulation have been shown to phosphorylate threonine 17 on PLB due to NO generation, suggesting Na^+/K^+ ATPase regulation is also a possibility. Suggested pathways of activation are via nitrosylation or cyclic guanosine

monophosphate (cGMP) signalling pathway or both. NO has also been reported to activate PKCε[179] and recently Pavlovic *et al*, has shown pacing induced PKCε phosphorylation of PLM Ser63 in rat myocytes by NO.[177] The NO regulation role of Na^+/K^+ ATPase may play an important role in disease processes during which NO signalling is significantly altered.

1.5.3 Additional functions of PLM

1.5.3.1 Regulation of NCX

As well as regulation of Na^+/K^+ ATPase, it has also been suggested that PLM may have another important functional role in regulating the NCX.[246] The NCX is an important electrogenic cardiac transport protein that can work in 2 modes: forward/Ca^{2+} efflux (exchanging $3Na^+$ ions into the cell for $1Ca^{2+}$ ion out) and reverse/Ca^{2+} influx (exchanging $3Na^+$ ions out of the cell for $1Ca^{2+}$ ion in).[35] The NCX normally works in the forward mode producing an inward ionic current resulting in a net inward movement of one positive charge. The reversal potential ($E_{Na/Ca}$) is determined by intra- and extra- cellular Na^+ and Ca^{2+} concentrations and E_m at any given time. Forward mode is favoured when $[Na^+]_i$ is low, removing Ca^{2+} from the cell; however when $[Na^+]_i$ is high reverse mode may be activated and Ca^{2+} is brought into the cell in exchange for Na^+. Regulation of the NCX1 (the cardiac isoform of the exchanger) by PLM has been proposed by the Cheung research group. To date there are no other accessory proteins that have been proposed to regulate NCX.

Cheung *et al*, present evidence that phosphorylation of PLM inhibits the NCX. Studies using HEK293 cells with co-expression of NCX and PLM showed that forskolin resulted in an additional suppression of I_{NCX} suggesting that PLM phosphorylation at Ser68 inhibits NCX.[231, 247] However, they also suggest that unphosphorylated PLM has little or no effect on NCX and a Ser68 to alanine PLM mutant has been shown to have no effect on I_{NCX}, Ca^{2+} transients or contractility.[246]

1.5.3.2 Co-localisation of NCX and PLM

In ventricular myocytes it has been shown that the α1 and α2 subunits of the Na^+/K^+ ATPase are functionally linked to NCX.[116] It has also been shown that PLM also immunoprecipitates with

NCX in cardiac sarcolemma.[231-233] It is proposed that PLM, Na^+/K^+ ATPase and NCX form a complex that helps control and maintain $[Na^+]_i$ and $[Ca^{2+}]_i$. However, it has been shown that PLM effects on NCX and Na^+/K^+ ATPase are completely independent of each other.[202, 231-233, 248]

1.5.3.3 Mechanism of NCX regulation

It would appear that phosphorylation of PLM at Ser68 may have opposing effects on Na^+/K^+ ATPase and NCX activity, stimulating one whilst inhibiting the other. Cheung has hypothesised that PLM phosphorylation of Ser68 under β-adrenergic stimulation would promote Na^+ extrusion by enhancing the activity of Na^+/K^+ ATPase. This Na^+ extrusion may offset any increase in Na^+ influx through increased heart rate (by favouring forward mode NCX) and may therefore limit the inotropic response at any time during "fight or flight" when increased contractility is desirable. Cheung further hypothesises that a concomitant inhibition of NCX (by phosphorylated PLM) will thus allow inotropy to be maintained in the face of enhanced Na^+ extrusion. Others, however, questioned the role of PLM regulating NCX and have argued that the inotropic "price" of enhanced Na^+ efflux on raising heart rate, is one that is "worth paying" as preventing Na^+ load enhances diastolic function and protects again arrhythmias.[45]

1.5.3.4 Evidence against NCX regulation

More recently, Bossuyt *et al*, 2006 showed that although NCX and PLM may co-immunoprecipitate when they used fluorescence resonance energy transfer (FRET) to measure the interaction they found no local signal indicative of close molecular proximity.[230] Though, this does not prove that there is no interaction between PLM and NCX. They did however find a good FRET signal between PLM and Na^+/K^+ ATPase.

There are conflicting findings in the literature regarding phosphorylation of NCX by β-stimulation with some reporting no effect[249-251] and others reporting stimulation.[252-255] A more recent study has also shown that PKA and PKC activation increases I_{NCX}.[256] Interestingly, none of these studies reported inhibition of NCX questioning the hypothesis of Cheung *et al*, for a role for PLM phosphorylation inhibiting NCX.

1.6 Functional effects of PLM on $[Na^+]_i$ in mouse models

Despa *et al*, 2005 have compared Na^+ measurements in quiescent myocytes from WT hearts and from PLM-KO hearts and showed that they have similar $[Na^+]_i$ (12.5±1.8mM in WT compared with 12.0±1.5mM in KO myocytes).[28] This is interesting considering it is hypothesised that PLM inhibits the pump and it has been shown that PLM-KO pump affinity for Na^+ is greater than in WT myocytes[28, 29, 33, 62] therefore potentially a lower $[Na^+]_i$ than in WT myocytes would be expected. However, protein expression of the total α subunit was also shown to be significantly lower in PLM-KO myocytes which may help to offset the increased Na^+ affinity of the pump in these mice resulting in relatively normal $[Na^+]_i$.[28, 33] It must also be noted that these Na^+ measurements were made in quiescent myocytes and will be affected by the basal phosphorylation status in the cell which may be high and is very dependent on Ca^{2+}. Therefore, if the WT myocytes following isolation are stressed and Ca^{2+} loaded, the basal phosphorylation may be increased and the pump affinity for Na^+ will be similar to that seen in PLM-KO myocytes resulting in similar $[Na^+]_i$. Additionally, these Na^+ measurements were made with sodium-binding benzofuran isophthalate (SBFI) in quiescent myocytes at room temperature which questions the physiological relevance of the result. The lack of action potential and Na^+ and Ca^{2+} influx combined with temperature effects on enzyme kinetics question the applicability of these measurements to the intact beating heart at 37°C.

Studies in beating perfused hearts comparing WT and PLM-KO mouse hearts showed a significantly lower LVDP in PLM-KO hearts[33] and indicated compromised contractility with development of mild hypertrophy.[34] This may be indicative of a lower $[Na^+]_i$ as this would reset the cellular Ca^{2+} load by forward mode NCX resulting in a lower intracellular Ca^{2+} and therefore a reduced contractility of the heart.

PKA and PKC stimulation help to highlight the importance of PLM and its effect on the pump and $[Na^+]_i$. Previous studies have shown a greater pump activity in KO myocytes, but this can be surmounted in WT by treatment with ISO. ISO increased pump activity in WT quiescent myocytes to the same amount as PLM-KO pumps (which showed no further increase in activity) demonstrating that phosphorylation relieves pump inhibition and even stimulates by PLM.[28] Na^+ measurements from the same cells shows ISO lowered the $[Na^+]_i$ in WT cells but did not affect PLM-KO myocyte $[Na^+]_i$.[28] The importance of this ISO effect on $[Na^+]_i$ was shown by Despa *et al*, 2008 who showed the pacing (2 Hz) induced rise in intracellular Na^+ could be reversed by ISO in WT but not PLM-KO myocytes.[32] This important observation shows that during situations of increased Na^+ influx, for example β-adrenergic stimulation in times of

"fight or flight" which will increase heart rate and action potential generation, that the rise in intracellular Na^+ with each heartbeat[53] will be counteracted by the increase in efflux rate of the Na^+/K^+ ATPase which has been disinhibited by PLM PKA phosphorylation.

1.6.1 The need for a mouse expressing unphosphorylatable PLM

A large amount of data discussed in this introduction has been gained using cardiac myocytes or HEK293 cells under a variety of conditions, some more physiologically relevant than others. Ideally what is needed at this point is to be able to measure $[Na^+]_i$ in an isolated perfused beating heart at 37°C allowing a more informed conclusion about changes to $[Na^+]_i$ during baseline cardiac physiology and during times of β-adrenergic stimulation to be made. When considering the appropriate mouse model to use, the current PLM-KO mouse has limitations, so a new genetically modified mouse, PLM^{3SA}, has been developed which has an unphosphorylatable PLM protein. Based on previous adenoviral work where constructs were made that had the 3 serine phosphorylation sites (Ser63, Ser68 and Ser69) mutated to alanine a mouse with the same mutations was created to allow further investigation into what would happen to mouse heart cardiac function when the Na^+/K^+ ATPase can no longer be disinhibited or stimulated. This could potentially affect the heart during periods of β-adrenergic stimulation as Na^+ efflux by the Na^+/K^+ ATPase could not be attenuated and increased to balance the increased Na^+ influx. A consequence of this may be Na^+ overload which in turn would affect $[Ca^{2+}]_i$ and could have severe consequences for the animal with respect to cardiac contractility and Ca^{2+} overload. As suggested previously an increase in $[Na^+]_i$ may lead to an increase in $[Ca^{2+}]_i$ via the reverse mode NCX resulting in Ca^{2+} overload which has been suggested to contribute to altered cardiac contractility, arrhythmias and even heart failure.[45, 52, 257]

This PLM mutant mouse (PLM^{3SA}) has not been previously characterised and the general aim of this thesis is to provide the first characterisation of this mouse using biochemical and functional approaches.

1.7 Hypothesis

The inability to phosphorylate phospholemman in the new PLM^{3SA} mouse may cause $[Na^+]_i$ overload, contractile dysfunction and cardiac arrhythmias. Of particular interest is heart function during periods of β-adrenergic stimulation, increases in heart rate and Na^+/K^+ ATPase inhibition.

1.8 Aims

To test this hypothesis, the following aims will be addressed:

- To investigate the biochemical phenotype of the PLM^{3SA} mouse heart.
- To investigate the basic cardiac function of the perfused PLM^{3SA} mouse heart.
- To investigate cardiac function of PLM^{3SA} mouse heart during β-adrenergic stimulation and increased pacing rate.
- To measure $[Na^+]_i$ in PLM^{3SA} mouse hearts and WT littermates using:
    a) Flame photometry
    b) ^{23}Na NMR

2 CHAPTER 2 – GENERAL METHODS

2.1 Reagents

All chemicals were supplied by Sigma-Aldrich or VWR unless otherwise stated. Details of the primary antibodies used for immunoblotting are listed in Table 2.7 with secondary antibody details listed in Table 2.8. Those used for immunocytochemistry are detailed in Table 2.10 and Table 2.11. Anti-Phospho(Ser63)-PLM and Anti-Phospho(Ser68)-PLM were gifts from J Randall Moorman (University of Virginia). Anti-PLM (C2) kindly supplied by Joe Cheung (Temple University School of Medicine, USA).

2.2 Mouse colony development, breeding and maintenance

Animals used in all studies were from our in-house PLM^{3SA} (FXYD-1 knock-in) mouse transgenic colony. Animals were housed in a controlled environment at a maintained temperature of 25^{o}C with a 12 hour light dark cycle and food and water ad libitum. All experiments performed were in accordance with the Home Office guidance in the Operation of the Animals (Scientific Procedures) Act 1986. All animals used were male and approximately 15 weeks of age (approximately 25-30g), with the exception of NMR data where animals were 8-10 weeks of age (approximately 20-25g).

2.2.1 Development of transgenic model

To investigate the functional effect of PLM phosphorylation on pump activity, a knock-in mouse has been generated in which the 3 serine phosphorylation sites (Ser63, Ser68 and Ser69) have been mutated to alanine resulting in a globally expressed unphosphorylatable PLM protein which is under the endogenous PLM promoter. This mouse, PLM^{3SA} mouse (or FXYD-1 knock-in), was developed by Genoway.

Genoway performed a detailed analysis of the FXYD-1 gene based on the DNA sequence (NM_05992). It was decided that the generation of a point mutation FXYD-1 knock-in model would be achieved by the replacement of FXYD-1 gene sequences using homologous

recombination in embryonic stem cells (ES) from 129/SvPas mice. A targeting vector was constructed containing homology arms flanking PLM sequences encompassing exons 5-7 with site directed mutagenesis of serine to alanine at residues 63, 68 and 69 and a neomycin resistance cassette flanked by LoxP sites integrated within FXYD-1 locus. Diphtheria toxin A subunit gene was incorporated into the plasmid outside the 5' homology domain. The construct was then transfected into embryonic stem (ES) cells and those that had undergone successful recombination were positively selected for using neomycin. Constructs that had inserted by illegitimate recombination were selected against using the diphtheria toxin. Selected ES cells were genotyped by PCR and Southern blotting to screen for correct placement of the construct. Successfully modified stem cells were transfected into C57BL/6 blastocysts which were implanted into female C57BL/6 mice to obtain male chimeric offspring. Chimeras were then backcrossed with C57BL/6 mice and those with the targeted ES cells, and therefore the construct, in the germ line produced agouti offspring. Following genotyping the heterozygous agouti male mice were used as founder mice to cross breed with C57BL/6 females and their offspring were termed Generation 1. Generation 1 heterozygotes were mated, and produced Generation 2 mice in an approximate ratio of 1 +/+ : 2 +/- : 1 -/-. Generation 2 heterozygotes were subsequently crossed and the +/+ and -/- offspring (Generation 3) were used in experiments. Generation 2 homozygotes were also crossed to produce additional +/+ and -/- offspring (Generation 3) for use in experiments. Mice used in experiments were all Generation 3 and either littermates or cousins. Currently the PLM^{3SA} mice have not been backcrossed on a pure C57BL/6 background.

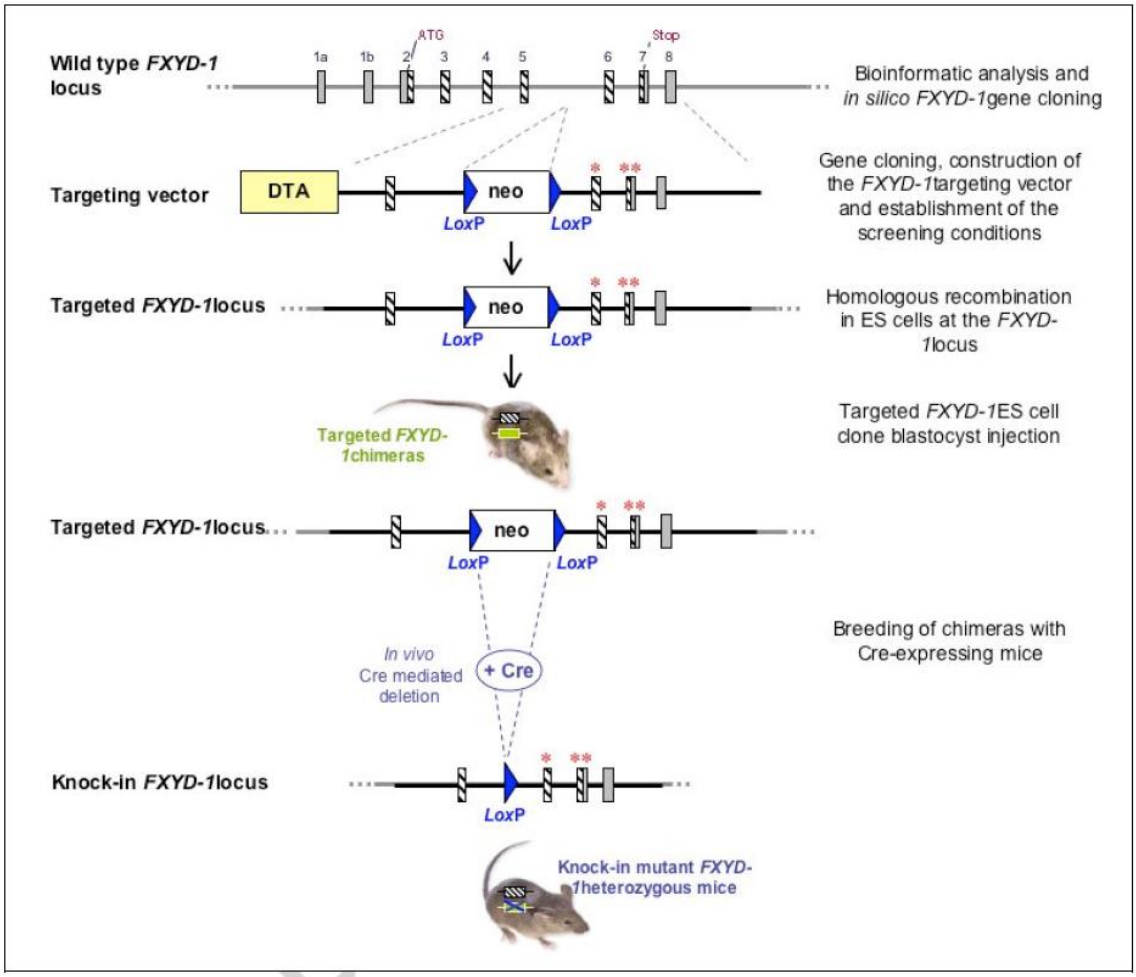

Figure 2.1: Schematic representation of the generation of the knock-in FXYD-1 mutated mouse (PLM^{3SA}) by Genoway.
Shows detailed description of the process used to create the genetically modified knock-in FXYD-1 (PLM^{3SA}) mice.

2.2.2 Colony maintenance

Mice generated from the heterozygous breeding pairs were genotyped using a standard protocol. Ear clippings from the offspring were digested in a 2ml Eppendorf tube with 500µl of master mix (500µl lysis buffer (100mM TRIS, 200mM NaCl, 5mM EDTA, 0.2% SDS) + 1µl proteinase K (20mg/ml) per ear sample) overnight in an Eppendorf Thermomixer at 55^{o}C shaking at 1000rpm. The following day tail debris was spun down at 10000 x *g* using an Eppendorf bench top centrifuge (5417R) for 5 minutes. 450µl of the supernatant was transferred to a fresh 2ml Eppendorf containing 500µl of isopropanol and spun down again at 13000 x *g* for 10 minutes. The supernatant was aspirated and the DNA pellet rinsed with 1ml ethanol (70% v/v) and again spun at 10000 x *g* for 2 minutes. The supernatant was aspirated

and allowed to dry at 37°C for 10 minutes. The DNA pellet was resuspended in 100µl tris-EDTA (TE: 10mM TRIS, 1mM EDTA, pH 8.0) at 37°C for 3 hours prior to polymerase chain reaction (PCR). Primers designed to complement the PLM knock-in sequence were used in the PCR reaction (see Table 2.2) and are listed below, Table 2.1. The PCR products were run on a 1.5% agarose gel made with 1x TAE (1L 50x TAE stock: 242g Tris, 57.1ml glacial acetic acid (100% v/v), 100ml EDTA (500mM, pH 8.0)) containing 3µl/50ml GelRed nucleic acid stain (Cambridge Bioscience) for 1hour at 120V and studied using a UV light. The knock-in allele yields an amplification product of 370bp whereas the PLM wild-type allele yields an amplification product of 259bp.

Primer Name	Sequence, 5′-3′
PLM KI F	TCT GCG TGC TAA GAT GAT CAC AGA TGC
PLM KI R	CTT GAC TTT GTT GGG AGA GGG ACG G

Table 2.1: Primers used for determining mouse genotype.

Reaction Mix		Reaction Conditions			
Genomic DNA	10ng	**Step**	**Temp.**	**Time**	**Cycles**
Primers	each 15pmol	Denaturing	94°C	120s	1 x
Reaction Buffer	0.5mM	Denaturing	94°C	30s	
Taq	2.6U	Annealing	65°C	30s	30 x
$MgCl_2$	2mM	Extension	68°C	120s	
dNTPs	0.5mM each	Completion	68°C	480s	1 x
Reaction volume	50µl				

Table 2.2: Optimised PCR conditions for the detection of the FXYD-1 knock-in allele.

2.3 Langendorff perfusion

2.3.1 Principles

The first published study of attempted organ perfusion dates back to 1849 by Loebel. However, it was Oscar Langendorff in 1895 who devised the perfusion technique which, although modified, is still used today.[258] In his original studies the apparatus used by Langendorff was cumbersome and involved a large aspirator connected to a blood perfusion flask held at a constant pressure by an ingenious electrical device.[258] Today the technique is simpler and consists of reservoirs containing solutions, which provide similar ion concentrations to that in blood, connected to a cannula from which the organ is hung. Gravity or a pump controller (described in Section 2.3.8) is used to infuse the organ with solutions contained in the reservoir at a constant pressure of 80mmHg.

The main purpose of this technique is to supply an isolated heart with oxygen and metabolites to study the effects of metabolic and pharmacological interventions on heart function.[259] This technique uses retrograde perfusion of the heart via the coronary arteries. The aorta is hung onto a cannula and the subsequent retrograde flow of the oxygenated perfusate forces the aortic valve to close. The pressure in the root of the aorta forces the perfusate through the coronary ostia and coronary arteries which supply the heart. Perfusate drainage is via the coronary sinus through the right atrium with the remainder exiting through the heart chambers via Thebesian drainage.

2.3.2 Langendorff basic set-up

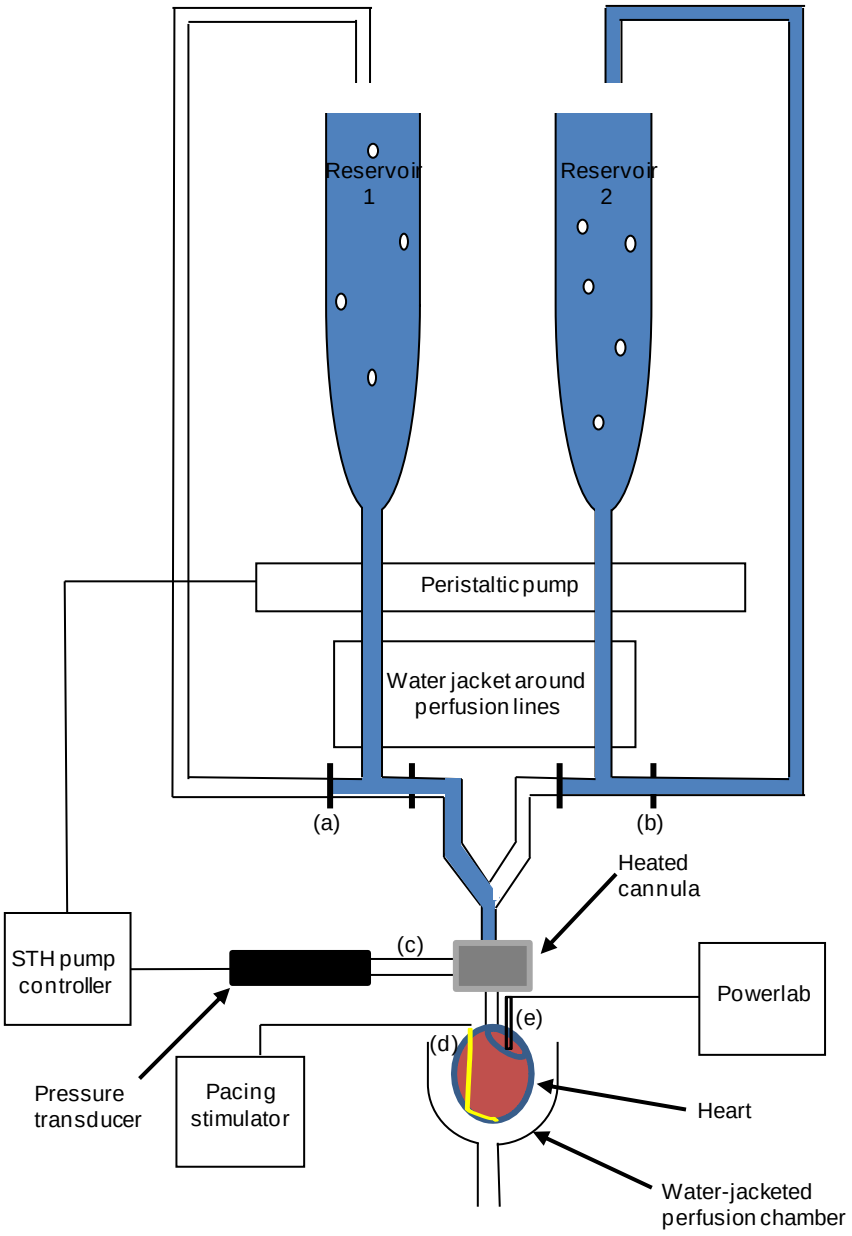

Figure 2.2: Basic Langendorff set-up used in the studies throughout this thesis. Reservoir 1 supplies perfusate to the heart through a heated cannula at 37^{o}C whilst reservoir 2 recirculates perfusate. By closing (a) and opening (b) tubing clips the reservoir supplying the heart can be changed to administer different perfusate interventions. A side arm from the cannula (c) connects to a pressure transducer and measures aortic pressure. This feeds back to the STH pump controller that adjusts the perfusion rate to maintain a constant pressure of 80mmHg. When required, a pacing wire (d) is positioned at the apex of the heart. An intraventricular balloon is placed in the left ventricle (e) to measure LVP by connection to a pressure transducer and Powerlab-Chart capture system.

In this thesis, the Langendorff apparatus has been modified for each individual study but the basic set-up consists of 2 separate reservoirs which attach to a cannula onto which the heart is hung (see Figure 2.2). The use of 2 reservoirs allows the administration of different solutions and pharmacological agents and both are oxygenated with 95% O_2/5% CO_2 and heated to provide perfusate at the cannula tip at 37^{o}C. Each reservoir has tubing clips allowing the easy transference from one solution to another at the cannula. The Langendorff set-up can use gravity flow to provide perfusate at 80mmHg pressure at the cannula; however the set-up used in this thesis (above) has an additional piece of equipment, the STH pump controller.[260] This allows the perfusion pressure to be set at 80mmHg without the need for the correct hydrostatic height and also measures coronary flow automatically. This STH pump controller works by passing the tubing from the reservoirs around a peristaltic pump before they enter the heart through a heated cannula at 37^{o}C. The peristaltic pump itself is operated by a feedback loop from a pressure transducer that is attached to a cannula arm measuring perfusion pressure in the aortic root. This pressure transducer records values using a bridge amplifier connected to the Powerlab-Chart system which feeds back to the peristaltic pump allowing constant perfusion pressure of 80mmHg to be maintained by adjusting coronary flow accordingly. Unless stated the studies here have been performed at constant pressure.

2.3.3 Heart excision and cannulation

Mice were anaesthetised by a combined intraperitoneal injection of sodium pentobarbitone (200mg/kg) with sodium heparin (200IU/kg). The depth of anaesthesia was checked using the loss of pedal withdrawal reflex and slowing of breathing rate. The thorax was located using the sternum as reference and a transabdominal incision was made using scissors (Fine Science Tools; fine iris scissors) exposing the diaphragm. This was then cut through and the thorax was opened by lateral incisions through the left and right sides of the ribs to the clavicles. To expose the heart, the ribcage was removed and the heart excised along with the lungs and placed immediately in 10ml 4^{o}C Krebs-Henseleit solution (KHB), see Table 2.3, to ensure the heart arrests. To cannulate the heart, first the lungs, thymus and fatty tissue were removed to expose the aortic arch which was cut through to leave the untruncated aorta. Using Dumont #5 fine tip forceps (Fine Science Tools) on either side of the aorta, it was slid onto the cannula (a previously blunted and scored 21 gauge needle) and secured using 4/0 surgical silk (Johnson and Johnson). After successful cannulation the perfusion pressure was rapidly increased to 80mmHg using STH pump controller to reduce the risk of ischemia and pre-conditioning. A

heated water-jacketed chamber filled with KHB was placed around the heart to ensure a heart temperature of 37°C.

2.3.4 Perfusion buffer

The main perfusion buffer used in these studies was modified Krebs-Henseleit bicarbonate buffer. However, depending on the needs of some studies this was further modified. Tables 2.3-2.5 list the buffer compositions used for the various studies. All solutions were filtered using a 5μm filter to remove undissolved chemicals and gassed with 95% O_2/5% CO_2 helping to maintain a pH of 7.4, except intracellular Na^+ studies washout solution Table 2.5 which was gassed with 100% O_2.

Paced and unpaced mouse heart studies

Reagent	Molarity (mM)
NaCl	118.5
$NaHCO_3$	25.0
KCl	4.7
$MgSO_4.7H_20$	1.2
KH_2PO_4	1.18
Glucose	11.1
Na Pyruvate	2.0
$CaCl_2$	1.4

Table 2.3: Krebs-Henseleit buffer (KHB) used in the majority of isolated mouse studies.
Na pyruvate has been added to help eliminate mouse heart cycling.[261, 262] In unpaced studies, 0.05mM ascorbate was added as a vehicle control due to subsequent ISO studies containing ascorbate to prevent the oxidation of ISO.

Rubidium uptake mouse heart studies

Reagent	Molarity (mM)
NaCl	118.5
$NaHCO_3$	25.0
$MgSO_4.7H_20$	1.2
NaH_2PO_4	1.2
Glucose	11.1
$CaCl_2$	1.4
RbCl	4.7
Bumetanide	0.05

Table 2.4: Modified Krebs-Henseleit buffer used in rubidium uptake studies.
KCl has been replaced by RbCl; KH_2PO_4 has been replaced by NaH_2PO_4. Bumetanide was added to block the NKCC.

Intracellular Na^+ studies mouse heart washout solution

Reagent	Molarity (mM)
NMDG	149.4
HEPES	2.38
$MgSO_4.7H_20$	1.2
EGTA	2.0
Glucose	10

Table 2.5: Composition of buffer used in intracellular Na^+ flame photometer studies for extracellular washout.
Removal of Na^+ from the perfusion buffer enables washout of Na^+ from the extracellular space. Removal of Ca^{2+} from the perfusion buffer ensures NCX is immobilised. Washout solution was buffered to pH 7.4 with KOH and gassed with 100% O_2.

2.3.5 Studies using paced mouse hearts

Mouse hearts were electronically paced at a frequency of 550 beats per minute (bpm) using a silver electrode placed in the apex of the heart and a reference electrode clipped onto the cannula to provide an earth. The electrodes were connected to a Student Stimulator that applied single square wave pulses of 1msec duration at 1.5x the pacing threshold for each heart, which was approximately 5V.

2.3.6 Studies using unpaced mouse hearts

For studies using unpaced mouse hearts an apparatus modification was made in order to maintain a high and stable heart rate. Due to the poor vascular perfusion of the right atrium and hence sino-atrial node by normal retrograde perfusion, an additional superfusion system was set-up to provide heated oxygenated KHB to the right atrium. An extra 2 reservoirs, again to administer different perfusate solutions, were set-up on the right hand side of the rig and the tubing passed around a peristaltic pump before entering a heated glass coil and exiting through a 21 gauge blunted needle placed close to the right atrium. The peristaltic pump was set to a flow rate of 3ml/min and the temperature was maintained at 37^{o}C.

2.3.7 Studies using paced mouse hearts inside NMR magnet

Although the techniques for perfusing hearts inside the NMR magnet incorporate elements of the methods for studies using paced hearts (Section 2.3.5) and the basic set-up (Section 2.3.2) it is a much more complicated set-up. The NMR magnet is very large, distant to the perfusion rig and requires the heart to be completely enclosed inside an NMR tube of outer diameter (O.D) maximum 1.0cm with an internal diameter (I.D) of 0.8cm. A modified NMR perfusion rig was developed which incorporated extended perfusion lines requiring water-jacketing to enable perfusion of the heart inside the magnet (which was also heated) at 37^{o}C, however due to heat loss from tubing in the NMR probe the heart was cannulated at room temperature. Following cannulation the heart was perfused at constant flow of 3ml/min. Constant flow perfusion was adopted, due to the inability of the pressure transducer to feedback to the STH pump controller because of perfusate line length. A balloon was fed into the left ventricle and LVEDP was set between 4-8mmHg and the heart was paced at 550bpm. The heart was then placed in the NMR

tube and coronary effluent was removed from the tube via a siphoning tube positioned at the top of the NMR tube. A more detailed description of this rig is found in Chapter 6, Section 6.3.2.

2.3.8 Measurement of cardiac function

Many cardiac function measurements were derived from real time left ventricular pressure (LVP) measurements. LVP measurements were obtained by removing the left atria and inserting a cling-film balloon into the left ventricle. The balloon was attached to a pressure transducer and fluid filled until a left ventricular end diastolic pressure (LVEDP) reading of 4-8mmHg was recorded by a Powerlab recorder using Chart programme software for data capture. The volume inside the balloon was then kept constant throughout the experiment providing isovolumetric measurements. Using the LVP measurements, left ventricular developed pressure (LVDP), heart rate and LVEDP were derived. Pressure transducers were calibrated at the start of each experimental day using a sphygmomanometer.

Aortic pressure or perfusion pressure was measured directly from the aortic root. The cannula sits in this aortic space and is linked to a pressure transducer which records values using a bridge amplifier connected to the Powerlab-Chart system. Using the STH pump controller the pressure was set to 80mmHg. Coronary flow was measured by calibrating the signal used to drive the peristaltic pump. Temperature was measured using a Hanna thermomister placed in the right ventricle. Temperature stability was maintained by submersion of the mouse heart into a KHB filled, temperature controlled chamber.

2.4 Protein expression determination using SDS-PAGE

2.4.1 Isolated heart sample preparation for SDS-PAGE

Following Langendorff perfusion, hearts were removed from the cannula and placed on blotting paper. The right atria was removed using fine spring scissors (Fine Science Tools) and the heart was blotted to remove any excess perfusion buffer from the ventricles before being snap frozen by dropping into liquid nitrogen. The whole process was done rapidly to ensure ‘in situ’ protein status was maintained.

Hearts were weighed using a Sartorius research balance and homogenised in a PBS (0.01M Phosphate buffer, 0.027M KCl, 0.137M NaCl) based homogenisation buffer with 1mM EDTA containing 100mg/ml (10%) phosphatase (Sigma; Phosphatase Inhibitor Cocktail 3) and 10mg/ml (1%) protease inhibitors (Calbiochem; Protease Inhibitor Cocktail Set III, EDTA-free) using a motor driven glass pestle and mortar (Fisher; FB56675) kept 'on ice' until the solution was able to pass through a 200µl gel tip (approximately 3 minutes). Heart homogenates were diluted 1:1 with 2x sodium dodecyl sulphate (SDS) sample buffer (100mM TRIS, 5% (v/v) β-mercaptoethanol, 4% SDS, 0.2% (w/v) bromophenol blue, 20% glycerol, pH6.8) was performed and the samples pipetted up and down 5 times with a 200µl Gilson pipette. The samples were then heated at 55^{o}C for 10 minutes to remove IgG from possible remaining blood. All samples were spun at 15000 x *g* using Eppendorf bench top centrifuge (5417R) for 5 minutes and supernatant removed for future gel loading.

NB. Samples to be probed for PLB were subjected to temperatures of 85^{o}C for 10 minutes to break the pentameric structure of PLB.

2.4.2 Protein assay

A simple protein assay, based on the method of Bradford, was performed to measure protein concentrations in samples loaded using equal volume. Bio-Rad protein assay kit (Bio-Rad 500-0006) was used and involved the addition of an acidic dye to each protein containing solution. The kit solution was diluted 1:5 to make a working stock solution. A BSA standard curve was constructed with this stock solution using a BSA free blank and five BSA standards covering the concentration range of 2 to 10µg/ml in increasing increments of 2µg/ml. Homogenates (without sample buffer) were added to the diluted stock solution in cuvettes and read at an absorbance wavelength (λ) of 595nm. Heart homogenates were tested at appropriate dilutions relating to the BSA standard curve. Protein concentrations of the samples were subsequently determined from the BSA standard curve. Samples that fell within 2 standard deviations of the group mean were considered suitable for equal volume protein loading.

2.4.3 SDS-PAGE and immunoblotting

Proteins were separated by SDS Polyacrylamide Gel Electrophoresis (SDS-PAGE) according to their molecular weight. Gel matrices used were 15% (v/v) acrylamide (Protogel, National Diagnostics) gels for PLM and PLB protein and 10% (v/v) acrylamide gels for Na^+/K^+ ATPase and larger proteins. An upper layer of 4.5% (v/v) acrylamide stacking gel was placed on top of the gel matrices to help separate proteins as they enter the higher percentage gel matrix. Samples were loaded in equal volumes and proteins were separated using the Mini Protean III gel electrophoresis system (Bio-Rad) at a constant voltage of 200V for 42 minutes in a reservoir buffer (0.025M TRIS, 0.19M glycine, 0.1% (w/v) SDS). A protein standard (Precision Plus Protein Standards, Bio-Rad) was run on each gel to enable protein identification by molecular weight. The compositions of the gels are listed in Table 2.6.

Reagents	**Stacking Gel**	**Running Gel**		**Concentration**
	4.5%	*10%*	*15%*	
1M TRIS-HCl	0.625ml	3.75ml	3.75ml	0.12/0.38M
10% SDS	50µl	0.1ml	0.1ml	0.1% w/v
30% (v/v) Acrylamide	0.75ml	3.33ml	5ml	4.5/10/15% v/v
ddH_2O	3.465ml	2.762ml	1.092ml	
TEMED	10µl	5µl	5µl	0.17% w/v
10% Ammonium Persulphate	70µl	70µl	70µl	0.11% w/v

Table 2.6: Table showing the components of stacking and running gels for SDS-PAGE.
Volume for stacking gel totals 5ml, volume for running gels totals 10ml and is adequate for 2 gels. TRIS used in stacking gel is at pH 6.8 and for running gel at pH8.8 adjusted with 1M HCl.

Proteins were then transferred onto polyvinylidene difluoride (PVDF) membranes (Amersham) (pre-soaked in methanol followed by transfer buffer, each for 5 minutes) using a semi-dry transfer unit at 10V for 37 minutes or 15V for 25 minutes with current set to 250mA per mini-gel in transfer buffer (0.025M TRIS, 0.19M glycine, 0.1% (w/v) SDS, 20% (v/v) methanol, pH

8.3). The membranes were then placed in 5% non-fat milk (Marvel) made with Tween-Phosphate Buffered Saline (T-PBS: 0.01M Phosphate buffer, 0.027M KCl, 0.137M NaCl, 0.1% (v/v) Tween-20) for 2 hours on an orbital shaker in order to block non-specific proteins before probing with the required primary antibody, see Table 2.7. Following primary antibody incubation membranes were washed repeatedly (every 10 minutes for 1 hour) in 15ml T-PBS and then incubated with appropriate secondary antibodies as listed in Table 2.8. Again following this incubation membranes were washed repeatedly (every 10 minutes for 1 hour) in 15ml with T-PBS before being prepared for chemiluminescence analysis.

Primary antibodies

Antibody	Species	Source	Dilution	Incubation
Anti-Phospho(Ser63)-PLM (Ser63)	Rabbit	J Randall Moorman	1:10 000	60mins RT
Anti-Phospho(Ser68)-PLM (Ser68)	Rabbit	J Randall Moorman	1: 10 000	60mins RT
Anti-Phospho(Ser/Thr69)-PLM (Ser69)	Sheep	In-house KCL	1:100	30mins RT
Anti-PLM (N1)	Chicken	In-house KCL	1:100	60mins RT
Anti-Na^+/K^+ ATPase α1 subunit	Mouse	Millipore	1:1000	60min RT
Anti- Na^+/K^+ ATPase α2 subunit	Rabbit	Millipore	1:1000	60mins RT
Anti-Na^+/K^+ ATPase α5 (total α subunit)	Mouse	DSHB	1:100	60mins RT
Anti- Na^+/K^+ ATPase β1 subunit	Mouse	Millipore	1:500	60mins RT
Anti- Na^+/K^+ ATPase β2 subunit	Rabbit	Millipore	1:1000	60mins RT
Anti-Phospho(Ser16)-PLB (S16)	Rabbit	Badrilla	1:5000	Overnight 4°C
Anti-PLB	Mouse	Badrilla	1:1000	60mins RT
Anti-SERCA2A ATPase	Mouse	Pierce Antibodies	1:1000	60mins RT
Anti-NCX (R3F1)	Mouse	Swant	1:1000	60mins RT
Anti-Actin	Mouse	DSHB	1:100	60mins RT
Anti-Calsequestrin	Rabbit	Abcam	1:1000	60mins RT

Table 2.7: Table of primary antibodies used for immunoblot analysis.
The table details the antibody used, the species of origin, the source, dilution used and incubation times.

Secondary antibodies

Antibody	Species	Source	Dilution	Incubation
Anti-Rabbit IgG HRP-linked	Donkey	GE Healthcare	1:1000	60mins RT
Anti-Sheep IgG HRP-linked	Rabbit	Thermo Scientific	1: 5000	60mins RT
Anti-Chicken IgY HRP-linked	Rabbit	Promega	1:1000	60mins RT

Table 2.8: Table of secondary antibodies used in immunoblot analysis.
The table details the antibody used, the species of origin, the source, dilution used and incubation times.

2.4.4 Chemiluminescence of immunoblots

Chemiluminescence is the emission of light produced by a chemical reaction. In this case secondary antibodies are linked to the enzyme horse radish peroxidase (HRP) which in the presence of enhanced luminescent reagents (ECL) undergoes an enzymatic reaction resulting in the emission of light. Membranes were incubated in equal volumes of ECL reagents (GE Healthcare) for 1 minute. They were then placed in Clingfilm in a photographic cassette and exposed to high performance chemiluminescent film (Hyperfilm, Amersham) for differing exposure times dependent on the antibody. Films were developed using a Fuji RGII automatic processor.

2.4.5 Quantification of protein bands

Exposed films were scanned using a Bio-Rad GS-800 Calibrated Densitometer which is operated by the Quantity-One software. Using this program the intensity of each band was measured and quantified for further analysis.

PVDF membranes were also stained with 10ml Coomassie blue (2.4mM Coomassie Brilliant Blue R, 10% (v/v) acetic acid, 50% (v/v) methanol) for 30 minutes before being washed in destain (10% (v/v) acetic acid, 50% (v/v) methanol) until protein bands are clearly visible. Staining with Coomassie allows visualisation of transfer quality and equal protein loading.

2.4.6 Phos-tag phosphate affinity SDS-PAGE and immunoblot

Protein samples were separated by electrophoresis at a constant current of 25mA per gel on Phos-tag SDS-gel containing 40µM Phos-tag ligand and 80µM $MnCl_2$ (percentage of gel is dependent on the protein molecular weight) in 1x reservoir buffer. Composition of the gels used is detailed in Table 2.9, stacking gel composition as before Table 2.6. Prior to protein transfer, gels were incubated in transfer buffer (Section 2.4.3) containing 1mM EDTA to chelate the Manganese (II) ions (Mn^{2+}) for 10 minutes on an orbital shaker, before incubation of the gel in transfer buffer alone (no EDTA) for a further 10 minutes. Proteins were transferred from the gel to a PVDF membrane (pre-soaked in methanol, followed by transfer buffer as for SDS-PAGE) in transfer buffer at 15V for 25 minutes using semi-dry electrophoretic transfer (Section 2.4.3) and detected using standard immunoblotting techniques (Section 2.4.3 and Section 2.4.4).

Reagents	**Phos-tag Gel**		**Final Concentration**
	10%	*15%*	
4 x Running Buffer	1.25ml	1.25ml	
30% (v/v)Acrylamide	1.68ml	2.52ml	10/15%(v/v)
ddH_2O	2.07ml	1.23ml	
10mM $MnCl_2$	40µl	40µl	80µM
5mM Phos-tag	40µl	40µl	50µM
10% APS	50µl	50µl	0.125% (w/v)
TEMED	5µl	5µl	0.125% (w/v)

Table 2.9: Composition of Phos-tag SDS-PAGE gels used.
4x Running buffer: 1.5M Tris-base, pH 8.7, 14mM SDS.

2.5 Isolation of adult mouse ventricular myocytes

Cells were isolated from adult mouse hearts, aged approximately 15 weeks (25-30g), by collagenase-based enzymatic digestion, as previously described.[263]

Hearts were excised and cannulated as described in Section 2.3.3. Hearts were perfused at 37°C in the standard Langendorff mode at a constant flow rate of 3ml/min in 3 sequential stages as follows: with (1) modified Tyrode's solution (130mM NaCl, 5.4mM KCl, 1.4mM $MgCl_2$, 0.4mM NaH_2PO_4, 4.2mM HEPES, 10mM glucose, 20mM taurine, 10mM creatine, pH 7.3 at 37°C) containing 0.75mM $CaCl_2$ for 2 minutes, (2) calcium-free modified Tyrode's containing 2mM EGTA for 4 minutes, (3) modified Tyrode's containing 0.1mM $CaCl_2$ and 125U/ml collagenase (Type II; Worthington Biochemical Corp) for 8 minutes. The coronary flow rate was maintained at 3ml/min using a Gilson Minipuls peristaltic pump. All solutions were maintained at 37°C and gassed with 100% O_2.

Following this perfusion protocol the heart was cut down from the cannula; ensuring only ventricles were taken, and dissected into small pieces in stage (3) solution. The tissue fragments were gently bubbled with 100% O_2 until the tissue started to break down, about 10 minutes. Using a 2ml plastic pipette, the tissue fragments were gently titrated to facilitate cell dispersion, before being filtered through gauze of 200µm pore size. Filtered cells were allowed to pellet down by gravity for 5-10 minutes before being washed with modified Tyrode's solution containing 0.5mM $CaCl_2$. A second pellet and wash step were performed during which $CaCl_2$ was increased to a final concentration of 1mM. Cells remained in the final solution at room temperature until experimentation.

Cells used in this thesis were prepared by Dr Shiney Reji, Kings College London.

2.6 Confocal microscopy

2.6.1 Culture of adult mouse ventricular myocytes for immunocytochemistry

Isolated adult mouse ventricular myocytes (AMVM) cells were kept in short term culture to ensure a high yield for confocal imaging. Nunc 35mm single vented round cell culture dishes (Nunc) were coated with laminin (Engelbreth-Holm-Swarm) prior to cell culture. 150µl of laminin, a murine sarcoma basement membrane, was added to 10ml ddH_2O making a final concentration of 15µg/ml and 1ml was added to each required dish. Dishes were incubated at room temperature in the cell culture hood for 1.5 hours. Laminin was then removed and stored at -20°C until re-use (total of 3 uses) and dishes washed with 1ml pre-warmed M199 culture medium (containing Hanks salts, 25mM HEPES, L-glutamic acid and L-amino acids, Invitrogen catalogue number 22350) supplemented with taurine (5mM), creatine (2mM) and L-carnitine

(2mM). Additionally 1% PenStrep (Gibco; 50mg/ml) was added. From AMVM isolation, the Tyrode solution was aspirated and cells washed in 10ml modified M199 medium (as above) incubated at 37°C and allowed to pellet under gravity (approx. 5 minutes) at room temperature. The supernatant was removed by aspiration and 4ml of culture medium added to make a cell suspension that was mixed by gentle inversion. 1ml of cell suspension was pipetted into each pre-laminated dish using a 5ml Gilson pipette and tip. Cells were allowed to adhere for 90 minutes in a humidified tissue culture incubator at 37°C with 5% CO_2 (Heraeus Hera Cell incubator).

2.6.2 Fixing of myocytes

Medium was aspirated from AMVM maintained in culture and cells were washed in 1ml 1x phosphate buffered saline (PBS, Invitrogen) at room temperature which was removed prior to fixing in 4% (v/v) paraformaldehyde (PFA; Agar Scientific) in PBS, 1ml/dish for 10 minutes avoiding movement of the dishes to optimise cell structure alignment. Cells were then washed with 1ml PBS (three 5 minute washes), before being stored in PBS at 4°C until antibody staining.

2.6.3 Adult mouse ventricular permeabilisation and staining

Fixed cells were permeabilised with 1ml/dish 0.2% (v/v) Triton X-100 in PBS for 5 minutes at room temperature. Cells were then washed with 1ml PBS for 5 minutes at room temperature. PBS was removed and the edge of the dish dried using a cotton bud and marked with a wax pen. To reduce non-specific secondary antibody binding 100µl of 5% (v/v) non-specific goat serum (NSG) diluted in 1% (w/v) bovine serum albumin (BSA)/gold buffer (20mM Tris-base, 155mM NaCl, 2mM EGTA, 2mM $MgCl_2$, pH 7.5) was added to the dish which was placed on an orbital shaker at room temperature for 20 minutes. This was removed and cells were then incubated in 100µl of primary antibody prepared in 1% (w/v) BSA/gold buffer solution in a humid chamber, on a shaker, overnight at 4°C. The next day cells were washed three times at 5 minute intervals before incubating with 100µl secondary antibody for 3 hours in a humid chamber on a shaker at room temperature. Cells were again washed three times at 5 minute intervals with 1ml PBS. PBS was removed by aspiration and a drop of Lisbeth's mounting medium (30mM Tris, pH 9.5, 70% (v/v) glycerol, 5% (w/v) n-propyl gallate) was added to the cells. A round cover slip was

carefully placed on top of the cells and the sides of the dish removed using a hot wire leaving the circular base. The base was then glued to a glass slide using superglue around the perimeter and the cover slip was fixed in place with clear nail varnish. Slides were stored at 4^{o}C until examination with the confocal microscope. Details of all antibodies and fluorescent dyes are detailed in Table 2.10 and Table 2.11.

Primary antibodies

Antibody	Species	Source	Dilution
Anti-PLM (C2)	Rabbit	J Cheung	1:100
Anti-Na^+/K^+ ATPase α1 subunit	Mouse	Millipore	1:100

Table 2.10: A list of primary antibodies used for immunocytochemistry.
The table details antibody dilution used, the species of origin and the source.

Secondary antibodies

Antibody	Species	Source	Dilution
Cy3-conjugated anti-rat IgG	Goat	Jackson ImmunoResearch	1:100
Cy5-conjugated anti-mouse IgG	Goat	Jackson ImmunoResearch	1:100
4'6-Diamidino-2-phenylindole dihydrochloride (DAPI)	-	Sigma Aldrich	1:100

Table 2.11: A list of secondary antibodies used for immunocytochemistry.
The table details antibody dilution used, the species of origin and the source.

2.6.4 Confocal microscopy imaging

Images of immunofluorescent labelled specimens were acquired by confocal laser scanning as described.[264] A Leica SP5 II system equipped with an Argon lasers (458, 476, 488 and 514nm), Helium-Neon lasers (HeNe 543 and 633) and a UV-diode (405nm) was used to acquire the images. Optical myocyte slices (approx. 1µm) were captured using a HCX PL APO 63x/1.4 oil immersion lens, a frame size of 1024 x 1024 pixels at a pixel depth of 8 bit, and scan frequency

of 400Hz. Further image processing was carried out using LAS AF software (Leica). The excitation and emission/detection wavelengths (λ) for the fluorescent proteins and dyes used in these experiments are listed in Table 2.12.

Antibody	Excitation λ	Emission λ
Cy3-conjugated anti-rat IgG	543nm	555-650nm
Cy5-conjugated anti-mouse IgG	633nm	650-750nm
4'6-Diamidino-2-phenylindole dihydrochloride (DAPI)	405nm	430-495nm

Table 2.12: Excitation and emission wavelengths used in confocal microscopy experiments.
Table details fluorophores and the excitation and emission wavelengths used for their detection.

2.7 Subcellular fractionation of adult mouse ventricular myocytes

AMVM were isolated as described in Section 2.5 and used for subcellular fractionation as described in Yin *et al*, 2010.[265] Myocytes were pelleted down under gravity for 5 minutes before the Tyrode solution was aspirated and replaced with 1.5 ml fresh Tyrode solution at room temperature. This cell suspension was then transferred to a 2ml eppendorf (VWR) using a 5ml Gilson pipette and tip, and a small 50µl sample was removed to another eppendorf and diluted 1:1 with 2x SDS sample buffer (Section 2.4.1) for the input control. The remaining cells were allowed to pellet down and the modified Tyrode's solution was replaced with 200µl of 4°C PBS based lysis buffer (Section 2.4.1) containing 0.05% digitonin and kept on ice for 5 minutes with frequent vortexing. Myocytes were then centrifuged at 10000 x *g* for 2 minutes at 4°C using an Eppendorf bench-top centrifuge (5417R). The supernatant contains the cytoplasmic fraction which was removed to a fresh pre-cooled Eppendorf tube and 200µl 2x SDS sample buffer was added. The remaining pellet was then resuspended in 200µl PBS based lysis buffer supplemented with 1% Triton X-100 by vortexing and incubated for 5 minutes on ice. The suspension was again centrifuged at 10000 x *g* for 2 minutes at 4°C and the supernatant containing the Triton-soluble membrane fraction was removed completely to a fresh Eppendorf tube and 200µl of 2x SDS sample buffer was added. The remaining pellet was resuspended in 400µl 2x SDS sample buffer and yields the Triton-insoluble myofilament fraction. All samples

were kept on ice throughout the fractionation procedure, and were heated to 55°C for 5 minutes after addition of sample buffer. Samples were centrifuged at 15000 x *g* for 5 minutes before being immunoblotted as described in Section 2.4.3. Fraction antibody markers are listed in Table 2.13.

Antibody	Species	Source	Dilution	Fraction
Anti-GAPDH-HRP conjugated	Mouse	Abcam	1:1000	Cytoplasm
Anti-Na^+/K^+ ATPase α1	Mouse	Millipore	1:1000	Membrane
Anti-cTroponinI	Mouse	Santa Cruz Biotechnology	1:1000	Myofilament

Table 2.13: A list of antibodies used as subcellular fraction markers.
The table includes details of antibody dilution used, the species of origin, the source that supplies each antibody, and the fraction it confirms.

2.8 Flame photometry

2.8.1 Principles

Flame photometry is a technique used to measure the amount of ions e.g. Na^+ or K^+ in a biological sample. It works on the principle that an alkali metal salt when drawn into a non-luminous flame will ionise, thus absorbing energy from the flame and emitting a light of a characteristic wavelength as the excited atoms return to an unexcited state. A photocell in the flame photometer then detects the emitted light and converts it to a voltage that can be measured and recorded. Na^+ emits an orange light of wavelength 589nm whilst K^+ emits a purple light of wavelength 766nm. Different ions can be distinguished by using coloured filters to detect the different wavelengths emitted. Consequently the voltages recorded give a measurement of the specific ion detected.

Flame photometry studies were used in this thesis to measure intracellular Na^+ content in the intact mouse myocardium and to determine Na^+/K^+ ATPase activity in the intact mouse myocardium by measuring tissue accumulation of rubidium (Rb^+) which was used as a K^+ substitute. For the latter study a rubidium filter was used to detect the ion. Rb^+ also burns with a purple flame at a wavelength of 780-794nm.

2.8.2 Isolated heart sample preparation for flame photometry

Hearts were excised and perfused on the standard Langendorff perfusion rig at constant pressure as previously described (Section 2.3 and 2.3.3). The perfusion protocols used in these studies are shown in Figure 2.4 using buffers detailed in Table 2.3 to Table 2.5. A washout perfusion period was used to remove extracellular ions before the hearts were cut down from the cannula, blotted to remove any residual fluid and snap frozen in liquid nitrogen until further analysis. To determine myocardial Na^+ or Rb^+ content, hearts were then dried overnight in an oven at 80°C for 16 hours. Hearts were then weighed before being finely chopped using scissors in 50µl/mg of 50% trifluoroacetic acid (TFA)[266] for Rb^+ uptake hearts and 20µl/mg for Na^+ content hearts (average mouse heart dry weight ~30mg). The mixture was shaken at 55°C for 24 hours using an Eppendorf Thermomixer Compact before being centrifuged at 15000 x *g* for 10 minutes and the supernatant collected and diluted in dH_2O. The Na^+ or Rb^+ content was measured using a Sherwood 410 Classic Flame Photometer (with correct filter set) using NaCl or RbCl standards to produce a linear calibration line.

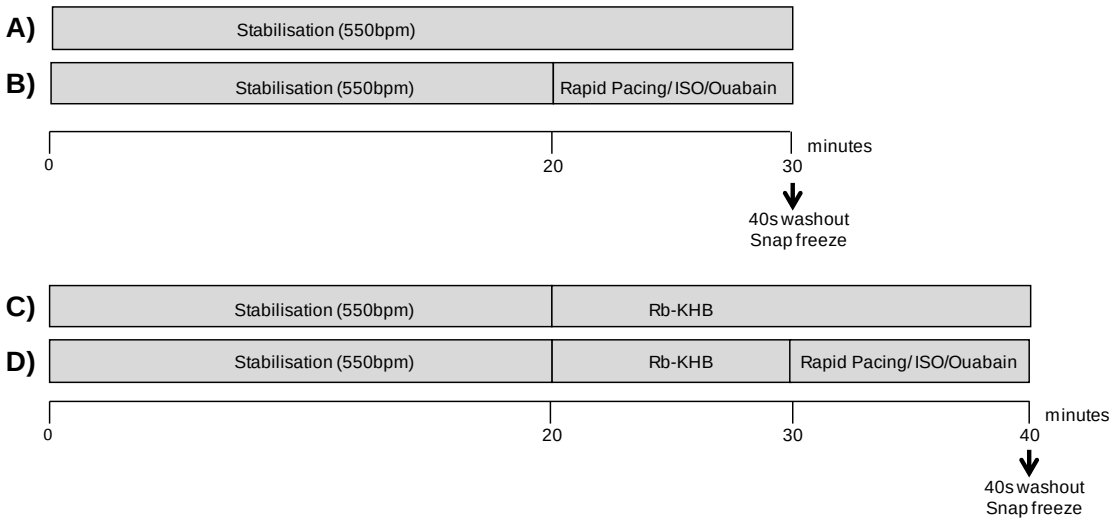

Figure 2.3: Flame photometer protocols for measuring intracellular Na^+ content or rubidium uptake in intact mouse myocardium.
A) KHB stabilisation period for Na^+ study; B) KHB stabilisation period + intervention period for Na^+ study; C) KHB stabilisation period followed by Rb^+-KHB perfusion for Rb^+ uptake study; D) KHB stabilisation period followed by Rb^+-KHB perfusion + intervention for Rb^+ uptake study. All protocols followed by 40 second washout with appropriate buffer and hearts snap frozen at end of protocol.

2.8.3 Flame photometer operation

Once the flame photometer had been primed for the fuel type, in this case natural gas, the equipment was turned on ensuring the flame is on. The nebuliser was washed through by placing it in a beaker of ddH_2O for a minimum of 30 minutes. The equipment then required calibration to the necessary standard curve e.g. Rb^+ or Na^+. To do this the standard curve dilutions were made and introduced to the flame photometer starting at the highest concentration. The nebuliser was placed in the sample for 20 seconds and using the coarse and fine sensitivity controls the reading manipulated to an appropriate arbitrary figure i.e. 50mg/ml top concentration of Rb^+ standard curve was set to 50.0. The nebuliser was removed from the solution and remained in air for at least 10 seconds, after which it was placed back into the diluent solution for washing, which in this case was ddH_2O. The next standard curve solution was then introduced to the nebuliser for 20 seconds, after which time the highest reading shown in the next 10 seconds was taken as the reading for that solution. This was necessary because of the degree of fluctuation by the flame. A standard curve was constructed and heart samples diluted accordingly with ddH_2O in 4ml glass tubes (Fisher) to fall on this curve. (For Rb^+ standard curve see Chapter 5, Section 5.4.1; for Na^+ standard curve see Chapter 5, Section 5.4.3). The nebuliser was placed in the tubes containing the diluted heart sample and readings were obtained in the same way as previously i.e. for a minimum of 20 seconds, followed by 10 seconds of measuring.

2.8.4 Measurement of Rb^+ by flame photometer

For Rb^+ measurement using the flame photometer 50µl of digested heart extract was further diluted into 3.95ml ddH_2O and measured according to the above method following the calibration of the equipment with an RbCl standard curve with concentrations ranging from 0mg/L to 50mg/L.

2.8.5 Measurement of Na^+ by flame photometer

For Na^+ measurement using the flame photometer 25µl of digested heart extract was further diluted into 3.975ml ddH_2O and measured according to the manufacturer's instructions

following the calibration of the equipment with a NaCl standard curve with concentrations ranging from to 0mg/L to 5mg/L.

2.9 ^{23}Na Nuclear magnetic resonance

2.9.1 Basic set-up

The NMR Langendorff perfusion system is described in detail in Chapter 6. However, a basic description of the experimental set-up is detailed here. Following excision of the mouse heart (Section 2.3.3) it was cannulated on a modified NMR Langendorff rig and perfused at constant flow of 3ml/min. Constant flow perfusion was adopted, due to the inability of the pressure transducer to feedback to the STH pump controller because of perfusate line length. A balloon was fed into the left ventricle and LVEDP was set between 4-8mmHg and the heart was paced at 550bpm with function measured using the Powerlab-Chart software. The heart was positioned inside a 1.0cm outer diameter (O.D) NMR tube which was placed in the centre of a 10mm Na microimaging coil (Bruker) connected within the NMR probe. The coronary effluent was removed from the tube via a siphoning positioned at the top of the NMR tube. The probe was subsequently placed inside the Bruker Avance III 400MHz Spectrometer 9.4 Tesla (T) NMR magnet core. Warm air was blown into the bottom of the magnet core at a pre-measured temperature and flow rate that would ensure the bore of the magnet was maintained at 37^{o}C. See Figure 2.4 for a detailed diagram of this procedure.

Once the probe was positioned correctly inside the magnet so that the heart was exactly in the centre of the magnetic field, the radio frequency cable was attached and using the Topspin software (Bruker) the resonance frequency was set using tuning and matching adjustment controls on the column. Due to the lack of deuterium channel, the field lock was removed. A pre-set Na shim file was read into the software which was then fine-tuned using mainly the z, z^2 and z^3 functions in order to create the most homogeneous magnetic field. This improves the signal to noise ratio which was important due to the small size of the intracellular ^{23}Na signal. Once the shim was optimal the heart ^{23}Na signal was measured.

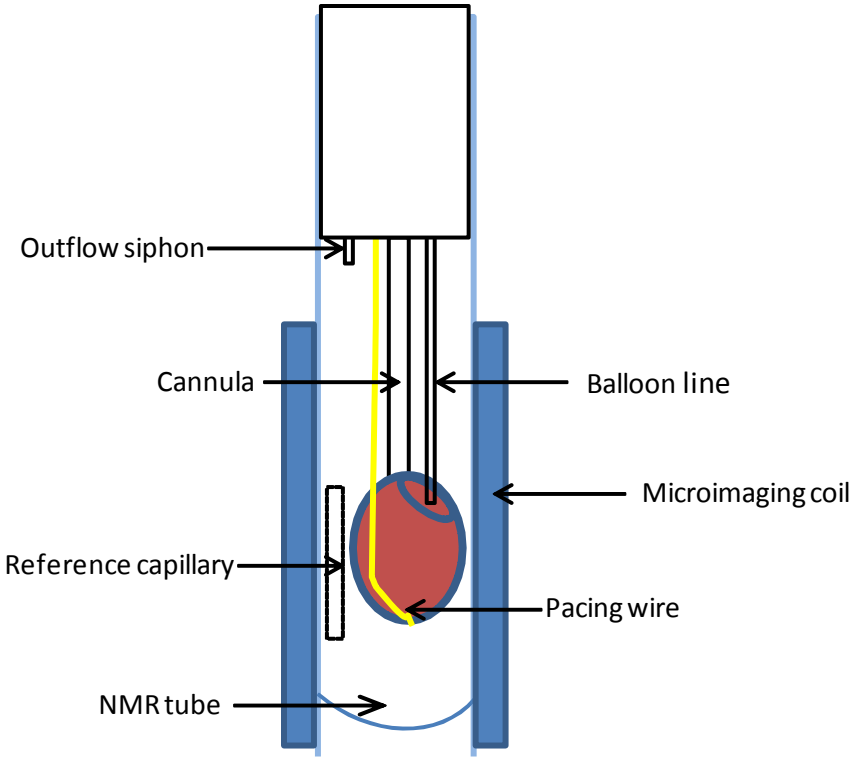

Figure 2.4: Diagram of the positioning of the Langendorff perfused heart inside the NMR tube and ^{23}Na microimaging coil.
The heart is cannulated and balloon placed in the left ventricle to measure cardiac function. A pacing wire is inserted into the apex for pacing at 550bpm. The heart is then placed in a 1.0cm (O.D) NMR tube and held in position by silicone bung. A siphoning tube is positioned at the top of the tube for removal of coronary effluent. A reference capillary is inserted next to the heart for future ^{23}Na concentration calculations (Section 2.9.5). The NMR tube is positioned in the centre of the microimaging coil (coloured in blue). This whole system is then inserted into the core of the 9.4 Tesla magnet.

2.9.2 Studies using shift reagent

Both the intracellular and extracellular ^{23}Na signals resonate at the same frequency on the NMR spectrum.[267] Therefore to measure the intracellular signal it was necessary to "shift" the extracellular ^{23}Na signal to a different resonant frequency. This was done by perfusing the heart with the a paramagnetic shift reagent Thulium (III) (1,4,7,10-Tetraazacyclododecane-1,4,7,10-tetra(methylene phosphonate)) ($Tm(DOTP)^{5-}$). After the heart had equilibrated to the magnet environment, a 30 minute stability perfusion period with standard KHB (Table 2.3) followed. The heart was then perfused with KHB containing 3.5mM $Tm(DOTP)^{5-}$ and supplemented Ca^{2+}

for 25 minutes until the extracellular ^{23}Na signal was shifted. Throughout the perfusion ^{23}Na spectra were acquired using Bruker Topspin NMR software as described in Section 2.9.4.

2.9.3 Studies using triple quantum filtering

Triple quantum filtering (TQF) enables the measurement of intracellular Na^+ signal without the use of a toxic shift reagent.[268] It works on the principle that ^{23}Na is a 3/2 spin nuclei and can spin in 4 different orientations resulting in different transition states. When ^{23}Na nuclei experience macromolecular structures e.g. in the intracellular space, electric fields are generated and allow the generation of these transition states which can be filtered for using Bruker Topspin NMR software. TQF thereby allows measurement of intracellular Na^+ signal by filtering out the signal from nuclei not experiencing this triple quantum transition state and hence not within the intracellular space (for a more detailed explanation see Chapter 6, Section 6.1.1.2).

Following heart equilibration inside the magnet, hearts were perfused with KHB (Table 2.3) for a stability period of 30 minutes and throughout ^{23}Na TQF signals were acquired as detailed in Section 2.9.4. Ten minute interventions of ISO, rapid pacing and ouabain were administered following the initial stability period and ^{23}Na TQF signals were acquired throughout.

2.9.4 NMR spectra acquisition

Time resolved ^{23}Na NMR spectra were acquired at 105.7MHz using conventional pulse-acquire experiments or triple quantum filtered experiments. All experiments were acquired with a 32μs 90^o rf pulse and a 200msec recycle delay. Triple quantum filtered ^{23}Na spectra were obtained with the pulse sequence 90^o_{φ} $-\tau/2-180^o_{\varphi+90}-\tau/2-90^o_{\varphi+90}-\delta-90^o_x-$(acquire) where the phase φ was incremented through 30, 90, 150, 210, 270 and 330º with the receiver alternated by 180º for each step. The triple quantum preparation time was τ = 5msec and a delay δ = 40μs. The acquisition parameters used in each experiment are as follows:

Shimming was carried out on the ^{23}Na signal with an acquisition employing 4 scans per spectrum acquired with 16384 points in FID, 773msec acquisition time, sweep width of 100ppm, 10Hz line broadening.

Following this a stability period was carried out employing a time resolved ^{23}Na TQF experiment with 192 scans per spectrum acquired with a resolution 2048 points in FID, 194msec acquisition time, sweep width of 50ppm, 10Hz line broadening. A total of 24 TQF spectra were acquired in an experiment time of 30mins.

Shift reagent, 3.5mM Tm(DOTP)$^{5-}$, was injected into the perfusion line at the constant flow rate of 3ml/min and conventional time series of 1D ^{23}Na spectra were obtained with 4 scans per spectrum with 2048 points in FID, 194msec acquisition time, sweep length of 50ppm, 20Hz line broadening. A total of 1024 spectra were acquired in an experiment time of 27mins 40s.

Following injection of shift reagent a second TQF experiment was acquired with the same parameters as the stability period with 4 spectra acquired in a total experiment time of 5mins.

For NMR experiments employing TQF measurements only an extended capture of ^{23}Na TQF experiment with 192 scans per spectrum acquired with a resolution 2048 points in FID, 194msec acquisition time, sweep width of 50ppm, 10Hz line broadening was performed. It was noted at which scan the intervention had been initiated for later analysis. An additional 40 TQF spectra could be acquired following the initial 24 TQF stability spectra as above.

2.9.5 Analysis of $[Na^+]_i$ signal from shift reagent perfused mouse hearts

For quantification of the $[Na^+]_i$ signal two factors must be known:

1) the number of moles in the acquired Na^+ signal

2) the volume of intracellular space in the heart.

A sealed glass reference capillary containing a solution of known Na^+ concentration with shift reagent (20µl volume of 145mM NaCl with 10mM Tm(DOTP)$^{5-}$) was placed inside the NMR tube in the same plane as the mouse heart. The shift reagent concentration is greater than that used for heart perfusion in order to shift the ^{23}Na reference (Na_{ref}) capillary spectral peak to a more distal frequency than the extracellular ^{23}Na spectral peak. Following perfusion with shift reagent, 3 sodium peaks were visible on the ^{23}Na spectrum: intracellular Na^+ peak, extracellular Na^+ peak and reference capillary Na^+ peak. Using Bruker Topspin NMR integral software the integral peak area was defined for both the intracellular Na^+ peak and the reference Na^+ peak allowing ratiometric comparison.

The peak size, or signal, detected by NMR was proportional to the number of Na^+ moles present.

$$^{23}\text{Na Reference Capillary Signal} \quad \boldsymbol{\alpha} \quad \text{no. of moles } Na^+$$

And as concentration is equal to number of moles divided by volume of solution.

$$\text{Concentration} = \frac{\text{no. of moles}}{\text{volume}}$$

Rearranging the equations it can be seen that the signal is proportional to concentration multiplied by volume:

$$^{23}\text{Na Reference Capillary Signal} \quad \boldsymbol{\alpha} \quad \text{concentration x volume}$$

The above allows quantification of the number of moles of Na^+ represented by the ^{23}Na reference capillary spectral peak. It was now possible to use this reference capillary peak to compare to the intracellular ^{23}Na peak and thereby determine the amount of moles of Na^+ in the intracellular signal. In order to determine the concentration of intracellular Na^+ in the heart, the volume of the intracellular space was now required.

The total extracellular and intracellular heart volumes were determined by taking the wet weight and dry weight ratios of each heart and using previous literature values from Jelicks *et al*, 1989 [269] who estimated that 0.44ml/g wet weight of the heart was cytosolic or Askensasy *et al*, 1997[270] who estimated that 2.5mg/g dry weight was cytosolic the intracellular volumes were calculated. Therefore the heart was cut down, blotted to remove perfusate in the ventricles and vasculature, and snap frozen at the end of the protocol and wet weight recorded. The heart was then dried for 24 hours at 80^{o}C to obtain the dry weight and the conversion factors used to calculate the intracellular volume for each heart. These were then used in conjunction with the estimate of the number of moles of Na^+ in the intracellular Na^+ signal to gain a measure of intracellular Na^+ concentration in each heart.

2.10 Statistics

Quantitative data was analysed and expressed as mean ± standard error of the mean (SEM). n represents the number of independent experiments. Where appropriate, statistical analysis was performed using GraphPad Prism 5 software with Students *t*-test or analysis of variance (ANOVA), and further post-tests performed as necessary. The statistical analysis method used is denoted for each figure and statistical significance marked by an asterisk (*). $P<0.05$ was considered significant.

3 CHAPTER 3 – BIOCHEMICAL PHENOTYPING OF PLM^{3SA} MOUSE

3.1 Introduction

In order to understand the role of PLM phosphorylation in cardiac physiology an important first step is to characterise the basic cardiac phenotype of the PLM^{3SA} mouse. It is possible, for example, that a global mutation of Ser63, Ser68 and Ser69 to Ala may affect PLM protein folding and trafficking to the sarcolemma. The mutation of Ser to Ala is one of the simplest substitutions with both amino acids being similar in size and structure. However, Ser has an uncharged polar side chain which has been replaced with Ala carrying a non-polar hydrophobic side chain, though this change in environment should not affect PLM structurally.

Under normal conditions PLM is known to regulate the Na^+/K^+ ATPase by acting as a brake on pump activity which is relieved by phosphorylation,[28, 29, 32, 33] therefore the presence of an unphosphorylatable PLM is most likely to be an undesirable pump accessory. Hence the effect of this mutation on protein expression levels of the key PLM and Na^+/K^+ ATPase subunits is vital to understand the biochemistry of this animal. Indeed studies in the PLM-KO mouse revealed small but non-significant changes in α2 and β1 subunits and most notably a 25% decrease in the α1 subunit expression.[33] If these effects can occur with the removal of PLM then it suggests that there may potentially be some differences in the PLM^{3SA} mouse. The use of phospho-antibodies will also be essential to ensure that the point mutations have been successful. Phospho-specific antibodies Ser68, Ser63 and Ser69 will be able to confirm whether an unphosphorylatable PLM protein has been created and total PLM antibody will measure the expression of PLM protein present as this antibody binds to the N-terminal of the PLM protein, which remains unchanged.

By introducing an unphosphorylatable PLM into the cell, the hypothesis suggests there may be changes to the intracellular Na^+ load, however there may also be other compensatory changes in the cell to try to counter-act this higher $[Na^+]_i$. For example, there is speculation that PLM regulates the NCX,[271] if so unphosphorylatable PLM may alter NCX expression. Even if PLM does not regulate NCX directly there may be an indirect effect on NCX expression to compensate for the hypothesised increase in $[Na^+]_i$ in PLM^{3SA} myocytes. Therefore protein expression levels of other E-C Coupling proteins will also be investigated.

Finally it is important to ensure that although PLM is present in the PLM^{3SA} mouse it is in the correct location and that it interacts with the Na^+/K^+ ATPase pump. Subcellular localisation will be investigated and co-immunoprecipitation and immunohistochemistry studies will confirm if co-localisation occurs.

3.2 Aims

The aims of the studies undertaken in this chapter were to:

1. Observe any gross phenotypic changes in PLM^{3SA} mice compared with PLM-WT littermates.

2. Ensure that PLM^{3SA} has been successfully mutated at all 3 phosphorylation sites: Ser63, Ser68 and Ser69.

3. Characterise the PLM^{3SA} mouse heart protein expression levels of PLM, Na^+/K^+ ATPase subunits and other E-C coupling proteins and compare with WT hearts.

4. Ensure mutated PLM has trafficked correctly to the sarcolemmal membrane and successfully co-localises with Na^+/K^+ ATPase subunits.

3.3 Methods

3.3.1 Preparation of whole heart homogenates

Hearts from PLM-WT and PLM^{3SA} littermates (n=6) were excised and cannulated on the Langendorff rig as described in Chapter 2, Section 2.3. To ensure the removal of blood from the coronary vasculature, the hearts were aerobically perfused at a constant pressure of 80mmHg for 5 minutes whilst being paced at a frequency of 550bpm. Following perfusion, the hearts were rapidly cut down, blotted and snap frozen in liquid nitrogen prior to homogenisation (approximately under 30 seconds).

Hearts were weighed and a 10% homogenate was made using the wet weight values. Homogenisation was in a PBS based buffer with 1mM EDTA containing phosphatase and protease inhibitors using a motor driven glass pestle and mortar kept 'on ice'. For immunoblot analysis experiments a sample of each homogenate was diluted 1:1 with 2x SDS sample buffer containing 5% β-mercaptoethanol and stored at -20^{o}C. Undiluted aliquots for IP were stored at -80^{o}C until use.

3.3.2 SDS-PAGE and immunoblot analysis

Detection of proteins by SDS-PAGE and immunoblot analysis was carried out as detailed in Chapter 2, Sections 2.4.3-2.4.5 unless otherwise stated. Gel matrices used were 15% acrylamide gels for PLM and PLB antibodies and 10% acrylamide gels for all Na^+/K^+ ATPase subunits and larger proteins. All antibody conditions were detailed in Table 2.7 and Table 2.8. Homogenates diluted in sample buffer were heated at 55^{o}C for 10 minutes and spun at 15000 x *g* prior to loading, except for samples probed for PLB which were heated to 85^{o}C for 10 minutes. A protein assay was also performed to determine the protein concentration in each homogenate, Table 3.1. Due to possible inaccuracies introduced by the protein assay methodology, all values that were within 2 standard deviations of the mean for each group were accepted (PLM-WT: mean 15.7 ± 2.3mg/ml, acceptable range 11.1 to 20.3mg/ml; PLM^{3SA}: mean 15.2 ± 1.9mg/ml, acceptable range 11.4 to 19.1mg/ml). For the SDS-PAGE and Phos-tag phosphate affinity SDS-PAGE experiments, samples were loaded into each well in equal volumes thus assuming equal protein loading. Coomassie staining of a run SDS-PAGE gel was performed to check for equal loading, see Figure 3.1.

Heart	PLM-WT (mg/ml)	PLM^{3SA} (mg/ml)
1	15.79	14.00
2	16.28	17.52
3	14.28	15.14
4	19.86	12.76
5	13.38	17.52
6	14.55	14.48

Table 3.1: Protein concentrations of heart homogenates.
Table showing the protein concentration (mg/ml) of heart homogenates (WT: 1-6; PLM^{3SA} 1-6) used in subsequent Western blotting experiments. Protein concentrations were determined using a simple protein assay for mouse hearts homogenised using wet heart weight. n=6 for each genotype.

Finally to ensure equal protein loading Westerns were run and analysed using actin and calsequestrin antibodies, proteins that should not be affected by point mutations of the PLM protein or any subsequent morphological changes. These can be seen in Figure 3.6E & F. From these results loading was considered equal.

NB. All membranes were Coomassie stained following transfer.

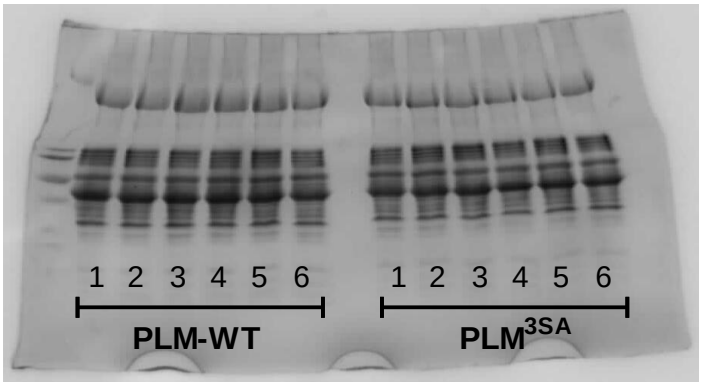

Figure 3.1: Coomassie stained SDS-PAGE gel.
Heart homogenates were loaded in equal volumes into a 15% gel. Following protein separation by electrophoresis the gel was Coomassie stained to show equal protein loading of all samples. PLM-WT samples loaded in order of hearts 1-6; PLM^{3SA} samples loaded in order of hearts 1-6.

3.3.3 Phos-tag phosphate affinity SDS-PAGE of heart homogenates

Homogenates were resolved on 15% Phos-tag SDS gels for PLM antibodies (Ser63, Ser68, Ser69 and total PLM) and 10% Phos-tag SDS gels for PLB antibodies (total PLB) containing 40µM Phos-tag ligand and 80µM $MnCl_2$ by electrophoresis at 25mA per gel. Gels were incubated in transfer buffer containing 1mM EDTA for 10 minutes, then transfer buffer alone prior to electrophoretic protein transfer onto PVDF membrane as described previously in Chapter 2, Section 2.4.6. Membranes were subsequently probed with antibodies as detailed in Table 2.7 and Table 2.8. Membranes were Coomassie stained following antibody probing and chemiluminescence.

3.3.4 Subcellular fractionation of AMVM

Fractionation was first attempted using the previously used mouse heart homogenates but due to preliminary findings i.e. control antibodies were not in the correct fractions, it was concluded that the homogenisation technique was too vigorous to maintain subcellular fractions and freshly isolated AMVM were used as an alternative. AMVM were isolated as previously described in Chapter 2, Section 2.5 and allowed to equilibrate prior to start of fractionation protocol. An input sample was taken to ensure each antibody marker could be detected in the total protein sample. AMVM were lysed in 200µl lysis buffer before fractionation into cytoplasmic, membrane and myofilament fractions (Chapter 2, Section 2.7) each of which were suspended in 400 µl total volume using 2x sample buffer. All samples were stored at -20^{o}C for subsequent immunoblot analysis using a variety of antibodies. Fractions and antibody markers were: (1) cytoplasm and glyceraldehyde 3-phosphate dehydrogenase (GAPDH), (2) membrane and Na^{+}/K^{+} ATPase α1 subunit, and (3) myofilament and cTroponinI (cTnI). See Table 2.7 and Table 2.8 for antibody conditions.

3.3.5 Confocal microscopy

AMVM to be immunolabelled and imaged using confocal microscopy were fixed in 4% PFA and permeabilised with 0.2% Triton X-100 as described in Chapter 2, Section 2.6. Following incubation in 5% NSG in 1% BSA/gold buffer to reduce non-specific antibody binding, cells were labelled with the primary rabbit monoclonal PLM-C2 at a dilution of 1:100, and mouse

monoclonal Na^+/K^+ ATPase α1 subunit at a dilution of 1:100, both in 1% BSA/gold buffer overnight at 4^{o}C. Secondary antibodies for mouse monoclonal were Cy5-conjugated anti-mouse IgG and assigned red in the Leica images, and rabbit monoclonal were Cy3-conjugated anti-rat IgG and the fluorescence assigned green in the Leica images both at 1:100 dilution in 1% BSA/gold buffer for 3 hours at room temperature. 4'6-diamidino-2-phenylindole dihydrochloride (DAPI) was also added with secondary antibodies at a dilution of 1:100. Samples were mounted onto microscope slides and imaged using confocal microscopy as detailed in Chapter 2, Section 2.6.4.

3.4 Results

3.4.1 PLM-WT and PLM^{3SA} growth curves

To check for normal development of mice and that there are no gross phenotypic differences between littermates, mice were weighed every week for 15 weeks. The growth curves are shown in Figure 3.2 and it can clearly be seen that there were no differences between mouse weights at any time point. There was a rapid weekly increase in weight, as would be expected in developing mice, until 10 weeks of age where a growth plateau was reached. Normally mice reach sexual maturity ranging from 6-10 weeks and physical maturity between 3 and 5 months of age depending on strain. In PLM-WT and PLM^{3SA} littermates as the weight curve plateaus by 15 weeks this was considered an appropriate age for future studies.

Mice were also observed over the course of a year (data not shown) and there were no obvious complications or premature deaths.

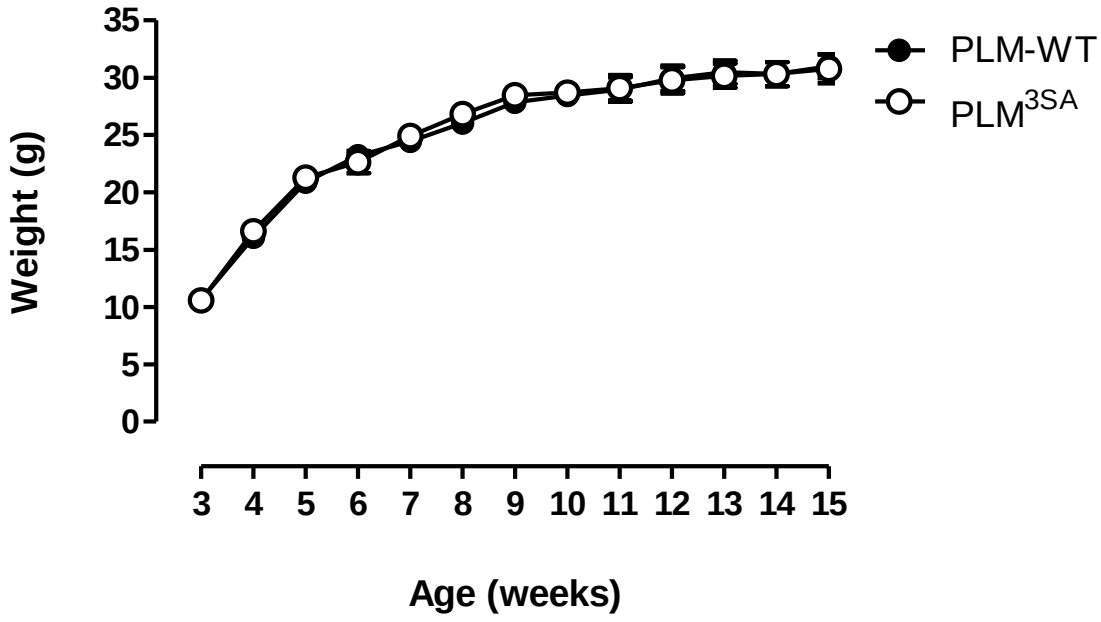

Figure 3.2: Growth curves of PLM-WT and PLM^{3SA} mice at weekly intervals.
n=8-12. All data expressed as mean±sem and analysed by repeated measures two-way ANOVA with Bonferroni post-test, P<0.05 was considered significant.

3.4.2 Western immunoblot analysis for cardiac proteins

3.4.2.1 Phospho-specific antibodies

To ensure that successful mutation of the PLM protein had occurred, Western blots were run and probed with previously characterised PLM phospho-specific antibodies. Figure 3.3 shows the results for immunoblot analysis with the phospho-specific antibodies Ser63, Ser68 and Ser69. Protein signals were observed in all PLM-WT homogenate samples with all three antibodies, whilst there was no protein signal in any of the PLM^{3SA} heart homogenates. This can be seen in the membrane blots in Figure 3.3A. A very low density signal was seen in PLM^{3SA} homogenates on the Ser63 blot which is undetectable by the densitometer and is most likely the result of cross binding at the N-terminal by this antibody; which has previously been noted in-house.[30] In WT heart homogenates, there was slight variability within Ser68 (PLM-WT: 0.27±0.1) and Ser69 (PLM-WT: 0.35±0.1) protein expression but due to perfusion stress affecting phosphorylation status within the heart, this may be have been due to the variability of the viability (and Ca^{2+} load) of individual heart perfusions.

3.4.2.2 PLM and Na^+/K^+ ATPase antibodies

To investigate the effect that mutation of PLM has on the total amount of PLM protein present in the PLM^{3SA} hearts and other important proteins, SDS-PAGE immunoblot analysis using total PLM antibody and antibodies for all Na^+/K^+ ATPase subunits was investigated (see Figure 3.4 and Figure 3.5). Total PLM protein expression was significantly decreased in PLM^{3SA} hearts compared to PLM-WT by 71% (PLM-WT: 0.78±0.16; PLM^{3SA}: 0.23±0.03, P<0.006). Whilst investigation of the Na^+/K^+ ATPase pump unit expression showed Na^+/K^+ ATPase α1 subunit, α2 subunit and total α subunit expression was similar in both PLM-WT and PLM^{3SA} homogenates. Na^+/K^+ ATPase β1 subunit expression was decreased by 25% in PLM^{3SA} homogenates and by 54% for β2 subunit expression; neither result was significant. When examining antibody blots for both β1 and β2 subunits (Figure 3.4) it can be seen that they are very dirty blots with some non-specific binding suggesting the antibody affinity for these proteins was poor, which places doubt on the reliability of these results.

Table 3.2 has all the analysed optical density measurements for each studied protein.

3.4.2.3 E-C coupling antibodies

The protein expression of other major E-C coupling in WT and PLM^{3SA} homogenates was also determined in case the mutation of PLM and the possible hypothesised subsequent increase in $[Na^+]_i$ had caused other proteins to be upregulated/downregulated as a consequence. Figure 3.6A shows membrane immunoblots of E-C coupling proteins relevant to this study and Figure 3.7 shows the representative graphs of the analysed protein expression. Expression of Ser16, the PLB PKA phosphorylation site, showed that there was no difference between expression in PLM-WT and PLM^{3SA} homogenates. However, total PLB protein expression levels were significantly decreased by 33% in PLM^{3SA} mouse hearts (PLM-WT 1.98±0.21; PLM^{3SA} 1.34±0.09, P<0.02). There was equal expression of SERCA2A in both genotypes and NCX expression which was also unchanged in both genotypes.

Table 3.2 has all the analysed optical density measurements for the studied proteins.

3.4.2.4 Loading control antibodies

The samples were also probed for proteins that are highly conserved within the cell and remain unchanged by external forces such as stress from Langendorff perfusion and possible disease processes activated in the new mouse by Ser to Ala mutation. The expression of these proteins was then used as loading controls for the heart homogenates to ensure equal protein loading had occurred. The results for actin expression (Figure 3.6B and Figure 3.7E), a protein that is highly conserved and is involved in cell motility, structure and integrity, showed that loading was equal for each sample (PLM-WT 0.58±0.04, n=6; PLM^{3SA} 0.55±0.04, n=6). Calsequestrin was also probed for, which is a sarcoplasmic reticulum Ca^{2+} binding protein shown to be stably expressed and frequently used as a loading control.[272] The results (Figure 3.6B and Figure 3.7F) showed that there was equal expression of calsequestrin in both mouse genotypes (PLM-WT 0.35±0.04, n=6; PLM^{3SA} 0.37±0.04, n=6). Therefore after all the extensive protein concentration analysis of the heart homogenates it was concluded that protein loading was equal and the above results were therefore true observations of protein expression.

Table 3.2 has all the analysed optical density measurements.

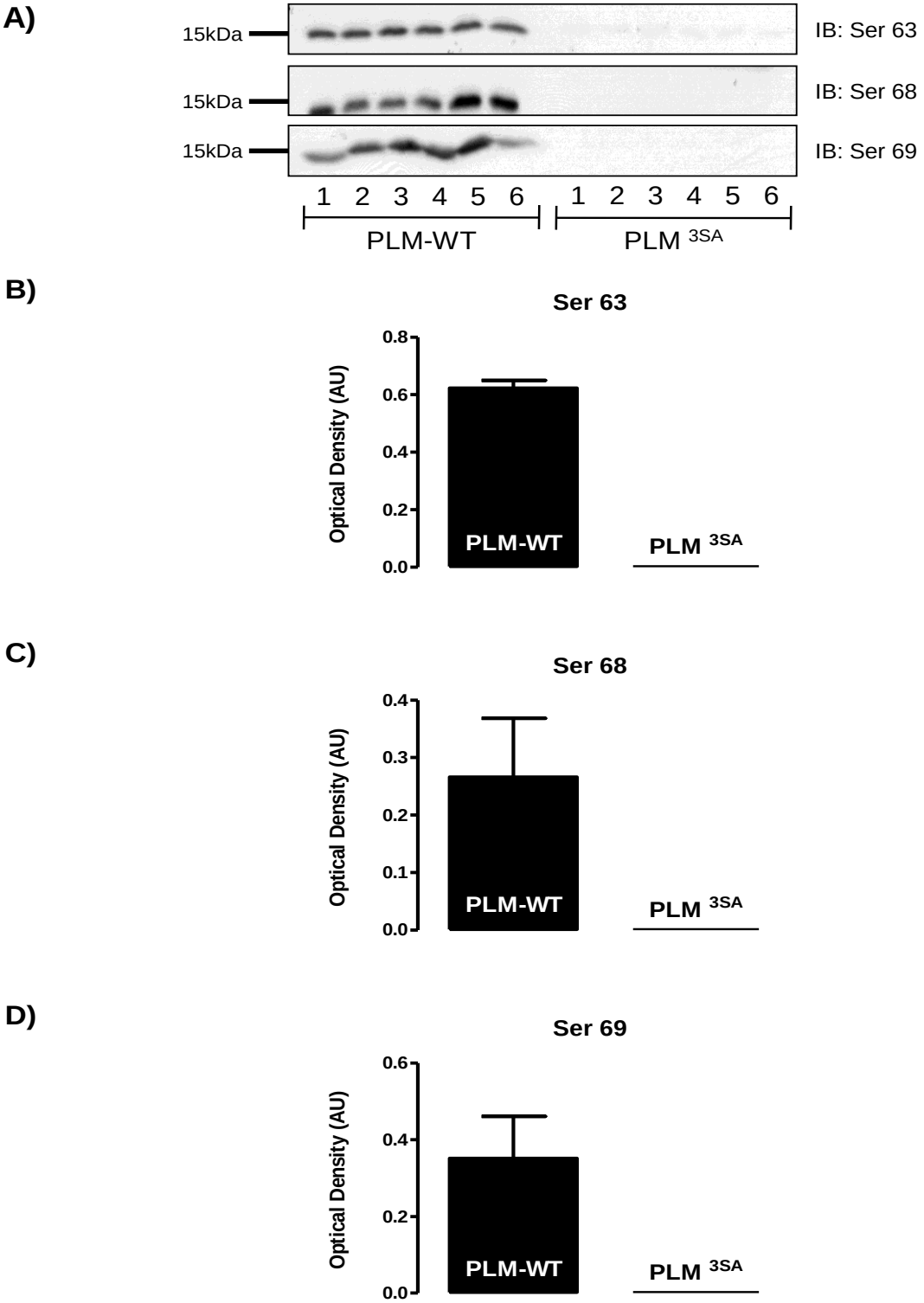

Figure 3.3: SDS-PAGE immunoblot (IB) analysis of PLM phosphorylation sites using PLM phospho-specific antibodies and correlating representative graphs of protein expression in PLM-WT and PLM^{3SA} mouse hearts homogenates.
A) IB analysis using Ser63, Ser68 and Ser69 phospho-specific antibodies; B) Representative graph of Ser63 expression; C) Representative graph of Ser68 expression; D) Representative graph of Ser69 expression. n=6. All data expressed as mean±sem. No further statistical analysis due to the absence of detectable signal in the PLM^{3SA} hearts.

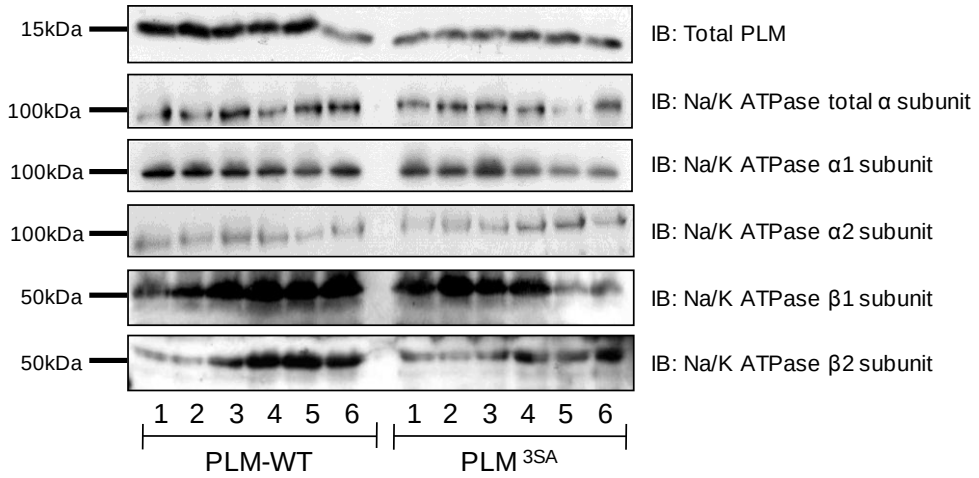

Figure 3.4: SDS-PAGE immunoblot analysis of PLM and Na^+/K^+ ATPase proteins. Antibodies used included: total PLM, Na^+/K^+ ATPase total α subunit, Na^+/K^+ ATPase α1 subunit, Na^+/K^+ ATPase α2 subunit, Na^+/K^+ ATPase β1 subunit and Na^+/K^+ ATPase β2 subunit.

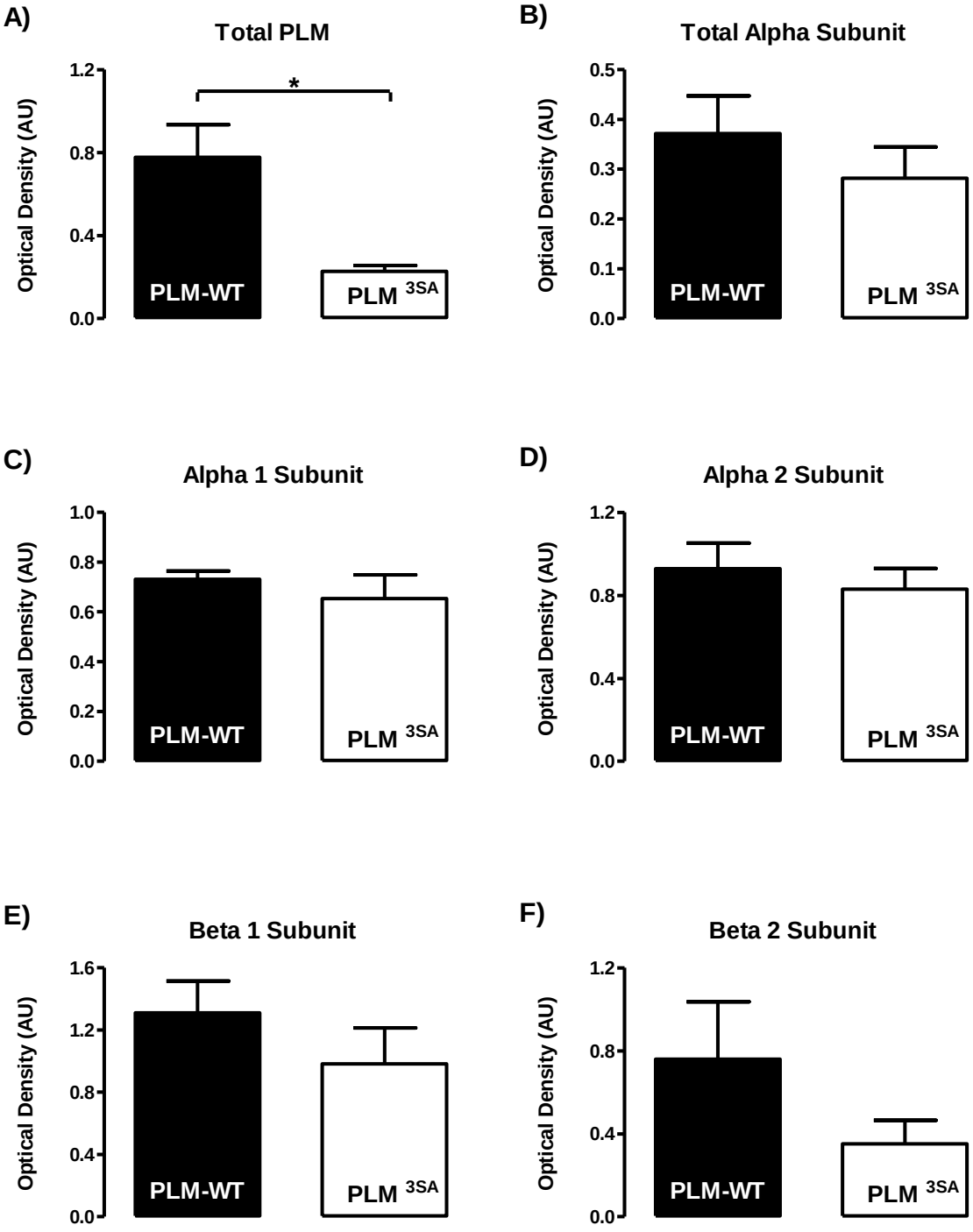

Figure 3.5: Representative graphs of protein expression of PLM and Na^+/K^+ ATPase pump proteins in PLM-WT and PLM^{3SA} mouse heart homogenates.
A) Total PLM; B) Total alpha subunit; C) Alpha 1 subunit; D) Alpha 2 subunit; E) Beta 1 subunit; F) Beta 2 subunit. n=6. All data expressed as mean±sem and analysed by Student's *t*-test, P<0.05 was considered significant (PLM-WT 'v' PLM^{3SA} denoted by *).

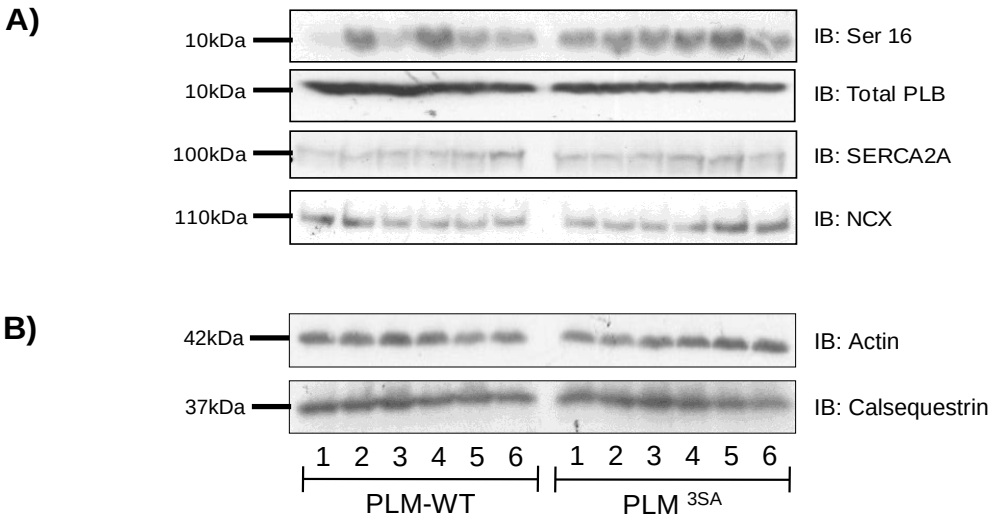

Figure 3.6: SDS-PAGE immunoblot analysis of E-C coupling proteins and loading controls.
Antibodies used included A) Ser16, Total PLB, SERCA2A, NCX; B) Actin and Calsequestrin.

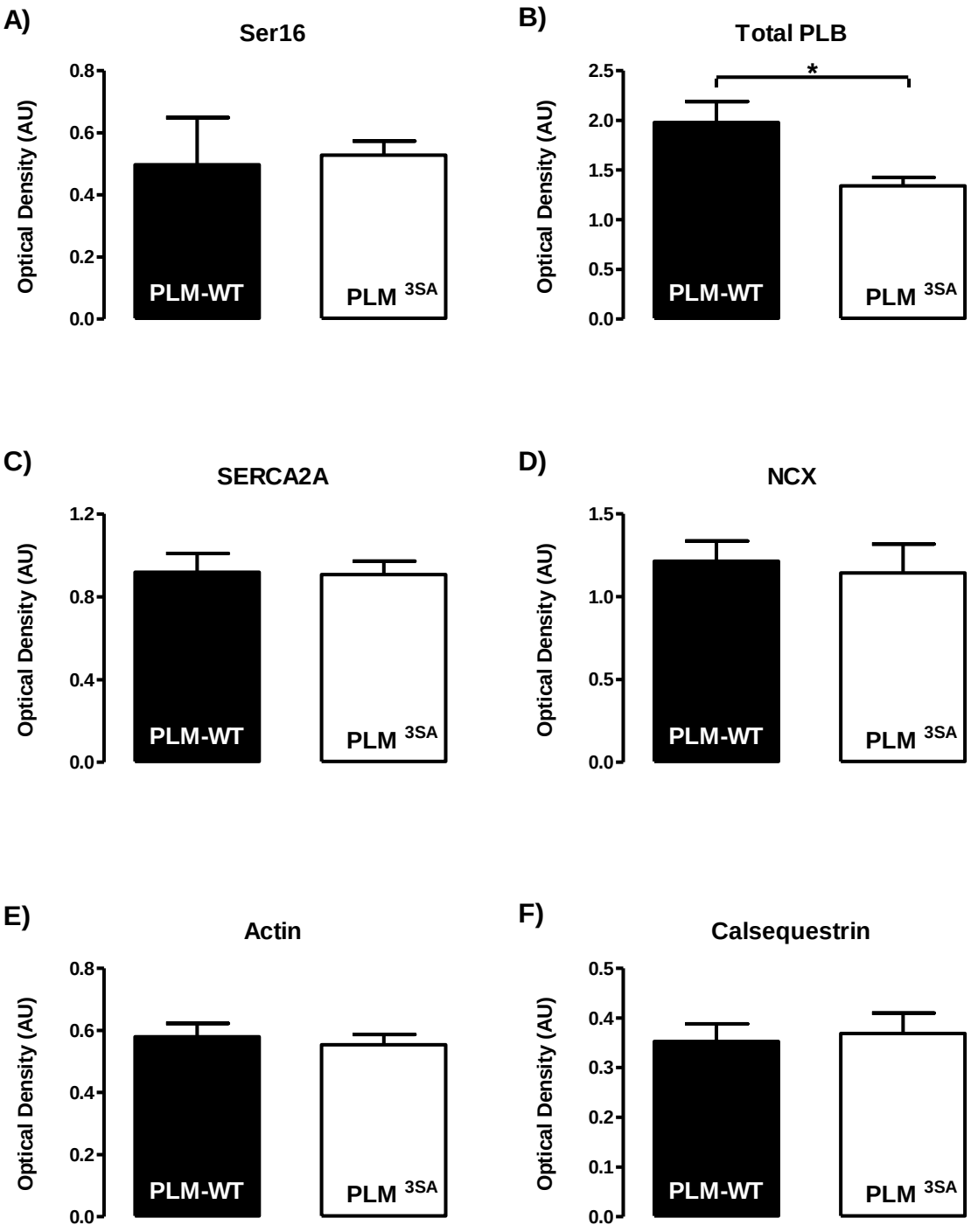

Figure 3.7: Representative graphs of analysed protein expression of E-C coupling proteins and loading controls in PLM-WT and PLM^{3SA} mouse hearts.
A) Ser16; B) Total PLB; C) SERCA2A; D) NCX; E) Actin; F) Calsequestrin. n=6. All data expressed as mean±sem and analysed by Student's *t*-test, P<0.05 was considered significant (PLM-WT 'v' PLM^{3SA} denoted by *).

Protein	PLM-WT (Optical Density, AU)	PLM^{3SA} (Optical Density, AU)	P Value
Ser63	0.62 ± 0.03	-	NA
Ser68	0.27 ± 0.1	-	NA
Ser69	0.35 ± 0.1	-	NA
Total PLM	0.78 ± 0.16	0.23 ± 0.03	P<0.006
Na^+/K^+ Alpha 1 Subunit	0.73 ± 0.03	0.65 ± 0.1	ns
Na^+/K^+ Alpha 2 Subunit	0.93 ± 0.12	0.83 ± 0.1	ns
Total Alpha Subunit	0.37 ± 0.08	0.28 ± 0.06	ns
Na^+/K^+ Beta 1 Subunit	1.31 ± 0.2	0.98 ± 0.23	ns
Na^+/K^+ Beta 2 Subunit	0.76 ± 0.28	0.35 ± 0.11	ns
Ser16 PLB	0.5 ± 0.15	0.53 ± 0.05	ns
Total PLB	1.98 ± 0.21	1.34 ± 0.09	P<0.017
SERCA2A	0.92 ± 0.09	0.91 ± 0.09	ns
NCX	1.21 ± 0.12	1.14 ± 0.08	ns
Actin	0.58 ± 0.04	0.55 ± 0.03	ns
Calsequestrin	0.35 ± 0.04	0.37 ± 0.04	ns

Table 3.2: Optical density measurements of analysed protein expression levels from PLM-WT and PLM^{3SA} heart homogenates.
Averaged optical density measurements for PLM phosphoproteins, total PLM, Na^+/K^+ ATPase subunits, E-C coupling proteins and loading controls. n=6. All data expressed as mean±sem and analysed by Student's *t*-test (PLM-WT 'v' PLM^{3SA}), P<0.05 was considered significant.

3.4.3 Detection of phosphorylated PLM using Phos-tag phosphate affinity SDS-PAGE

Phos-tag phosphate affinity SDS-PAGE was used to ensure that the lack of signal with the phospho-specific antibodies (Ser63, Ser68 and Ser69) in PLM^{3SA} heart homogenates was due to successful global eradication of the phosphorylation sites. If for example, Ser68 mutation had not occurred but Ser69 mutation to Ala had been successfully, this may cause a conformational change that affects Ser68 phospho-antibody binding to the Ser68 site, even though it may possibly be phosphorylated. To investigate this further, the previously used heart homogenates were resolved on Phos-tag SDS-PAGE gels and subjected to immunoblot analysis using total PLM antibody. The use of Phos-tag SDS-PAGE allows visualisation of phosphorylation sites within a protein sample due to the Phos-tag molecule binding to each phosphate group and changing the migration rate of the phosphoprotein through the gel.[273] Depending on the protein it is often possible to see individual phosphorylation sites due to differences in the surrounding amino acid environment which will affect the protein migration rate.[274, 275]

Figure 3.8A shows Phos-tag SDS-PAGE immunoblot analysis using total PLM antibody. It can be seen that in the PLM-WT hearts there were several phosphorylation sites present ranging from 25kDa to 50kDa and a faint band lower down at 15kDa which represents normally seen unphosphorylated PLM. Unfortunately protein from PLM-WT heart 1 did not run adequately for all blots, which is often the case for the protein lane adjacent to the marker in Phos-tag gels, and has been removed from further analysis. From the primary sequence there are 4 known potential phosphorylation sites in PLM[22, 220] however from the Phos-tag results it appears that there are potentially 5-6 phosphorylation sites in the PLM-WT hearts, although there was variation in band intensities. When comparing PLM-WT homogenates with PLM^{3SA} homogenates there was an absence of phosphorylation sites between 37kDa and 50kDa which correlates to the mutated sites. Additionally there appears to be 2 faint bands present at 2 sites which can also be seen in PLM-WT homogenates. These could be due to non-specific binding, but as can be seen from the SDS-PAGE IB using total PLM antibody (Figure 3.8B), this antibody shows good affinity to unphosphorylated PLM protein at 15kDa with a specific band and clean blot. Therefore it may be worth considering that these extra bands in both PLM-WT and PLM^{3SA} hearts are a real phenomenon and potentially worth investigating further.

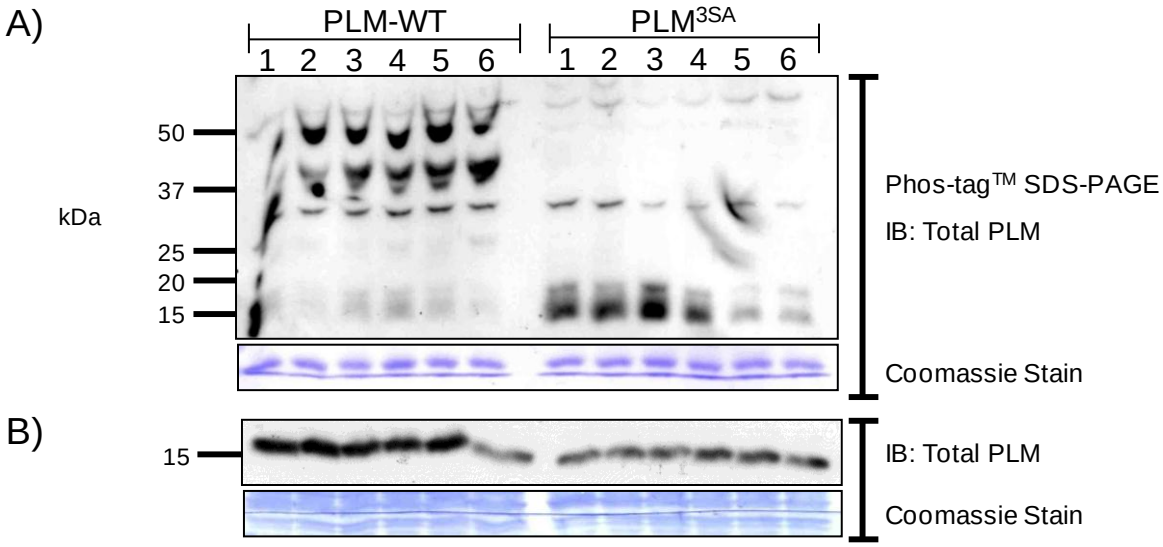

Figure 3.8: Phos-tag phosphate affinity SDS-PAGE and immunoblot analysis in PLM-WT and PLM^{3SA} heart homogenates using total PLM antibody.
A) Phos-tag immunoblot analysis using total PLM antibody run with heart homogenate samples from WT and PLM^{3SA} mice and corresponding Coomassie stained membrane at PLM unphosphorylated region; B) SDS-PAGE immunoblot analysis with total PLM antibody run with the same heart samples and corresponding Coomassie stained membrane. n=6.

In order to further distinguish which detected phosphorylation sites related to which Ser residue, the same homogenates were resolved with Phos-tag gels and subjected to immunoblot analysis using PLM phospho-specific antibodies. Finally it is known in-house that Ser68 antibody cross-reacts with the PLB PKA phosphorylation site, Ser16, the same samples were again resolved on Phos-tag gels and immunoblot analysed using the total PLB antibody.[130]

Phos-tag resolved membranes analysed with PLM phospho-specific antibodies can be seen in Figure 3.9. Panel A shows the immunoblot analysed using Ser69 antibody and bands can be seen in the WT samples at 50kDa which appear to correlate to the top dark band on the total PLM Phos-tag immunoblot (Figure 3.8A). Panel B shows the immunoblot analysed with Ser63 antibody and there were two bands present, one at 50kDa (similar to the band on Ser69 immunoblot) and one at 37kDa in the WT heart samples. This contribution to 2 bands could be due to the Ser63 antibody detecting both mono- and dual- phosphorylated sites.[275] The top band correlates to the same position as the band detected on the Ser69 immunoblot and most probably they will both contribute to the same band on the total PLM Phos-tag immunoblot. Panel C shows the Phos-tag immunoblot analysed with Ser68 antibody and multiple bands can be seen

in both PLM-WT and PLM^{3SA} heart samples, unlike the previous 2 phospho-specific antibodies that only have bands in PLM-WT. However, further investigation using total PLB antibody to probe a separate Phos-tag immunoblot suggests that some of these bands are due to the ability of Ser68 to cross-react with Ser16 on PLB hence the presence of bands in PLM^{3SA} homogenates (Figure 3.9D). It is extremely likely that Ser68 contributes in part to some of the bands seen on the total PLM Phos-tag immunoblot but this cannot be distinguished further. The only true way to be certain which residues contribute to which phospho band would be to individually mutate each residue in turn to Ala and repeat the total PLM Phos-tag immunoblot.

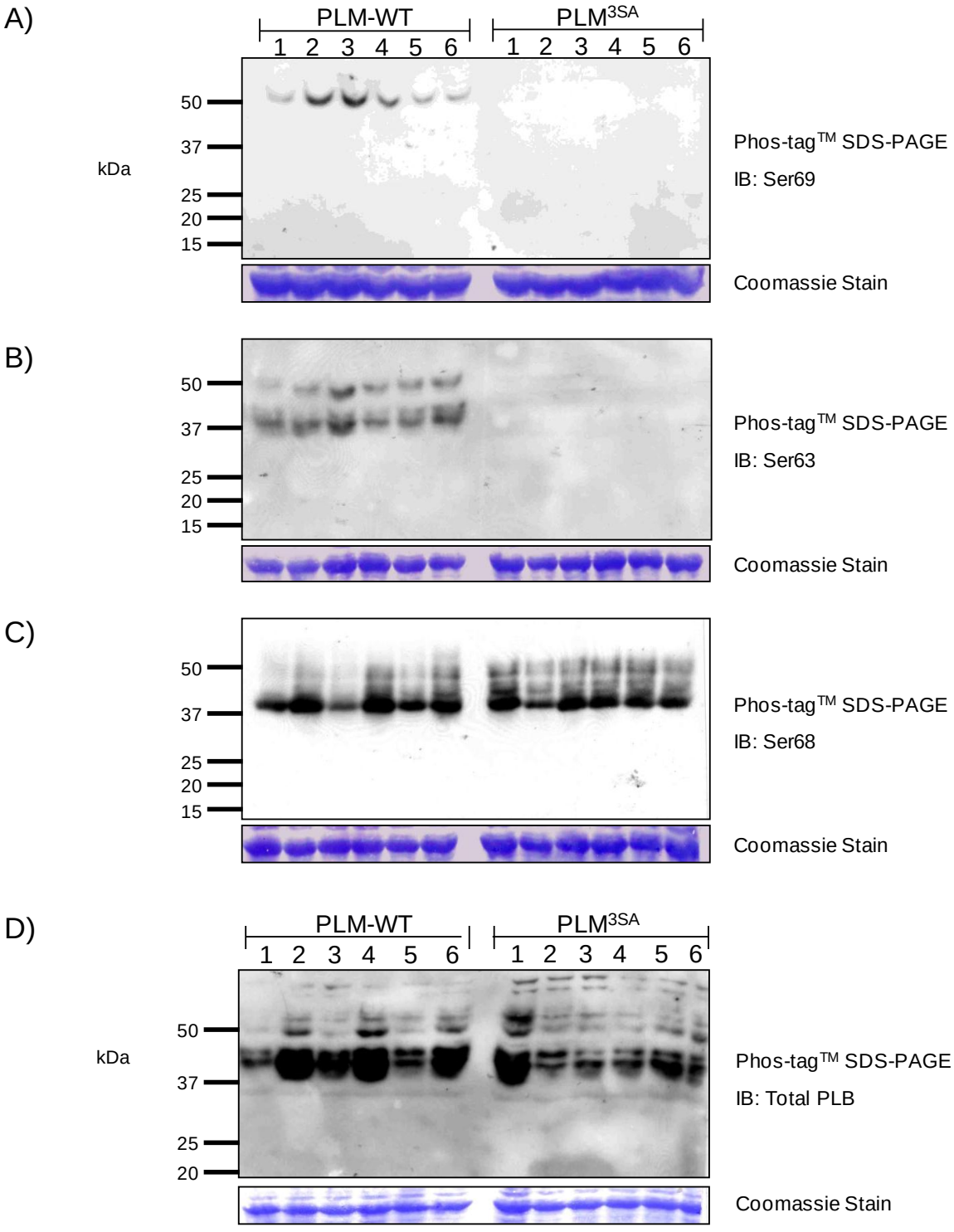

Figure 3.9: Phos-tag phosphate affinity SDS-PAGE immunoblot analysis using PLM phospho-specific antibodies and total PLB in WT and PLM^{3SA} heart homogenates.
A) Phos-tag immunoblot analysis with Ser69 phospho-specific antibody and corresponding Coomassie stained membrane; B) Phos-tag immunoblot analysis with Ser63 phospho-specific antibody and corresponding Coomassie stained membrane; C) Phos-tag immunoblot analysis with Ser69 phospho-specific antibody and corresponding Coomassie stained membrane; D) Phos-tag immunoblot analysis with total PLB antibody and corresponding Coomassie stained membrane. n=6.

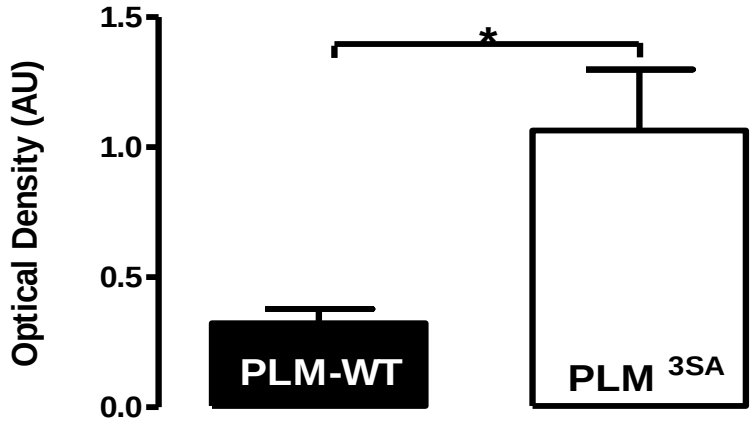

Figure 3.10: Graphical representation of unphosphorylated PLM expression densitometered from Phos-tag SDS-PAGE immunoblots analysed using total PLM antibody.
Unphosphorylated PLM expression in PLM-WT and PLM^{3SA} heart homogenates. n=6. All data expressed as mean±sem and analysed by Student's *t*-test, P<0.05 was considered significant (PLM-WT 'v' PLM^{3SA} denoted by *).

Following densitometry of unphosphorylated PLM bands in both WT and PLM^{3SA} homogenates from Phos-tag SDS-PAGE immunoblots analysed with total PLM it was seen that the majority of PLM in the PLM^{3SA} hearts was unphosphorylated which would be expected with successful Ser to Ala point mutations. However, graphical representation (Figure 3.10) of WT and PLM^{3SA} unphosphorylated PLM expression showed there was a significant difference between the unphosphorylated states in each of the genotypes (PLM-WT 0.32±0.06, n=5; PLM^{3SA} 1.07±0.23, n=6; P<0.05). This suggests that in PLM-WT hearts only a small amount of the protein was in the unphosphorylated state.

3.4.4 Investigation of subcellular PLM localisation by fractionation of AMVM from WT and PLM^{3SA} hearts

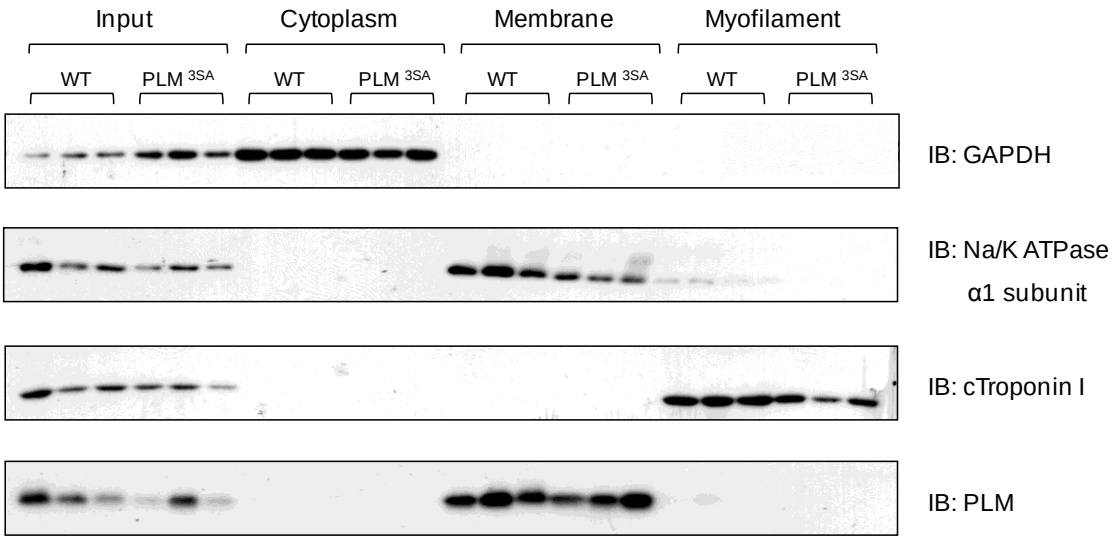

Figure 3.11: SDS-PAGE and immunoblot analysis of AMVM from PLM-WT and PLM^{3SA} hearts subjected to subcellular fractionation.
AMVM were fractionated from PLM-WT and PLM^{3SA} hearts into cytoplasmic, membrane and myofilament fractions. All fractions, including input were subjected to SDS-PAGE and immunoblot analysis using GAPDH (cytoplasmic marker), Na^+/K^+ ATPase α1 subunit (membrane marker) and cTnI (myofilament marker). Correct segregation of fraction markers was observed. Finally fractions were subjected to immunoblot analysis using total PLM antibody. n=3.

In order to confirm the localisation of mutated PLM in the PLM^{3SA} mice and ensure that the mutations have not affected trafficking to the membrane, myocytes from PLM-WT and PLM^{3SA} hearts were subjected to subcellular fractionation into cytoplasmic fraction, triton-soluble membrane fraction and triton-insoluble myofilament fraction. These fractions were resolved by SDS-PAGE and immunoblots analysed using antibodies for specific protein markers to determine the purity of each fraction. Fractions were subjected to immunoblot analysis to determine the content of fraction markers: GAPDH for cytoplasmic fraction, Na^+/K^+ ATPase α1 subunit for membrane fraction and cTnI for the myofilament fraction. Representative blots of different marker proteins are shown in the above Figure 3.11 for AMVM from both PLM-WT and PLM^{3SA} hearts. It was shown that correct segregation of the different fraction markers occurred, with enrichment in the corresponding fraction and absence in the 2 remaining fractions. GAPDH, in the top panel, can be seen in the input fraction and enriched in the

cytoplasmic fraction for both PLM-WT and PLM^{3SA} AMVM, whilst being absent from the membrane and myofilament fractions. Na^+/K^+ ATPase α1 subunit, in the second panel, was found in the input fraction and enriched in the membrane fraction. There was slight carry over into the myofilament fraction but as this band was faint it is likely to be from left over membrane in the myofilament fraction that did not detach easily. cTnI can be seen in the third panel enriched in the myofilament fraction compared with the input and absent from the membrane and cytoplasmic fraction.

To determine the subcellular localisation of the mutated PLM in the PLM^{3SA} mice the same fractions were subjected to immunoblot analysis using the total PLM antibody. The results clearly showed that PLM in the PLM^{3SA} mouse was present in the membrane fraction, which was in agreement with PLM in the PLM-WT myocytes, and absent in the cytoplasmic and myofilament fractions. So as expected, the point mutations of PLM have not affected the trafficking of the protein to the membrane.

It is of note that in the previous Western Blot analysis of total PLM in heart homogenates (Figure 3.5A) that the protein expression of PLM was significantly lower in PLM^{3SA} homogenates compared to PLM-WT and yet in this figure the protein expression levels appear reduced but not significantly. It is worth mentioning that the AMVM isolation technique (Chapter 3.4.4) yields different protein concentrations per heart depending on the success of the isolation technique and the above fractions were not normalised for protein concentration before loading.

3.4.5 Co-immunoprecipitation of PLM and Na^+/K^+ ATPase α1 subunit in PLM-WT and PLM^{3SA} heart homogenates

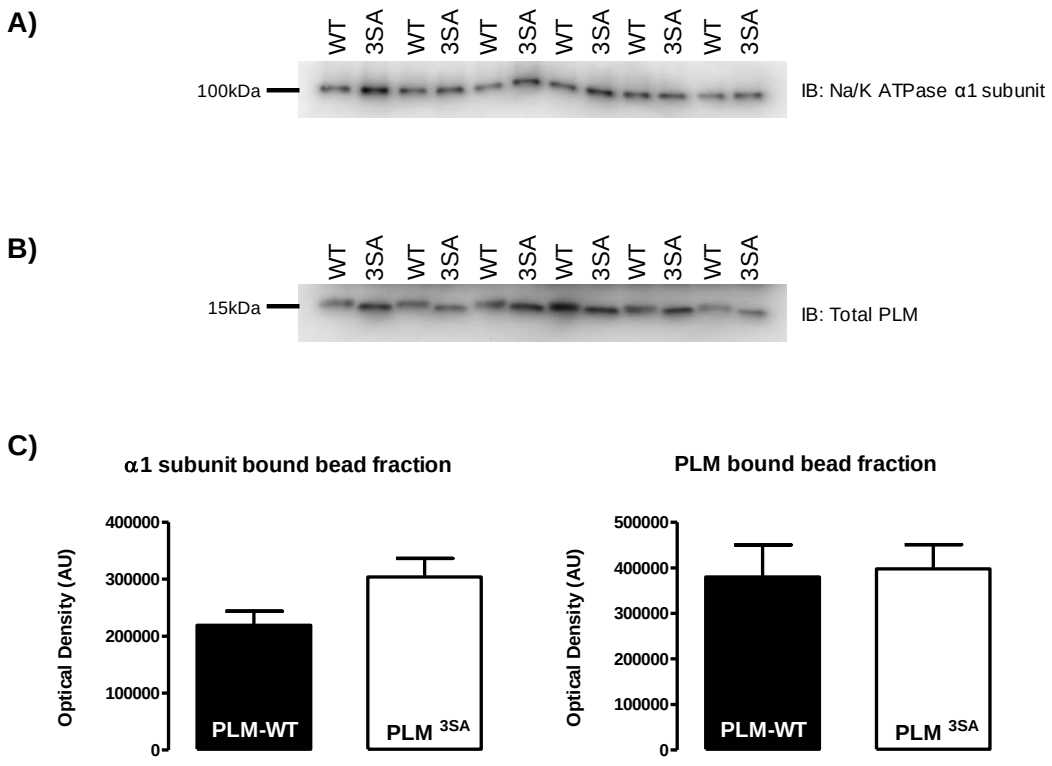

Figure 3.12: SDS-PAGE and immunoblot analysis of PLM-WT and PLM^{3SA} heart homogenate co-immunoprecipitation (co-IP) samples looking for interaction complexes of Na^+/K^+ ATPase α1 subunit and PLM.
A) Na^+/K^+ ATPase α1 subunit IB of bound bead fraction from WT and PLM^{3SA} heart co-IP; B) Total PLM IB of bound bead fraction from WT and PLM^{3SA} co-IP; C) Graphical representation of α1 subunit and PLM bound bead fractions from WT and PLM^{3SA} heart co-IP. n=6. All data provided by Dr Will Fuller, University of Dundee.

It can be seen in Figure 3.12 that when using Na^+/K^+ ATPase α1 subunit antibody for co-IP PLM was successfully pulled down. Figure 3.12A shows the bead fraction probed for Na^+/K^+ ATPase α1subunit confirming effective capture of the subunit on the beads. Figure 3.12B then shows the same bead fraction probed for total PLM suggesting that PLM and Na^+/K^+ ATPase α1subunit form a complex together in PLM-WT and PLM^{3SA} mouse hearts. Graphical representation of each IB in Figure 3.12C show similar amounts of PLM and Na^+/K^+ ATPase α1subunit are bound in both WT and PLM^{3SA} heart homogenates.

NB. Co-immunoprecipitation studies were undertaken by Dr Will Fuller at the University of Dundee using methods described in Fuller *et al*, 2009.[63]

3.4.6 Investigation of subcellular localisation of PLM relative to Na^+/K^+ ATPase α1 subunit in AMVM from PLM-WT and PLM^{3SA} hearts, by confocal microscopy

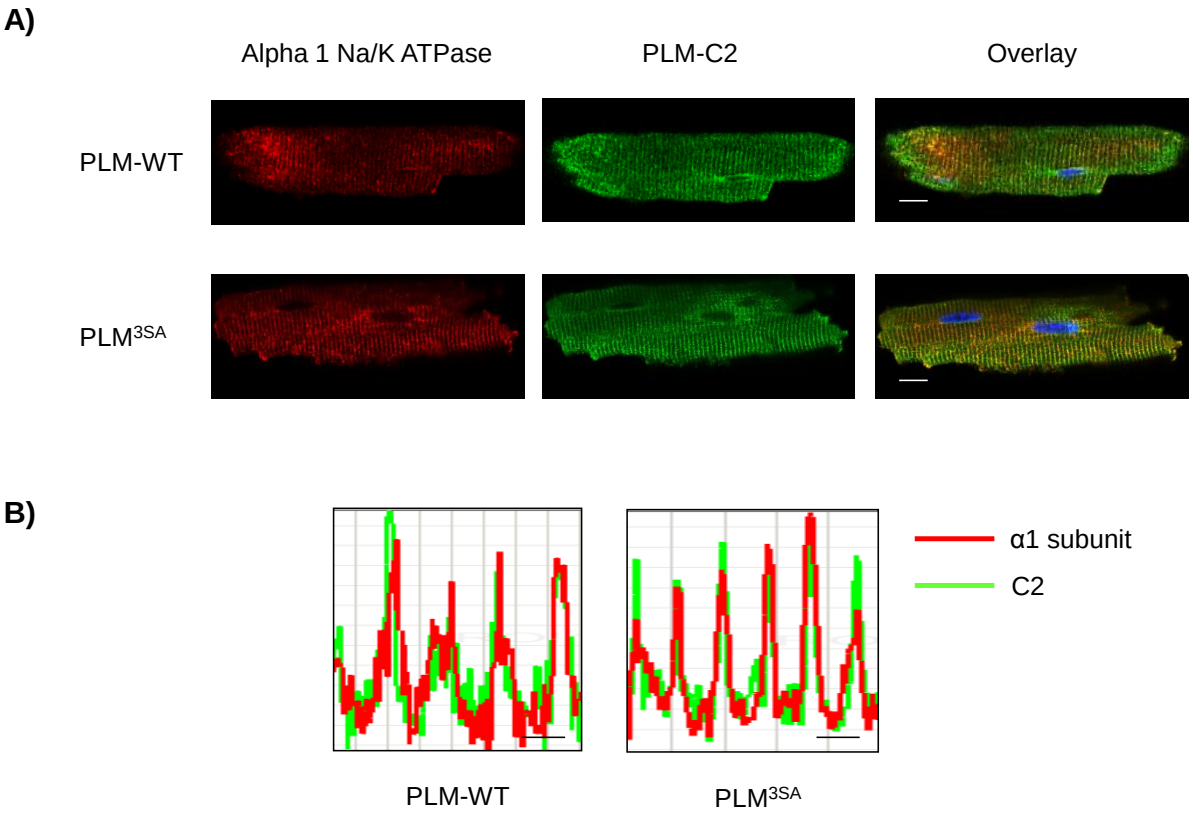

Figure 3.13: Confocal microscopy images showing co-localisation of PLM with Na^+/K^+ ATPase α1 subunit in AMVM from PLM-WT and PLM^{3SA} hearts.
A) Fixed and permeabilised cells were immunolabelled with Na^+/K^+ ATPase α1 subunit (red) and PLM-C2 (green) primary antibodies and imaged using confocal microscopy. Cy5-labelled Na^+/K^+ ATPase α1 subunit (red) and Cy3-labelled PLM-C2 (green) are shown in separate channels and as a merged image for both WT and PLM^{3SA} myocytes. B) Relative intensities are shown graphically below. Nuclei are stained with DAPI (blue). Scale bar on confocal image = 10μM, scale bar on intensity plot = 2μM.

Now that it has been established that mutated PLM in the PLM^{3SA} mouse was located in the membrane subcellular fraction it was also important to confirm that it co-localises with the Na^+/K^+ ATPase pump as suggested by previous co-IP data. The majority of literature has suggested that PLM co-localises with the Na^+/K^+ ATPase α1 subunit[26, 63] and Silverman *et al*,[30] show co-localisation with the Na^+/K^+ ATPase α1 subunit using immunocytochemistry experiments. Therefore using immunocytochemistry it was investigated whether mutated PLM co-localises with Na^+/K^+ ATPase α1 subunit. Initially control experiments were performed to

determine the correct antibody concentrations. The requirement for antibodies to be raised in different species limits which antibodies could be used to image PLM and Na^+/K^+ ATPase α1subunit together. Several PLM antibodies were tested such as B8 (dog PLM antibody) and total PLM (data not shown) however they showed no selectivity for PLM. The PLM-C2 rabbit monoclonal which binds to the PLM N-terminal was finally used and antibody concentrations determined. For Na^+/K^+ ATPase subunit labelling, the previously used Na^+/K^+ ATPase α1 subunit mouse monoclonal antibody from Millipore (Chapter 2 Table 2.7) was optimised.

In Figure 3.13A PLM-C2 (green) stained the myocyte at the t-tubule invaginations[276] in both PLM-WT and PLM^{3SA} myocytes in a striated pattern. Na^+/K^+ ATPase α1 subunit, imaged in red, can be seen at the t-tubular surface and at the membrane edge. In the overlay in Figure 3.13A it can be seen that there was co-localisation of both antibodies in PLM-WT and PLM^{3SA} myocytes, indicated by the yellow labelling which occurs when the 2 images are lying on top of each other. This confirmed that the mutated PLM protein in PLM^{3SA} mice co-localised with the Na^+/K^+ ATPase α1 subunit.

It is of note that these antibodies were not ideal for use in confocal microscopy but there were limited tools available. To further support that the 2 antibodies co-localised, a region of interest was taken for each cell and the relative intensities are shown in Figure 3.13B. It can be seen that the relative intensities for PLM-C2 and Na^+/K^+ ATPase α1 subunit overlay each other providing further evidence of co-localisation of PLM with the Na^+/K^+ ATPase in both WT and PLM^{3SA} myocytes.

3.5 Discussion

The main findings of the results presented in this chapter showed that the PLM^{3SA} mouse grows normally and has no obvious gross phenotype. At the molecular level, the mutation of PLM phosphorylation sites appears successful with bands corresponding to Ser63, Ser68 and Ser69 absent from both SDS-PAGE and Phos-tag affinity SDS-PAGE immunoblots analysed with phospho-specific PLM antibodies. The PLM protein was not only successfully mutated but appears to traffic to the membrane fraction (as shown by differential purification), was found located in the membrane (immunostaining and confocal microscopy) and co-associated with the Na^+/K^+ ATPase α subunit (shown by co-IP experiments and confocal microscopy).

3.5.1 Mutation of PLM protein

Successful mutation of PLM in PLM^{3SA} mice was shown using immunoblot analysis with phospho-specific antibodies. The absence of bands in all of the PLM^{3SA} crude ventricular homogenates at previously phosphorylatable PLM sites Ser63, Ser68 and Ser69 with phospho-specific antibodies suggests successful mutation of the PLM protein so that it can no longer be phosphorylated at these sites. However, when mutating a Ser residue to Ala there may be a change in the structural conformation of the PLM protein. Therefore, to ensure that a lack of binding by these phospho-specific antibodies was due to elimination of all 3 phosphorylation sites, and not due to the inability to reach the antibody binding site, Phos-tag phosphate affinity SDS-PAGE immunoblot analysis with total PLM antibody was used to confirm that PLM phosphorylation sites had indeed been successfully removed. Interestingly though, in PLM-WT homogenates, not only were the expected phosphorylation bands detected for the known phosphorylation sites but additional bands were also detected. These bands were also detected in the PLM^{3SA} homogenate samples. Potentially these additional bands could suggest the presence of more unconfirmed phosphorylation sites. In the PLM mouse sequence there are 5 serine residues Ser37, Ser62, Ser63, Ser68 and Ser69.[220, 22] However, the ability of the Phos-tag molecule to bind to a phosphorylation site is dependent on the presence of a phosphate group at the Ser residue.[273] As Ser37 is the last residue found in the transmembrane domain it is unlikely that it is in a position to be phosphorylated, whilst all other Ser residues are found in the cytoplasmic tail. Previous work on the cytoplasmic Ser sites in Xenopus oocytes using sequential mutations to Ala showed that by mutating Ser62 there was no phosphorylation at this site by PKA, PKC or NIMA kinase ("never in mitosis" kinase)[277] and it was assumed that this

site has no role in protein function.[277] Of course other residues can be phosphorylated such as tyrosine and histidine; however these are not present in the PLM cytoplasmic tail sequence. The cytoplasmic tail is aspartate and glutamate rich, which has been shown to be important in providing negative charge to PLM cytoplasmic tail helping to release PLM from the endoplasmic reticulum for translocation to the membrane.[278] Whether Asp is phosphorylated and therefore binds Phos-tag molecule to produce a non-specific band on the Phos-tag gel is debatable in eukaryotic cells.[279] The only other question remaining with the use of Phos-tag gel is how selective is the Phos-tag molecule for simply negatively charged phosphates. The negative charge on the Asp and Glu amino acids at positions Asp54, Glu52, Glu55 and Glu56 present in PLM protein could bind Phos-tag molecule directly. This may possibly explain the extra bands seen in Figure 3.8.

The use of phospho-specific antibodies to distinguish which phosphate moieties correlate to which Ser phosphorylation site also provides some interesting findings. The binding of Ser63 at two phosphate sites, one of which is the same site as Ser69, suggests that Ser63 can detect when PLM is mono- and dual- phosphorylated. As basal phosphorylation of PLM has been attributed to PKC and Ser63 is the major site of PKC phosphorylation it fits that this site under normal conditions is mono-phosphorylated and additional phosphorylation of other sites causing dual phosphorylation may also be detected.[130]

The other interesting observation from the Phos-tag SDS-PAGE immunoblot analysis was the amount of unphosphorylated protein seen in the PLM-WT hearts compared to the unphosphorylated bands in PLM^{3SA}. In these studies the unphosphorylated WT band was 30% of the unphosphorylated signal in PLM^{3SA} homogenates, suggesting that 70% of PLM in the WT was phosphorylated. Basal phosphorylation of PLM has been reported as at least 30% at Ser68 in one study[62] and as much as 46% at Ser68 in another.[232] Fuller *et al*, 2008, proposed that in rat ventricular myocytes basal phosphorylation in unstimulated myocytes was approximately 30% at Ser68 with an additional 50% at Ser63 mainly due to phosphorylation by PKC, leaving 40% of PLM phosphorylated at neither residue.[130] This estimate of unphosphorylated PLM fits with the comparison of unphosphorylated PLM in WT compared with PLM^{3SA} in this study. Basal phosphorylation measurements are highly dependent on the preparation of the tissue sample. Ventricular myocytes have been shown following isolation to be highly phosphorylated due to stress and Ca^{2+} loading which reduces over time, therefore reported basal phosphorylation may differ depending on when experimentation was started. Some factors that may influence the phosphorylation status of the isolated beating heart could be the stress of removing the heart

from the animal[259] and an adequate perfusion period prior to snap freezing thereby allowing proteins to re-equilibrate to an *in vivo* phosphorylation state. Perfusion of these hearts was 5 minutes at an *in vivo* pacing rate of 550bpm and the phosphorylation status measured was similar to that from hearts resolved on a Phos-tag SDS-PAGE that had been perfused for 60 minutes (data not shown). By using a positive phosphorylation control on these gels such as homogenate from hearts perfused with high concentration of ISO (PKA activator) or phorbol myristate acetate (PKC activator) the amount of basal phosphorylation observed could potentially be put into context.

One further question to address would be whether the use of Phos-tag molecule affects the affinity of total PLM antibody to bind to PLM. Although the Phos-tag molecule binds to phosphates at PLM Ser sites and slows their migration, it remains fixed in the gel matrix and does not transfer to the membrane due to chelation by EDTA of the divalent cation, Mn^{2+}, which enables Phos-tag molecule to bind in the first instance. Therefore the affinity of the antibody to bind to the PLM protein should not be affected.

3.5.2 Protein expression: PLM and Na^+/K^+ ATPase

The primary PLM phosphorylation sites: Ser63, Ser68 and Ser69, have been shown to be successfully mutated and the consequent effects on protein expression of total PLM, Na^+/K^+ ATPase subunits and other E-C coupling proteins have been investigated. The significant reduction in total PLM expression seen in PLM^{3SA} mice compared with PLM-WT accompanied by equal protein expression of Na^+/K^+ ATPase α1 subunit was not completely unexpected. Previously in PLM-KO mice a reduction in total Na^+/K^+ ATPase α subunit expression was reported.[33] If, as previously hypothesised, PLM acts as a brake on Na^+/K^+ ATPase pump, with the removal of this brake the myocyte has regulated its own pump activity by reducing the number of active units as observed in PLM-KO mice.[28] Therefore in a myocyte expressing a permanent PLM brake on the Na^+/K^+ ATPase pump, the myocyte may have modified protein expression in order to maintain a normal net pump current helping to regulate $[Na^+]_i$. Within our laboratory I_{Pump} has been measured in both WT and PLM^{3SA} myocytes using perforated patch clamping and no differences were found in the affinity of the pump for Na^+ (K_m) or maximal pump turnover rate (V_{max}). Thus suggesting that the myocytes have found an adaptation to maintain normal pump function and hence $[Na^+]_i$ under basal conditions. However, it must be taken into consideration that the similar I_{Pump} measurements may have been

influenced by the basal phosphorylation state of the myocytes they were measured in. If, following myocyte isolation, cells had been incubated at room temperature for a long period of time the basal phosphorylation state of the quiescent WT myocytes may have decreased significantly thereby mimicking PLM^{3SA} myocyte pump activity. It is possible that under normal *in vivo* phosphorylation control PLM^{3SA} myocytes may have a reduced pump activity when compared with WT and this will be investigated by measuring $[Na^+]_i$ and Rb^+ uptake in later studies within this thesis.

For a decrease in PLM expression to normalise pump current it is important to consider the relationship between PLM and the α subunit, especially the stoichiometry of this partnership. Previous work has indicated that PLM has a 1:1 stoichiometry with Na^+/K^+ ATPase subunits,[129] but PLM has also been reported to form tetramers.[217, 280] Recent studies in HEK293 cells have shown that PKC/PKA activation of PLM monomer can cause increased PLM oligomerisation. These tetramers, which have been termed a reserve pool, may not bind or regulate Na^+/K^+ ATPase at all.[230] Therefore, it may be possible that in WT hearts some Na^+/K^+ ATPase molecules do not associate with PLM. If so, could perhaps this also occurs in PLM^{3SA} myocytes to help modulate pump activity. Since oligomerisation may be influenced by phosphorylation, this ratio of associated to unassociated or monomeric to multimeric PLM may be different in PLM^{3SA} myocytes, bearing in mind that even the formation of oligomers may also be affected by the fact that PLM cannot be phosphorylated at all in these mice. Immunoprecipitation experiments have reported that PLM forms a complex with Na^+/K^+ ATPase α1 subunit[63] which is supported by co-IP studies within this Chapter. However, these experiments have limitations and may only be studying a select population of PLM and Na^+/K^+ ATPase subunits. Indeed Pavlovic *et al*,[62] report preliminary data whereby immunoprecipitation of all of PLM only co-precipitates 44% of total Na^+/K^+ ATPase α1 subunit, whereas immunoprecipitation of Na^+/K^+ ATPase α1 subunit co-precipitates all (100%) of PLM. This suggests the possibility of either a subpopulation of pump units that are functional at the cell surface but not attached to PLM, or a subpopulation of pump units that are not functional within the cell. Very recently Fuller *et al*, have observed the existence of PLM-PLM multimers under physiological conditions which supports this idea.[242] Therefore reduction of PLM expression in PLM^{3SA} hearts may decrease PLM units per Na^+/K^+ ATPase pump unit and consequently enable the myocyte to maintain normal $[Na^+]_i$. Measurement of $[Na^+]_i$ in intact beating hearts in both genotypes will be essential to answer these questions.

PLM can also associate with the Na^+/K^+ ATPase α2 subunit in HEK293 cells;[129] however in guinea pig myocytes it has also be shown that PLM does not associate with Na^+/K^+ ATPase α2 subunit.[30] In mice, using α1 and α2 knock-out model, James *et al*,[87] concluded that only the α2 subunit is involved in regulating $[Ca^{2+}]_i$ in cardiac myocytes. Therefore it was important to look at protein expression of both subunits in PLM^{3SA} mouse which was shown to be similar to WT. However, it has been suggested that the Na^+/K^+ ATPase α2 subunit contributes little to the overall pump activation and function within the cell. Berry *et al*, 2007, showed in mouse myocytes that the α2 subunit current ($I_{\alpha2}$) contributes only 6% of the total Na^+/K^+ ATPase pump current (I_{Pump}) for Na^+ efflux whilst the α1 subunit current contributes to 94%.[82] The amount of contribution to I_{Pump} by the α2 subunit could be quantified in the new mouse by exploiting the ouabain binding site in the α1 subunit and measuring I_{Pump} in myocytes by patch clamping techniques. Expression of both β1 and β2 subunit appeared decreased in PLM^{3SA} homogenates but not significantly and was most probably due to the low affinity of the antibody to bind to the protein. There were no major changes in other proteins involved in E-C coupling.

Finally the subcellular localisation of the mutated PLM protein was investigated. It has been shown using site-directed mutagenesis of residues within the cytoplasmic domain of PLM in Madin-Darby Canine Kidney cells that a negative charge at Ser69 is necessary for the shift of PLM to the membrane.[278] Although Ala also carries a negative charge, it is possible that mutating the Ser69 residue may affect PLM trafficking to the membrane. The results from the fractionation experiments show that this does not appear to be the case. Mutated PLM correctly trafficks to the sarcolemmal membrane in PLM^{3SA} myocytes probably due to the glutamate and aspartate rich cytoplasmic tail providing negative charge to release PLM from ER, as previously mentioned. Confocal data confirms this finding and shows mutated PLM present in the sarcolemmal membrane and t-tubules. It also supports co-IP data by showing co-localisation of PLM with the Na^+/K^+ ATPase α1 subunit. Although it is now clear that PLM associates with the α1 subunit in PLM^{3SA} mice, future experiments using FRET signalling would be useful to confirm interaction.[129]

3.6 Summary

In this chapter it was shown that the PLM^{3SA} mouse is viable and grows normally with no obvious gross phenotype. Mutation of the PLM phosphorylation sites appears successful with bands corresponding to Ser63, 68 and 69 absent from SDS-PAGE immunoblots analysed with phospho-specific antibodies and similarly from Phos-tag phosphate affinity SDS-PAGE immunoblots analysed with total PLM antibody. Trafficking of the mutated PLM protein to the membrane appears unaffected in PLM^{3SA} hearts with co-IP and confocal studies supporting co-localisation of the mutated protein with Na^+/K^+ ATPase α subunit. Finally protein expression studies show total PLM expression is decreased in PLM^{3SA} mouse hearts compared with WT.

4 CHAPTER 4 – PHENOTYPING OF PLM^{3SA} MOUSE BY LANGENDORFF PERFUSION

4.1 Introduction

The PLM^{3SA} mouse has a newly created genetic profile which has never before been characterised for basic cardiac function. In order to fully understand the model and use it to test hypotheses outlined in this thesis, it was first necessary to assess contractility, coronary flow and LVEDP under basal conditions paced at a physiological heart rate. These studies are important as a launch pad for further investigation into the role PLM plays in kinase-mediated Na^+/K^+ ATPase regulation. These baseline measurements can then be used to establish the effects of pacing protocols and β-adrenergic stimulation on PLM^{3SA} hearts.

Firstly, the basic contractility of the heart under paced *in vivo* heart rate conditions (550bpm) will be investigated. Previous Langendorff studies by our group in PLM-KO mice showed a difference in basal cardiac function, with depressed contractility in PLM-KO compared to PLM-WT hearts.[33] This is indicative of a lower $[Na^+]_i$ due to relief of inhibition of the Na^+/K^+ ATPase and the differences could imply that permanent inhibition on the pump by unphosphorylatable PLM may affect contractility in the new PLM^{3SA} mice. If, as hypothesised, the PLM^{3SA} mouse has a higher $[Na^+]_i$ then changes in contractility may be seen when animals are compared with their WT littermates, such as increased LVDP.

However, by pacing the hearts at 550bpm any differences in heart rates of each genotype may be masked. It is possible that the genetically modified mouse has developed adaptations in heart rate to enable normal function. Of course these adaptations would be under autonomic control *in vivo* which cannot be investigated in the Langendorff preparation; however it is possible to investigate any potential heart rate differences by looking at unpaced Langendorff heart preparations. This information is also essential to look at the true effect of ISO β-adrenergic stimulation on each heart type. ISO causes inotropic and lusitropic responses in the heart, but also chronotropic effects which cannot be investigated in electrically paced preparations. Therefore unpaced Langendorff mouse hearts preparations will also be investigated as well as the effects of β-adrenergic stimulation.

Paced heart Langendorff preparations may not permit the investigation of ISO chronotropic effect, but do allow the control of stimulated heart rate increases, and thus the effect of pacing on PLM^{3SA} hearts can be investigated. Force-frequency relationships (FFR) were first described by Bowditch in 1871[281]

and describe the effects of increasing chronotropy on cardiac contractility. Changes in force development are directly related to intracellular Ca^{2+} transients whose frequency and magnitude increase with increased rate.[282] This is partly due to decreases in diastolic relaxation time and hence less time for Ca^{2+} to leave the cell thereby reducing Ca^{2+} extrusion. Also reverse mode NCX may be activated by an increase in $[Na^+]_i$, caused by increased Na^+ influx through voltage-gated Na^+ channels with increased heart rate,[283] and this influences the amount of Ca^{2+} entering the cell in exchange for Na^+ extrusion. It is of note that the FFR in mouse and rats is negative, which is due to a number of complex reasons. It is believed that because rodents have a higher resting $[Na^+]_i$ than other mammals[284] this causes $[Na^+]_i$ to affect Ca^{2+} entry via NCX more readily and Ca^{2+} entry at rest is favoured.[8] It is well known that at rest rat ventricles show potentiation and gain in SR Ca^{2+} and therefore on stimulation there is a net Ca^{2+} loss, hence why contractility decreases with increased frequency rate in rats.[8] The same theory can be applied to mouse ventricles which like the rat heart has elevated $[Na^+]_i$ and a short action potential duration. There is therefore a loose correlation between the direction and slope of the FFR and intracellular Na^+ concentration.[285] It is hypothesised that the new mouse may have higher $[Na^+]_i$ than WT hearts so consequently may display a steeper negative FFR.

The use of pacing to establish the relationship between heart rate and contractility is, however, an artificial one. It is rare (other than in tachycardias) that heart rate is substantially elevated *in vivo* in the absence of β-receptor occupation. So, in addition, the studies described in this chapter will examine the FFR in the presence of β-adrenergic stimulation in WT and PLM^{3SA} mice.

4.2 Aims

The aims of the studies undertaken in this chapter were to:

1) Characterise the Langendorff perfused PLM^{3SA} mouse heart at physiological pacing rates.

2) Characterise the Langendorff perfused PLM^{3SA} mouse heart in the absence of electrical pacing to observe any heart rate differences between WT littermates and any subsequent effects on cardiac function.

3) Investigate the FFR in PLM^{3SA} mouse hearts and WT littermates.

4) Study the effects of β-adrenergic stimulation on cardiac function of PLM^{3SA} mouse hearts.

5) Assess the effect of β-adrenergic stimulation on FFR in PLM-WT hearts and to look at the effects of unphosphorylatable PLM on this relationship.

4.3 Methods

4.3.1 Basic contractile function

As previously described in general methods Chapter 2 Section 2.3, hearts from PLM-WT and PLM^{3SA} littermates were excised and cannulated on the standard Langendorff rig. They were aerobically perfused with KHB for 20 minutes at a constant pressure of 80mmHg and paced at 550bpm. An intraventricular balloon was placed in the left ventricle of each heart and LVEDP was set between 4-8mmHg. Baseline measurements of LVDP and coronary flow were recorded continuously throughout the experiment. Arrhythmia score was calculated retrospectively as described in Section 4.3.5.

For unpaced contractile function measurements hearts were perfused as above but were allowed to free-run at their intrinsic heart rate without electronic stimulation. Unless unavoidable there are a very limited number of Langendorff mouse heart studies that are performed unpaced due to the unpredictable nature of mouse hearts *ex vivo* which, in our experience, are very sensitive to external factors such as temperature and positioning of the intraventricular balloon. *In vivo* heart rates for mice are 500-600bpm[286, 287] however, using the basic Langendorff set-up *ex vivo* heart rates are usually 400bpm or lower. Due to the need for right atrial superfusion to help maintain a more physiological heart rate, the standard Langendorff rig was modified (see Chapter 2 and Figure 4.1 below) and the right atrium was superfused at a constant flow of 3ml/min. Again cardiac function parameters LVDP, LVEDP, coronary flow and heart rate were measured using an intraventricular balloon and were recorded for the duration of the experiment.

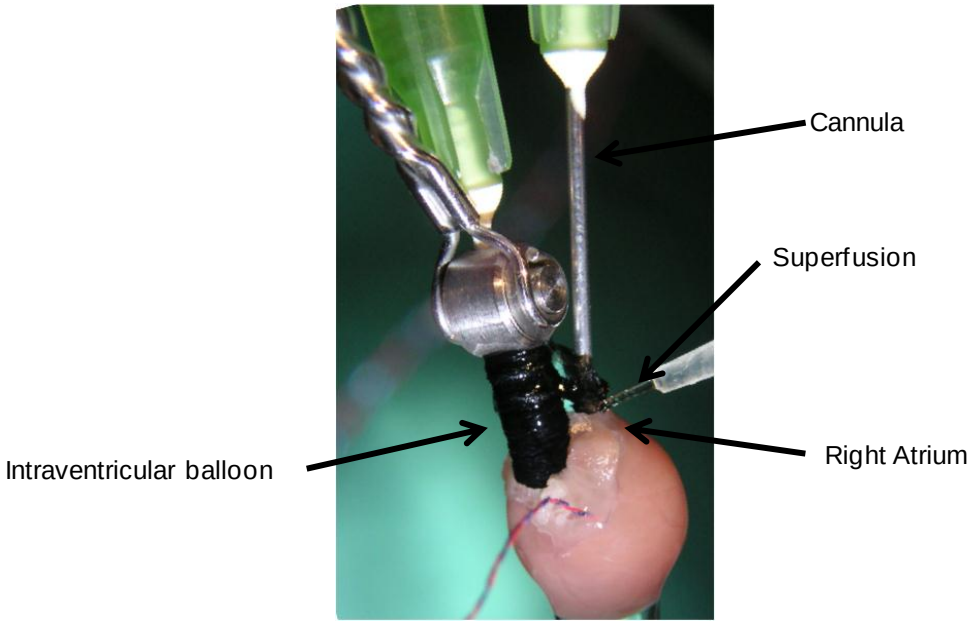

Figure 4.1: Photograph of Langendorff perfused mouse heart on standard set-up with superfusion of the right atrium.
Heart is cannulated on a metal cannula and secured using suture. An intraventricular balloon is inserted into the left ventricle and is connected to a pressure transducer allowing measurement of LVDP, LVEDP and heart rate. Constant superfusion of the right atrium is supplied by an extra cannula connected to a calibrated peristaltic pump supplying flow at 3ml/min. For basic Langendorff set-up simply remove superfusion.

4.3.2 Force-frequency relationship

Langendorff perfusion of PLM^{3SA} and PLM-WT littermate hearts was set-up as for paced hearts above (Section 4.3.1). Following a 20 minute stabilisation period at 550bpm the frequency of pacing was adjusted over time in order to investigate the FFR in each mouse genotype. Firstly the frequency was stepped to 400bpm and then increased in increments of 50bpm to 750bpm. The hearts were perfused at the lower frequencies (400-600bpm) for 5 minutes and at the higher frequencies (650-750bpm) for 3 minutes to avoid heart function deterioration. An intraventricular balloon measured changes in cardiac function parameters LVDP, LVEDP, coronary flow and heart rate throughout the experiment.

4.3.3 Isoprenaline study

PLM-WT and PLM^{3SA} hearts from littermates were cannulated and perfused as described in Section 4.3.1 with superfusion to the right atria and without electronic stimulation. Following 20 minutes of stabilisation perfusion ISO at either 1nM or 100nM concentration was administered. Previous work

on full ISO concentration response curves proved difficult due to heart function decline between concentrations. However, to address the question of β-adrenergic stimulation effect on our mice simply a low concentration (1nM) and a high concentration (100nM) of ISO were administered. These concentrations were derived from previous work (not shown) in isolated cells where ISO EC_{50} was measured as 10nM (n=4). ISO perfusion was maintained for 10 minutes to ensure short term and long term effects could be measured.

4.3.4 FFR in presence of isoprenaline Study

FFR experiments were conducted in the presence of 1nM ISO. Following successful cannulation, mouse hearts underwent a 20 minute stabilisation period at a frequency of 550bpm before being perfused with 1nM ISO which was maintained throughout the duration of the experiment. After 10 minutes of ISO perfusion the above FFR protocol (Section 4.3.2) was implemented starting at 400bpm increasing to 800bpm in 50bpm increments. An intraventricular balloon was used to measure changes in cardiac function parameters LVDP, LVEDP, coronary flow and heart rate throughout the experiment.

4.3.5 Heart rate variability analysis

Heart rate variability (HRV) analysis has been investigated to give a quantitative measure of the frequency of ectopic arrhythmias in hearts during paced, unpaced and ISO studies. This analysis is of particular use in paced heart studies and gives an index of the number of "escape" ectopic beats, usually presenting as ventricular premature beats (VPBs) in a normal Langendorff perfused heart. This allows an insight into the electrical stability of the heart and comparison between genotypes.

Analysis of HRV was performed using HRV software supplied by ADInstruments for LabChart Pro. HRV module is designed to measure natural variations in the beat-to-beat intervals of the heart *in vivo*. It does this by measuring the interval between each heartbeat and calculates statistics accordingly. It calculates the standard deviation (SD) of changes in consecutive beat-to-beat intervals (SD of ΔNN) providing a non-subjective, quantitative measure of VPB frequency. A period of 10 minutes of LVDP trace for each heart was analysed using this method and the "arrhythmia score" that was obtained provides a correlation of arrhythmia incidence in the heart trace and a quantified

arrhythmia score. Below in Table 4.1 is a summary of the observed heart function and corresponding arrhythmia score.

Subjective Assessment	**Arrhythmia Score** (AU)
Sinus Rhythm	0-5
Low incidence of ectopic beats	5-10
High incidence of ectopic beats	10-20
Severe ventricular ectopics	20-30
Chaotic rhythms (includes VF)	30+

Table 4.1: Subjective assessment of heart function and corresponding arrhythmia score. HRV analysis quantifies the incidence of ventricular ectopic beats in LVDP traces and assigns them an arrhythmia score. This score can then be correlated to a subjective assessment of function. Sinus rhythm has low arrhythmia scores (0-5) whilst increasing incidence of ventricular ectopic beats shows increasing arrhythmia scores (5-10, 10-20). The more severe episodes of ventricular ectopic beats score highly (20-30) and VF scores highest of all (+30).

NB. It is of note that this analysis does not detect regular and persistent bursts of arrhythmias such as ventricular tachycardias.

4.4 Results

4.4.1 Contractile function of paced mouse hearts

To understand the effects of the PLM mutation in PLM^{3SA} mice basic cardiac function at a physiological heart rate was investigated. Figure 4.2 shows the baseline measurements of LVDP and coronary flow in WT and PLM^{3SA} hearts. It can be seen that LVDP in PLM^{3SA} hearts was significantly higher at all time points for the duration of the stabilisation period. However, coronary flow showed no differences between PLM^{3SA} and PLM-WT hearts and averaged at just under 4ml/min. Table 4.2 shows the measured parameters at the end of the 20 minute stabilisation period and highlights the previous findings.

It was hypothesised that the PLM^{3SA} mouse may be more prone to arrhythmias caused by increased $[Na^+]_i$ therefore the stability period for both genotypes was analysed for heart rate variability (HRV) using Chart software and the arrhythmia scores were compared. The results can be found in Table 4.3 and show that there was no difference in arrhythmia scores in PLM-WT and PLM^{3SA} mouse hearts paced at 550bpm.

Parameter	PLM-WT	PLM^{3SA}	P value
LVDP (mmHg)	87±5	112±7	P<0.05
Coronary flow (ml/min)	3.8±0.5	3.7±0.2	ns

Table 4.2: Summary of paced cardiac function.
Summary of cardiac function in paced PLM-WT and PLM^{3SA} hearts at the end of the 20 minute stabilisation period. n=12. All data expressed as mean±sem and analysed by Student's *t*-test (PLM-WT 'v' PLM^{3SA}), P<0.05 was considered significant.

Parameter	PLM-WT	PLM^{3SA}	P value
Arrhythmia score	5±1	8±1	ns

Table 4.3: Arrhythmia scores during paced Langendorff perfusion.
Table showing arrhythmia scores during the stability period in paced PLM-WT and PLM^{3SA} mouse hearts. n=12. All data expressed as mean±sem and analysed by Student's *t*-test (PLM-WT 'v' PLM^{3SA}), P<0.05 was considered significant.

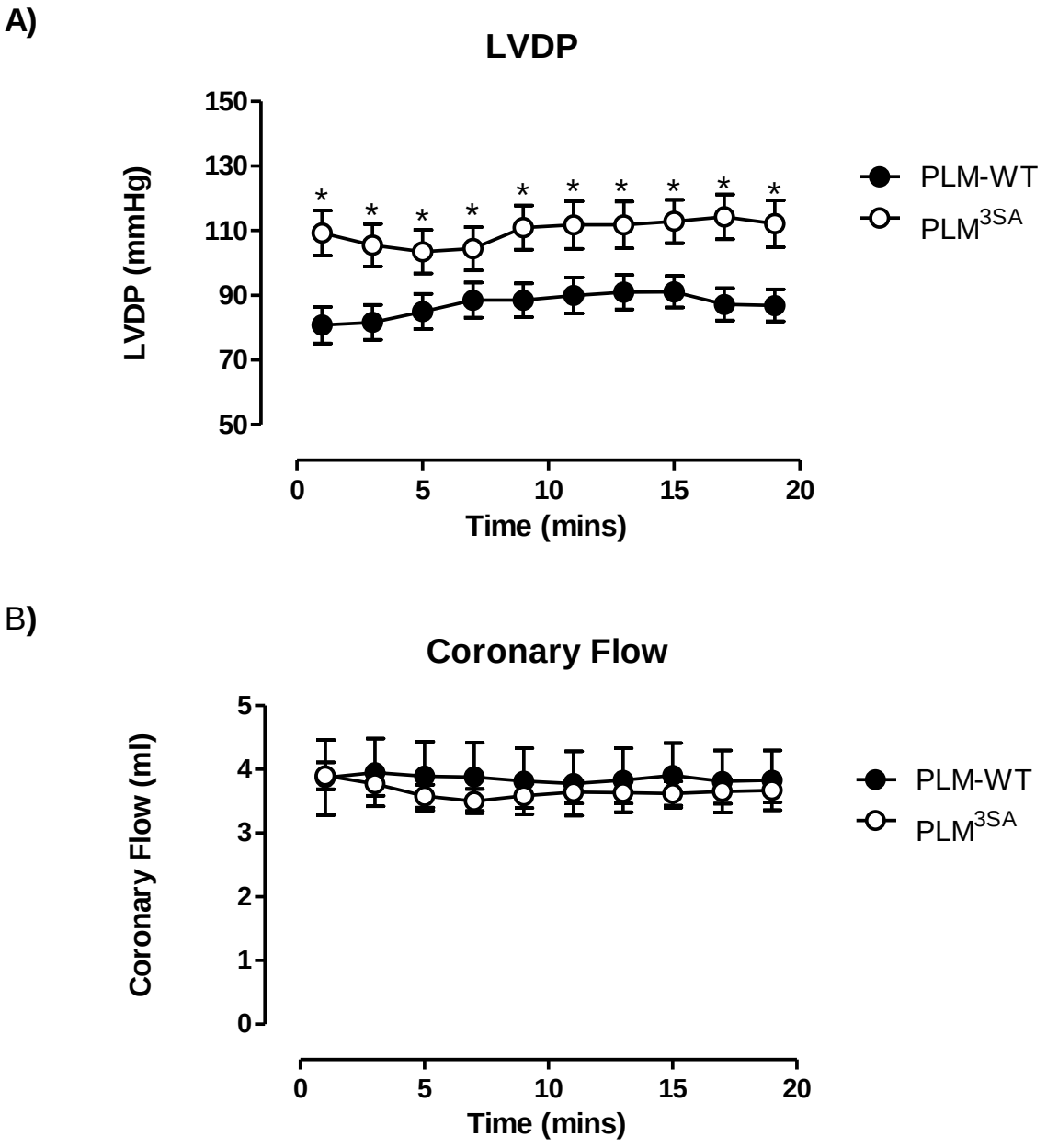

Figure 4.2: Cardiac function of paced PLM-WT and PLM^{3SA} mouse hearts during 20 minutes of aerobic Langendorff perfusion.
A) LVDP; B) Coronary flow. n=12. All data expressed as mean±sem and analysed by two-way ANOVA followed by pairwise Bonferroni post-hoc test, P<0.05 was considered significant (PLM-WT 'v' PLM^{3SA} denoted by *).

4.4.2 Contractile function of unpaced mouse hearts

In order to determine any heart rate differences between PLM^{3SA} and WT hearts and to later study the effects of ISO on the unphosphorylatable PLM^{3SA} hearts, it was necessary to investigate unpaced stability of the hearts over 60 minute. Figure 4.3 shows the HR, LVDP and coronary flow over the 60 minute perfusion period and the measurements at the end of the standard 20 minute stabilisation period are listed in Table 4.4. At the 20 minute standard time point LVDP, HR, LVEDP and coronary flow were not significantly different in PLM-WT hearts compared with PLM^{3SA} hearts. Throughout the full 60 minute perfusion period HR, LVDP, coronary flow and LVEDP were not significantly different in PLM^{3SA} hearts compared to PLM-WT hearts at any time point. Heart rate did however decrease over 60 minutes in PLM-WT hearts by 13% and in PLM^{3SA} hearts by 12%, these decreases were not significantly different from each other but the decrease in PLM-WT heart rate was significant from its starting heart rate. LVDP decreased non-significantly by 29% in PLM-WT compared with 16% in PLM^{3SA} hearts over 60 minutes, both are non-significant with respect to the starting values.

Parameter	PLM-WT	PLM^{3SA}	P value
LVDP (mmHg)	132±14	121±17	ns
Heart Rate (bpm)	487±16	441±29	ns
LVEDP (mmHg)	-0.8±2	1.5±1	ns
Coronary Flow (ml/min)	3.6±0.2	3.8±0.6	ns

Table 4.4: Baseline measurements of unpaced cardiac function.
Table detailing baseline cardiac function measurements in unpaced PLM-WT and PLM^{3SA} hearts at the end of the standard 20 minute stabilisation period. n=6. All data expressed as mean±sem and analysed by Student's *t*-test (PLM-WT 'v' PLM^{3SA}), P<0.05 was considered significant.

It is of note that LVEDP was below the standard 4-8mmHg setting value, although the balloon was originally set for these values. This could be due to the reduction in heart rate over time. Without a constant pacing rate the contractility of the heart will be affected by the decrease in heart rate due to there being more time for relaxation of the heart and therefore LVEDP will decrease. Unfortunately it could also be due to not enough time spent at the start of the stabilisation period ensuring the heart has relaxed fully to the introduction of the balloon to the ventricle. The LVEDP although below 4mmHg did stabilise after 10 minutes hence making the previous observations valid. Due to this observation

subsequent Langendorff perfusion experiments incorporated an increased balloon manipulation period prior to recording stabilisation measurements.

Again HRV was analysed and the arrhythmia scores can be found in Table 4.5 and show that there was no difference between arrhythmia scores in PLM-WT and PLM^{3SA} mouse hearts. It is of note though that compared to paced study arrhythmia scores, these values were significantly higher P<0.02. This highlights the complexity of unpaced heart studies and the tendency of these hearts to have a much higher incidence of spontaneous arrhythmias.

Parameter	PLM-WT	PLM^{3SA}	P value
Arrhythmia Score	15±3	19±5	ns

Table 4.5: Arrhythmia scores during unpaced Langendorff perfusion.
Table showing arrhythmia scores during Langendorff perfusion stability period in unpaced PLM-WT and PLM^{3SA} mouse hearts. n=6. All data expressed as mean±sem and analysed by Student's *t*-test (PLM-WT 'v' PLM^{3SA}), P<0.05 was considered significant.

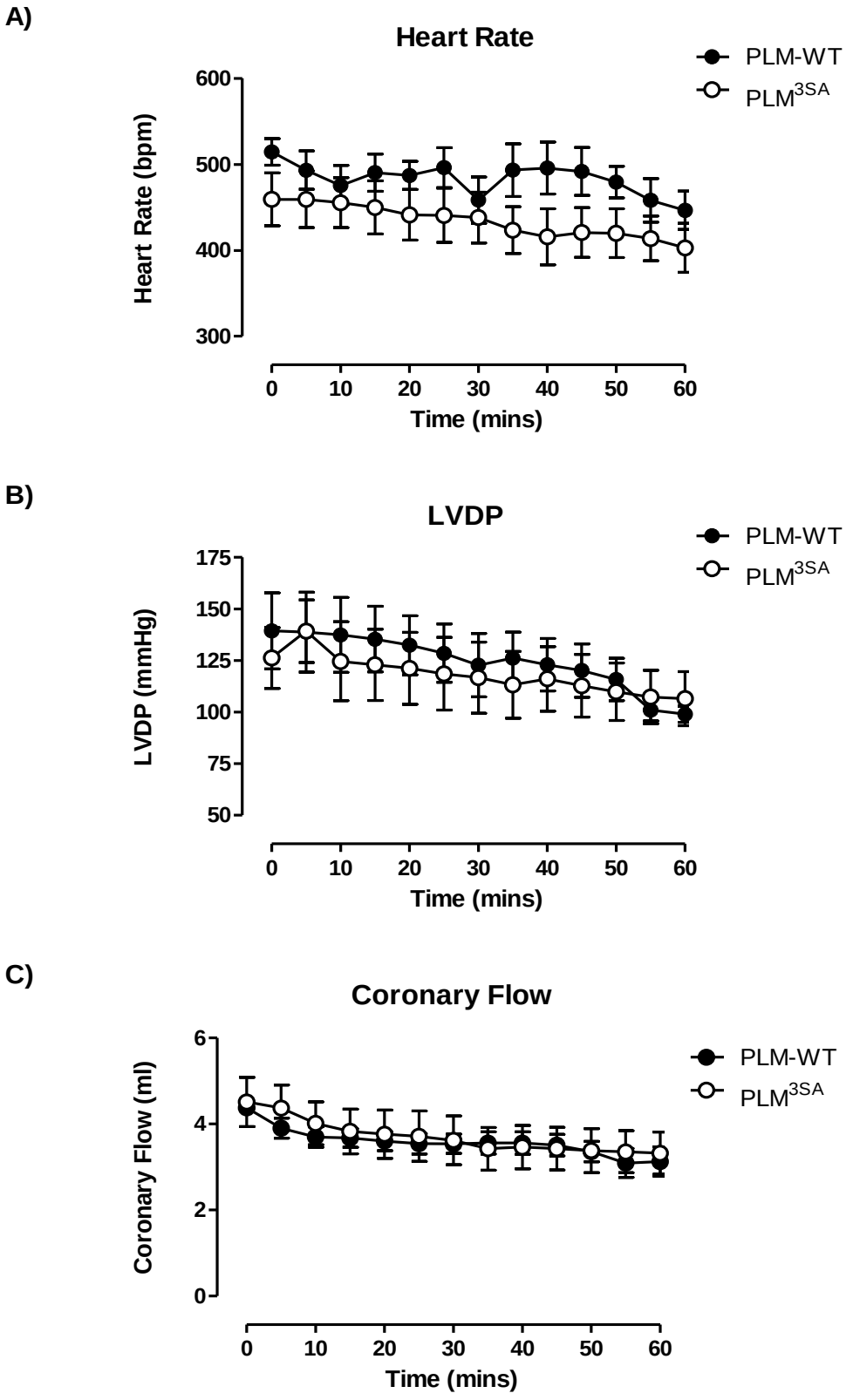

Figure 4.3: Cardiac function of unpaced PLM-WT and PLM^{3SA} mouse hearts during 60 minutes of aerobic perfusion.
A) Heart rate; B) LVDP; C) Coronary flow. n=5-7. All data expressed as mean±sem and analysed by two-way ANOVA followed by pairwise Bonferroni post-hoc test. P<0.05 was considered significant (PLM-WT 'v' PLM^{3SA} denoted by *).

4.4.3 Force-frequency relationship

As discussed, the force-frequency relationship is influenced by the intracellular Na^+ concentration and hence is a good indicator of intracellular Na^+ concentration.[8] The FFR was first described by Bowditch in 1871 and describes the chronotropic effects on cardiac output and force during a contraction.[281, 288] In large mammals, including humans and dogs, FFR is positive;[289] however in small mammals whilst this is the same *in vivo* in *ex vivo* this relationship is negative,[282, 290-292] the reasons behind which are complex.

Intracellular Na^+ is not the sole determinant of the negative force-frequency relationship but studies have shown that it is important.[285, 293-296] It seems likely therefore that if Na^+ extrusion, particularly at high heart rates, is compromised in the PLM^{3SA} heart then the slope or "steepness" of the negative FFR may be altered.

Force-frequency relationship results are shown in Figure 4.4. Both PLM^{3SA} and WT hearts displayed a negative force-frequency relationship with increasing heart rate which was mostly linear for the chosen range. Due to the previously observed increased baseline LVDP in paced PLM^{3SA} hearts compared to PLM-WT hearts (Figure 4.2), LVDP was significantly higher in PLM^{3SA} hearts in the range of 400bpm to 650bpm. At higher heart rates of 700 and 750bpm, LVDP was not significantly different between genotypes due to the slope of the PLM^{3SA} hearts becoming steeper than the slope of the PLM-WT hearts (Figure 4.4A).

However, when analysed over the full frequency range, the gradients of the FFR of PLM^{3SA} and PLM-WT hearts were not significantly different, as can be seen in Figure 4.5. PLM^{3SA} FFR gradient was -0.1 ± 0.02mmHg/bpm, n=6 and PLM-WT FFR gradient was -0.08 ± 0.02mmHg/bpm, n=6.

Coronary flow was similar in both genotypes throughout the range of frequencies. Flow increased in both genotypes at 750bpm but this rise was non-significant from the starting flow rate in both hearts. LVEDP remained independent of heart rate in both genotypes from 500-600bpm, however there was a dramatic increase at frequencies greater than this (650-750bpm). LVEDP in PLM^{3SA} hearts increased more steeply than in WT and was significantly different at 600 and 650bpm; however they both reached similar LVEDP values at 750bpm.

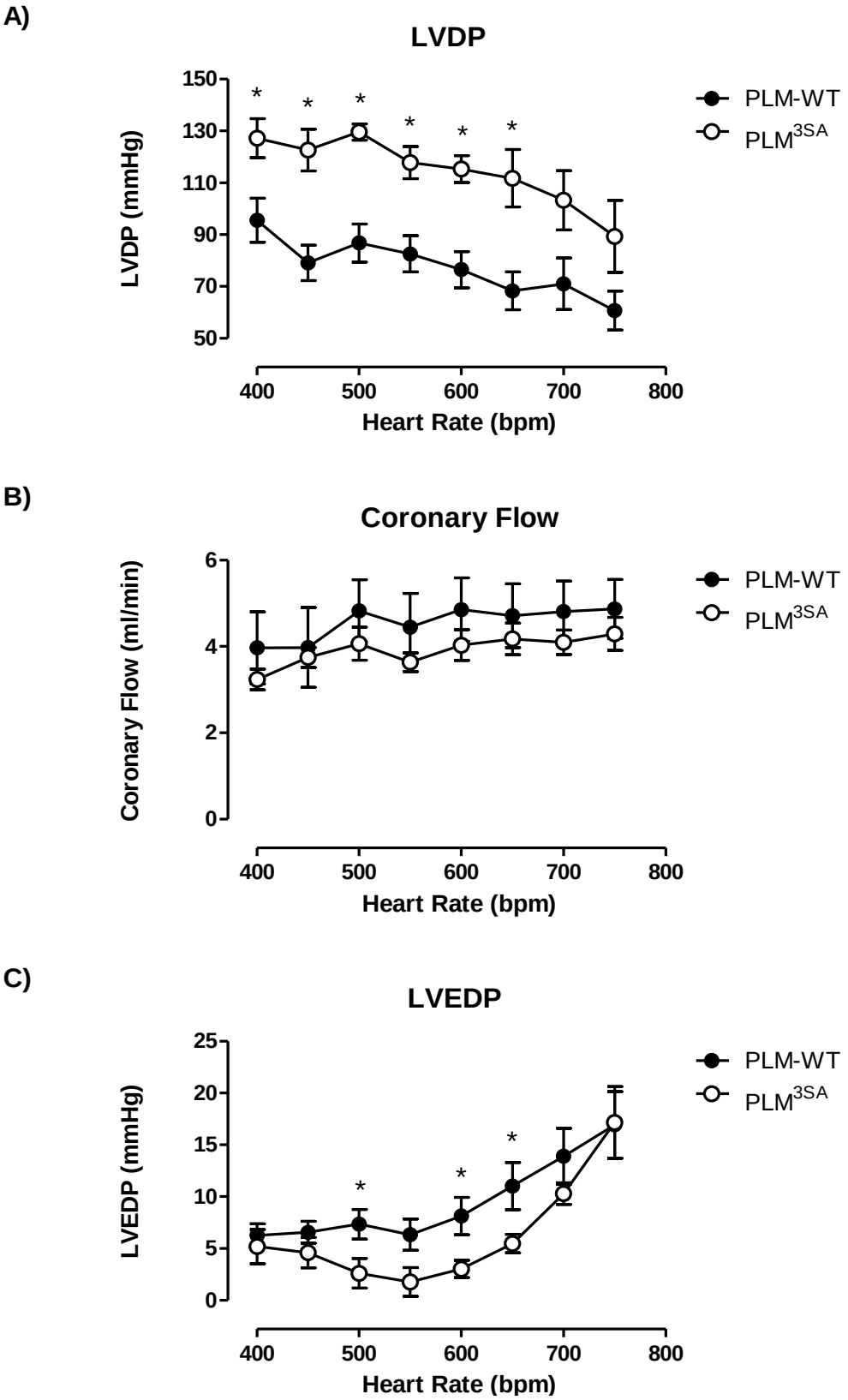

Figure 4.4: FFR in PLM-WT and PLM^{3SA} mouse hearts.
A) LVDP; B) Coronary flow; C) LVEDP. n=6. All data expressed as mean±sem and analysed by two-way ANOVA followed by pairwise Bonferroni post-hoc test, P<0.05 was

considered significant (PLM-WT 'v' PLM^{3SA} denoted by *).

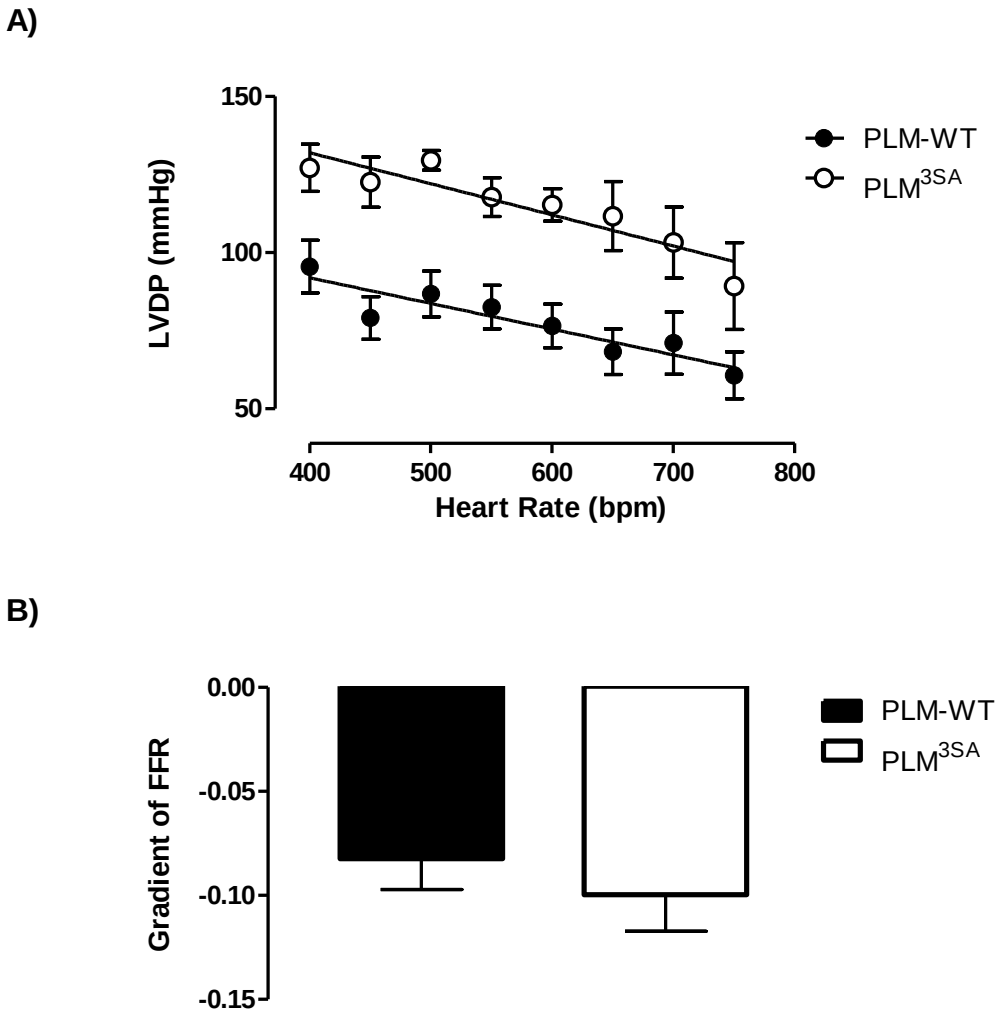

Figure 4.5: Gradients of FFR from PLM-WT and PLM^{3SA} mouse hearts.
A) Line of best fit through LVDP results over full frequency range; B) Graphical representation of FFR gradients from line of best fit. n=6. All data expressed as mean±sem and analysed by Student's *t*-test, P<0.05 was considered significant (PLM-WT 'v' PLM^{3SA} denoted by *).

4.4.4 Effect of isoprenaline on PLM^{3SA} mice compared with PLM-WT

As described previously, it was hypothesised that the presence of unphosphorylatable PLM in the PLM^{3SA} mouse may result in a Na^+/K^+ ATPase pump that cannot be regulated resulting in compromised Na^+ extrusion which potentially may load the cell with Na^+ - especially at high heart rates. Differences in PLM^{3SA} force-frequency relationship and evidence of Na^+ and Ca^{2+} overload at higher frequencies i.e. diastolic dysfunction and arrhythmias were anticipated. However, the failure to see any significant changes in the FFR may be due to the unphysiological nature of external electrical pacing. As mentioned previously, *in vivo* heart rate increases are usually accompanied by β-receptor stimulation and it is possible that even in the WT mouse hearts, the lack of β-stimulation leaves the pump unstimulated at high frequencies. Potentially explaining why PLM^{3SA} and WT mouse hearts produced similar results. However, if heart rate was to be raised more physiologically i.e. by β-receptor stimulation, this may reveal differences between PLM^{3SA} and WT hearts.

Results for Langendorff perfused ISO stimulation of PLM-WT and PLM^{3SA} mouse hearts are shown in Figure 4.6-8. ISO increased LVDP, coronary flow and heart rate at both 1nM and 100nM concentrations in PLM-WT and PLM^{3SA} hearts. Table 4.6 and Table 4.7 show the cardiac function parameters before and after ISO treatment for PLM-WT and PLM^{3SA} mice.

With 1nM ISO heart rate increased slightly in both genotypes, 17% in PLM-WT and 15% in PLM^{3SA} hearts, and with 100nM ISO PLM-WT heart rate increased by 49% and 55% respectively (Figure 4.7). Heart rate increases at each ISO concentration were not significantly different between genotypes however increases with 100nM were significantly different from starting heart rate values for each genotype. LVDP increased dramatically with 1nM ISO by 82% in PLM-WT and 60% in PLM^{3SA}; however this was not significant (Table 4.6) and was most likely reflective of the differences in basal contractility. With 100nM ISO LVDP did not increase further in PLM-WT hearts at 82% but increased slightly in PLM^{3SA} hearts to 76% compared to 1nM ISO results. Also, coronary flow increased with 1nM ISO by 32% in PLM-WT and 29% in PLM^{3SA} hearts and with 100nM ISO by 92% in PLM-WT and 80% in PLM^{3SA}. Neither of these increases was significant when comparing PLM-WT with PLM^{3SA} hearts at each concentration. LVEDP changes were most dramatic by decreasing below 0mmHg, the results can only be described qualitatively not quantitatively due to the inaccuracy of negative numbers caused when the ventricle relaxes so much that the balloon no longer fills it, contraction is no longer isovolumic and suction forces act on the balloon to create a negative value. With this in mind it can be seen that LVEDP decreases in both PLM-WT and PLM^{3SA} with 1nM and 100nM ISO by similar amounts.

Decline in LVDP over 10 minutes of 1nM ISO perfusion was negligible (PLM-WT: 4.4%; PLM^{3SA} 7.0%) and for 100nM ISO there was even a small increase in LVDP (PLM-WT: 5.2%; PLM^{3SA} 1.0%).

Again an arrhythmia score was estimated from function measurements prior to ISO perfusion and during 10 minutes of ISO perfusion, the results can be found in Table 4.8. There were no significant differences between WT and PLM^{3SA} arrhythmia scores with either 1nM ISO or 100nM ISO. Also, when comparing WT hearts before and during ISO treatment there were no differences at both concentrations and the same was true for PLM^{3SA} hearts.

Parameter	**PLM-WT**		**PLM^{3SA}**	
	0 ISO	**10min ISO**	**0 ISO**	**10min ISO**
Heart Rate (bpm)	417±15	487±11	449±31	504±16
LVDP (mmHg)	95±10	164±6	116±12	176±8
Coronary Flow(ml/min)	2.6±0.2	3.4±0.1	3.2±0.2	4.0±0.2

Table 4.6. Effect of 1nM ISO on cardiac function of unpaced PLM-WT and PLM^{3SA} hearts.

Parameter	**PLM-WT**		**PLM^{3SA}**	
	0 ISO	**10min ISO**	**0 ISO**	**10min ISO**
Heart Rate (bpm)	423±7	629±37	419±28	639±7
LVDP (mmHg)	83±7	154±20	92±10	156±13
Coronary Flow(ml/min)	2.1±0.2	4.1±0.5	2.7±0.2	4.7±0.3

Table 4.7. Effect of 100nM ISO on cardiac function of unpaced PLM-WT and PLM^{3SA} hearts.

Arrhythmia Score	**PLM-WT**			**PLM^{3SA}**		
	0 ISO	**10min ISO**	**P**	**0 ISO**	**10min ISO**	**P**
1nM ISO	16±4	20±5	ns	9±3	19±4	ns
100nM ISO	11±3	12±2	ns	18±5	12±2	ns

Table 4.8. Table showing heart rate variability measurements.
Taken during Langendorff perfusion during pre-ISO stability period and during 10 min ISO period PLM-WT and PLM^{3SA} mouse hearts. n=5-6. All data expressed as mean±sem and analysed by Student's *t*-test (PLM-WT 'v' PLM^{3SA}), P<0.05 was considered significant.

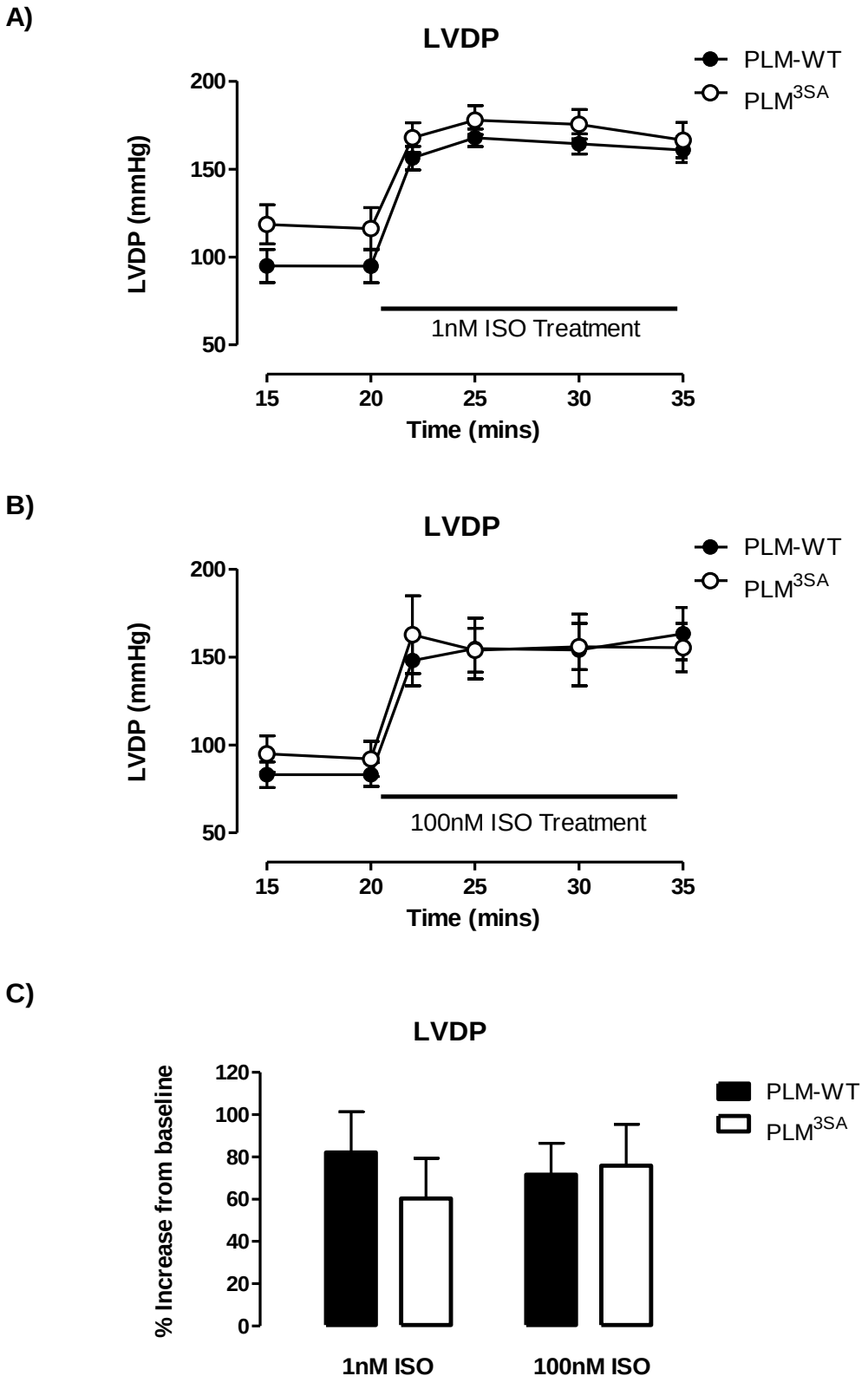

Figure 4.6: Effect of 1nM and 100nM ISO on LVDP in PLM-WT and PLM^{3SA} hearts.
A) LVDP with 1nM ISO; B) LVDP with 100nM ISO; C) % LVDP changes for 1 and 100nM ISO. n=5-6. All data expressed as mean±sem and analysed by two-way ANOVA followed by pairwise Bonferroni post-hoc test or Student's *t*-test, P<0.05 was considered significant (PLM-WT 'v' PLM^{3SA} denoted by *).

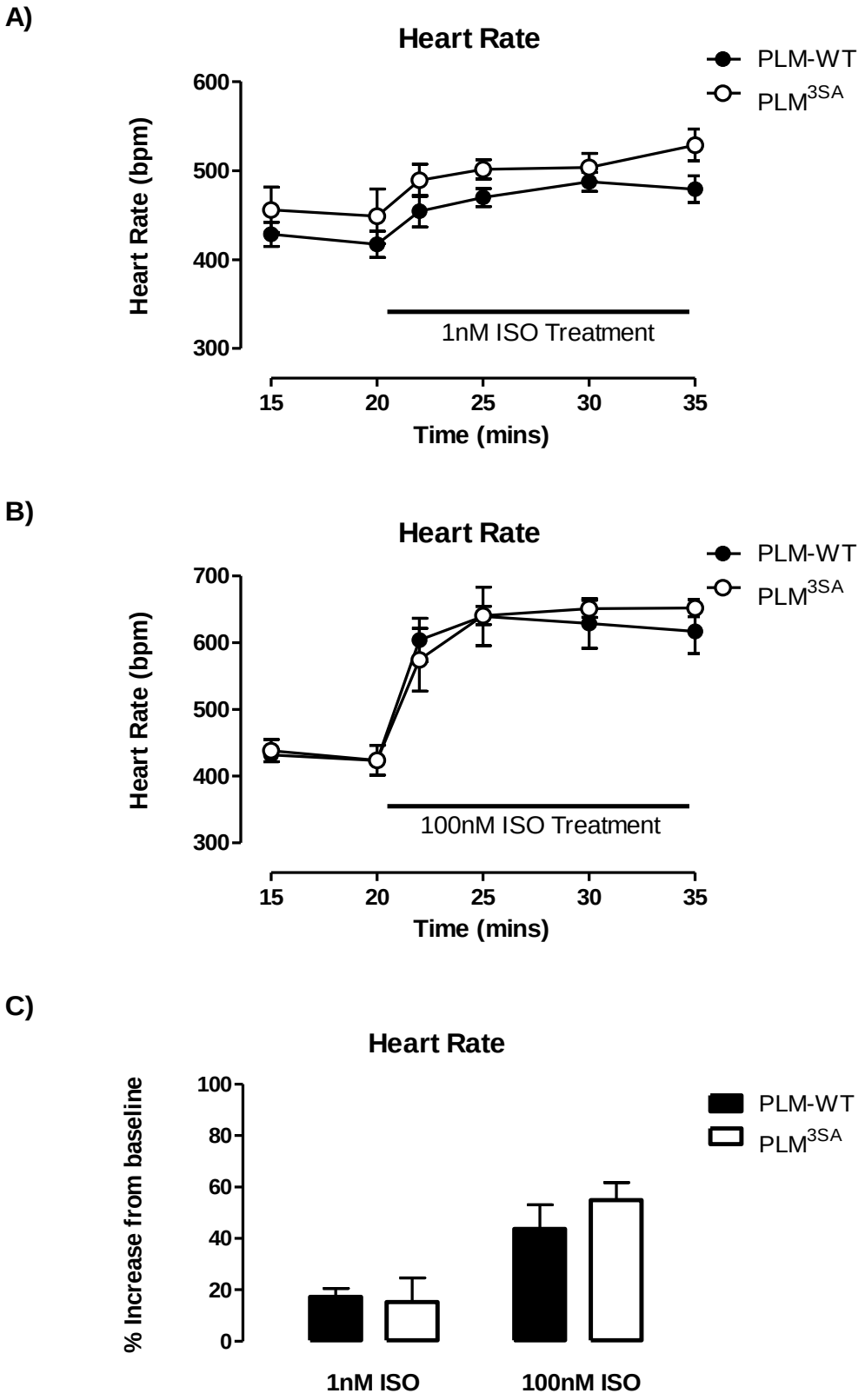

Figure 4.7: Effect of 1nM and 100nM ISO on heart rate in PLM-WT and PLM^{3SA} hearts.
A) HR with 1nM ISO; B) HR with 100nM ISO; C) % HR changes for 1 and 100nM ISO. n=5-6. All data expressed as mean±sem and analysed two-way ANOVA followed by pairwise Bonferroni post-hoc test or by Student's *t*-test, P<0.05 was considered significant (PLM-WT 'v' PLM^{3SA} denoted by *).

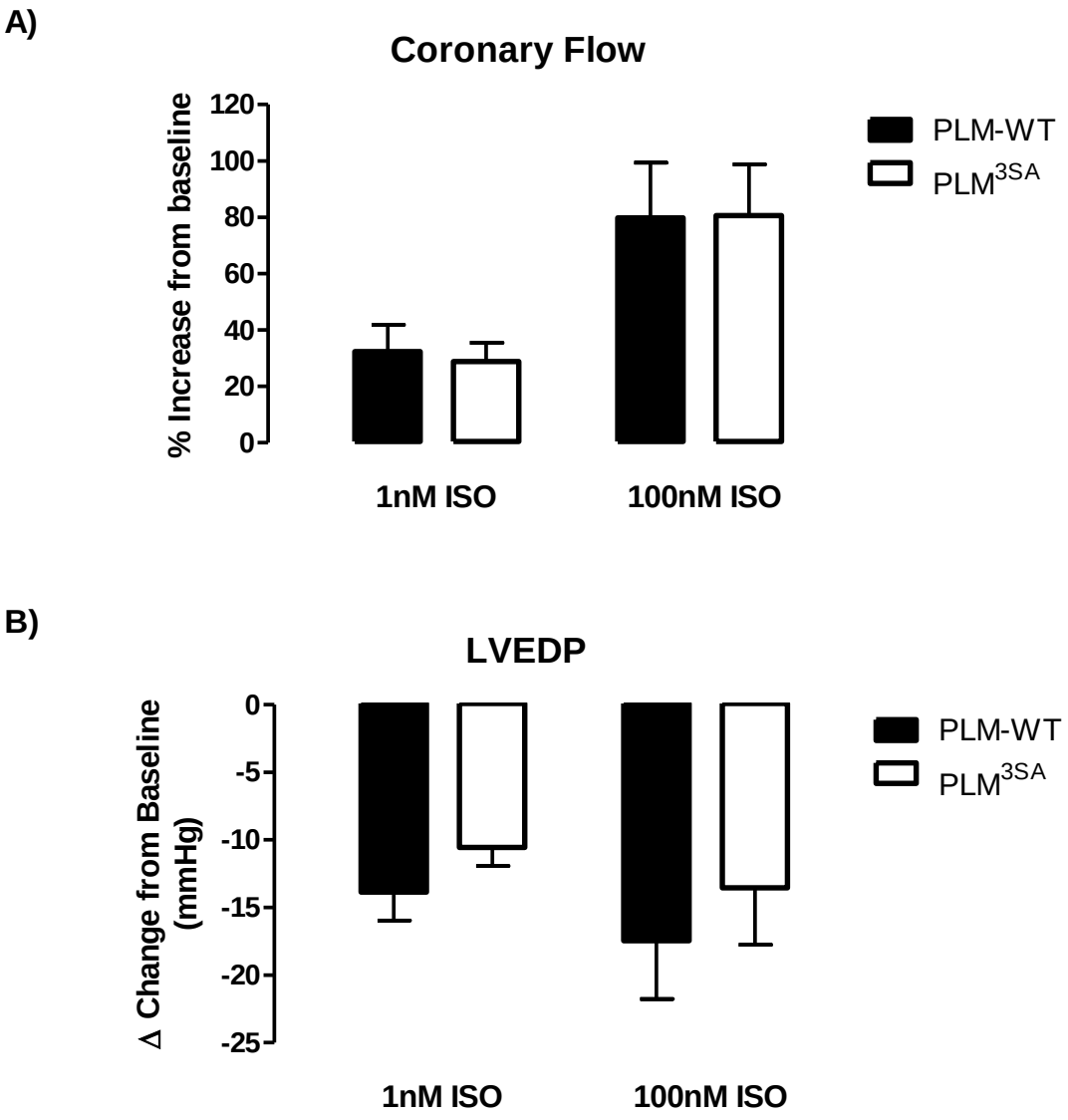

Figure 4.8: Effect of ISO (1nM and 100nM) on coronary flow and LVEDP in PLM-WT and PLM^{3SA} mouse hearts.
A) Coronary flow % change with 1 and 100nM ISO; B) LVEDP % change with 1 and 100nM ISO. n=6. All data expressed as mean±sem and analysed by Student's *t*-test, P<0.05 was considered significant (PLM-WT 'v' PLM^{3SA} denoted by *).

4.4.5 Force-frequency relationship with isoprenaline

Finally, as previously discussed, *in vivo* increases in heart rate are almost always accompanied by β-adrenergic stimulation. Therefore the final aim in this series of studies was to perform FFR in the presence of ISO. The concentration of ISO used was important in this study due to the need for PLM phosphorylation at Ser68 without excessive heart rate effects; otherwise the heart would have difficulty following the FFR pacing protocol without multiple escape rhythms. Different ISO concentrations (0.01nM – 100nM) were perfused through PLM-WT mouse hearts and homogenised before SDS-PAGE and immunoblot analysis using Ser68 phospho-specific antibody (data not shown). 1nM ISO created the perfect profile displaying both Ser68 phosphorylation and LVDP elevation in Langendorff experiments (Figure 4.6) but without a large increase in heart rate from unpaced basal heart rate measurements (PLM-WT: 417±15 to 487±11, an increase of 17%; PLM^{3SA}: 449±31 to 504±16, an increase of 15%). Hearts were paced at 550bpm for the stabilisation period and ISO pre-treatment followed by FFR protocol from 400bpm to 800bpm.

In Figure 4.9 the contractile function measurements for FFR in the presence of 1nM ISO can be seen. ISO stimulation showed increases in LVDP, heart rate and coronary flow similar to the results in Figure 4.6-8 (data not shown). During the FFR protocol, LVDP initially increased at 400bpm in both genotypes but then steadily decreased with incremental heart rate increases. The FFR gradients were analysed (Figure 4.10) and it can be seen that the gradients were similar in both genotypes with PLM-WT gradient of -0.08 ± 0.01mmHg/bpm, n=7 and PLM^{3SA} gradient of -0.06 ± 0.01mmHg/bpm, n=5.

In contrast to previous FFR data without ISO, LVEDP decreased with increasing heart rate reaching a plateau at 600bpm to 800bpm for both PLM-WT and PLM^{3SA} hearts. Additionally in both genotypes coronary flow remained stable until 600bpm, approximately 3.2ml/min, at which point it increased to 4ml/min. This increase was not significant from baseline for either genotype.

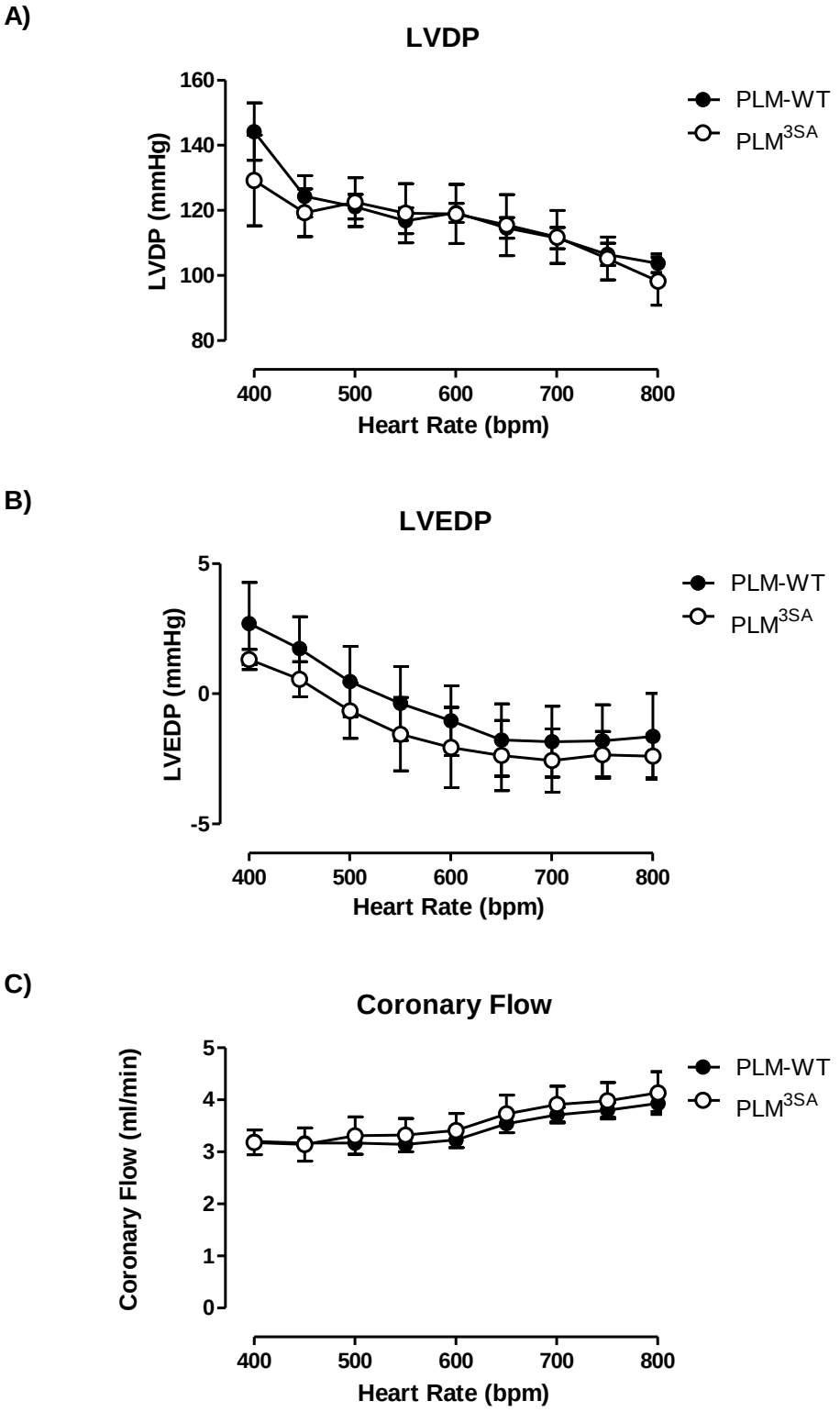

Figure 4.9: FFR in PLM-WT and PLM^{3SA} mouse hearts in the presence of 1nM ISO.
A) LVDP; B) LVEDP; C) Coronary flow. n=6. All data expressed as mean±sem and analysed two-way ANOVA followed by pairwise Bonferroni post-hoc test, P<0.05 was considered significant (PLM-WT 'v' PLM^{3SA} denoted by *).

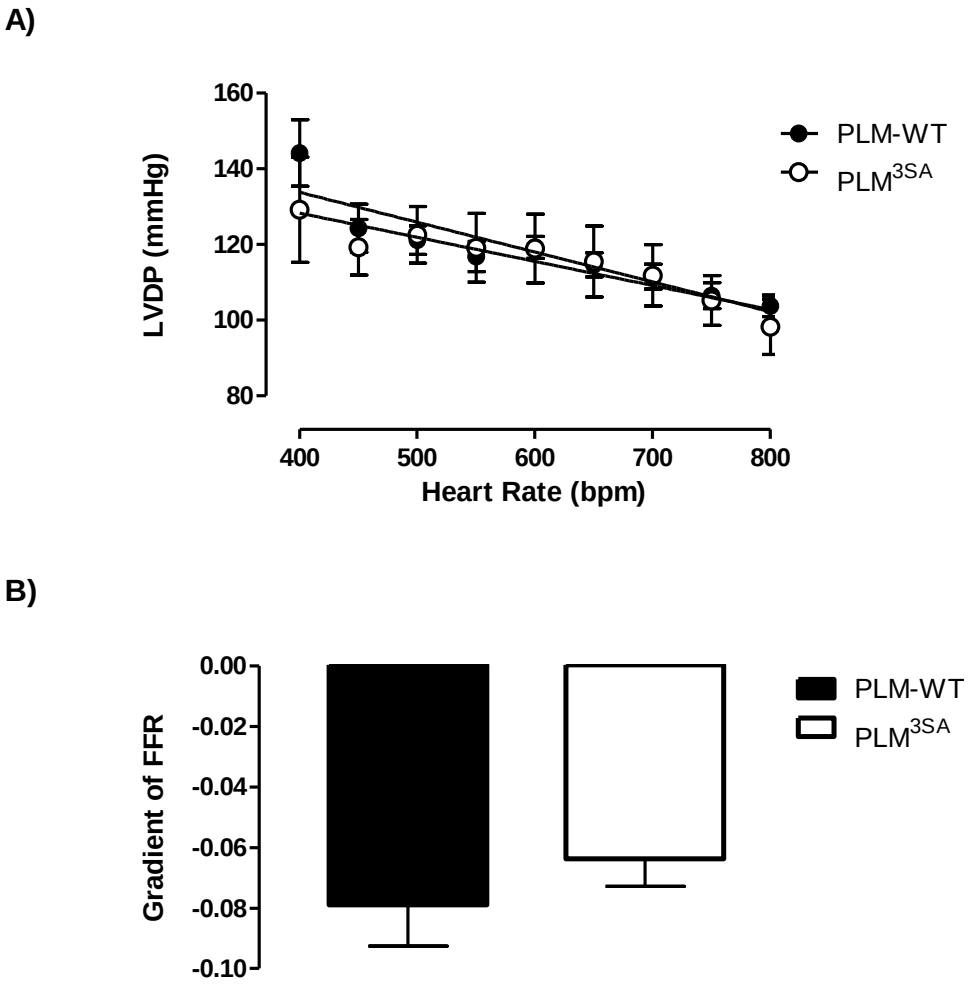

Figure 4.10: Gradients of FFR slopes in PLM-WT and PLM^{3SA} mouse hearts in the presence of 1nM ISO.
A) Line of best fit through LVDP results over full frequency range; B) Graphical representation of gradients of line of best fit slopes. n=5-7. All data expressed as mean±sem and analysed by Student's *t*-test, P<0.05 was considered significant (PLM-WT 'v' PLM^{3SA} denoted by *).

A)

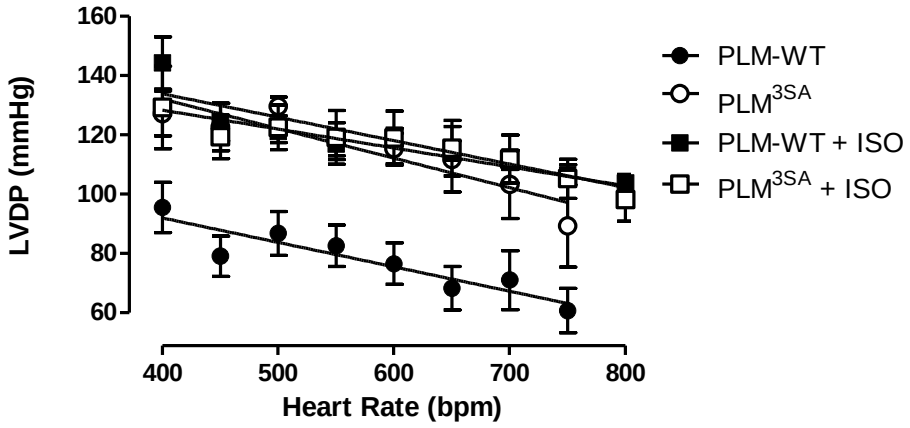

B)

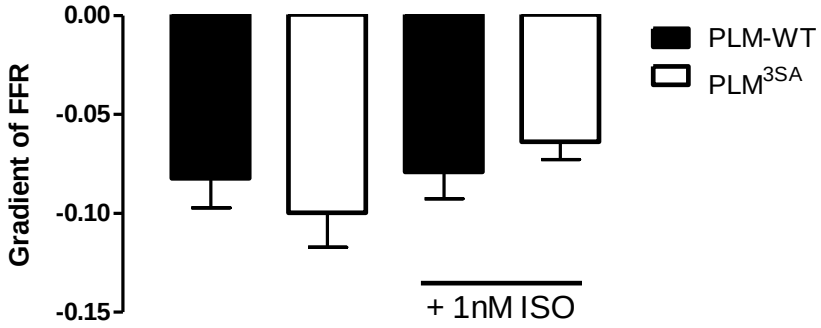

Figure 4.11: Summary of FFR gradients in PLM-WT and PLM^{3SA} mouse hearts with and without 1nM ISO present.
A) Line of best fit through LVDP results over full frequency range; B) Graphical representation of FFR gradients from line of best fit. n=5-7. All data expressed as mean±sem and analysed by one-way ANOVA with Tukey post-test, P<0.05 was considered significant (PLM-WT 'v' PLM^{3SA} denoted by *).

Compiling this data set with previous FFR gradient data it can be seen that whilst PLM-WT gradients were similar in both experiments, the gradient of the PLM^{3SA} mouse hearts differed. PLM^{3SA} FFR gradient in the presence of ISO was shallower than PLM^{3SA} FFR gradient alone but not significantly. PLM^{3SA} gradient is -0.1 ± 0.02mmHg/bpm, n=6 and PLM^{3SA} + ISO gradient is -0.06 ± 0.01mmHg/bpm, n=5.

4.5 Discussion

In this chapter it has been shown that PLM^{3SA} mouse hearts have increased basal cardiac contractility compared with WT when paced at 550bpm. However, unpaced Langendorff studies showed no differences in contractility between genotypes which were shown to have similar LVDP, coronary flow and LVEDP measurements. PLM^{3SA} hearts did show lower heart rates than WT but this was not significant. PLM^{3SA} hearts have a negative FFR, as do WT hearts; however the FFR gradients were not significantly different. The addition of ISO to unpaced preparations caused expected increases in contractility, HR and coronary flow, and a decrease in LVEDP in both genotypes to a similar extent. ISO addition to the FFR has no significant effect on the previously seen negative gradient or coronary flow but does decrease LVEDP in a manner similar to ISO alone.

4.5.1 Basic function

4.5.1.1 Basally paced hearts

Paced cardiac function at 550bpm in the PLM^{3SA} mouse shows significantly increased contractility compared with PLM-WT hearts. This is in keeping with the hypothesis that PLM^{3SA} hearts may have a higher $[Na^+]_i$ at basal pacing rates. It follows that an increased $[Na^+]_i$ would cause an accumulation of intracellular Ca^{2+} via the NCX by forcing the NCX to work in a reverse mode thus removing Na^+ from the cell in exchange for Ca^{2+}.[53] This additional intracellular Ca^{2+} would then contribute to an increased contraction during an action potential compared to WT. Recent studies have suggested that increased Ca^{2+} may also help trigger more SR CICR causing further increases in cardiac contraction.[257, 297] Small changes in cytosolic Na^+ can cause a significant shift in the NCX mode of action. Despa, *et al*, in 2002[11] showed that the NCX stoichiometry renders the reversal potential of the transporter extremely sensitive to cytosolic Na^+ and therefore even small changes in global Na^+ are likely to mediate significant changes in I_{NCX}. Thus, a small increase in intracellular Na^+ can significantly increase the intracellular Ca^{2+} load and compromise diastolic dysfunction. In these studies, a crude index of arrhythmias (the arrhythmia score reflecting ventricular ectopic beats during pacing) did not reveal a significant increase in arrhythmia propensity in PLM^{3SA} hearts.

A rise in intracellular Na^+ may compromise diastolic function and raise LVEDP. Initially LVEDP is set by adjusting the balloon volume but once set; a compromised Ca^{2+} extrusion

could be reflected in an elevated LVEDP, particularly at higher heart rates. However, in these studies LVEDP remained stable and the relationship between LVEDP and heart rate was not different in PLM^{3SA} hearts compared with WT providing no evidence for diastolic dysfunction.

Interestingly, an *in vivo* investigation by our group using echocardiograph (ECHO) measurements showed no difference in basal cardiac function (such as cardiac output, stroke volume etc.) between PLM^{3SA} hearts and PLM-WT hearts which is in contrast to the above paced study findings where a significant basal inotropy was observed. This could be due to the heart *in vivo* being subjected to adaptive autonomic control mechanisms to maintain normal cardiac function and that the Langendorff preparation isolates the heart from this control and can therefore expose the effects of the point mutations directly on cardiac function. Indeed further studies by our group have suggested that PLM^{3SA} mice have a higher parasympathetic control than WT and that sympathetic drive is greatly reduced (unpublished data). *In vivo* this change in autonomic control may compensate for the changes in developed pressures observed in the isolated Langendorff heart.

4.5.1.2 Free-running hearts

Observations made in the unpaced studies mimic those seen *in vivo* with contractility measurements similar in both genotypes. PLM^{3SA} hearts have lower heart rates than WT hearts when perfused on an unpaced Langendorff system, although this was not significant. Heart rates in PLM^{3SA} mice were 50bpm lower than WT littermate controls and decrease over time by the same amount, LVDP falling at a similar rate. It must be noted however, that there are few Langendorff mouse heart studies that are unpaced. This is due to the unpredictable nature of mouse hearts *ex vivo* which are very sensitive to external factors such as temperature and positioning of the intraventricular balloon. *In vivo* heart rates for mice are 500-600bpm[286, 287] however, using the basic Langendorff set-up *ex vivo* heart rates are usually 400bpm or lower in the absence of right atrial superfusion. In the current study heart rates close to 500bpm were observed which is more akin to *in vivo* heart rates but still artificial due to lack of β-adrenergic stimulation, which is known to be basally active *in vivo*. Interestingly though, *in vivo* heart rates have been shown by our group using ECHO to be lower in PLM^{3SA} mice which supports these unpaced study findings.

Arrhythmia score analysis highlights the difficulties that accompany unpaced Langendorff perfusion. Compared to paced Langendorff perfusion there was a significantly greater incidence rate of arrhythmias in unpaced hearts in both WT and PLM^{3SA} hearts. Pacing regulates the heart into a normal rhythm and results from these studies are hence uncomplicated by arrhythmias.

It can be seen that over the 60 minutes of unpaced perfusion heart rate decreases over time as does LVDP and coronary flow. The initial decrease in heart rate was probably due to the wash-out of catecholamines from the heart. When the mouse is anaesthetised there is an associated stress which will be accompanied by the release of catecholamines from the nerve terminals at the SA node manifested in a high heart rate when the heart is first perfused. Over time these catecholamines are washed out. Heart rate has an effect on LVDP, LVEDP and coronary flow therefore these measurements also follow the pattern of heart rate decline over time. The total decline in these measurements was not unexpected as it has previously been documented by Sutherland *et al*, 2000[259] that some decline in Langendorff preparations over time is a certainty and none of the measurements made were significantly decreased with respect to their starting values.

These studies into the basal cardiac function of the PLM^{3SA} hearts raise the question as to why the gain in contractility seen in the paced PLM^{3SA} studies was not seen in the unpaced preparations, and which one is more representative of the *in vivo* situation. As previously stated, ECHO measurements have revealed that cardiac function measurements show no differences between genotypes and that HR is decreased in PLM^{3SA} mice compared with WT. This would suggest that the unpaced study results are more reflective of the *in vivo* situation and that the pacing of hearts to 550bpm may over amplify differences in contractile function.

The maximal unpaced heart rate after 20 minutes of perfusion in PLM^{3SA} mouse hearts was approximately 441bpm, which decreased by 12% over an hour. Perhaps by pacing at 550bpm and reducing the diastolic interval, the time available for Ca^{2+} removal is limited and results in greater contractile function. Therefore when observing the FFR in these hearts increasing heart rate would cause incremental increases in developed pressures when compared with WT; however this was not the case. ISO stimulation should also evoke differences in LVDP by increasing heart rate to the same extent in both genotypes; again this was not the case. Therefore this rate dependent exposure of contractility differences helps strengthen our hypothesis of PLM phosphorylation influencing $[Na^+]_i$. Either PLM^{3SA} hearts have a higher basal $[Na^+]_i$ as previously suggested which would influence Ca^{2+} accumulation via reverse mode

NCX or the faster heart rates will increase Na^+ influx which cannot be extruded as efficiently by unphosphorylatable PLM in the PLM^{3SA} mouse heart and influences Ca^{2+} accumulation and contractility accordingly. Of course this second mode of action may also be influenced by pacing-induced phosphorylation of PLM which would see more efficient handling of increased Na^+ influx in WT compared to PLM^{3SA} hearts and will be discussed in more detail with FFR studies.

4.5.2 Effects of pacing

The force-frequency relationship was first described by Bowditch in 1871 and describes the chronotropic effects on cardiac output and force during a contraction.[281, 298] Changes in force development are directly related to intracellular Ca^{2+} transients[299] and increased frequency of action potentials leads to an influx of Ca^{2+} through the L-type Ca^{2+} channels causing loading of the SR. Increase in frequency will also reduce the time for diastolic relaxation and Ca^{2+} extrusion may be reduced. Additionally, more Ca^{2+} enters the cell via the NCX which is influenced by the increase of $[Na^+]_i$ due to increased Na^+ influx through voltage-gated channels seen with increased heart rate.[298] Calcium handling proteins such as PLB and SERCA may also be affected and may influence Ca^{2+} overload.[282] In theory this increase in SR Ca^{2+} and hence Ca^{2+} transients should cause an increase in force and generate a positive FFR; this is true for large mammals such as humans and dogs[289] where heart rate varies over a 3 fold range and contractile function can double.[300] However for small mammals such as rat and mouse, where there is not the same capability for heart rate and contractility to increase, this relationship *ex vivo* is flat or negative whilst *in vivo* is positive.[8] The cellular mechanism underlying the negative *ex vivo* FFR are complex and the previously reported negative FFR could be the result of experimentation parameters such as unphysiological frequencies used (250 - 400bpm)[292, 296, 301] and temperature. As previously stated there is an intrinsic β-adrenergic tone *in vivo* and studies in conscious mice have shown a predominant sympathetic tone with little parasympathetic input on heart function,[300] therefore frequency stimulation in the absence of β-adrenergic stimulation is a situation that would never occur in a physiological *in vivo* setting and may contribute to this negative FFR seen *in vitro*. A further contributing factor could be the higher resting $[Na^+]_i$ and lower I_{NCX} activation threshold with the shorter action potential found in rats and mice than larger mammals.[41] This causes a net SR Ca^{2+} gain during rest periods and resumption of activation causes a net SR Ca^{2+} loss thereby reducing contractility with increased frequency.[8]

Previous studies in PLM-KO mice within our group have shown FFR with a positive staircase. This was assumed to be due to lower $[Na^+]_i$ from a more active unregulated Na^+/K^+ ATPase pump. It was hypothesised that the PLM^{3SA} mouse may have a higher $[Na^+]_i$ because of the permanent inhibition on the Na^+/K^+ ATPase pump which should cause $[Na^+]_i$ to increase with increasing frequency therefore a negative FFR might be predicted. Indeed the FFR was negative, however was not different to that seen in WT hearts suggesting that if pacing-induced PLM phosphorylation occurs it does not protect the heart against Na^+ or Ca^{2+} overload at high heart rates.

4.5.2.1 Pacing, high heart rate, nitric oxide and PLM phosphorylation

Having established that heart rate may not usually increase *in vivo* in the absence of β-receptor stimulation, there is still reason to propose that pacing-induced increases in heart rate may phosphorylate PLM and increase Na^+/K^+ ATPase activity. Firstly, pacing is known to release noradrenaline from nerve terminals[302, 303] so it is possible at higher heart rates that PLM may be phosphorylated through a classical PKA-dependent pathway. In addition, recent studies by our group, Pavlovic *et al*, 2013,[177] show that pacing induces NO-dependent phosphorylation of PLM by PKC-dependent pathway in AMVM.

If pacing does phosphorylate PLM with respect to the FFR studies, a negative but shallow FFR was expected in WT hearts. However, in PLM^{3SA} hearts since PLM can no longer be phosphorylated a steeper FFR was expected due to the potentially greater rise in $[Na^+]_i$. This was, however, not observed and FFR in WT and PLM^{3SA} hearts had similar FFR gradients.

Additional work by our group using Western blot analysis of paced Langendorff rat hearts show no increased phosphorylation of PLM at any residue with pacing protocols whilst others show phosphorylation (data not shown). Pacing of myocytes (0-3Hz) in the Pavlovic study does not mimic physiological heart rates (~10Hz) and this may account for the lack of phosphorylation in hearts paced at more physiological pacing rates. This may explain why the FFR gradients are equal in these experiments because if PLM is not further phosphorylated during increased pacing in WT hearts then it will be acting in a manner similar to unphosphorylatable PLM and will regulate $[Na^+]_i$ in a similar way.

Pacing induced NO release and subsequent PKA activation in theory should lower LVEDP values due to the lusitropic PKA effects on Troponin I and PLB. However, in these experiments

LVEDP rises as frequency rises. Potentially the reduced time for diastolic relaxation at each frequency, and therefore the reduced time for Ca^{2+} extrusion from the cell, cause SR Ca^{2+} loading which overrides any PKA lusitropic effects by NO activation. This Ca^{2+} load will continue to increase with rate and may cause diastolic dysfunction, indeed at 800bpm some hearts have been seen to go into ventricular fibrillation (VF) as they cannot cope with this Ca^{2+} overload. Future VF threshold experiments may determine any differences in mouse phenotype. However, no differences were observed between genotypes suggesting that PLM phosphorylation in the WT mouse either does not occur (as suggested by the Western blot data) or is unimportant in the regulation of Na^+ and Ca^{2+}.

4.5.3 Effects of catecholamines

A recurring theme throughout these studies is the presence of β-adrenergic stimulation under normal conditions or during physiological changes in heart rate. Therefore it was important to ascertain the effect of β-adrenergic stimulation by perfusing PLM^{3SA} hearts with ISO. As expected, ISO at 1nM and 100nM evoked chronotropic, inotropic and lusitropic effects in WT and PLM^{3SA} hearts. It was a surprise that 1nM ISO increased LVDP to almost the same extent as 100nM ISO however; heart rate was only 40% of heart rate increase seen with 100nM ISO. This could be due to the increase of cAMP and consequently PKA causing enough phosphorylation of E-C coupling proteins to allow maximal LVDP effects at 1nM but the cAMP level, which directly activates the hyperpolarising cAMP nucleotide channels of the SA node to increase heart rate, is not sufficient at 1nM to obtain maximal heart rate effects. Coronary flow increases with both 1nM and 100nM ISO due to the presence of β_2 receptors in smooth muscle. Activation of these receptors causes increased Ca^{2+} efflux with decreased Ca^{2+} influx and this lack of $[Ca^{2+}]_i$ results in a decrease in actin-myosin interactions and the tissue relaxes. This can be seen with the increase in coronary flow at 1nM and 100nM ISO.

The surprising finding in this data set is the lack of differences between PLM-WT and PLM^{3SA} FFR. It was hypothesised that Na^+ may be elevated in PLM^{3SA} hearts particularly in the presence of ISO or when heart rate is elevated by rapid pacing. In WT hearts PLM will be phosphorylated at Ser68 in the presence of ISO and will be able to handle massive increases in contractility and heart rate by having a pump that is able to remove enhanced Na^+ influx[30] which in turn will help control Ca^{2+}. In PLM^{3SA} hearts the lack of phosphorylation at Ser68 and the predicted increase in $[Na^+]_i$ and therefore $[Ca^{2+}]_i$ via the NCX should cause the heart to initially

contract to a greater extent than WT hearts, however this was not the case. Further to this Despa *et al*, 2008, suggested that ISO stimulation induces a delayed decrease in $[Na^+]_i$ in PLM-WT animals due to a lag in the activation of the pump,[32] supported by Wang *et al*, 2010,[361] however when observing changes during 10 minutes of ISO infusion it was seen in WT hearts that developed pressure was maintained throughout and at a similar level to PLM^{3SA} hearts. Perhaps the role of Na^+/K^+ ATPase in the overall ISO stimulated E-C coupling cycle is only small and any differences are obscured by other PKA substrates important to Ca^{2+} handling e.g. PLB, SERCA, L-type Ca^{2+} channels, Ryanodine receptors.

One point of interest was that LVEDP in both mice decreased in the presence of ISO to such an extent to give negative pressure measurements. The lusitropic effect of ISO on end diastolic pressure has been well documented[53, 304] and is due to PKA effects on PLB accelerating SR Ca^{2+} reuptake and troponin I decreasing myofilament sensitivity to Ca^{2+} resulting in faster Ca^{2+} dissociation from troponin C and faster relaxation.[53] What is interesting in these studies is that although LVEDP decreases in both WT and PLM^{3SA} hearts that there was less (non-significant) relaxation in PLM^{3SA} hearts possibly suggesting a higher $[Ca^{2+}]_i$ which in turn may suggest higher $[Na^+]_i$. Of course concluding anything from negative balloon values is not possible but potentially an interesting observation.

Finally, heart rate in both mice increased with ISO, especially with 100nM ISO. As previously discussed, in the mouse heart, LVDP should decrease at higher rates and it was anticipated that this would be particularly marked in PLM^{3SA} mice that have unphosphorylatable Ser68 and therefore no pump activation. This was not seen however due to the fact that β-adrenergic stimulation increases of heart rate will provide a positive FFR as seen during *in vivo* situations.[300]

4.5.4 Effects of pacing and catecholamines

In the studies where the pacing-induced FFR was generated in the presence of low-dose ISO (1nM) negative FFR were observed in both WT and PLM^{3SA} hearts with no differences in FFR gradients. Possibly the concentration of ISO used was insufficient to significantly phosphorylate PLM and changes to Na^+ efflux were too small to affect FFR. However additional data from Western blot studies showed 1nM ISO induces PLM phosphorylation and voltage-clamp studies performed by other members of our group show 1nM ISO can stimulate

pump current in isolated myocytes (data not shown). It is clear, however, that 1nM ISO did not replicate the positive FFR observed in PLM-KO hearts – perhaps suggesting that 1nM ISO does not stimulate the pump to the same degree as PLM deletion. It would have been interesting to repeat these FFR studies with higher ISO concentrations to see if the negative staircase could be converted to a positive one. However, in these pacing-induced FFR it was not possible to investigate higher ISO concentrations as the concomitant chronotropic effects cause escape rhythms which preclude adequate pacing, particularly at the lower frequencies. The data from free-running hearts (Figure 4.6 to Figure 4.8) however shows that a higher ISO concentration (100nM) elevates heart rate and contraction similarly in both PLM^{3SA} and WT hearts suggesting that the inotropic response to ISO (and elevated heart rate) is not moderated by rendering PLM unphosphorylatable.

The slope of the FFR gradients for WT hearts with and without 1nM ISO were identical. The only difference observed in the LVDP gradients was with PLM^{3SA} hearts which showed a reduced FFR slope with 1nM ISO. Again this is difficult to explain as it was expected that $[Na^+]_i$ would be increased with combined ISO and pacing stimulus protocols and should therefore be dramatically steeper than without ISO. These results again highlight that ISO effects on Langendorff hearts are mainly via direct Ca^{2+} handling proteins which can override and compensate for any changes in $[Na^+]_i$.

The difficulty in interpreting the data in this chapter emphasises the need for measurement of intracellular Na^+ in isolated hearts beating at physiological rates and temperatures.

4.6 Summary

It was hypothesised that PLM^{3SA} mouse hearts may exhibit a normal or increased $[Na^+]_i$ due to permanent pump inhibition which in turn would favour an increase in $[Ca^{2+}]_i$ via the NCX, loading the SR stores and causing a greater inotropic effect than in PLM-WT hearts. An increased basal contractility was seen in paced hearts. In unpaced studies, the decrease in intrinsic heart rate of PLM^{3SA} hearts may allow developed pressures to be comparable to WT which may be the case *in vivo* to allow the mouse to function normally. There are a number of possible explanations for the lack of a genotypic effect on the FFR:

1. In the absence of β-receptor stimulation PLM phosphorylation does not change in the WT heart and hence Na^+ influx, Na^+ extrusion and $[Na^+]_i$ are similar in both genotypes.

2. $[Na^+]_i$ may be different in the 2 genotypes but Na^+ plays a limited role in influencing contractility (this seems unlikely given the known effects of Na^+ elevation).

3. Na^+ extrusion is different between the genotypes but other E-C coupling mechanisms have adapted and compensated to give no net effect.

4. In the presence of β-receptor stimulation, PLM is phosphorylated in WT but not the PLM^{3SA} mouse but again, either (a) this does not affect $[Na^+]_i$, (b) affects $[Na^+]_i$ but $[Na^+]_i$ is unimportant in determining contractility or (c) the effects of Na^+ handling are swamped by the altered regulation of other E-C coupling targets of PKA phosphorylation.

On the basis of the data presented in this chapter it is difficult to distinguish between these possibilities. These data do, however, emphasis that for a better understanding of the PLM^{3SA} mouse, it is essential that methods are developed to measure $[Na^+]_i$ at physiological heart rates and temperatures.

5 CHAPTER 5 –MEASUREMENT OF $[Na^+]_i$ IN PLM^{3SA} MOUSE HEARTS USING FLAME PHOTOMETRY

5.1 Introduction

Data in the previous chapter indicates the importance of measuring intracellular Na^+ concentration in PLM-WT and PLM^{3SA} mouse hearts under basal and stressed conditions. The "gold-standard" for measuring $[Na^+]_i$ at physiological heart rates and temperatures is ^{23}Na NMR and the use of this technique is one of the eventual objectives of this thesis. However, at the time of the experiments within this chapter, the ^{23}Na mouse coil was still in development. Therefore an alternative way of measuring $[Na^+]_i$ in PLM-WT and PLM^{3SA} mouse hearts was required.

5.1.1 Measurement of Intracellular Na^+

There are several methods for measuring intracellular Na^+; the most frequently used are listed below. The different methods are discussed briefly with their relative merits.

- *SBFI (Sodium-binding Benzofuran Isophthalate)*
- *Ion-selective electrodes*
- *^{23}Na NMR*
- *Flame Photometry*

5.1.1.1 SBFI

SBFI is a dual excitation ratiometric fluorescent dye whose fluorescence changes as a function of Na^+ concentration.[305] SBFI, once inside the cell, binds to Na^+ ions by the presence of a crown ether chelator linked to the fluorophore. The selectivity of the dye for Na^+ is due to the size of the cavity on the chelator and although K^+ can bind, SBFI is 18 fold more selective for Na^+ over K^+. Once Na^+ is bound, the fluorescent yield of the dye increases resulting in a narrower excitation peak which is also shifted to shorter wavelengths. This changes the ratio of fluorescence intensities excited at 340/380nm and allows calculation of the amount of Na^+

present in the cell. SBFI is a reliable technique for Na^+ measurements in isolated cardiac myocytes[7] and in the PLM field SBFI has been used to indicate the intracellular Na^+ concentration in PLM-WT and PLM-KO myocytes with/without ISO.[28, 32] The advantages with this technique are that it does not damage the tissue and it is possible to measure $[Na^+]_i$ changes over time. However, although this technique has been used extensively in single cells, its use in whole tissues such as Langendorff hearts has been limited.[306] The main limitations are that the SBFI dye leaks from the cell rapidly at 37°C in paced myocytes. It has therefore been almost exclusively used in quiescent cells at room temperature. Hence it is unsuitable for measuring $[Na^+]_i$ at 37°C at physiological pacing rates (5-10Hz).

5.1.1.2 Ion-selective electrodes

Ion-selective electrodes are an alternative way of measuring cations in solution[307] and consist of an ion-sensitive membrane (ion-exchange glass or Na^+ ionophore) that is exposed to the ion of investigation in solution on one side and on the other, a solution of known ion activity which is in contact with a reference electrode e.g. Ag^+/AgCl. A potential is set up across this semi-permeable membrane according to the Nernst equation and this potential can be measured by a voltmeter. The recorded voltage gives an indication of the ion concentration. Although these electrodes can be highly selective for the ion of interest and provide measurements without tissue destruction they are difficult to use, have high impedance and require double-junction electrodes (or double-barrelled structure) to allow simultaneous recording of membrane potential.[308-309] Consequently they are inherently unstable and unsuitable for use in contracting and moving preparations such as cardiac tissue paced at physiological rates and temperatures.

5.1.1.3 ^{23}Na NMR

In this thesis ^{23}Na NMR in a perfused mouse heart was considered to be the optimal method for measuring intracellular Na^+ in hearts beating at physiological rates at 37°C and will be discussed further in Chapter 6. However, at the start of these studies, ^{23}Na NMR was not available and therefore the appropriateness of flame photometry as a method for estimating intracellular Na^+ in beating hearts was investigated.

5.1.1.4 Flame photometry

The need to obtain quantitative measures of both Na^+ and K^+ in biological samples without the necessity of chemical separation led to the development of the flame photometer. The concept for flame photometry was first devised by Lundegardh circa 1929[310, 311] when he developed a basic piece of apparatus that fired cations in solution into a flame producing spectra that were photographed and compared to known spectra from standard solutions. In the mid 1940's more sophisticated instruments were developed in which the light produced from the flame was passed through optical filters onto a photosensitive element and the resultant current was measured.[312, 313] Today models are slightly more sophisticated again but all work on the same basic principle of emission spectroscopy.

Flame photometry relies on the fact that alkali metals, such as Na^+ and K^+, when drawn into a non-luminous flame will ionise and absorb energy from the flame causing the atoms to excite to a new energy state. As these atoms decay back to the unexcited ground state they emit light of a characteristic wavelength for each atom determined by the Planck-Einstein relationship. For example Na^+ emits light at a wavelength of 589nm which to the naked eye appears as orange and K^+ emits light at a wavelength of 766nm which is seen as a purple light. A photocell detects the intensity of the emitted light and converts it to a voltage which can then be recorded and related to the concentration of the ion present. As ions emit light at different wavelengths, filters can be used to isolate individual emission signals in the same sample.

5.1.1.5 Flame photometry disadvantages

Flame photometers use the most basic form of emission spectroscopy to determine the ionic content of a solution, i.e. the energy from alkali metals is of a low excitation magnitude and will not exceed the energy from the flame thus keeping spectra simple to detect and analyse. However, this in itself provides many disadvantages. For example the light intensity from the flame will be affected by the fuel used, rate of flow and pressure of gas to the photometer and the rate of nebulisation of the sample into the flame.[314] Flame photometry also requires full tissue destruction and adequate washout of the extracellular ion[305] but this can be controlled for. The other issue is that flame photometers respond linearly to an ion over a very small concentration range, especially in the case of Na^+. Therefore extreme dilutions of the sample may be required to obtain a reading on the appropriate scale.

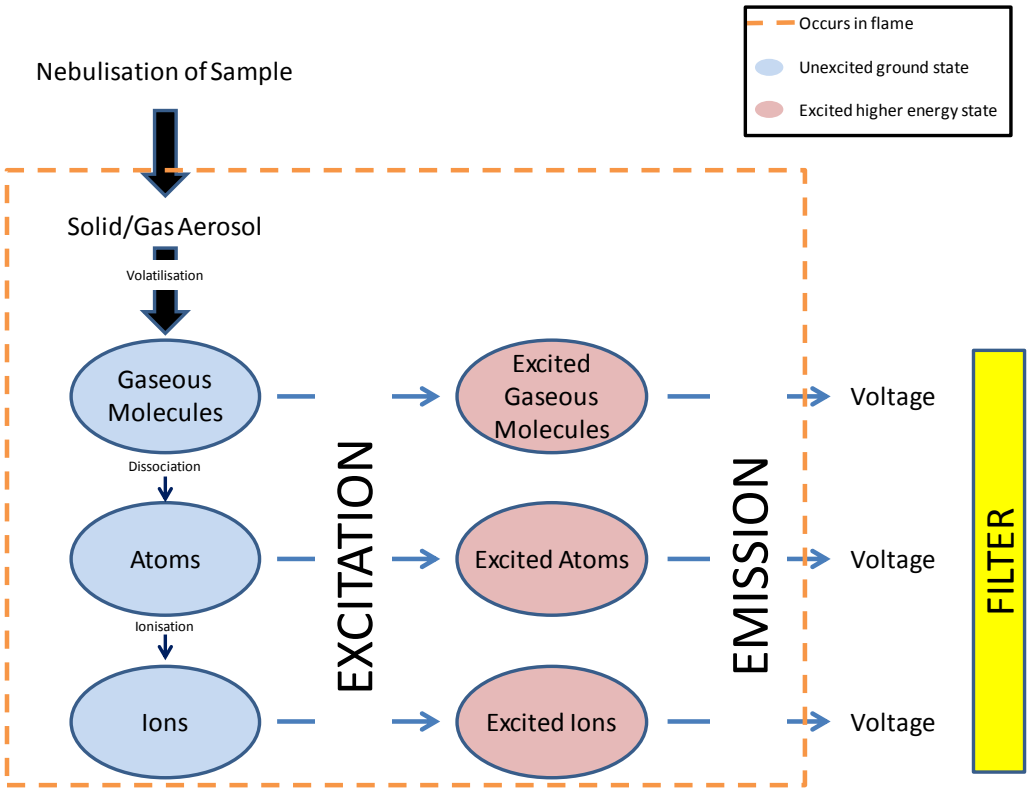

Figure 5.1: Schematic representation of how a flame photometer works.
Unexcited molecule/atoms/ions in solution are excited by passing through a non-luminous flame reaching a new energy state. As they return to the ground energy state they emit light of a characteristic wavelength that is detected by a photocell, converted to a voltage and measured by a voltmeter. The use of filters allows differentiation between ions.

5.1.2 Intracellular Na^+ in PLM-WT and PLM^{3SA} hearts

Flame photometry was used to measure basal intracellular Na^+ from Langendorff perfused PLM-WT and PLM^{3SA} mouse hearts paced at the physiological rate of 550bpm. Previous studies using SBFI measurements in PLM-KO myocytes at rest have shown that $[Na^+]_i$ is comparable to WT (PLM-WT: 12.5±1.8mM; PLM-KO: 12.0±1.5mM)[28] and was attributed to compensation by lower expression of Na^+/K^+ ATPase α subunit. Therefore, it is possible that the decreased PLM expression in PLM^{3SA} mouse hearts compared to WT (Chapter 3 Section 3.4.2.2), may compensate for reduced net activity and intracellular Na^+ may remain normal (as perhaps suggested by similar FFRs in WT and PLM^{3SA} hearts). Alternatively, it is possible that unphosphorylatable PLM may lead to elevations in $[Na^+]_i$ when hearts are rapidly paced or exposed to ISO.

Since the objective of these experiments was to investigate the effect of ISO on basal Na^+ (in the absence of changes in influx secondary to increases in heart rate) these experiments were all performed in hearts paced at 550bpm. The ISO concentration selected has inotropic and chronotropic effects and phosphorylates PLM but that was not so high as to lead to escape rhythms in hearts paced at 550bpm. Accordingly 10nM ISO was used in these experiments. It was hypothesised that ISO may cause a decrease in $[Na^+]_i$ in WT hearts compared to control due to Ser68 PLM phosphorylation and pump activation[28] whilst in PLM^{3SA} hearts which cannot regulate Na^+/K^+ ATPase Na^+ would remain unchanged.

Rapid pacing (800bpm) and ouabain interventions were also investigated for their effects on $[Na^+]_i$. It was hypothesised that both rapid pacing and ouabain should increase $[Na^+]_i$.[1, 8] Ouabain was used as a positive control for $[Na^+]_i$ and although mouse and rat hearts express ouabain-resistant Na^+/K^+ ATPase α subunits, a submaximal ouabain concentration was used in these experiments. 50μM ouabain was chosen as a concentration that induced a substantial inotropy (assumed to be due to rises in $[Na^+]_i$[315, 316]) but was not so high as to cause an irreversible contracture.[317-319] For each experiment PLM^{3SA} was compared to WT littermates.

5.1.3 Rubidium uptake in PLM-WT and PLM^{3SA} hearts

Flame photometry has been used extensively to quantitatively measure the K^+ content in biological solutions.[314] There are 3 significant routes of K^+ efflux from the cell shown in Figure 5.2; voltage-gated K^+ channels, ligand gated ATP sensitive channels (K_{ATP}) which are activated in response to metabolic stress and the possible reverse mode $Na^+/K^+/2Cl^-$ co-transporter. There is only 1 major route of K^+ influx though and this is via the Na^+/K^+ ATPase with a small contribution from $Na^+/K^+/2Cl^-$ co-transporter operating in its forward mode.

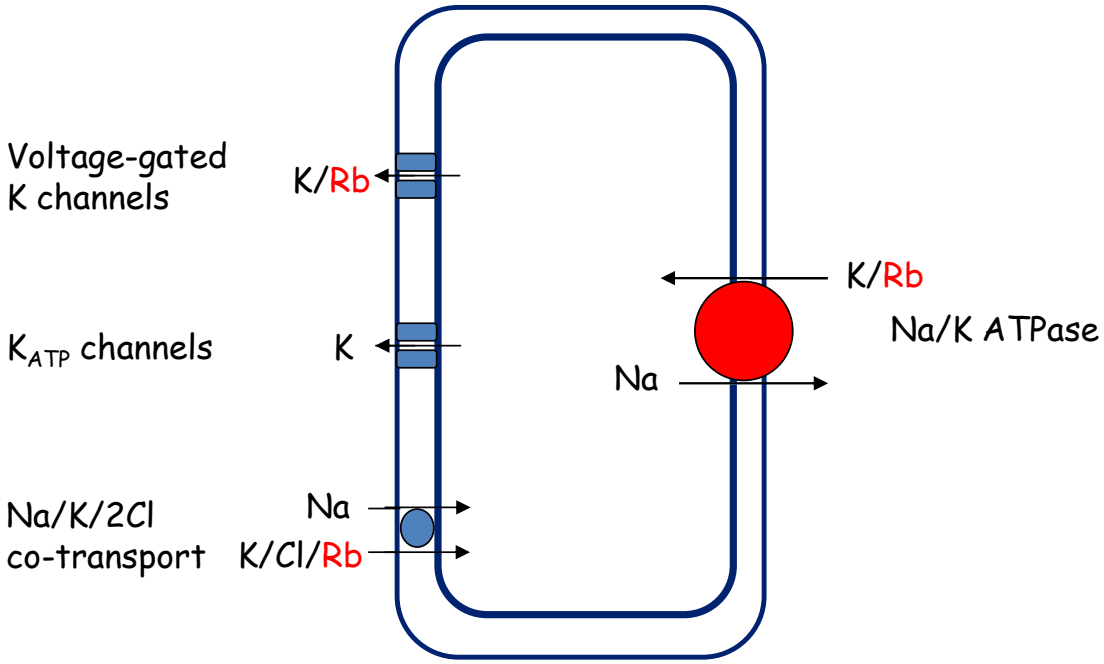

Figure 5.2: Schematic representation of major K^+/Rb^+ transport routes in the cell. Diagram showing major routes of K^+ influx and efflux with those that can be utilised by Rb^+ highlighted in red. $Na^+/K^+/2Cl^-$ can act in forward or reverse mode bringing K^+ into or out of the cell. K_{ATP} channels are activated in response to metabolic stress so under normal physiological conditions are not activated. Adapted from Kupriyanov *et al*, 2004.[320]

K^+ efflux from cells is quantitatively significant and will vary with activity and activation of cell signalling pathways. Thus, as an index of Na^+/K^+ pump function, measuring K^+ uptake (complicated by possible changes in K^+ efflux) is of limited value. However, Rb^+ is a K^+ congener[321] and can substitute for K^+ in the Na^+/K^+ ATPase transport cycle (see Figure 5.2). Since Rb^+ is not naturally occurring (i.e. there is no endogenous intracellular Rb^+) then Rb^+ influx is at least initially (before the cells load with Rb^+) a good index of Na^+/K^+ ATPase activity. This can be done using radioactive Rb^+ (typically ^{86}Rb) or as has been done in these experiments, by measuring tissue content after exposure to Rb^+-containing solutions.

In radioactivity studies ^{86}Rb is commonly used due to its similarity to ^{37}K, it has the same net charge and covalent radius but the half-life is significantly longer at 18.55 days. This isotope has been used in many membrane transport studies involving many different tissue types including erythrocytes, cerebral vessels and skeletal muscle.[322-325] Other studies using NMR have used the quadrupolar active isotope nuclei ^{87}Rb to look at influx rates for example in

perfused rat hearts.[326] Finally, many studies have also used non-radioactive rubidium or caesium and lithium as external activators of the pump to study Na^+/K^+ ATPase mechanisms.[327-329]

Rb^+, despite being twice the atomic weight of K^+, has a similar hydrated ionic radius (Rb^+: 2.93 Å; K^+: 2.76K Å) which determines biological properties of ions.[330] When considering substituting K^+ for Rb^+ the affinity and kinetic properties with respect to Na^+/K^+ ATPase and whether it would be able to activate the pump at the same rate must be taken into account. Work by Beauge *et al*, in 1968,[331] in red blood cells suggests that Rb^+ activates the pump with similar uptake rates as K^+ and other work has supported this in cardiomyocytes.[332-335] Beauge *et al*,[331] also showed that ouabain shifts the Rb^+ uptake curve to the left indicating the block of the pump by ouabain reduces Rb^+ uptake as may be predicted.

Rb^+ uptake has therefore been used as an index of Na^+/K^+ ATPase activity in WT and PLM^{3SA} hearts subjected to a variety of protocols.

5.2 Aims

The aims of the studies undertaken in this chapter were to:

1. Determine appropriate experimental parameters for digestion of Langendorff perfused hearts for use in subsequent flame photometry experiments.
2. Investigate intracellular Na^+ content during basal pacing conditions (550bpm) in PLM^{3SA} mice and littermate controls.
3. Investigate the effect of rapid pacing, ISO and ouabain perfusion on intracellular Na^+ in PLM^{3SA} and WT mouse hearts.
4. Determine the Rb^+ uptake during basally paced heart perfusion in both genotypes.
5. And finally determine the effect of rapid pacing, ISO and ouabain perfusion on Rb^+ uptake in PLM^{3SA} and WT littermate hearts.

5.3 Methods

5.3.1 Intracellular Na^+ in PLM-WT and PLM^{3SA} hearts

As described in general methods (Chapter 2, Section 2.3.3), hearts were excised from PLM-WT and PLM^{3SA} mice and cannulated for standard Langendorff perfusion. Following 20 minutes of paced Langendorff aerobic perfusion at 550bpm with standard KHB (see Chapter 2 Table 2.3), hearts were subjected to either:

- 10 minutes perfusion paced at 550bpm with standard KHB,
- 10 minutes perfusion paced at 550bpm with KHB + 10nM ISO,
- 10 minutes perfusion paced at 550bpm with KHB + 50µM ouabain or
- 10 minutes perfusion paced at 800bpm with standard KHB.

A washout of extracellular Na^+ was performed to ensure only intracellular Na^+ content was measured by flame photometry. Hearts were perfused with a mannitol based Na-free buffer for 40 seconds (for details see Chapter 2 Table 2.5) following the above interventions. Hearts were cut down, blotted and quickly snap frozen in liquid N_2 and dried for 16 hours at 80°C and weighed before being digested with 50% trifluoroacetic acid (TFA).[266] Analysis of heart samples using the flame photometer (Section 2.8) calibrated to a NaCl standard curve was then performed.

5.3.2 Rb^+ uptake in PLM-WT and PLM^{3SA} hearts

Following 20 minutes of paced Langendorff perfusion at 550bpm as above, hearts were perfused with K^+-free Rb^+-KHB[336] (see Chapter 2 Table 2.4) for 10 minutes before being subjected to either:

- 10 minutes perfusion paced at 550bpm with K^+-free Rb^+-KHB,
- 10 minutes perfusion paced at 550bpm with K^+-free Rb^+-KHB + 10nM ISO,
- 10 minutes perfusion paced at 550bpm with K^+-free Rb^+-KHB + 50µM ouabain or
- 10 minutes perfusion paced at 800bpm with K^+-free Rb^+-KHB.

To ensure washout of any extracellular Rb^+, hearts were perfused with standard KHB for 40 seconds following the above interventions. Bumetanide (BM) was present in all the K^+-free Rb^+-KHB perfusion buffers to block the $Na^+/K^+/2Cl^-$ co-transporter ensuring that any Rb^+

uptake was solely due to the Na^+/K^+ ATPase.[337-341] Control WT hearts were perfused with BM-free Rb^+-KHB to measure additional Rb^+ taken up by $Na^+/K^+/2Cl^-$ co-transporter (as shown in Figure 5.7). Hearts were again dried for 16 hours at 80^{o}C and weighed before being digested with 50% TFA and analysed using the flame photometer calibrated to an RbCl standard curve.

5.3.3 Flame photometry operation

The Sherwood Scientific Model 410 Classic Flame Photometer was set-up in accordance with manufacturer's directions (see Chapter 2, Section 2.8.3). The system was primed with natural gas (hydrocarbon gas containing methane and CO_2) and adjusted for optimum gain. Standard curves were constructed for Na^+ or Rb^+ using dilutions of NaCl or RbCl in the global diluent (ddH_2O) and correct flame photometer filters for Na^+ or Rb^+. The top standard curve concentration of each ion was set to an appropriate value on the flame photometer and subsequent concentrations were simply read off and noted. A standard curve was constructed. Digested heart samples were spun at 15000 x *g* for 10 minutes and diluted appropriately for the standard curve (see Chapter 2, Section 2.8.4 - 2.8.5). Samples were aspirated through the nebuliser into the flame and recordings allowed to stabilise for 20 seconds (due to fluctuation of flame photometer measurements) and the highest reading was recorded over the following 10 seconds.

5.4 Results

5.4.1 Heart digestion and ion extraction

Many of the methods used for flame photometry with whole heart samples require digestion of the tissue for at least 12-24 hours.[342] However, this has rarely been evaluated and certainly not documented, and so whilst optimising the methods for the following experiments it was decided to test whether a shorter extraction time could be used. Comparison of 1 hour and 24 hour digestion was done on hearts digested in 50% trifluoroacetic acid and then measured using the flame photometer. Heart digestion optimisation was performed using hearts from the Rb^+ uptake study. Figure 5.3A shows the Rb^+ standard curve that was used to estimate Rb^+ concentrations in each sample. As previously discussed, the flame photometer provides an almost 1:1 measure of an ion if it is present in the correct linear range. As can be seen in Figure 5.3A Rb^+ has a large concentration range where the ion has a linear correlation (0–50mM RbCl). The fit of the line, r^2, is 0.99 showing a good correlation between Rb^+ concentration and flame photometer reading. This was considered an appropriate scale to use for all further Rb^+ experiments.

Initially it can be seen in Figure 5.3B that 1 hour digestion in 50% TFA provides a considerable Rb^+ signal compared to control hearts which have been perfused with Rb^+-free KHB. Comparison of Rb^+ signals from hearts digested for 1 and 24 hours show almost identical signal magnitude (1 hour digestion: 23.09 ± 1.2AU Rb, n=7; 24 hour digestion: 23.34 ± 1.2AU, n=7), see Figure 5.3C, suggesting no further Rb^+ extraction following an additional 23 hours of digestion. However, although it appears that all of the Rb^+ can be extracted within 1 hour, at this time point the sample remains undigested with a large insoluble pellet and suspended large particles. These block the nebuliser of the flame photometer resulting in problems with the measurements and increased variability. After 24 hours digestion, although no further Rb^+ is extracted, the sample is more homogeneous with a much smaller insoluble fraction. It was therefore decided to use a 24 hour extraction protocol.

As a further quality control it was confirmed that 24 hour digestion extracts all Rb^+ to be measured. The solid remnants from the 24 hour digestion were re-digested in fresh 50% TFA and, as can be seen in Figure 5.3D there was no further Rb^+ extraction. These findings provided the basis for defining future protocols. That is, hearts were digested for 24 hours in 50% TFA before being measured by the flame photometer.

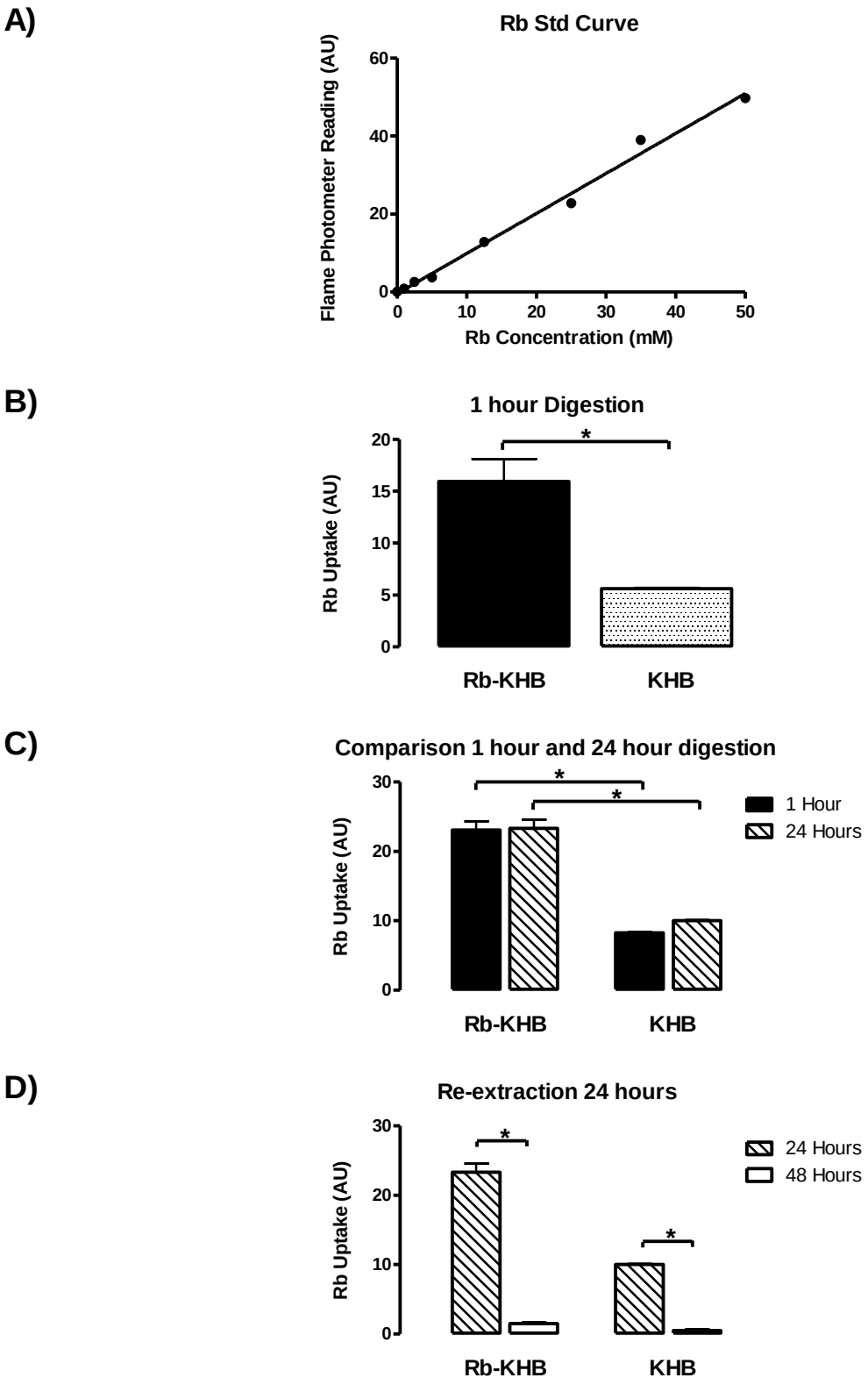

Figure 5.3: Determination of parameters for heart digestion in future experiments. A) RbCl std curve; B) 1hr digestion comparison between Rb^+-KHB and KHB hearts; C) Comparison of 1hr and 24hr digestion with Rb^+-KHB and KHB hearts; D) 24hr re-extraction of Rb^+-KHB and KHB hearts. n=3-7. All data expressed as mean±sem and analysed by one-way ANOVA and Student's *t*-test, $P<0.05$ was considered significant and denoted by *.

5.4.2 Extracellular washout period

A requirement of the flame photometry method is that all extracellular Na^+ or Rb^+ is washed out of the hearts before freezing. Flame photometry will measure all ions present in the heart sample at the time of digestion therefore residual ions from the extracellular space would be measured also. The length of time of the washout period is critical, too short a Na^+ (or Rb^+) free extracellular washout will leave residual contaminant ions which will add to the estimate of the intracellular ion content. Conversely, too long a washout and the reversal of the transmembrane gradient will result in Na^+ (or Rb^+) being lost from the intracellular compartment. The balance between extracellular wash out and intracellular loss is a fine one and therefore the correct extracellular washout period had to be determined for each ion. Effluent from the hearts during the washout perfusion period was collected in 10 second aliquots and analysed using flame photometry for both Rb^+ and Na^+. It can be seen in Figure 5.4 that the rate of loss for both Rb^+ and Na^+ was similar and started to plateau towards the end of the 40 second washout period. It can be concluded that 40 seconds is an adequate washout period to remove extracellular Rb^+/Na^+ without removing intracellular ions and should help give an accurate measure of the amount of Na^+ or Rb^+ content in the cells during each intervention.

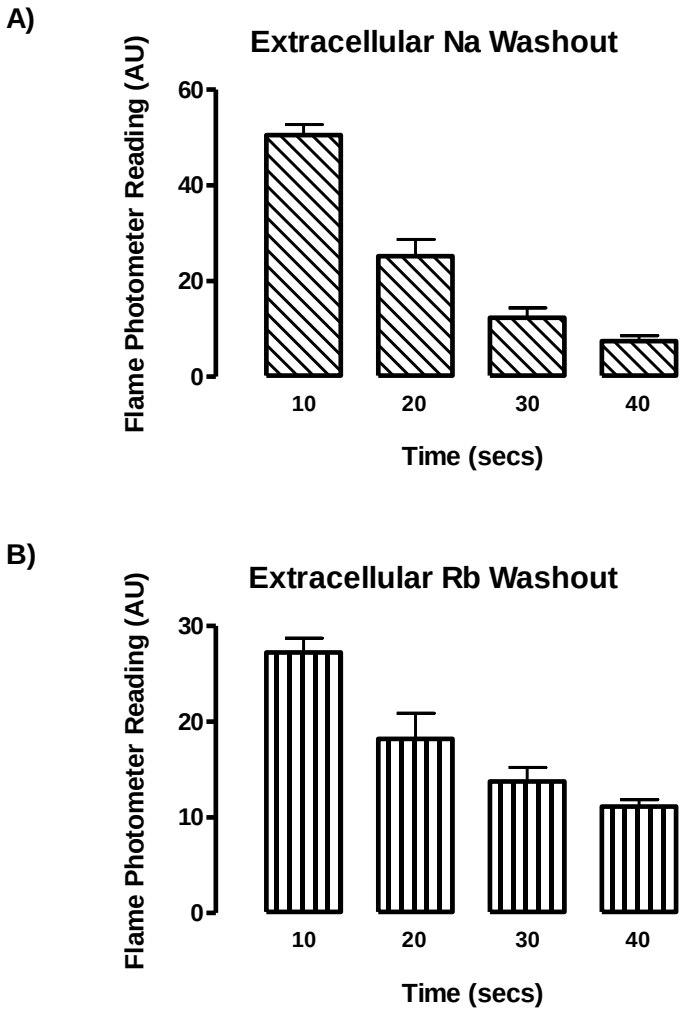

Figure 5.4: Determination of appropriate extracellular washout periods for Na^+ and Rb^+ measured from coronary effluent collected during sequential 10 second intervals. A) Rate of extracellular Na^+ loss; B) Rate of extracellular Rb^+ loss. n=6.

5.4.3 Intracellular Na^+ in PLM-WT and PLM^{3SA} mouse hearts

It is widely accepted that the linear range for Na^+ using the flame photometer is very narrow (0.5 to 10ppm) due to Na^+ self-absorption at higher values. Therefore samples were highly diluted to be able to measure Na^+ which may introduce inaccuracies and errors. It can be seen in Figure 5.5A that the Na^+ standard curve quickly becomes non-linear at moderately low concentrations (<5mM NaCl). To obtain a 1:1 relationship between signal and ion concentration the standard curve used is <1mM in range. Figure 5.5B shows the standard curve at the linear range for Na^+ ions, $r^2 = 0.9966$ showing a good correlation.

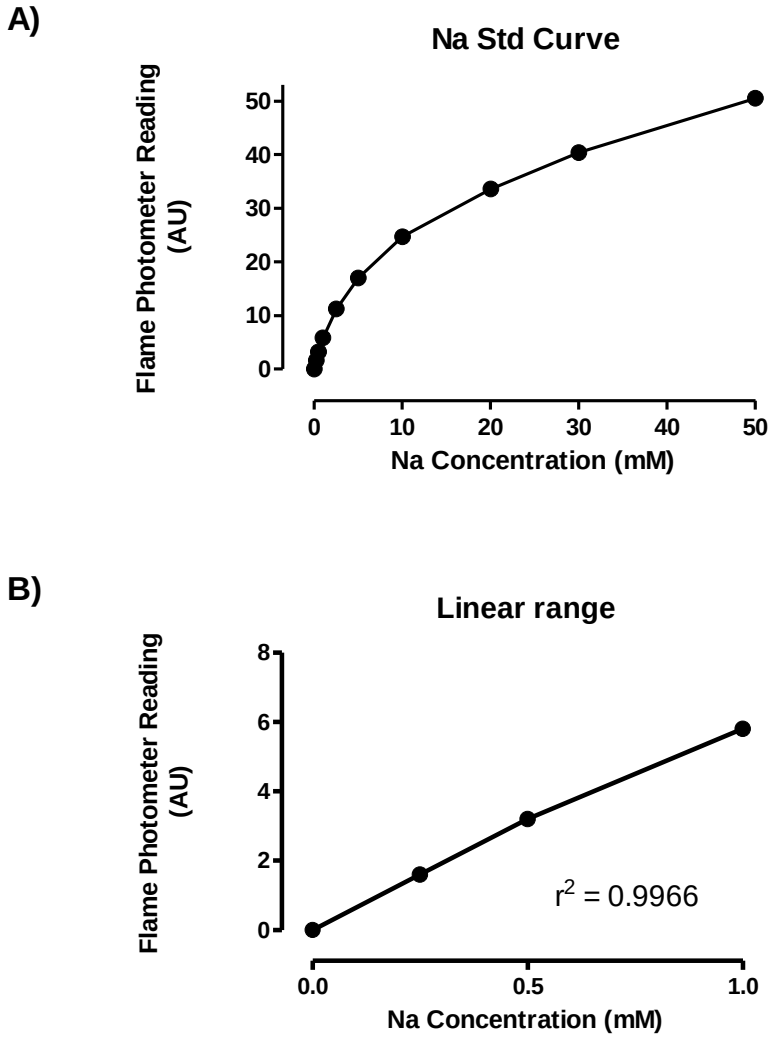

Figure 5.5: Determination of NaCl standard curve over a linear range for Na^+.
A) NaCl standard curve over 0-50mM range; B) NaCl standard curve over linear range 0-1mM.

Cardiac function profiles (not shown) when hearts were perfused with ISO or rapidly paced at 800bpm match those previously seen in this thesis (Chapter 4, Section 4.4.3 and 4.4.4). ISO caused an inotropic response, however any chronotropic response was masked by the continuous pacing of the hearts at 550bpm from which there were few escape rhythms. Rapid pacing at 800bpm was associated with a decrease in LVDP accompanied by an increase in LVEDP as previously seen in FFR for lower heart rates. Ouabain induced a positive inotropic response as expected.[317, 343-345] While 50μM ouabain will not completely block the α1 subunit of

the rat (or mouse) Na^+/K^+ ATPase[346] this concentration was used as it induced a clear positive inotropy without a significant rise in LVEDP.

Figure 5.6 shows the intracellular Na^+ content measured following these protocols by the flame photometer. The results show that there was no significant difference between intracellular Na^+ content in PLM-WT and PLM^{3SA} mouse hearts at basal pacing rate of 550bpm (PLM-WT: 3.02 ± 0.24AU; PLM^{3SA}: 3.6 ± 0.9AU, n=4-8). There were also no significant differences between intracellular Na^+ measurements in PLM-WT and PLM^{3SA} hearts following ISO, 800bpm rapid pacing or ouabain interventions. Intracellular Na^+ content appears to be lower than control values with ISO perfusion for both genotypes but this was non-significant. Also intracellular Na^+ content appears to be marginally greater than control values for both genotypes with ouabain perfusion, but again this was non-significant.

The failure to detect any significant increases in intracellular Na^+ using this technique raises the possibility that this technique has insufficient resolution to detect even the large changes that might be expected with ouabain or rapid pacing. The reasons for this are discussed in more detail in the discussion section of this chapter. However, the lack of resolution of this technique led to the consideration of Rb^+ uptake as another surrogate method for estimating Na^+/K^+ ATPase function.

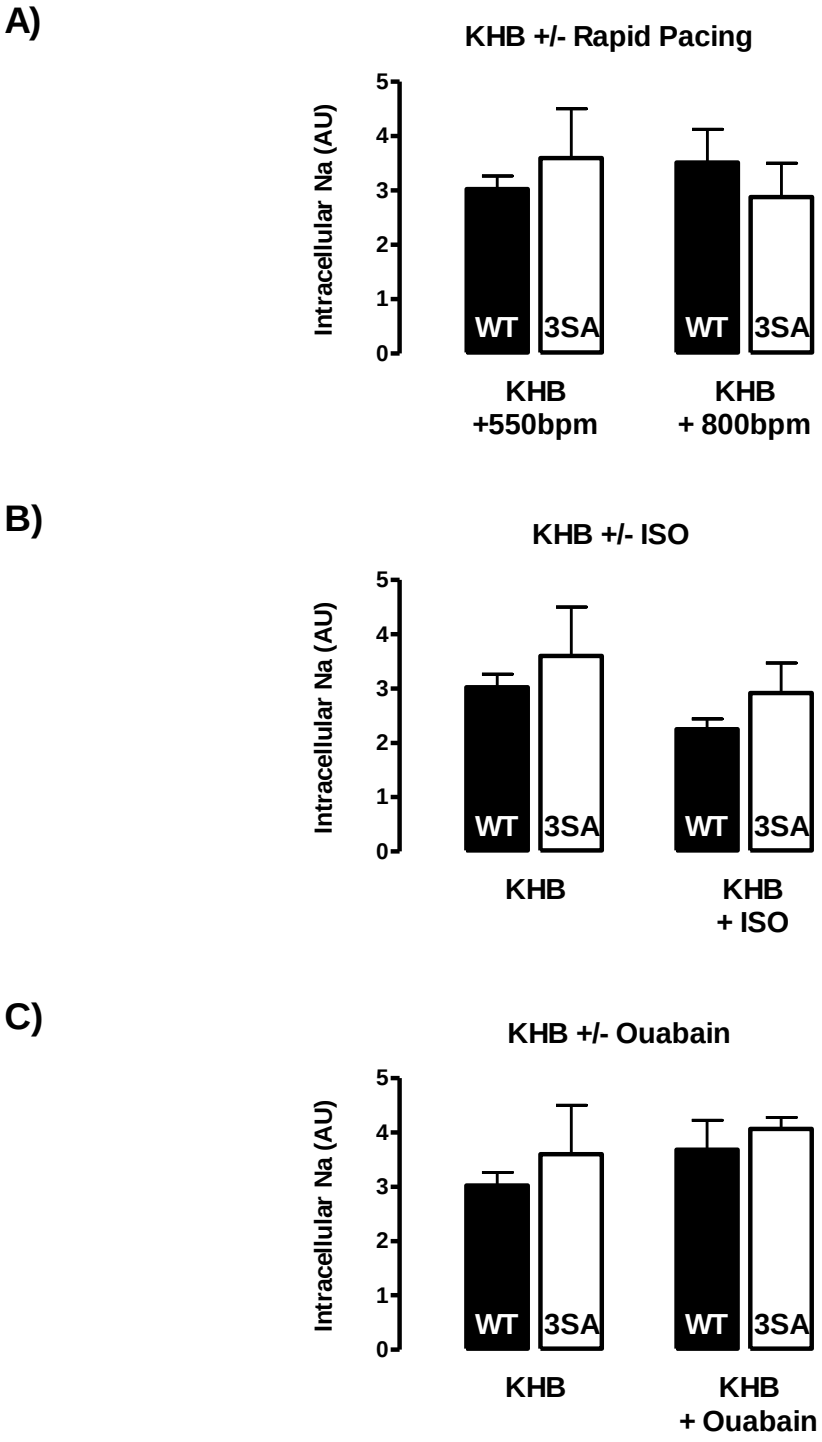

Figure 5.6: Flame photometer results for intracellular Na^+ content during different interventions comparing WT and PLM^{3SA} mouse hearts.
A) Rapidly paced (800bpm) intracellular Na^+ changes; B) 10nM ISO intracellular Na^+ changes; C) 50µM ouabain intracellular Na^+ changes. n=5-8. All data expressed as mean±sem and analysed by two-way ANOVA followed by Bonferroni post-hoc test, $P<0.05$ was considered significant.

5.4.4 Rb^+ uptake in PLM-WT and PLM^{3SA} mouse hearts

Similar RbCl standard curves to those previously shown in Figure 5.3A were used for flame photometer calibration in these experiments. When investigating Rb^+ uptake it is on the premise that $2K^+$ are exchanged for $3Na^+$ using the energy from the hydrolysis of one ATP molecule. If K^+ is replaced with Rb^+, an analogue ion, it can be assumed that any Rb^+ that exists intracellularly is due to uptake by the Na^+/K^+ ATPase pump. There is only one other way that Rb^+ could be taken up into the cell under normal physiological conditions and this is by the $Na^+/K^+/2Cl^-$ co-transporter. Therefore BM was added to Rb-KHB to block this pathway and its effect on Rb^+ uptake was measured in control hearts. It can be seen in Figure 5.7 that BM had only a small non-significant effect on Rb^+ uptake. However, in order to minimise the possibility that this admittedly small pathway could increase its contribution under different experimental conditions, BM was added to all perfusion buffers used in this series of studies.

Perfusion with Rb-KHB itself influenced LVDP, coronary flow and LVEDP. It is clear that Rb^+ exerts effects that are distinct from those of K^+ as switching from equimolar K^+ to Rb^+ perfusate induced transient effects (see Figure 5.8). LVDP initially rose in PLM^{3SA} hearts whilst decreasing in PLM-WT hearts which were significantly different from each other 3 minutes from the start of Rb^+-KHB perfusion. By the end of the Rb^+-KHB only perfusion period, LVDP in both genotypes had normalised to values similar to pre-Rb^+-KHB perfusion. Coronary flow and LVEDP followed a similar time-course to that of developed pressure changes with an increase in both parameters but identically in both genotypes. Both parameters had returned to baseline measurements by the end of the Rb^+-KHB only perfusion period showing that although K^+ substitution with Rb^+ exerted effects, they were transient.

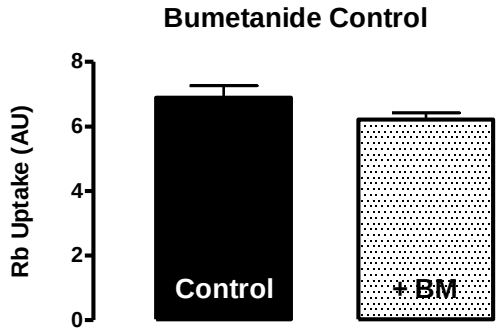

Figure 5.7: Effect of bumetanide on Rb^+ uptake in PLM-WT hearts.
Following a KHB stabilisation period, WT hearts were perfused with Rb^+-KHB +/-BM for 10 minutes before a subsequent 40 second extracellular washout and snap freezing in liquid nitrogen. Hearts were digested and analysed using the flame photometer with an Rb^+ filter. n=6. All data expressed at mean±sem and analysed by Student's *t*-test, $P<0.05$ was considered significant.

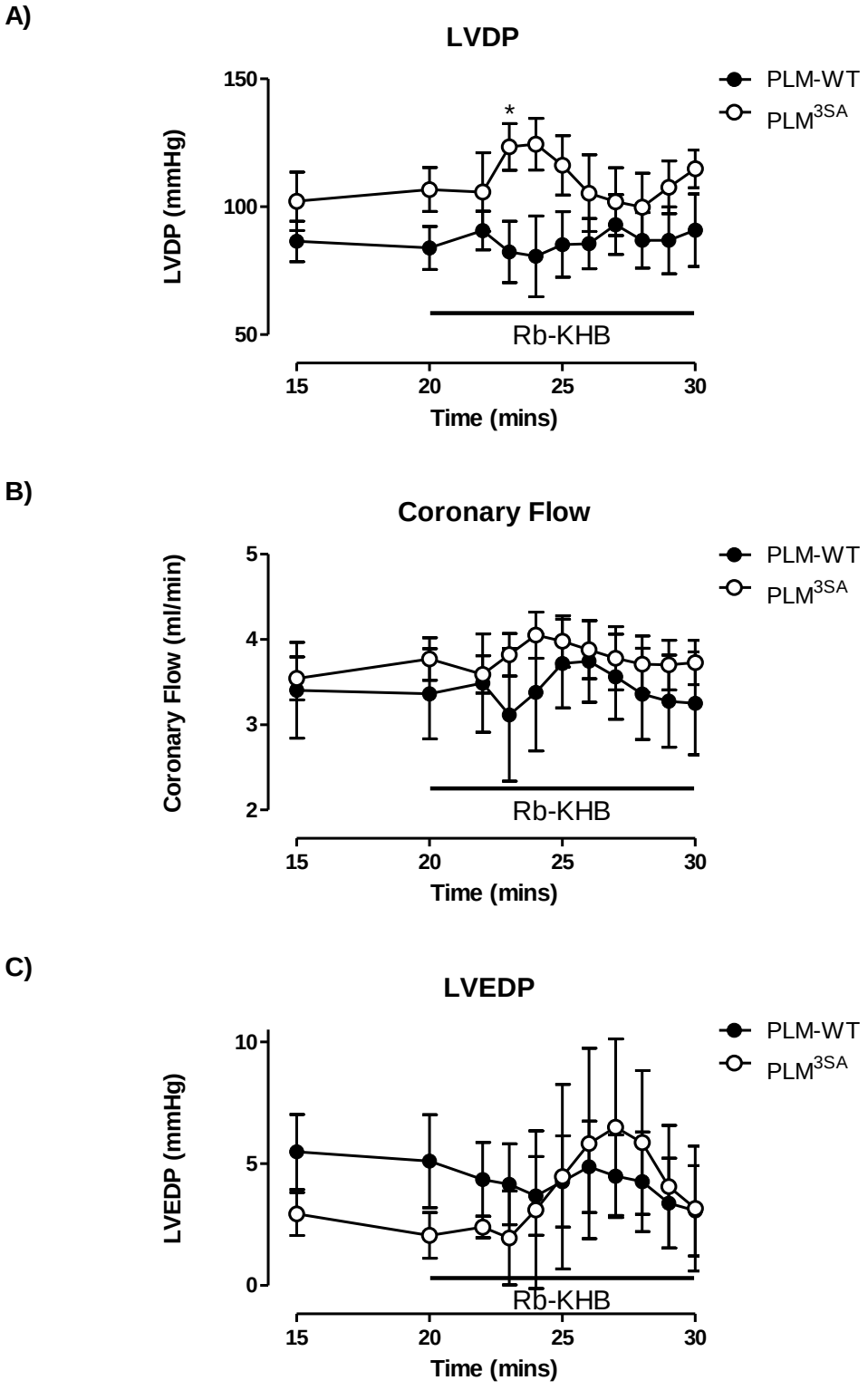

Figure 5.8. Effect of Rb^+-KHB perfusion on cardiac function.
A) LVDP; B) Coronary Flow; C) LVEDP. n=6. All data expressed as mean±sem and analysed by one-way ANOVA and Bonferroni post-hoc test, P<0.05 was considered significant (PLM-WT 'v' PLM^{3SA} denoted by *).

Figure 5.9 shows Rb^+ uptake measured by the flame photometer following a variety of perfusion protocols. It can be seen that there were no differences between the genotypes (PLM^{3SA} vs. WT) at baseline or in response to any intervention. Rapid pacing (Figure 5.9A) and ISO (Figure 5.9B) did not affect Rb^+ uptake compared to basal controls. Ouabain, however, significantly reduced Rb^+ uptake in both genotypes compared to basal controls.

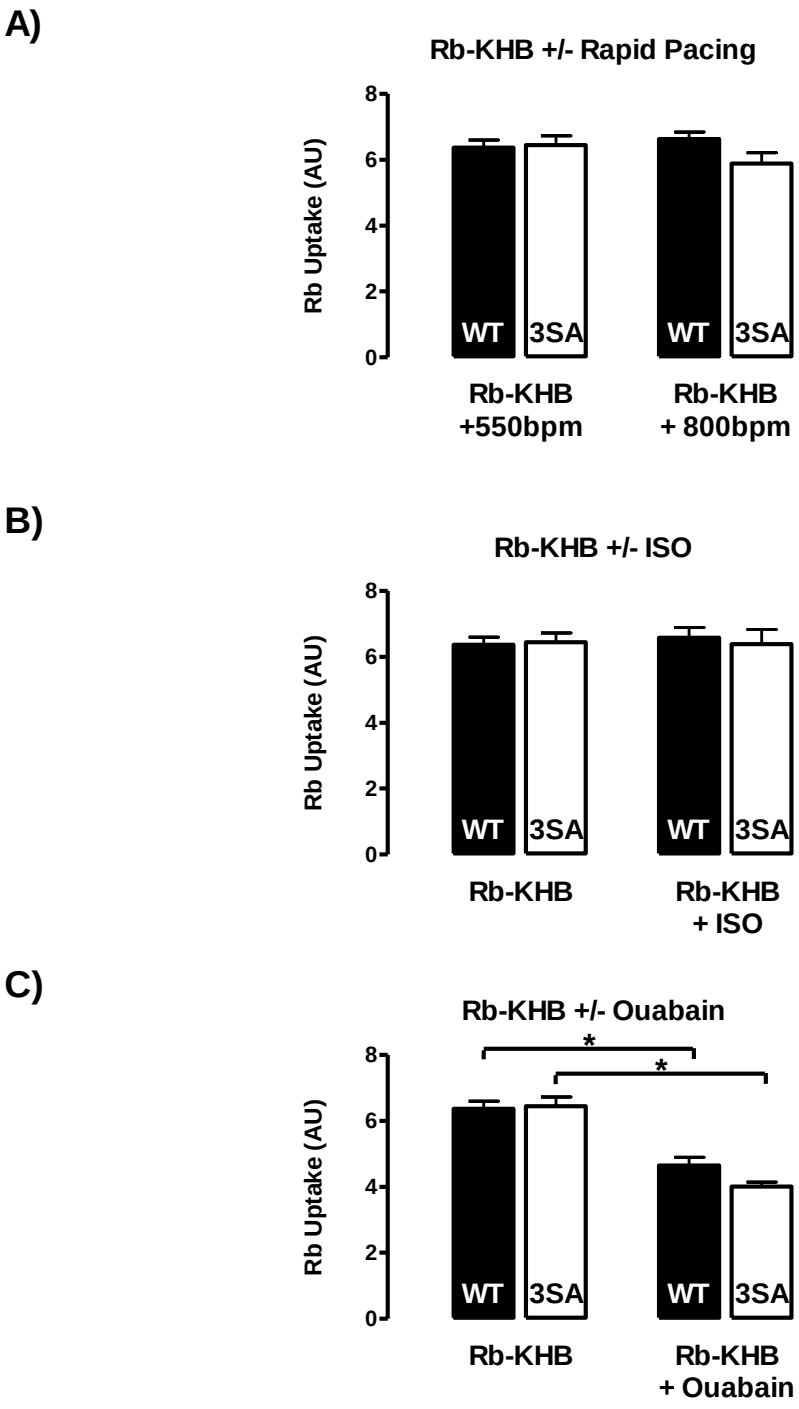

Figure 5.9: Flame photometer results comparing basal Rb^+ uptake with Rb^+ uptake during different interventions in WT and PLM^{3SA} mouse hearts.
A) Rb^+ uptake at during rapid pacing; B) Rb^+ uptake in the presence of 10nM ISO; C) Rb^+ uptake in the presence of 50µM ouabain. n=5-8. All data expressed as mean±sem and analysed by one-way ANOVA followed by Bonferroni post-hoc test, $P<0.05$ was considered significant denoted by *.

5.5 Discussion

In this chapter the experimental parameters for subsequent flame photometry studies were determined before intracellular Na^+ or Rb^+ uptake was measured in WT and PLM^{3SA} mouse hearts at basal pacing rates and during different protocols. Intracellular Na^+ content in basally paced WT and PLM^{3SA} hearts was the same and was unaffected by rapid pacing, ISO or ouabain perfusion in either genotype. In Rb^+ uptake studies, substitution of K^+ with Rb^+ had a transient effect on cardiac function measurements of LVDP, coronary flow and LVEDP. Rb^+ uptake by WT and PLM^{3SA} perfused hearts was the same under basal conditions and was unaffected by rapid pacing or ISO perfusion in either genotype. Ouabain however, significantly decreased Rb^+ uptake in both PLM-WT and PLM^{3SA} mouse hearts compared to their respective controls.

Some of the above findings, in particular the lack of effect of ouabain on intracellular Na^+, highlight the possibility that the results obtained using flame photometry may not be representative of the ion concentrations in these hearts, due to experimental limitations of the technique. However, it is appropriate that the results obtained are discussed as though the technique is not limiting and that these results are possibly real. Confirmation of these results with ^{23}Na NMR would be useful.

5.5.1 Intracellular Na^+

Flame photometry has been used in many studies with a range of species and tissue types to measure intracellular Na^+ with varying results. For example, in the guinea pig ventricle intracellular Na^+ concentration was reported as 36.7mM[347] whilst in the perfused rat and rabbit hearts estimations of $[Na^+]_i$ reported were lower at 20.2mM and 19.3mM respectively.[348, 349] Whilst these results differ considerably with each other, this could potentially be due to species differences. However, all of these estimations are greater than those reported in other studies which utilise alternative experimental methods (ion-selective electrodes, fluorescence resonance imaging (SBFI), ^{23}Na NMR) which have suggested that $[Na^+]_i$ can vary between 4-16mM.[2-10] In particular, one study by Malloy *et al*, measured $[Na^+]_i$ in the perfused rat heart by both flame photometry and ^{23}Na NMR and found vastly different results of 30.7mM and 6.2mM respectively.[350]

These conflicting results suggest that there is an over-estimation of $[Na^+]_i$ with flame photometry methods. For flame photometry measurements the total sample is consumed (i.e.

tissue is destroyed) and therefore all Na^+ present in the sample will be measured.[351] Therefore any residual Na^+ in the extracellular space and vasculature which isn't removed will contribute to the intracellular Na^+ measurement. Washout of the extracellular compartment is therefore critical for accurate $[Na^+]_i$ determination. However Na^+ washout from the extracellular space is associated with 2 complications: (1) washout may not be complete if too short; (2) washout may cause intracellular Na^+ loss down the Na^+ concentration gradient if too long. Additionally within the heart there may also be Na^+ present in both the intracellular and extracellular compartments in a bound form which would therefore contribute to the measured flame photometer intracellular Na^+ signal but may not be of functional relevance.[351] Both of which may contribute to an over-estimation of $[Na^+]_i$ when compared to results from other methodology.

In the studies presented in this chapter intracellular Na^+ content was measured in perfused WT and PLM^{3SA} mouse hearts paced basally at 550bpm by flame photometry following a suitable extracellular wash-out period. It was shown that intracellular Na^+ content was similar in both genotypes. Previous measurement of $[Na^+]_i$ by other techniques in mouse myocytes have been reported by Despa *et al*, 2005 using SBFI.[28] They measured $[Na^+]_i$ in resting cardiac myocytes from both WT and PLM-KO mice and showed that both had similar resting $[Na^+]_i$. The absence of PLM in knock-out mouse myocytes has previously been shown to significantly increase apparent affinity (K_m) of the pump for Na^+ compared with WT;[28, 62] therefore a lower $[Na^+]_i$ than in WT myocytes than PLM-KO was hypothesised. However, it was also shown in these studies that expression of the total α subunit protein was decreased in PLM-KO myocytes which supported the notion that the increased Na^+ affinity of Na^+/K^+ ATPase in PLM-KO mice might be offset by the decrease in pump protein expression thus resulting in similar $[Na^+]_i$ under basal conditions.[28]

The same reasoning may apply to the similar intracellular Na^+ signals seen in both WT and PLM^{3SA} hearts. In the PLM^{3SA} mouse the presence of unphosphorylatable PLM potentially places a permanent brake on the pump and may affect affinity of the pump for Na^+. It was hypothesised that this may affect $[Na^+]_i$ in these mice and potentially cause it to be greater than in WT mice. Indeed hearts perfused in this study were under basal physiological conditions of 550bpm pacing rate which has previously been shown in Chapter 4, Section 4.4.1 to have greater contractile function supporting the hypothesis of a greater intracellular Na^+ content. However, it was also shown in Chapter 3, Section 3.4.2.2 that total PLM protein expression was significantly decreased in PLM^{3SA} heart homogenates compared with WT; whilst total α subunit

protein expression was unchanged. Therefore under basal physiological conditions potentially the reduced PLM expression may result in similar net pump current in WT and PLM^{3SA} myocytes and hence similar intracellular Na^+ content. In support of this theory, other data from colleagues have shown similar Na^+/K^+ ATPase activity (I_{Pump} measurements) in PLM^{3SA} and WT quiescent myocytes using ruptured patch clamp techniques at both 25mM and 100mM pipette Na^+. Therefore under basal conditions similar intracellular Na^+ content in WT and PLM^{3SA} hearts may be explicable.

However, the experimental conditions under which each of these measurements was made must also be taken into consideration. Despa *et al*, made WT and PLM-KO SBFI measurements of $[Na^+]_i$ in quiescent myocytes at room temperature. The low temperature may affect ion channel window currents and exchanger protein equilibrium altering resting $[Na^+]_i$ and $[Ca^{2+}]_i$ equilibrium and so measurements of $[Na^+]_i$ potentially may not be physiologically relevant.[28] Similarly, although patch clamp studies in PLM^{3SA} were made at physiological temperatures of 35^{o}C the myocytes were quiescent. Quiescent myocytes lack action potentials and the rapid influx of Na^+ and Ca^{2+} which could significantly affect $[Na^+]_i$ measurements questioning their physiologically relevance. Another factor to consider is the length of time between myocyte isolation and experimentation. Following the stressful cell isolation procedure, cells are likely to be slightly Ca^{2+} loaded with high basal PLM phosphorylation. If SBFI measurements were taken at this point then WT and PLM-KO pump activity and affinity for Na^+ would be similar, thus resulting in the reported similar $[Na^+]_i$. In the PLM^{3SA} patch clamp data, if cells were left to rest for a long time prior to experimentation, basal PLM phosphorylation would reduce sufficiently in WT myocytes replicating pump conditions in myocytes with unphosphorylatable PLM present; again questioning the physiological relevance of these results. In theory, the flame photometry data was more representative of an *in vivo* situation being measured in perfused beating hearts at physiological heart rates and temperature. However, as previously stated flame photometry also has limitations such as incomplete washout affecting results and lack of sensitivity making small differences difficult to detect. Similar $[Na^+]_i$ measurements in PLM^{3SA} and WT hearts does conflict with isolated heart inotropy in PLM^{3SA} compared with WT which shows increased inotropy in PLM^{3SA} mice. However, small increases in $[Na^+]_i$ (1mM), which may be undetectable by the insensitive flame photometer, can cause a large increase in Ca^{2+} influx and hence contractility.[76]

5.5.1.1 Rapid pacing and intracellular Na^+

Rapid pacing of the hearts at 800bpm had no effect on intracellular Na^+ content in WT or PLM^{3SA} mouse hearts compared to controls. Increases in $[Na^+]_i$ have been reported with increases in stimulation frequency in a variety of species and preparations.[352-355] In the isolated perfused rat heart pacing induced changes in $[Na^+]_i$ have been reported using ^{23}Na NMR[356-359] due to increased Na^+ entry with increased heart rates.[1] The lag theory proposed by Langer in 1967 hypothesised that increases in pacing rate causes increased Na^+ influx rate which outbalances Na^+ efflux by Na^+/K^+ ATPase until a new $[Na^+]_i$ steady state is reached.[360]

The role of PLM phosphorylation in rapid pacing was investigated by Pavlovic *et al*, 2013 who showed PLM phosphorylation increases with pacing at 3Hz at both Ser63 and Ser68 residues and was attributed to an NO-dependent pump stimulation pathway.[177] Therefore, phosphorylation of PLM in WT hearts with rapid pacing at 800bpm would potentially result in removal of additional Na^+ influx induced by the increase in pacing rate. Whether pump activity would now be great enough to maintain a basal level of Na^+ is unlikely particularly, as discussed earlier, this NO-dependent pathway may be saturated even at 550bpm. An SBFI study by Despa *et al*, showed a 6mM $[Na^+]_i$ increase with pacing at 2Hz in both WT and PLM-KO mouse myocytes,[32] thus indicating that during pacing in WT myocytes the Na^+ pump works at the same rate as the unrestricted pump in PLM-KO myocytes. These studies (Pavlovic and Despa) both report an increase in intracellular Na^+ in myocytes induced by pacing; however no increase in intracellular Na^+ was observed in our flame photometry study. Additionally, if PLM phosphorylation by rapid pacing was able to reduce Na^+ content to a basal level then in this current study a clear difference between WT and PLM^{3SA} Na^+ content would be observed, however this was not the case. No difference in intracellular Na^+ content was observed between the genotypes suggesting that PLM phosphorylation does not play a role here. This is in agreement with FFR data from Chapter 4, Section 4.4.3 which showed a negative FFR in both WT and PLM^{3SA} mouse hearts but no differences in the gradient of the FFR slope, suggesting similar $[Na^+]_i$ in both genotypes.

These conflicting results could be due to differences in experimental set-up. SBFI measurements in myocytes were made at room temperature and pacing started from quiescent state therefore perhaps the initial Na^+ accumulation measured was due to the ionic balance of the cell being reset. The suggestion that rapid pacing phosphorylates PLM resulting in similar $[Na^+]_i$ changes in both WT and PLM-KO may simply be the result of the length of time cells were isolated prior to experimentation which has been shown to be critical to the basal

phosphorylation status of the cell. If experiments were performed soon after cell isolation then basal phosphorylation would be high and the WT myocytes would behave like PLM-KO myocytes without further PLM phosphorylation by rapid pacing. Additionally pacing at 2/3Hz is low (equivalent of 120-180bpm) and again not considered physiological.

Perhaps the difference lies in myocyte PLM phosphorylation compared to isolated whole heart preparations. Whole heart PLM phosphorylation Western blotting data in the lab is conflicting, with some colleagues revealing phosphorylation changes in whole hearts at 800bpm, whilst others do not. Perhaps rapid pacing does induce PLM phosphorylation in isolated hearts but is difficult to detect due to rapid dephosphorylation by phosphatases in the local environment within the time taken for hearts to be removed from the cannula and frozen. Alternatively perhaps PLM simply does not get phosphorylated by rapid pacing at 800bpm for 10 minutes in the isolated heart preparation, though this protocol has been established within the group and considered sufficient to induce relevant physiological changes. Or as previously discussed at 550bpm the pacing effect is likely to be saturated with no further phosphorylation of PLM at higher pacing rates.[177]

However, no change in intracellular Na^+ from basal Na^+ signal with rapid pacing was unexpected. ^{23}Na NMR studies, in particular studies by Simor *et al*, looking at FFR in rat hearts correlate increases in heart rate with decreases in LVDP (range 250-500bpm) and increases in $[Na^+]_i$.[358] In the study presented here, mouse hearts paced at 800bpm show decreased LVDP, as previously seen in FFR data Section 4.3.2, but with no additional change in intracellular Na^+ content. Interestingly, Simor *et al*, also showed the greatest changes in $[Na^+]_i$ with pacing occurred with low concentrations of extracellular Ca^{2+} (0.24mM), however accompanying LVDP decreases were small. At high extracellular Ca^{2+} concentrations (2.2mM) whilst changes in developed pressure were large the change in $[Na^+]_i$ was negligible. Finally 1.15mM extracellular Ca^{2+} revealed Na^+ changes of just 1mM accompanied by 60mmHg developed pressure changes at the highest pacing rate. In the current study Ca^{2+} was present extracellularly at a concentration of 1.4mM, which may explain why developed pressure changes were observed at 800bpm but intracellular Na^+ content changes were not. Perhaps in this range $[Na^+]_i$ changes were small (<1mM), too small to be detected by the insensitive flame photometer. No clear conclusion can be made from this study at this time and further testing of this model with ^{23}Na NMR may help resolve these results.

5.5.1.2 ISO and intracellular Na^+

ISO stimulation of the isolated hearts in this study caused an increase in inotropy but had no effect on intracellular Na^+ content in WT or PLM^{3SA}. Wang *et al*, 2010[361] showed similar *in vivo* inotropic effects with ISO in WT and PLM-KO hearts which peaked after 1-2 minutes and began to decline in WT but not PLM-KO hearts. Further work in paced myocytes (2Hz) showed the addition of ISO (1µM) caused maximal contraction in both genotypes after 2-4 minutes which then declined in WT but not PLM-KO hearts. $[Na^+]_i$ was measured using SBFI and revealed that in WT $[Na^+]_i$ increased with pacing and initial ISO addition and then declined in WT but not PLM-KO myocytes. Similar work by Despa *et al*, 2008[32] supports these findings that $[Na^+]_i$ decreases in paced cardiac myocytes (2Hz) upon the addition of ISO (1µM) in WT but not PLM-KO myocytes. All these findings indicate the importance of PLM phosphorylation by ISO in regulating $[Na^+]_i$. Therefore the absence of a significant decrease in flame photometer measurements of intracellular Na^+ in WT hearts was unexpected.

ISO perfusion in this study was for 10 minutes which has previously been shown to be adequate for $[Na^+]_i$ changes,[361] however the use of 10nM ISO compared with 1µM of other studies[32, 361] may have been too low a concentration to evoke detectable changes in intracellular Na^+ content. To ensure Na^+ influx was similar in both WT and PLM^{3SA} hearts pacing at 550bpm was maintained throughout the addition of ISO. This limited the concentration of ISO available for use due to the requirement to avoid escape rhythms caused by adding ISO at too great a concentration to follow the basal pacing protocol of 550bpm. Previous work using Western blotting to look for ISO induced PLM phosphorylation in WT hearts showed that 10nM ISO produced an increase in Ser68 phosphorylation therefore was considered adequate at the time of the study planning. However, potentially the concentration was too low to detect any differences in Na^+ efflux in WT hearts. This may also apply to the lack of differences seen between WT and PLM^{3SA} intracellular Na^+ content. It was hypothesised that PLM^{3SA} hearts may have greater $[Na^+]_i$ compared to WT with the addition of ISO due to the inability to phosphorylate PLM and activate the Na^+/K^+ ATPase, however this was not the case. At 550bpm Na^+ influx rate was similar in both WT and PLM^{3SA} hearts and may have been too great to detect changes to Na^+ efflux induced by PLM phosphorylation by 10nM ISO by the flame photometer. Again the limitations of the flame photometer sensitivity to detect small changes in Na^+ ion content may contribute to the lack of significant effects.

5.5.1.3 Ouabain and intracellular Na^+

Ouabain is a known inhibitor of Na^+/K^+ ATPase[330] and has been shown in multiple studies to cause an inotropic response in the heart due to inhibition of Na^+/K^+ ATPase resulting in increases in intracellular Na^+ and subsequent increase in Ca^{2+} via NCX.[315, 316, 362, 363] Initial studies by Ellis and Dietmer in sheep Purkinje fibres using Na^+ microelectrodes convincingly showed increases in intracellular Na^+ activity with the addition of ouabain.[364-366] They deduced that concentrations of ouabain greater than 100nM were sufficient to see significant changes in Na^+. However, in the current study no changes were seen in intracellular Na^+ content in either WT or PLM^{3SA} hearts with 50 µM ouabain. This concentration of ouabain was chosen as previously a large inotropic response had been observed without contracture. According to the previous publications this concentration should have been sufficient to observe changes in intracellular Na^+,[364-366] though this was not the case. However, these studies were performed in sheep Purkinje fibres so most probably the species and tissue type influence any ouabain changes seen. Additional studies in sheep papillary muscle using 0.5µM showed even greater Na^+ increases compared to Purkinje fibres in the same study[367] and studies in rat heart muscle showed low concentrations of ouabain (0.1, 0.5 and 1.0µM) produced concentration-dependent increases in intracellular Na^+.[346] Studies using ^{23}Na NMR also reported increases in intracellular Na^+ with 250µM ouabain of 32%.[368] Therefore the lack of any changes detected in this data set was unexpected. The fact that there were no differences between genotypes, however, was not unexpected as there was no reason to assume that a change to PLM protein would impact the ouabain binding site on the Na^+/K^+ ATPase pump. There are possibly 2 reasons for the absence of any ouabain effect: (1) the lack of sensitivity of the flame photometer to detect changes in intracellular Na^+; or (2) an incorrect washout protocol which caused loss of intracellular Na^+ as well as extracellular Na^+ down its concentration gradient resulting in similar Na^+ measurements for this and all the protocols. The failure to detect a rise in Na^+ with such a well characterised intervention such as ouabain, questions the ability of this technique, for whatever reason, to faithfully report intracellular Na^+ concentrations in perfused mouse hearts.

5.5.2 Rubidium uptake

The amount of rubidium taken up by PLM-WT and PLM^{3SA} perfused isolated hearts paced at a basal rate of 550bpm was similar. Rb^+ has been shown to activate the Na^+/K^+ ATPase in a manner similar to K^+ [332-335, 369, 370] with a similar apparent affinity constant.[371] This suggests that

pump activity will not be compromised by the substitution of K^+ for Rb^+ and that Rb^+ affinity for the pump in both genotypes will be similar. Na^+ extrusion by the pump will be dependent on extracellular Rb^+. However, as extracellular Rb^+ is present at 4.7mM and pump saturation has been reported with 4mM K^+ (and hence Rb^+),[124] Na^+ extrusion should be unaffected. The limiter for Rb^+ uptake will therefore be the actual pump activity itself in each genotype.

As previously discussed with the intracellular Na^+ content results, the lack of any differences between WT and PLM^{3SA} Rb^+ uptake could be attributed to similar pump activity in both mice resulting from the reduction in PLM protein expression in PLM^{3SA} heart homogenates normalising the net pump current to that of WT hearts. It has been reported that Rb^+ influx acts as a measure of Na^+ influx, because under steady state conditions Rb^+ uptake is tightly coupled to Na^+ entry assuming that reverse mode NCX is negligible.[326] Therefore under steady state conditions Na^+ efflux, and hence Rb^+ influx, must equal Na^+ influx. Since there is no reason to assume that Na^+ influx has changed in PLM^{3SA} hearts compared with WT at 550bpm then Na^+ efflux must be constant between genotypes, resulting in similar Rb^+ uptake in both hearts. However, it was hypothesised that the Na^+/K^+ ATPase in PLM^{3SA} hearts may be desensitised to Na^+, therefore to achieve the same Na^+ efflux (and Rb^+ uptake) as WT the $[Na^+]_i$ must rise more in these hearts. Since $[Na^+]_i$ in these flame photometry studies is the same in both genotypes then PLM^{3SA} hearts achieve the same Na^+ efflux as WT at similar $[Na^+]_i$ suggesting that the pump is equally sensitive to $[Na^+]_i$ activation. Perhaps this is because the WT pump is not significantly (or sufficiently) phosphorylated and so resembles the PLM^{3SA} pump, or that the flame photometry technique is too insensitive to detect changes in $[Na^+]_i$ as suggested by the lack of changes detected by ouabain intervention in the previous section (5.5.1.3), or finally that the basal Rb^+ measurement observed is incorrect, again due to an insensitive measuring technique.

The substitution of Rb^+ for K^+ caused transient effects in cardiac function measurements of developed pressure, coronary flow and LVEDP. The effect was short lasting, under 10 minutes, however a transient increase in inotropy was observed in PLM^{3SA} hearts but not WT. It has previously been suggested by Sala *et al*, 1991 that Rb^+ can cause voltage-gated K^+ channel blockade during the action potential.[372] This should potentially prolong action potential duration and may increase inotropy. However, in contrast, in guinea pig ventricular strips the opposite has been observed with depressed contractility following exposure with 5mM Rb^+.[373] In mouse hearts the cause behind this transient inotropy remains unclear.

Previous controls using BM to block any other potential Rb^+ influx pathway have shown that any Rb^+ measured in this protocol has been taken up by the pump alone. Incorrect washout timings may affect the amount of Rb^+ uptake measured and again the sensitivity of the flame photometer may be limiting.

5.5.2.1 Rapid pacing and Rb^+ uptake

Rapid pacing at 800bpm had no effect on rubidium uptake in either WT or PLM^{3SA} hearts. Historically rapid pacing has been shown to increase $[Na^+]_i$[352-359] and this increased Na^+ influx would be accompanied by increased Na^+ efflux, and hence Rb^+ uptake in both genotypes. Additionally, if rapid pacing causes further PLM phosphorylation, thereby increasing Na^+/K^+ ATPase affinity for Na^+ and hence activity,[28, 62] a greater increase in Rb^+ uptake in WT hearts compared with the desensitised PLM^{3SA} hearts may be seen. However, lack of Rb^+ uptake differences between basal controls and rapidly paced hearts in either genotype suggests that rapid pacing, contrary to published studies, has not affected $[Na^+]_i$ and Rb^+ influx remains unchanged. Again, the lack of sensitivity of the flame photometer to detect small changes in Rb^+ uptake may be responsible.

5.5.2.2 ISO and Rb^+ uptake

β-adrenergic stimulation by the addition of ISO had no effect on the amount of Rb^+ taken up by WT or PLM^{3SA} hearts. During ISO intervention hearts were continually paced at 550bpm, a rate greater than that induced by 10nM ISO, ensuring that Na^+ influx remained constant in both genotypes. Previous data shows phosphorylation of PLM by 10nM ISO at Ser68 (not shown) which is known to stimulate the pump and increase Na^+ affinity.[32, 361] Therefore whilst decreases in $[Na^+]_i$ were expected (but not seen), due to Na^+ influx rate remaining constant Rb^+ uptake was also expected to remain constant. Additionally, as influx is constant in both genotypes it was expected that there would be no differences in Rb^+ uptake in PLM^{3SA} hearts either. The data reflects this with no change in Rb^+ uptake between control and ISO perfused hearts or between genotypes was observed.

5.5.2.3 Ouabain and Rb^+ uptake

As previously discussed in Section 5.5.1.3, ouabain is an inhibitor of Na^+/K^+ ATPase and concentrations of >100nM are sufficient to see changes in intracellular Na^+ concentration. Therefore, it was hypothesised that 50μM ouabain, used in this study, would be sufficient to affect intracellular Na^+ content (which was not seen) and consequently decrease Rb^+ uptake. In both WT and PLM^{3SA} Rb^+ uptake was significantly decreased compared with basal controls suggesting that indeed the pump had been inhibited and the uptake of Rb^+ reduced. Reduction of Rb^+ uptake was approximately 30% compared with controls, which is similar to the reported increases in intracellular Na^+ with 250μM ouabain of 32% using ^{23}Na NMR.[368] Potentially such large changes in ion content are necessary for accurate measurement by the flame photometer and changes induced by other interventions were too small to be detected.

Ouabain significantly reduced Rb^+ uptake in both WT and PLM^{3SA} hearts by similar amounts. In both mouse heart homogenates there was similar protein expression levels of both α subunits (Chapter 3, Section 3.4.2.2) therefore differences in ouabain inhibition of the pump was not expected or seen.

5.5.3 Experimental limitations

Throughout this series of studies the lack of detection of any changes in intracellular Na^+ content with any intervention, especially ouabain was unexpected and questions the sensitivity of the methodology used to detect changes in Na^+ ion content. Perhaps the changes rapid pacing, ISO or ouabain induced were too small for accurate detection by the flame photometer and a larger number of hearts were required for the studies to show any significance. The only significant effect seen was in the Rb^+ uptake study with the addition of 50μM ouabain, which resulted in a 30% decrease in Rb^+ influx. The failure to detect an increase in Na^+ was unexpected in these conditions as changes of this magnitude have been detected by other techniques such as ^{23}Na NMR. Repeating these studies using a different method for measuring $[Na^+]_i$, such as ^{23}Na NMR, is therefore necessary.

5.6 Summary

Using flame photometry no differences were observed in intracellular Na^+ content between WT and PLM^{3SA} isolated mouse hearts under basal conditions. Rapid pacing to 800bpm had no effect on intracellular Na^+ content compared to control or between genotypes. ISO had no effect on WT or PLM^{3SA} intracellular Na^+ content. Ouabain, although causing an inotropic response, did not change intracellular Na^+ content in WT or PLM^{3SA} hearts. Thus, although it is possible to speculate about other limitations, the fundamental problem with this data set is it does not appear as if this method is suitable for measuring changes in Na^+ content in our hands.

The amount of rubidium uptake by WT and PLM^{3SA} mouse hearts was shown to be the same under basal conditions and with ISO perfusion as expected. However, Rb^+ uptake was unaffected by rapid pacing. Ouabain significantly decreased Rb^+ uptake in both genotypes from their respective control and suggested successful inhibition of the pump in both genotypes by a similar amount.

Flame photometry may not be the optimum method to detect small changes in ionic content in mouse hearts and ^{23}Na NMR will be utilised to gain a better understanding of changes in intracellular Na^+ in perfused beating mouse hearts.

6 CHAPTER 6- NMR MEASUREMENT OF $[Na^+]_i$ IN PLM^{3SA} AND WT LITTERMATE HEARTS

6.1 Introduction

Nuclear magnetic resonance (NMR) studies provide a non-invasive technique that allows the measurement of intracellular Na^+ in a perfused heart.[74, 374] Most NMR studies on perfused hearts have been performed in rat due to the complexity of the technique when miniaturising it for the mouse heart. Until 2004 only 2 labs in the world had published studies of ^{23}Na NMR in Langendorff perfused mouse hearts.[375] There are many technical complications presented by NMR spectroscopy in perfused mouse hearts some relating to the set-up of a Langendorff NMR perfusion rig and others associated with successful visualisation of ^{23}Na spectra. Development of reliable aerobic mouse heart perfusion requires particular consideration of:

- temperature maintenance through extended perfusion lines,
- O_2 saturation at the cannula,
- the introduction of metal pacing wires inside the magnet necessary for paced function
- and the effects of inertia, damping and hydrostatic pressure on cardiac function measurements derived from balloons positioned in the left ventricle and recorded remotely.

^{23}Na is considered a medium sensitivity nucleus for NMR visualisation[376] however, a number of technical challenges are introduced when attempting to visualise a ^{23}Na spectrum from a perfused mouse heart. These include:

- the difficulties in manufacturing small coils with sufficient precision to allow for homogeneous electric fields,
- the further limitations imposed by placing a small mouse heart inside a larger coil – poor "filling factor",
- the quantitatively small amount of sodium present in a mouse heart limits the signal: noise ratio,
- and the use of potentially toxic and relatively uncharacterised (in the mouse heart) shift reagents to enable visualisation of intracellular Na^+ signal.

The majority of the ^{23}Na spectrum is generated by the extracellular Na^+ component (145mM) and both extra- and intracellular Na^+ ions resonate at the same frequency.[267] In order to quantify $[Na^+]_i$ by NMR, extracellular and intracellular Na^+ signals must be differentiated and the relative intracellular and extracellular volumes must be known or determined.[377] The use of chemical shift reagents can help separate the two signals by binding to extracellular Na^+ ions causing them to resonate at a different frequency, thus 'shifting' the extracellular Na^+ signal. However there are additional complications with the use of shift reagent such as chelation of Ca^{2+} [378, 379] and biological toxicity.[380] The use of multiple quantum filtering (MQF) techniques can distinguish intracellular Na^+ without the need for shift reagent.[269] However these are restrictive in the size of Na^+ signal seen compared to the standard full ^{23}Na spectrum[381] and again have not been fully characterised in isolated mouse hearts.

The work in this chapter focuses firstly on the development of a reliable method for obtaining ^{23}Na spectrum in the perfused mouse heart and secondly quantification of the $[Na^+]_i$. To measure $[Na^+]_i$ two approaches were used:

1) the use of shift reagent to reveal the intracellular Na^+ signal component of the ^{23}Na single quantum (SQ) spectrum,

2) the use of MQF techniques to measure $[Na^+]_i$.

Once basal measurements were obtained changes to $[Na^+]_i$ induced by rapid pacing, ISO stimulation and ouabain were also investigated using MQF techniques.

6.1.1 Measurement of intracellular ^{23}Na

There are 2 ways that have been used to measure $[Na^+]_i$ in these NMR studies:

1) Use of a shift reagent
2) Triple quantum filtering

6.1.1.1 Use of shift reagents

As previously stated the major problem with measuring $[Na^+]_i$ using NMR is that extra- and intracellular ^{23}Na resonate at the same frequency on an NMR spectrum.[267] The use of shift reagents allows the separation of each peak by binding to the extracellular Na^+ ions and causing them to resonate at a different frequency, effectively "shifting" extracellular Na^+ to reveal intracellular Na^+. The application of the shift reagent technique has been known about since the late 1950's[382-384] but it was Hinckley in 1969[385] that first systematically developed this area of NMR spectroscopy.[386-388] Work in the ^{23}Na shift reagent field was advanced by R.K Gupta *et al*,[267] and M. Pike *et al*,[389] in the 1980's when they first used the hyperfine anionic shift reagent, bis(tripolyphosphate)dysprosium(III) or $Dy(PPP_i)_2^{7-}$, allowing direct observation of resolved resonances from both extra- and intracellular ^{23}Na. Complexes of lanthanide elements, dysprosium and thulium, are the most commonly used shift reagents.[390-392] A key characteristic of shift reagents is that they cannot pass through the cell membrane and therefore they and their bound components remain extracellular. Properties of shift reagents include a high negative charge and relatively large size which prevents them from penetrating the cell membrane.[393] They are reported to produce a shift by 2 possible modes of action: (1) shifts by contact and (2) shifts by pseudo contact with Na^+. Shifts by contact involve the formation of a covalent bond with the spare electron in ^{23}Na outer shell which causes a transfer of the electron spin density. Pseudo contact shifts involve the magnetic effects of the unpaired electron magnetic moment and the presence of shift reagent changes the environment of this magnetic moment thereby changing the spin density.

The major problem with shift reagents is that their anionic nature means that as well as Na^+ they can also bind Ca^{2+} [379] which reduces the concentration of free extracellular Ca^{2+} greatly impacting perfused heart function and contractile force.[358, 394] This can potentially be offset by adding additional Ca^{2+} to raise the free Ca^{2+} concentration of the solution.[374] To complicate matters, different shift reagents have different binding affinities for Ca^{2+}, for example $Dy(PPP_i)_2^{7-}$ has a high affinity for Ca^{2+} and induces Ca^{2+} precipitation which limits the additional free Ca^{2+} that can be added to the hearts.[395] Dysprosium triethylenetriamine hexaacetate or Dy(TTHA) also interacts with Ca^{2+} and needs a large supplementation of Ca^{2+} to achieve normal function but one advantage is that there is no Ca^{2+} precipitation. The major issue with this shift reagent though, is that it does not produce a great enough shift for good spectral resolution.[379] The shift reagent thulium 1,4,7,10-tetraazacyclododecane-N,N',N'',N'''tetra(methylenephosphonate) or $Tm(DOTP)^{5-}$, is another lanthanide complex,

which is less toxic[392] and although it shows a degree of Ca^{2+} chelation it can tolerate a greater supplementation of free Ca^{2+} without precipitation (1mM) and produces an adequate shift in the Na^+ resonance frequency.[379]

$Tm(DOTP)^{5-}$

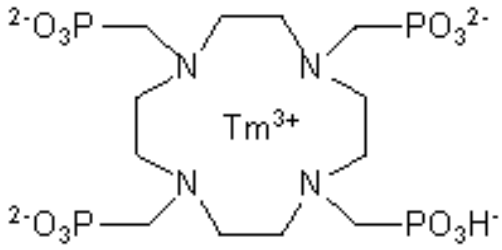

Mol Wt: 824.71

Figure 6.1: Chemical structure of $Tm(DOTP)^{5-}$, a lanthanide complex shift reagent.

Unfortunately the use of lanthanide complexes at high concentrations can cause line width broadening which causes a loss of spectral resolution. This in turn complicates the resolution of the intracellular ^{23}Na peak from the broader extracellular ^{23}Na peak as the peaks will not resolve completely from each other. High concentrations shorten the relaxation times, T1, which in turn broadens line widths. Previous studies in mouse perfused hearts have used $Tm(DOTP)^{5-}$ at 5mM and showed good spectral resolution with an addition of Ca^{2+} so that free Ca^{2+} was in the region of 0.8mM to obtain adequate function.[375] However, in rat hearts this shift reagent has also been used at 3.5mM with an adequate extracellular Na^+ shift.[379] Therefore there is a fine balance between using a $Tm(DOTP)^{5-}$ concentration great enough to resolve intra- and extracellular ^{23}Na peaks sufficiently without Ca^{2+} chelation and increased line width broadening and will be discussed in more detail later (Section 6.3.4).

6.1.1.2 Triple quantum filtering

Multiple quantum filtering is a technique that can be used to measure intracellular Na^+ concentrations without the use of a toxic shift reagent. There are 2 important assumptions for the use of multiple quantum filtering for measuring intracellular Na^+:

1) the contribution from the intracellular Na^+ ions to the MQF spectrum is large and responds to induced changes,
2) and that the extracellular signal size remains constant.[381]

Multiple quantum filtering exploits the fact that ^{23}Na is a quadrupolar spin 3/2-nucleus. This means there are 4 possible spin orientations resulting in: 3 possible single-quantum transitions (SQ), 2 double quantum transitions (DQ) and 1 triple quantum transition (TQ) (see Figure 6.2).[396] It has been proposed that when Na^+ is transiently bound to macromolecules, electric fields are generated which act as effective relaxation mechanisms[397] and allow the generation of multiple quantum transitions.[398, 399] In crystalloid perfused hearts, the intracellular space contains significantly more macromolecular structures than the extracellular space and hence intracellular ^{23}Na nuclei should produce a larger multiple quantum signal compared with extracellular ^{23}Na nuclei.[400] Additional ^{23}Na nuclei that enter the cell during interventions contribute to the non-averaged quadrupolar interactions and will be seen as an increase in intracellular multiple quantum filtering signal.[400] Studies in rat perfused hearts have shown this is the case and changes in $[Na^+]_i$ content can be monitored effectively using MQF.[400, 401]

The ability for ^{23}Na nuclei to spin in the 4 possible orientations is due to electrons in each electron shell (s, p and d for ^{23}Na) rotating differently when subjected to an external magnetic field. The nuclei can be captured in each of these transitions by setting the phase cycle correctly and effectively cancelling out or "filtering" the other transitions resulting in either DQ transition signal or TQ transition signal (SQ signal incorporates all the transitions and is the standard NMR spectrum signal) (see Figure 6.2). Studies comparing TQF and DQF signals with shift reagent SQ signals in perfused rat heart revealed that both TQF and DQF signals accurately represented the changes in $[Na^+]_i$ when extracellular volumes remained constant.[400, 402] Schepkin *et al*,[400] showed in rat heart that ^{23}Na TQF signal had a good linear correlation with intracellular Na^+ content so TQF was used for these studies. TQF does have limitations though and produce low intensity signals compared to SQ ^{23}Na signal. One study estimated the TQF signal to be proportional to 3% of the total SQ signal[400] and of that signal only 1% was estimated to be from intracellular ^{23}Na. TQF has a remaining component of extracellular ^{23}Na

incorporated into the signal. However, extracellular Na^+ should remain constant during the interventions used and because measurements were expressed as % change from baseline a good correlation in changes to $[Na^+]_i$ signal can be achieved.

The major advantage of the TQF approach is that it negates the need for using toxic, Ca^{2+} chelating shift reagent. One of the aims of these studies was to compare both approaches. TQF gives a reliable signal which in itself is not calibrated. So, ultimately the ideal protocol may involve TQF measurement, in the absence of shift reagent, of relative changes that can then be calibrated by a sequential short period of heart perfusion with shift reagent.

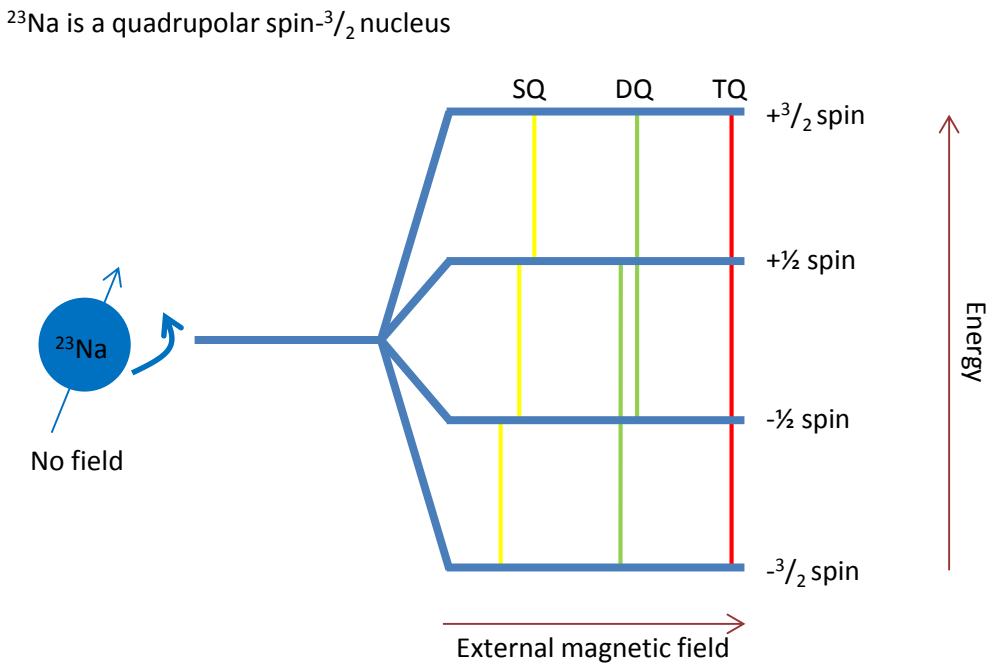

Figure 6.2: Multiple transition states of the quadrupolar nuclei ^{23}Na.
When ^{23}Na is placed in an external magnetic field is it capable of spinning in 4 possible orientations. A SQ transition (shown in yellow) is where a nucleus can move between single energy states i.e.-$^3/_2$ to -½ and the SQ spectrum is the sum of all of these transitions. There are 2 possible DQ transitions (green) which capture nuclei that move between 2 energy states i.e. -½ to +$^3/_2$. Finally TQ transitions (red) capture nuclei that can move between the highest and lowest energy state i.e. +½ to +$^3/_2$. By setting the phase cycle correctly the nuclei can be captured in each transition state.

6.2 Aims

The aims of the studies undertaken in this chapter were to:

1. Set-up a Langendorff perfusion system to perfuse paced mouse hearts inside a 9.4 Tesla NMR magnet.

2. Obtain good heart function during perfusion inside magnet.

3. Obtain good SQ ^{23}Na spectrum.

4. Using the shift reagent, $Tm(DOTP)^{5-}$, quantify the $[Na^+]_i$ for PLM^{3SA} hearts and WT littermates.

5. Using TQF detect changes in $[Na^+]_i$ signal during application of β-adrenergic stimulation, rapid pacing and ouabain.

6.3 Methods

The ^{23}Na NMR methods (and heart perfusion system) were not established prior to the start of these studies. The development, characterisation and refinement of these techniques is therefore described in detail in this chapter. At the time of writing this process was still evolving and therefore this chapter describes the progress thus far.

6.3.1 ^{23}Na mouse coil

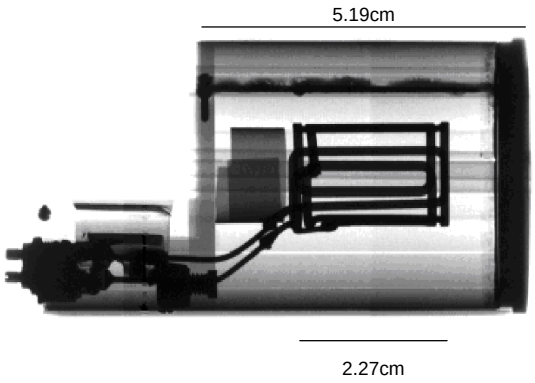

Figure 6.3: MRI image of mouse ^{23}Na coil inside probe body.
Actual body of the probe measures 5.19cm with the coil active region measuring 2.27cm. Coil itself is a birdcage wire configuration as can be seen in the central region.

A 10mm ^{23}Na mouse radio frequency coil was commissioned, designed and built by Bruker (Coventry, UK) using superconducting wire in a birdcage configuration to allow effective capture of the ^{23}Na signal. An MRI image of the coil can be seen in Figure 6.3 detailing the birdcage structure and enabling the precise location of the active region of the coil to be defined within the body of the probe. This will enable the heart to be correctly positioned at the centre of the active region producing the optimum ^{23}Na spectrum and maximising signal: noise ration.[269] At the left hand side of the probe are the tuning and matching rods used to tune the ^{23}Na spectrum. Shimming generates the optimum homogeneous magnetic field by manipulating current flow through the wires. Tuning defines the energy that will be applied to generate the energy difference in the ^{23}Na nucleus. The probe is locked into a 1m column which is then placed into the core of the magnet from underneath and secured in place at a pre-defined height that places the active region into the centre of the magnetic field.

6.3.2 NMR perfusion rig

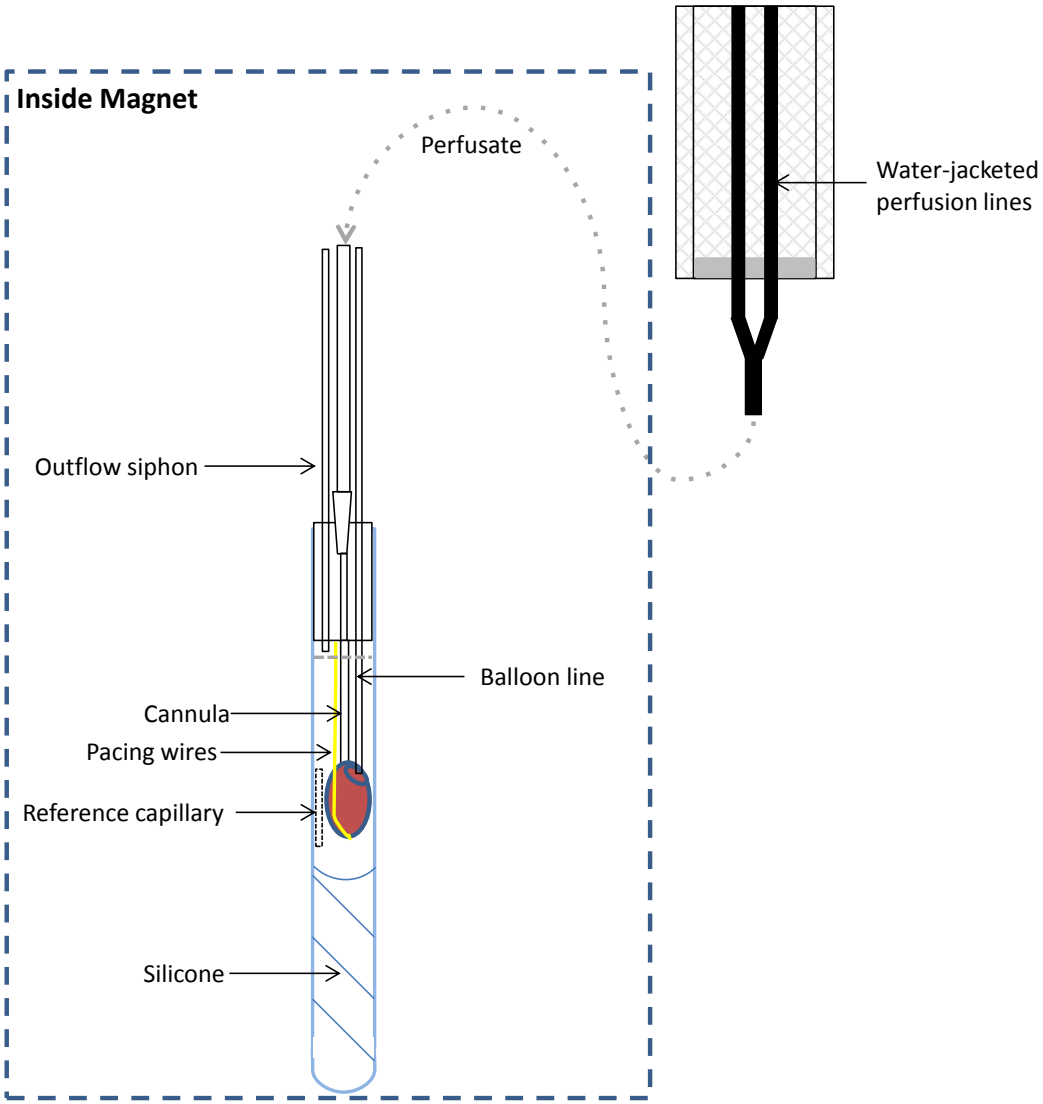

Figure 6.4: Schematic diagram showing NMR Langendorff perfusion rig.
The heart is cannulated on a carbon fibre cannula fed from extended water-jacketed perfusion lines. It is submerged in KHB in an NMR tube which has been filled with silicone to limit extracellular volume. The level of KHB in the tube is maintained by an outflow siphoning tube. Pacing wires are introduced into the ventricle and base of the heart to allow control of continuous pacing. A reference capillary is positioned alongside the heart so it is in the same active region field as the heart for spectral acquisition.

6.3.2.1 NMR Langendorff rig set-up

Perfusion inside the NMR magnet involved modifying the standard Langendorff set-up (see Chapter 2, Section 2.3.2) to allow perfusate to be delivered from the standard heated reservoirs to a cannula that can be inserted into an NMR tube and positioned inside the ^{23}Na coil in the core of the 9.4 Tesla NMR magnet. A schematic diagram is shown in Figure 6.4 with actual photographs of the NMR Langendorff rig that was used in Figure 6.5. The distance from the NMR magnet to the perfusion bench required 3m of perfusion tubing which was heated by passing it through a water-jacketed flexible heat exchanger. On exiting this water-jacket the perfusate tubing is reduced in diameter in order to fit inside the NMR probe that carries the ^{23}Na coil. This smaller tubing cannot be heated external to the magnet however once inside the magnet it can be heated using a thermo-circulator heating system designed to maintain the temperature of the bore of the magnet. Adjustment of both the perfusate heat exchanger and magnet bore heating system temperatures allows the perfusate to be delivered at 37^{o}C to the heart. Unfortunately, while this maintains a stable temperature in situ, when the probe is not inside the magnet, the lack of water-jacketing in the distal tubes cools the heart to room temperature. Hearts are therefore, by necessity, hypothermic during cannulation and set-up, and only achieve 37^{o}C when placed inside the magnet. All parameters such as balloon LVEDP and pacing rate were therefore initially set at room temperature which of course is not optimal for mouse heart perfusion.[259] In later iterations of this system, this problem has been addressed but this improved system was unavailable at the time of this thesis and therefore not used in the studies described here.

6.3.2.2 Cannula

The cannula was adapted for perfusion in a magnet as a non-metallic alternative to the standard cannula was required. A carbon fibre cannula was used with similar measurements to the standard metal perfusion cannula (O.D. 0.8mm and I.D. 0.4mm). The cannula passes through a silicone bung sealing the top of the glass NMR tube. See Figure 6.4 and Figure 6.4A, B and C.

6.3.2.3 Perfusion pressure

Perfusion pressure was measured using a transducer situated outside of the magnet and at the same height as the heart. Hearts were perfused at a constant flow of 3ml/min.

6.3.2.4 Balloon

A polyethylene balloon line was also passed through the silicone bung with an I.D. of 0.4mm and length marginally longer than the cannula. Externally this balloon line was attached to the standard balloon cannula which was connected to a 3 way tap and pressure transducer positioned in the body of the probe. A cling film balloon was made in the standard way on the free end of this balloon line and calibrated with the column in the horizontal position. Following insertion of the balloon into the cannulated heart, LVEDP was set at pressures between 4-8mmHg. See Figure 6.4 and Figure 6.4A, B, C and G.

6.3.2.5 Perfusate siphoning

To remove effluent from the sealed NMR tube a siphoning line was also passed through the silicone bung to a height just below the bung. This siphoning tube allows perfusate to be removed from the NMR tube using passive siphoning. Initially, perfusate was pumped out of the NMR tube using a peristaltic pump set at a flow rate equal to the coronary flow rate. However, small discrepancies in inflow and outflow rates created positive or negative pressures inside the tube which affected heart function. It is of note though that a siphoning system also results in a negative pressure within the sealed NMR tube and resulted in offsets in the balloon pressure recording which had to be corrected for when the heart was placed vertically in the magnet. See Figure 6.4 and Figure 6.4A, B and C.

6.3.2.6 Pacing

The heart was paced using silver wire pacing electrodes which again were passed through the silicone bung. The introduction of pacing wires into the NMR active region is unconventional.

Many workers studying isolated rat hearts in the NMR allow the hearts to 'free run' without external pacing as rat hearts beat at reasonably physiological rates. However, mouse hearts are intrinsically very arrhythmic and require external pacing for stability.[33, 403] In the few NMR studies that use pacing in Langendorff hearts, they have all used agar/KCl bridges as pacing electrodes. In studies described here, silver wire electrodes have been used with the addition of appropriate radio frequency (RF) filtering by placing a 1.5µH RF choke in series with the stimulating electrodes to remove unwanted high frequency noise. See Figure 6.4 and Figure 6.4A, B and C.

6.3.2.7 Extracellular volume

Finally the bottom of the NMR tube was filled with silicone to reduce dead space to accelerate the exchange of the extracellular solution when washing in and out the shift reagent. Inhomogeneous or slow exchange of this extracellular compound can lead to poor separation of intra- and extracellular Na^+ and multiple peaks on the ^{23}Na spectra.[393] See Figure 6.4 and Figure 6.4D.

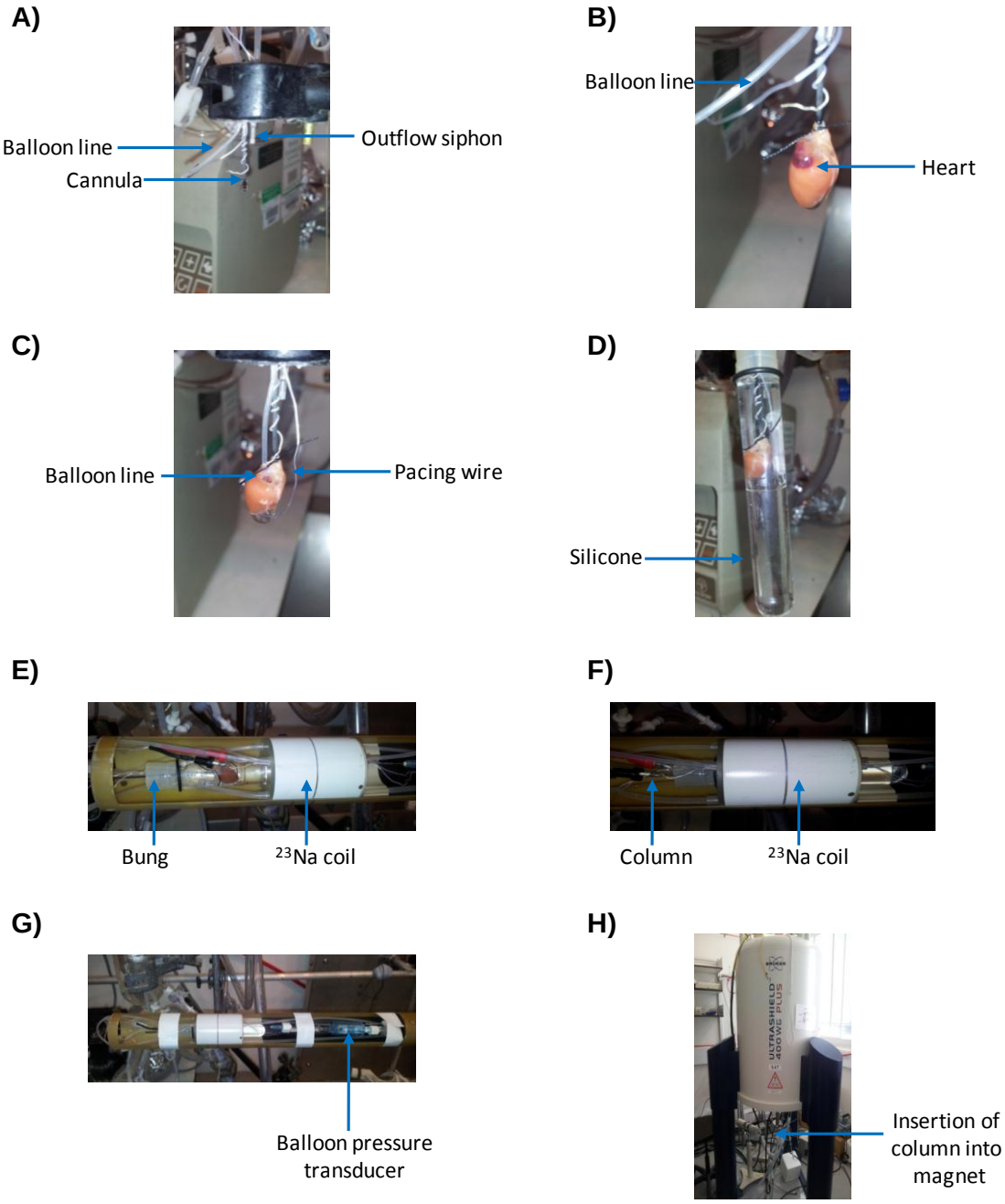

Figure 6.5: Photographs of heart perfusion system and sequence of events showing cannulation of heart, insertion of balloon and positioning of NMR tube inside probe before being inserted into the magnet core.
A) Bung positioned for mouse heart cannulation; B) Mouse heart cannulation; C) Balloon and pacing wires in place; D) Heart placed inside NMR tube; E) Insertion into Na coil; F) Heart in situ in NMR coil; G) All equipment secured in place in NMR column; H) Insertion of column into magnet core.

6.3.3 Heart function inside NMR magnet

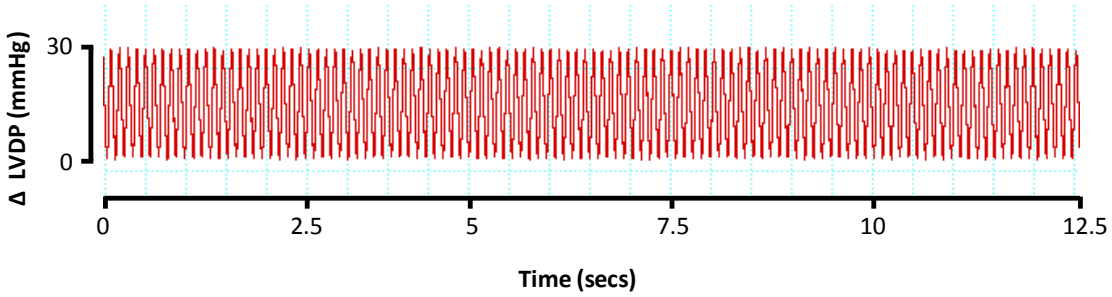

Figure 6.6: Chart traces for LVDP (mmHg) of hearts perfused inside NMR magnet. LVDP measured on previously described modified Langendorff NMR perfusion rig**.** Trace represents 12.5 seconds of perfusion at 550bpm.

Due to the inability to observe the heart throughout the experiment it was important to make accurate function measurements. Figure 6.6 shows an example of LVDP measurements from hearts perfused inside the magnet. It can be seen that the LVDP are much lower than previously shown pressures from hearts cannulated on the standard Langendorff rig (see Chapter 4, Section 4.4.1). This was due to pacing the hearts inside a closed system in order to prevent leaks inside the NMR magnet.

The nature of the "sealed" NMR tube and the extracellular volume connected to the siphoning tube imposes a significant inertia and dampening of left ventricular (LV) contraction. This damps the LVP signal in situ in the magnet, not seen in hearts perfused on the standard Langendorff set-up and not contained within a "sealed" NMR tube. Unfortunately the constraints of the system, and the need to avoid perfusate entering the NMR coil etc., mean that this was the only possible arrangement at this time. Thus, although it was recognised that LV function was lower than that seen usually in Langendorff mouse hearts, this was accepted and exclusion criteria were set at a lower threshold. Hearts were excluded if pacing stimulus was not followed, LVDP <20mmHg, or LVEDP was not stable throughout the protocol.

Again, in subsequent more recent iterations of this apparatus, this problem has been solved but this improved apparatus was not available at the time of these studies.

6.3.4 $Tm(DOTP)^{5-}$ perfusate concentration

$Tm(DOTP)^{5-}$ was used in these studies to reveal the $[Na^+]_i$ signal in the perfused hearts. As previously discussed (Section 6.1.1.1) $Tm(DOTP)^{5-}$ is a known Ca^{2+} chelator and the concentration used in these studies was a compromise between the reduction in Ca^{2+} (and associated decrease in heart function) and an adequate shift in the ^{23}Na spectrum. Preliminary work was done using both 3.5mM $Tm(DOTP)^{5-}$ and 5mM $Tm(DOTP)^{5-}$. 5mM $Tm(DOTP)^{5-}$ broadened the spectral line width effectively reducing the extracellular Na^+ shift compared with 3.5mM $TM(DOTP)^{5-}$. Additionally, Ca^{2+} chelation was greater with 5mM $Tm(DOTP)^{5-}$, as discussed below (Section 6.3.4.1). Therefore 3.5mM $Tm(DOTP)^{5-}$ was used in these studies as it gave an adequate shift of extracellular Na^+ from the intracellular Na^+ peak without excess Ca^{2+} chelation or ^{23}Na peak line width broadening.

6.3.4.1 $Tm(DOTP^{5-})$ chelation of Ca^{2+}

Free Ca^{2+} measurements ($[Ca^{2+}]_{free}$) were performed using standard KHB solutions with a range of Ca^{2+} additions ($[Ca^{2+}]_{added}$) in the presence of 3.5mM or 5mM $Tm(DOTP)^{5-}$ to investigate the effect of shift reagent on Ca^{2+} chelation. Samples were analysed using a blood gas analyser and results plotted.

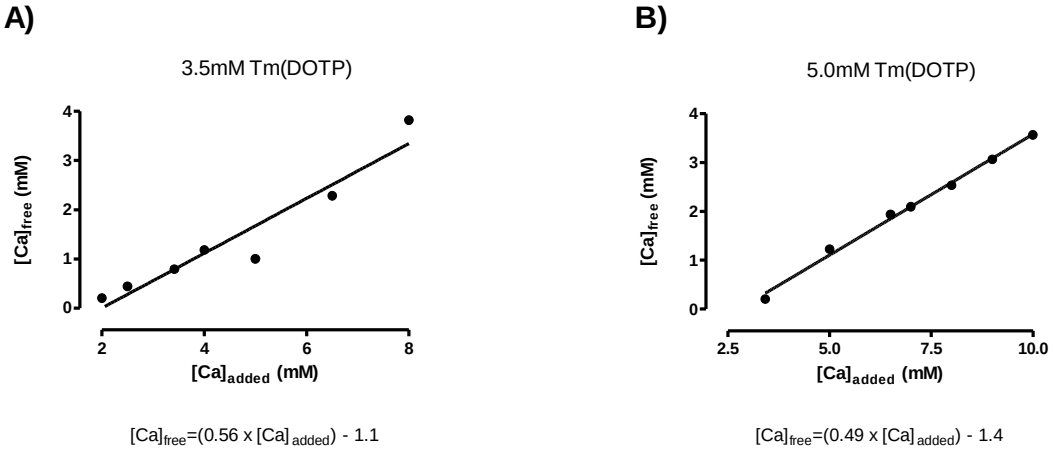

Figure 6.7: Effect of $Tm(DOTP)^{5-}$ on free Ca^{2+} concentration in standard KHB with additional Ca^{2+} supplementation.
A) 3.5mM $Tm(DOTP)^{5-}$ on $[Ca^{2+}]_{free}$ over a range of $[Ca^{2+}]_{added}$; B) 5mM $Tm(DOTP)^{5-}$ on $[Ca^{2+}]_{free}$ over a range of $[Ca^{2+}]_{added}$.

Standard KHB (no $Tm(DOTP)^{5-}$) contained 1.0mM free Ca^{2+}. Chelation of Ca^{2+} by 3.5mM and 5mM $Tm(DOTP)^{5-}$ concentrations are shown in Figure 6.7. It can be seen that both concentrations of $Tm(DOTP)^{5-}$ chelate Ca^{2+} extensively reducing free $[Ca^{2+}]_{free}$, with 5mM reducing $[Ca^{2+}]_{free}$ the most. Both $Tm(DOTP)^{5-}$ chelated 1.4mM $[Ca^{2+}]_{added}$ below the detection limit of the blood gas analyser. With 3.5mM $Tm(DOTP)^{5-}$ an additional 3.75mM $[Ca^{2+}]_{added}$ would be required to obtain a $[Ca^{2+}]_{free}$ of 1.0mM similar to standard KHB solution. Most studies describe adding additional Ca^{2+} to their shift reagent KHB however few indicate the amount added.[375] Some shift reagent rat perfusion studies adjust $[Ca^{2+}]_{free}$ to 0.8mM to maintain function albeit a reduced one,[374] however, none of these studies actually show the effect of shift reagent on LVDP traces. Preliminary data was obtained using 5mM $Tm(DOTP)^{5-}$, assuming that this would give us the greatest shift, with an additional $[Ca^{2+}]_{added}$ of 5mM Ca^{2+} to help maintain normal heart function. Unfortunately though, although heart function remained normal, no adequate shift was observed due to line broadening of the Na^+ peak. However, using 3.5mM $Tm(DOTP)^{5-}$ with additional $[Ca^{2+}]_{free}$ maintained function with adequate shift for exposure of $[Na^+]_i$. Therefore for these studies 3.5mM $Tm(DOTP)^{5-}$ with additional Ca^{2+} was used due to the good spectral extracellular Na^+ shift.

6.3.5 Perfusion protocol

Hearts were cannulated and perfused at a constant flow of 3ml/min with a balloon placed in the left ventricle and LVEDP set between 4-8mmHg in the horizontal column position. Function measurements were derived from the balloon as previously described in Chapter 2, Section 2.3.8. For shift reagent studies once hearts had equilibrated inside the magnet, they underwent a 34 minute stability period before perfusion solutions were exchanged for standard KHB (Chapter 2, Table 2.3) containing 3.5mM $Tm(DOTP)^{5-}$ for 25 minutes. For TQF studies once hearts had equilibrated inside the magnet, they underwent a 20 minute stability period before perfusion solutions were exchanged for standard KHB containing 10nM ISO, 50μM ouabain or standard KHB with rapid pacing at 800bpm for 10 minutes.

6.3.6 NMR spectra acquisition

Spectra acquisition details can be found in Chapter 2, Section 2.9.4. Each perfused heart underwent a series of SQ spectrum acquisition or TQF spectrum acquisition during stability period and interventions e.g. $Tm(DOTP)^{5-}$ perfusion, pacing, ISO perfusion and ouabain perfusion.

6.3.7 Quantification of $[Na^+]_i$ from NMR $Tm(DOTP)^{5-}$ perfusion

It is important to be able to quantify the size of the intracellular ^{23}Na peak obtained in the ^{23}Na spectrum and ideally obtain a value of $[Na^+]_i$ for each heart. For this 2 factors must be known: (1) the relative size of the intracellular ^{23}Na peak and (2) the heart intracellular volume. Firstly, measurement of intracellular ^{23}Na peak size can be estimated by the addition of a reference capillary, inside the NMR tube, which carries a known amount of Na^+ for comparison.[377] The reference capillary ^{23}Na peak (Na_{ref}) must be distinguishable from the intra- and extracellular ^{23}Na peaks so therefore must contain a larger concentration of $Tm(DOTP)^{5-}$ to 'shift' the Na_{ref} further along the frequency scale.

6.3.7.1 Use of reference capillary

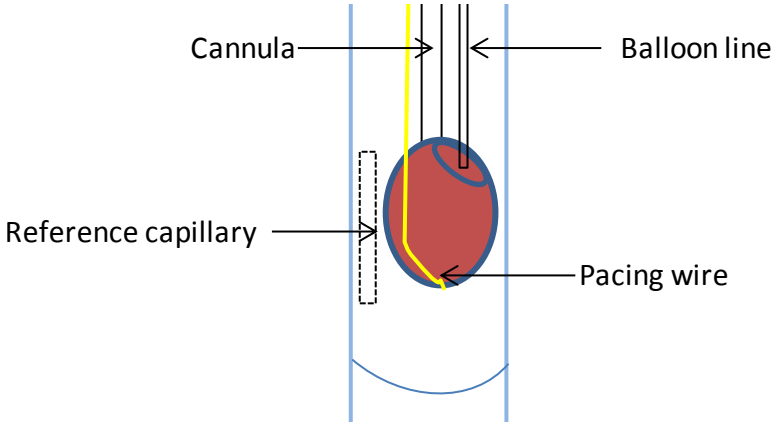

Figure 6.8: Enlarged cross-section of set-up inside NMR tube.
Reference capillary can be seen slotted down the side of the heart in the active region of the coil.

A reference capillary was placed along the side of the heart in the centre of the active region of the ^{23}Na coil. It was necessary to place it in the same plane as the heart so that the ^{23}Na signals were comparable. The reference capillary consisted of a sealed glass capillary tube carrying a known volume and concentration of Na^+ and $Tm(DOTP)^{5-}$. The peak this produced on the spectrum, Na_{ref}, represented the size of ^{23}Na peak for a given number of moles of Na^+ in solution. This was then used to ratio the intracellular ^{23}Na peak on the spectrum to enable the calculation of the number of Na^+ moles in the peak. This could also be done with extracellular ^{23}Na peak but as $[Na^+]_i$ quantification was the main objective the amount of Na^+ inside the reference capillary was similar to expected intracellular Na^+ peak size. Additionally $Tm(DOTP)^{5-}$ concentration used was greater than the concentration used in the final shift reagent study to produce a larger shift. 5mM and 10mM $Tm(DOTP)^{5-}$ were tested with different NaCl concentrations in a 20µl volume capillary (due to small size of active region) to estimate the most appropriate reference capillary solution.

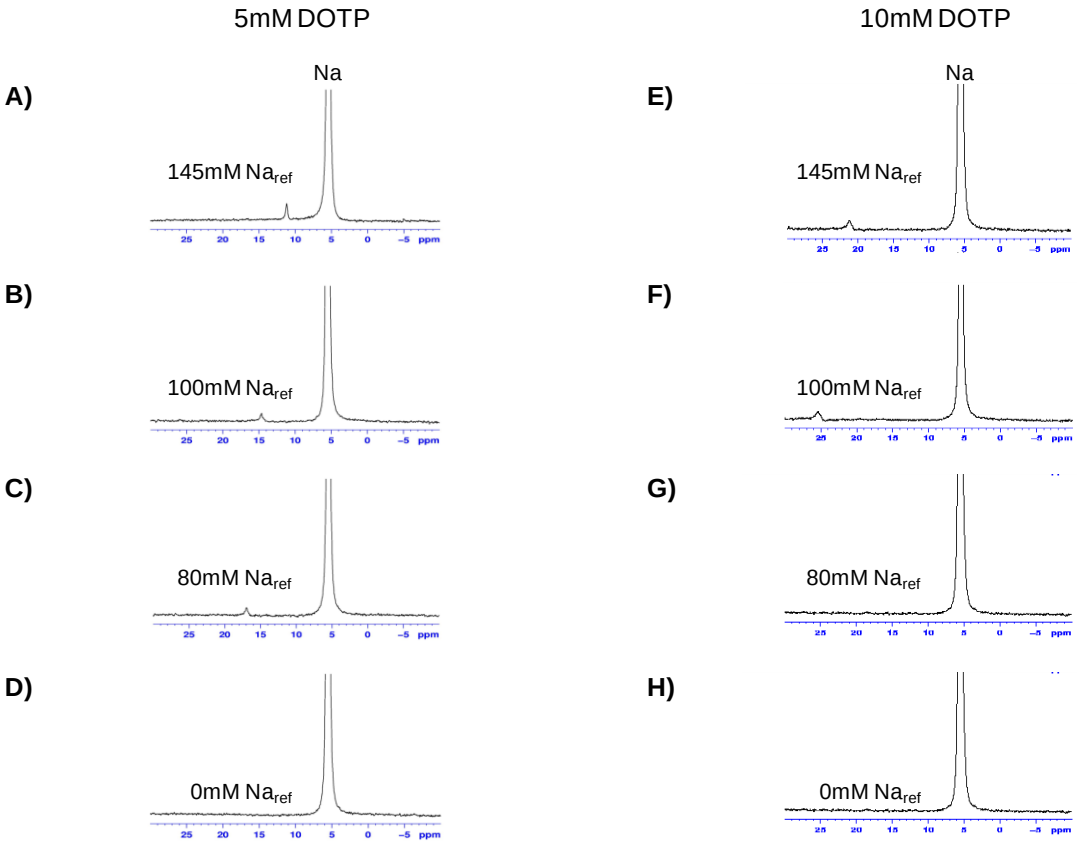

Figure 6.9: Reference capillary peaks.
A) 145mM NaCl + 5mM DOTP; B) 100mM NaCl + 5mM DOTP; C) 80mM NaCl + 5mM DOTP; D) 0mM NaCl + 5mM DOTP; E) 145mM NaCl + 10mM DOTP; F) 100mM NaCl + 10mM DOTP; G) 80mM NaCl + 10mM DOTP; H) 0mM NaCl + 10mM DOTP.

It was decided that a 20µl volume capillary containing 145mM NaCl with 10mM $Tm(DOTP)^{5-}$ would be used for future experiments in shift reagent determination of intracellular Na^+ peak. This reference capillary contains 2.9µmoles of Na^+.

6.3.7.2 Quantification of signal

The integral for each peak area was obtained using Bruker Topspin NMR analysis software and recorded. The integral area of the reference capillary signal was then used to ratiometrically obtain an estimate of the number of moles present in the intracellular ^{23}Na signal as described below:

The peak size, or signal, detected by NMR is proportional to the number of Na^+ moles present. It was then possible to use this reference capillary peak to compare to the intracellular Na^+ peak and thereby determine the number of moles of Na^+ contributing to the intracellular signal. The intracellular volume of each heart was calculated using previous literature values from Jelicks *et al*, 1989[269] who estimated that 0.44ml/g wet weight of the heart was cytosolic or Askensasy *et al*, 1995[270] who estimated that 2.5ml/g dry weight was cytosolic the intracellular volumes were calculated. Therefore the heart was cut down, blotted to remove perfusate in the ventricles and vasculature, and snap frozen at the end of the protocol and wet weight recorded. The heart was then dried for 24 hours to obtain the dry weight and the conversion factor used to calculate the intracellular volume for each heart. This was then used in conjunction with the estimate of the number of moles of Na^+ in the intracellular Na^+ signal to gain a measure of intracellular Na^+ concentration in each heart.

6.3.8 Triple quantum filtering

TQF signals were captured at the same time as single quantum spectra throughout the stabilisation period. Due to the cardio-depressant effect of shift reagent on heart function in experiments where relative changes were sufficient, the TQF signal was used to measure changes from baseline during interventions such as the addition of 10nM ISO, rapid pacing at 800bpm and the addition of 50µM ouabain. Note that these were the same interventions used during the Na^+ uptake flame photometer protocols. For TQF spectra acquisitions see Chapter 2, Section 2.9.4.

6.3.8.1 Analysis of TQF signal

The integral for each TQF scan was obtained using Bruker Topspin NMR analysis software and the area for each peak was recorded. Due to TQF signal variation dependent on the heart shimming, tuning and signal: noise ratio, the changes from baseline stability for each intervention were determined for each heart.

6.4 Results

6.4.1 Function of hearts inside the NMR magnet

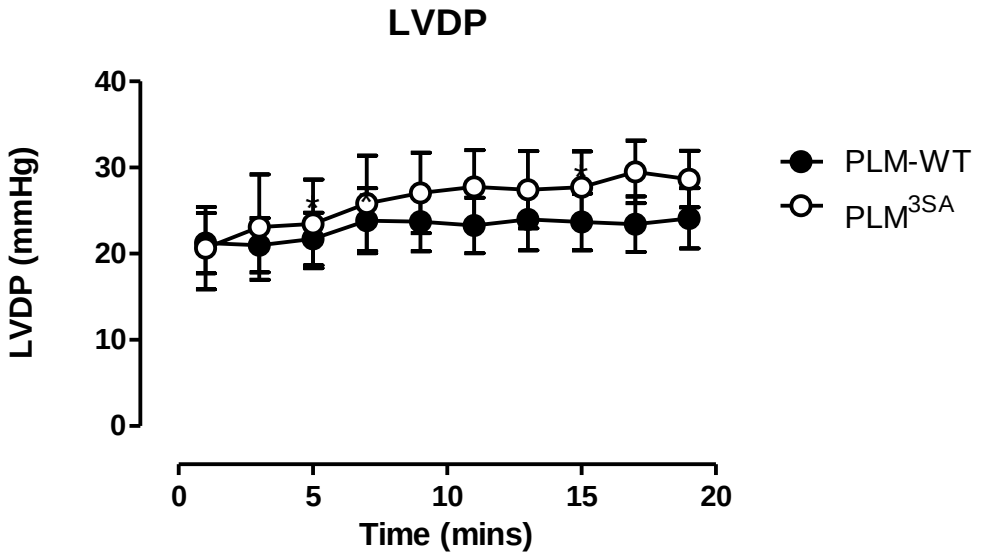

Figure 6.10: NMR cardiac function measurements.
Function measurements from hearts perfused on NMR perfusion rig inside the magnet for PLM-WT and PLM^{3SA} hearts, n=5-6.

As previously discussed in Section 6.3.3 heart function inside the magnet was not optimal when compared with LVDP data for hearts perfused on the standard Langendorff rig. However, heart function inside the magnet for both genotypes was stable over the 20 minute equilibration period and there was little variation between hearts in each group. Developed pressures were approximately ⅓ the amplitude of those seen on the standard perfusion rig. Despite the difficulty in measuring function inside the magnet, PLM^{3SA} hearts showed approximately 17% higher LVDP than WT hearts although this difference, whilst consistent with the significant differences measured earlier (Chapter 4, Figure 4.2), was not significant.

6.4.2 ^{23}Na SQ spectrum

Figure 6.11 shows a ^{23}Na spectrum obtained after optimising the homogeneity of the magnetic field by shimming, matching and tuning the probe. The ^{23}Na peak in this spectrum represents the sum of both extra- and intracellular Na^+ content. The ^{23}Na peak resonates between 0 and 1 (parts per million) ppm.

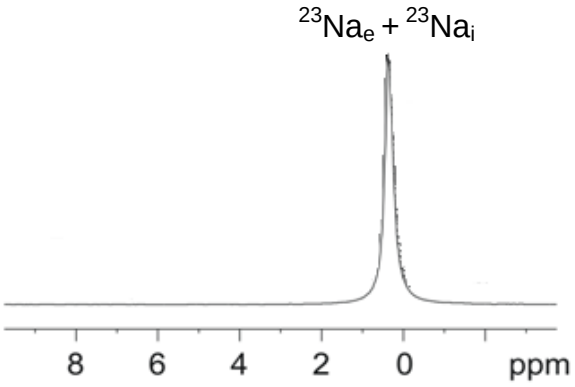

Figure 6.11: Single quantum acquisition of ^{23}Na spectrum.
^{23}Na spectrum acquired from perfused mouse heart paced at 550bpm.

6.4.3 Shift reagent, $Tm(DOTP)^{5-}$, shift of extracellular ^{23}Na peak

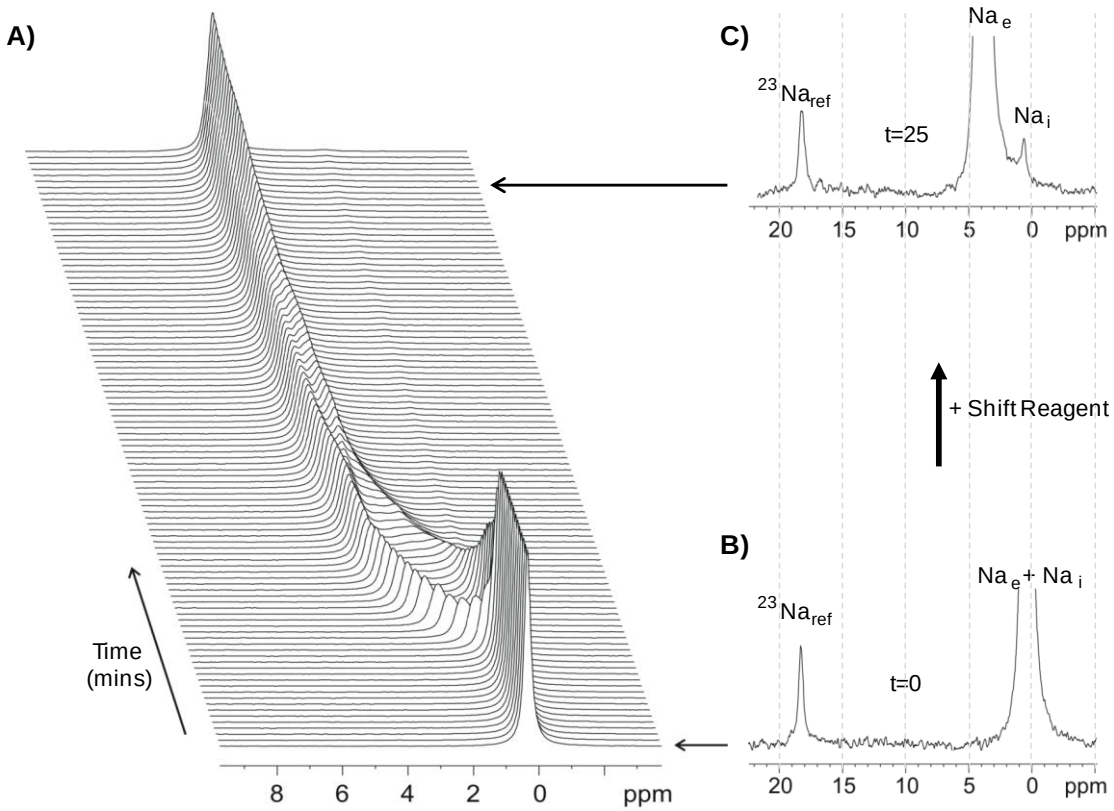

Figure 6.12: Multiple spectra of ^{23}Na acquired from Langendorff perfused mouse heart over time detailing the addition of 3.5mM $Tm(DOTP)^{5-}$.
A) 2D scans showing $Tm(DOTP)^{5-}$ "shifting" extracellular ^{23}Na peak to the left revealing intracellular ^{23}Na peak. B) 1D spectrum of ^{23}Na at time=0 or start of the $Tm(DOTP)^{5-}$ addition; C) 1D spectrum of ^{23}Na at time=25 minutes showing separate extra- and intracellular ^{23}Na peaks.

Using parameters previously defined in methods section (Section 6.3.4) the effect of 3.5mM $Tm(DOTP)^{5-}$ on extracellular ^{23}Na peak was determined. Following the stability period (Figure 6.12B, time=0) hearts were perfused with 3.5mM $Tm(DOTP)^{5-}$ and spectra were acquired over the following 25 minutes. Figure 6.12A shows consecutive ^{23}Na spectrum prior to $Tm(DOTP)^{5-}$ perfusion and then as $Tm(DOTP)^{5-}$ was introduced. It can be seen in Figure 6.12A that the extracellular peak starts to shift slowly to more positive values of ppm scale in a biphasic manner. The sharp time=0 ^{23}Na peak becomes broader and more shallow for approximately 10 minutes after which it again starts to sharpen and increase in height.

The most likely interpretation of this sequence of events is that there are differences in the shifts of vascular and interstitial Na^+ [269] compared with the large extra cardiac volume of perfusate Na^+. The smaller vascular and extracellular Na^+ shifts more quickly to higher ppm than the larger extra cardiac volume of perfusate Na^+; hence the initial shift was not only to the left but also downwards. As the shift reagent gradually accumulated in the larger volume of perfusate surrounding the heart in the NMR tube, this gradually shifted to the left increasing the size of the peak until a single extracellular ^{23}Na peak forms once the shift reagent becomes homogeneously distributed. The shifted extracellular ^{23}Na peak reveals the small intracellular ^{23}Na peak at 0-1ppm seen in Figure 6.12C.

6.4.4 Shift reagent, $Tm(DOTP)^{5-}$, determination of $[Na^+]_i$ in ^{23}Na in PLM-WT and PLM^{3SA} hearts

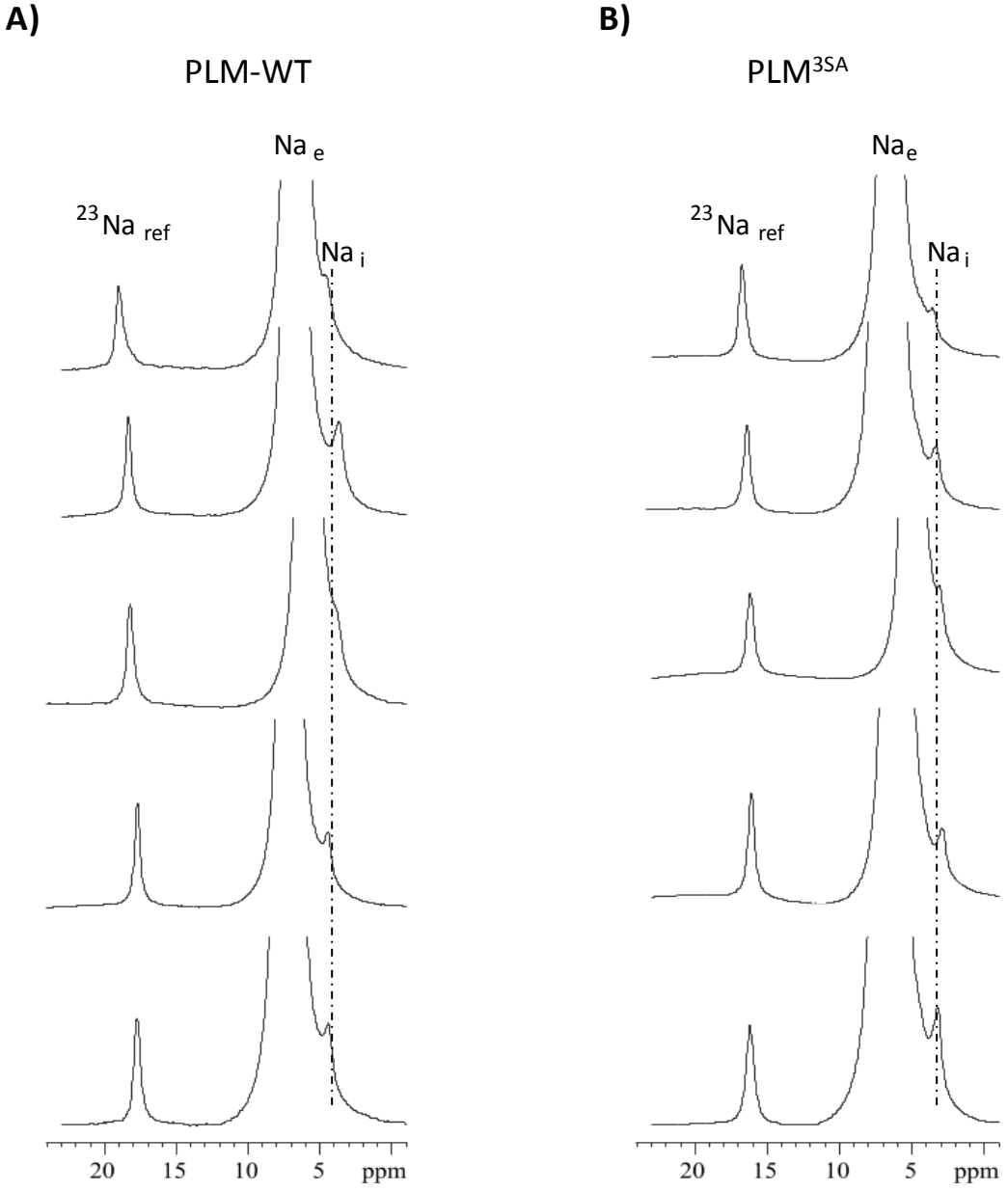

Figure 6.13: ^{23}Na spectra obtained from PLM^{3SA} and WT hearts.
Averaged spectra (4 scans) were obtained in each of 5 PLM-WT (Panel A) and PLM^{3SA} (Panel B) hearts. Spectra were obtained at the end phase of 3.5mM $Tm(DOTP)^{5-}$ perfusion. The Na_{ref} peak represents 2.9µmoles of Na^+.

Each heart was subjected to $Tm(DOTP)^{5-}$ perfusion but the magnitude of the extracellular ^{23}Na shift from the intracellular ^{23}Na peak was dependent on many factors including heart function and the homogeneity of the NMR magnetic field by successful shimming. The broad line width of both the ^{23}Na peaks can be seen and in order to gain an accurate peak integral area for

intracellular ^{23}Na peak, this peak had to be extrapolated from the shoulder of the extracellular ^{23}Na peak. Therefore to obtain the most accurate integral size for intracellular Na^+, spectra were averaged (4 scans) from the end phase of the $Tm(DOTP)^{5-}$ perfusion as shown in Figure 6.12A prior to analysis by Bruker Topspin NMR software. It can be seen that some $[Na^+]_i$ peaks were better separated than others which may reflect the state of the heart during $Tm(DOTP)^{5-}$ perfusion and highlights the need for optimising perfusion.

6.4.5 Quantification of $[Na^+]_i$

Hearts were frozen at the end of the $Tm(DOTP)^{5-}$ experiments and both wet weights and dry weights were taken for all hearts in order to calculate IC volumes using Askenasy *et al*, and Jelicks *et al*, conversion factors.[269, 270] No differences were observed between WT and PLM^{3SA} heart wet or dry weights. See Table 6.1.

Using Bruker Topspin NMR analysis software the averaged 1D spectrum (Figure 6.13) was separated into extra- and intracellular ^{23}Na peaks and integral areas measured for intracellular and reference ^{23}Na peaks. The values for Na_i:Na_{ref} ratio were calculated to obtain the no. of moles in each heart intracellular Na^+ peak. This was then converted using either Jelicks *et al*,[269] or Askenasy *et al*,[270] conversion factors to calculate $[Na^+]_i$ for WT and PLM^{3SA} hearts. These measurements can be found in Table 6.1. It can be seen that using either conversion factor that $[Na^+]_i$ for WT and PLM^{3SA} hearts are the same.

	PLM-WT	PLM^{3SA}	P Value
Wet weight (mg)	201±13	185±9	ns
Dry weight (mg)	33±2	31±1	ns
Wet/Dry Ratio	6±0.2	6±0.3	ns
$[Na^+]_i$ (mM) (*Jelicks*)	14.4±1.9	12.7±2.5	ns
$[Na^+]_i$ (mM) (*Askenasy*)	15.5±1.9	13.0±2.3	ns

Table 6.1: Table of parameters used to calculate $[Na^+]_i$ for WT and PLM^{3SA} hearts.
Table showing averaged wet weight, dry weight and wet: dry weight ratio for PLM-WT and PLM^{3SA} shift reagent perfused hearts paced at 550bpm. n=5 Averaged $[Na^+]_i$ for both genotypes also shown using either wet weight (Jelicks conversion factor[269]) or dry weight (Askenasy conversion factor[270]) for determination. All data expressed as mean±sem and analysed by Student's *t*-test (PLM-WT 'v' PLM^{3SA}), $P<0.05$ was considered significant.

6.4.6 TQF spectra and intracellular ^{23}Na signal

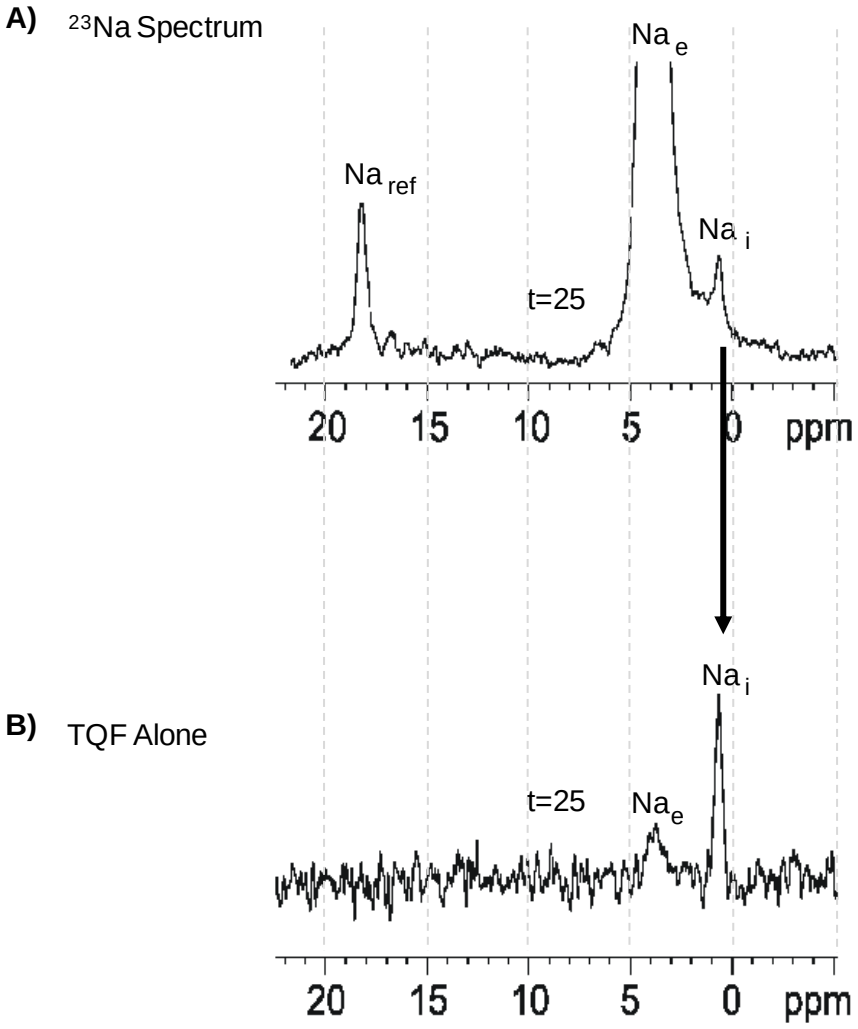

Figure 6.14: TQF analysis of ^{23}Na in the presence of $Tm(DOTP)^{5-}$ to emphasise the contribution of extra- and intracellular ^{23}Na to the total TQF signal.
A) 1D spectrum showing ^{23}Na in the presence of $Tm(DOTP)^{5-}$ at time=25 minutes; B) TQF spectrum for the same heart following $Tm(DOTP)^{5-}$ perfusion protocol.

Although TQF signals are mostly representative of $[Na^+]_i$ signal there still remains a component of extracellular Na^+ signal too. TQF ^{23}Na signals are a combination of intra- and extracellular ^{23}Na signals and in order to measure the contribution of each to the TQF signal, the TQF signal was investigated in the presence of $Tm(DOTP)^{5-}$. Figure 6.14 shows the 1D single quantum ^{23}Na spectrum at the end of the shift reagent perfusion protocol (Panel A), with the accompanying TQF signal (Panel B). It can be seen that the extracellular ^{23}Na peak was greatly

reduced compared with the SQ extracellular ^{23}Na signal. Comparing both extra- and intracellular ^{23}Na peaks it was clearly seen that the $[Na^+]_i$ signal was proportionally much larger, thereby confirming that the majority of the TQF signal was from intracellular Na^+. Using the Bruker Topspin software the relative size of each peak contribution to the TQF signal was measured and $[Na^+]_i$ contribution was estimated as 64% of the TQF signal with 36% from extracellular Na^+.

6.4.7 TQF signal stability

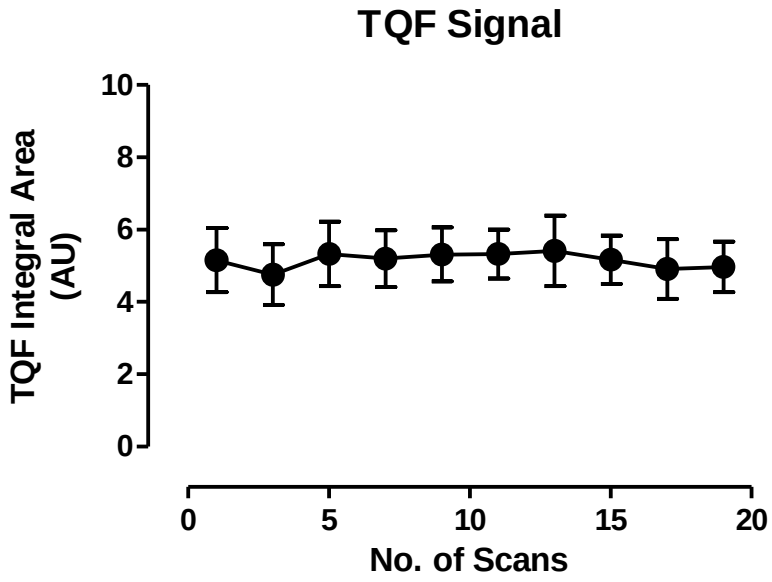

Figure 6.15: TQF signal stability during equilibrium period.
TQF signal stability from mouse hearts perfused in the magnet during stability period. n=6. All data captured on same receiver gain and expressed as mean±sem.

In order to quantify relative changes in TQF signal with rapid pacing, ISO or ouabain perfusion the baseline TQF signal must be stable. Previously it was shown that LVDP during the equilibrium period was stable (Figure 6.10) and TQF scans captured throughout this same period are shown above. Figure 6.15 shows the averaged signals from a random sample of 6 WT hearts and it can be seen that the TQF signal was stable throughout the stability period. The signal was also stable for PLM^{3SA} hearts. It is important to note that all signals were captured at the same receiver gain making it possible to report the mean data for all 6 hearts and observe the TQF signal stability.

6.4.8 TQF changes during rapid pacing, ISO and ouabain stimulation of PLM-WT and PLM^{3SA} Hearts

TQF signals were analysed to quantify any changes induced by rapid pacing or ISO/ouabain perfusion on PLM-WT and PLM^{3SA} hearts. Baseline measurements were defined as the mean of the last 4 scans of the equilibrium period; whilst intervention changes were defined as the mean of the final 4 scans of the intervention period. Relative changes from baseline are shown in Figure 6.16 and were subsequently expressed as % changes which can be seen in Figure 6.17.

Rapid pacing significantly increased the TQF signal in both WT and PLM^{3SA} hearts by a similar amount (approximately 12%). ISO perfusion at constant pacing rate of 550bpm also significantly increased the TQF signal from baseline in both genotypes by a similar amount. Ouabain perfusion greatly increased the TQF signal (>40%) in both genotypes. There were no differences in TQF signal percentage changes from baseline between WT and PLM^{3SA} hearts with rapid pacing, ISO or ouabain.

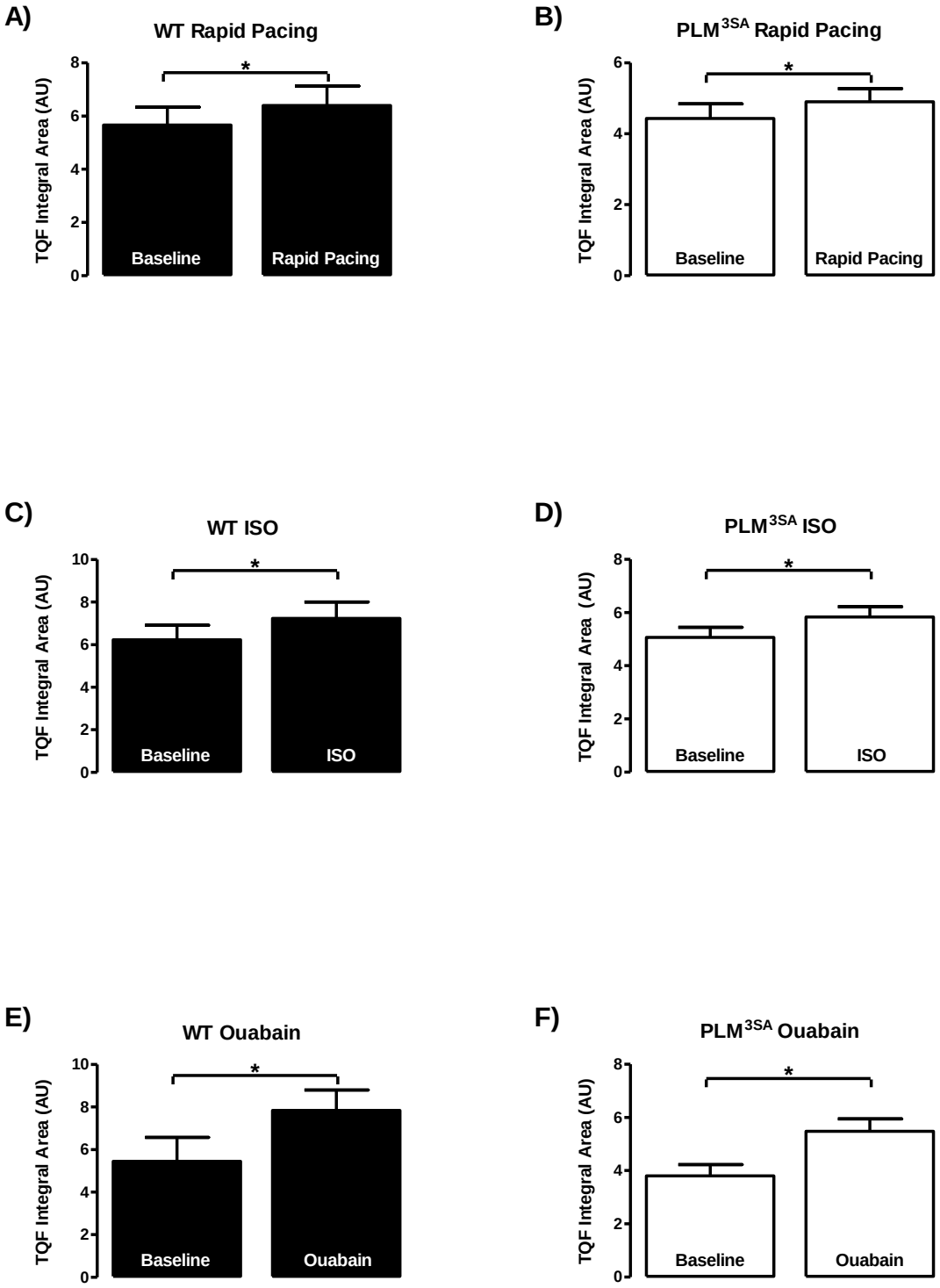

Figure 6.16: TQF relative signal changes with different perfusion interventions in PLM-WT and PLM^{3SA} mouse hearts.
A) Rapid pacing changes to TQF signal in PLM-WT; B) Rapid pacing changes to TQF signal in PLM^{3SA}; C) ISO changes to TQF signal in PLM-WT; D) ISO changes to TQF signal in PLM^{3SA}; E) Ouabain changes to TQF signal in PLM-WT; F) Ouabain changes to TQF signal in PLM^{3SA}. n=4-6. All data expressed as mean±sem and analysed by Paired Student's *t*-test, P<0.05 was considered significant (PLM-WT 'v' PLM^{3SA} denoted by *).

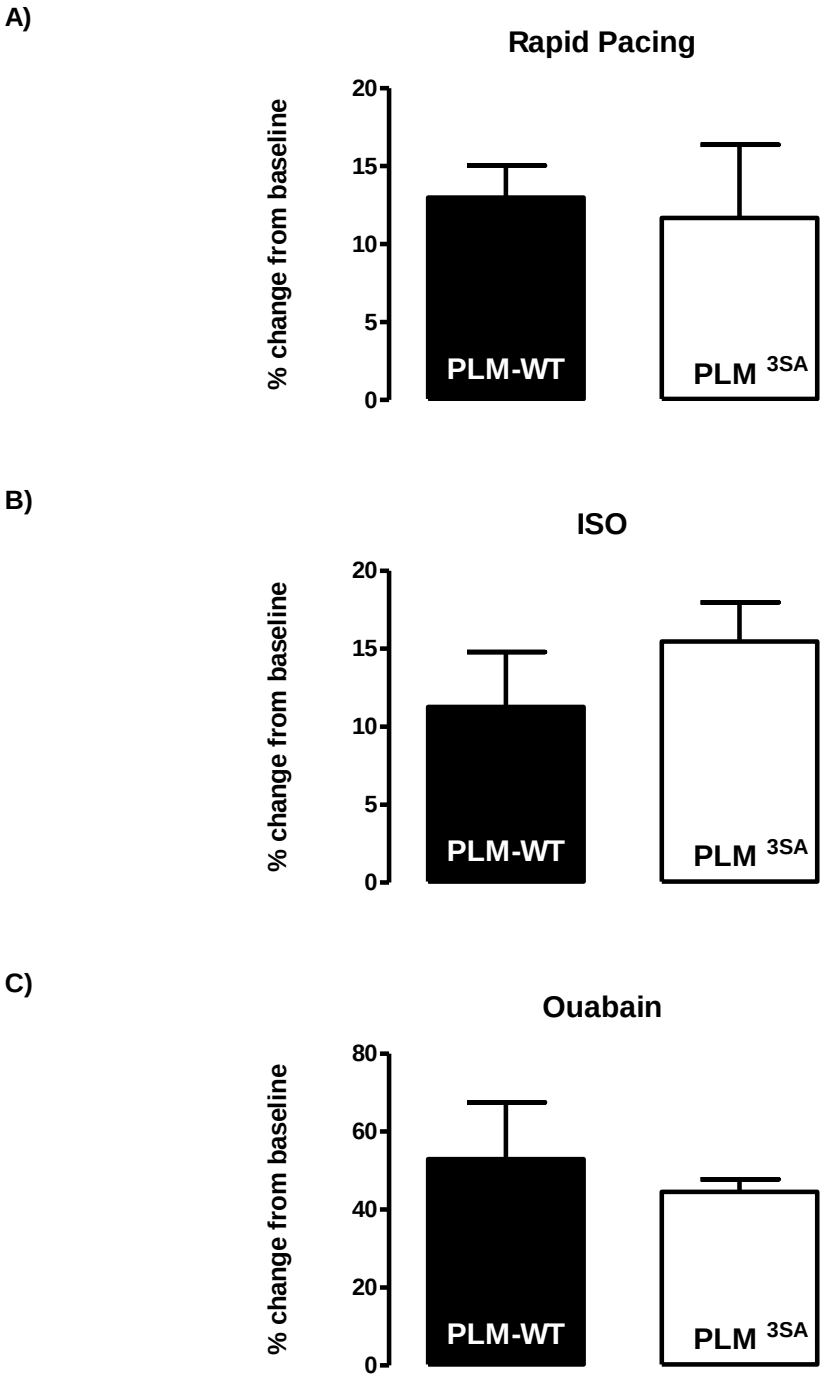

Figure 6.17: TQF signal % changes from baseline in PLM-WT and PLM^{3SA} mouse hearts.
A) % changes from baseline with rapid pacing; B) % changes from baseline with ISO; C) % changes from baseline with ouabain. n=4. All data expressed as mean±sem and analysed by Student's *t*-test, P<0.05 was considered significant (PLM-WT 'v' PLM^{3SA} denoted by *).

6.5 Discussion

In this chapter the development of a Langendorff perfusion rig that allows perfusion of an isolated mouse heart inside a 9.4T magnet was described. Cardiac function measurements from hearts perfused on this rig were shown to be stable in both WT and PLM^{3SA} hearts but depressed when compared to hearts perfused on a standard Langendorff rig. Single quantum ^{23}Na spectra were obtained and separate extra- and intracellular ^{23}Na peaks were resolved with the use of the shift reagent, $Tm(DOTP)^{5-}$. The extracellular ^{23}Na peak was 'shifted' away to a different resonant frequency revealing the intracellular ^{23}Na peak. The presence of a reference capillary, of known Na^+ content, within the active region of the ^{23}Na coil enabled the quantification of $[Na^+]_i$ in WT and PLM^{3SA} hearts. There were no differences in $[Na^+]_i$ between WT or PLM^{3SA} hearts basally paced at 550bpm. An alternative method for measuring $[Na^+]_i$ without the requirement of toxic shift reagent was also investigated and it was shown that TQF signals could be obtained and represented both extra- and intracellular Na^+, with the majority being from $[Na^+]_i$. Rapid pacing at 800bpm, ISO and ouabain all showed relative increases in ^{23}Na signal which were assumed to reflect changes in intracellular Na^+ in the absence of changes to extracellular Na^+.

6.5.1 Establishment of mouse heart perfusion

The initial aim of this chapter was to establish reliable and stable cardiac function of isolated mouse hearts inside the NMR magnet. Particular consideration was given to the maintenance of temperature ensuring that hearts perfused in the magnet were at 37^oC, especially important in mouse heart perfusion.[259, 403] The double water jacketed perfusion lines were essential to this temperature maintenance. Of equal importance was the requirement to pace the hearts at a physiological pacing rate which was done using electrically stimulated pacing wires without introducing significant electrical interference. Despite these considerations cardiac function, although stable, was reduced when compared with LVDP from a standard Langendorff perfusion rig. On a standard Langendorff apparatus perfusion and transducer tubing are kept to a minimum and hearts perfused on a heated cannula and positioned in an unsealed water-jacketed bath containing KHB. With this arrangement hearts paced at 550bpm typically generate 80mmHg – 120mmHg LVDP. However, in the present studies using NMR Langendorff apparatus, LVDP was 20-30mmHg. The reason for this depression of function was two-fold; firstly the constraints of the current system design meant that the heart was perfused

inside a sealed NMR tube which placed large hydrostatic pressures on the heart damping the LV contraction. Secondly the tubing used to connect the balloon to the distal pressure transducers was of small diameter and long length which further compromised the ability to record the already depressed LVP. Both of these factors combined contributed to the measurement of depressed function. The limitations of this system will be addressed and corrected in future perfusion system designs; however for these studies the stability of function, and ATP and creatine phosphate (CP) metabolites measured with ^{31}P NMR (data from studies not shown) suggest that the ^{23}Na NMR data obtained during these studies was reliable.

6.5.2 Use of appropriate shift reagent

In ^{23}Na NMR studies the use of shift reagents to observe intracellular ions has commonly been used. There are several shift reagents available for use each with differing properties for Ca^{2+} chelation and Na^+ shift. It was decided to use $Tm(DOTP)^{5-}$ due to the reports of lower Ca^{2+} affinity and greater tolerance of additional Ca^{2+} supplementation than other shift reagent[379] whilst producing an adequate extracellular Na^+ shift. However, $Tm(DOTP)^{5-}$ in these studies was observed to have a strong relationship between the extent of spectral shift and Ca^{2+} concentration. It appeared that Na^+ and Ca^{2+} both functionally compete for $Tm(DOTP)^{5-}$ binding sites i.e. at low Ca^{2+} concentrations extracellular Na^+ shift is greatest, but at high Ca^{2+} concentrations extracellular Na^+ shift is negligible. Also a higher $Tm(DOTP)^{5-}$ concentration did not necessarily translate to a greater extracellular peak shift but to a greater competition of Na^+ and Ca^{2+} for the binding site. Therefore it was necessary to choose the correct concentration of $Tm(DOTP)^{5-}$ (and additional Ca^{2+} supplementation) to allow optimal discrimination of extra- and intracellular ^{23}Na peak whilst maintaining a more physiological Ca^{2+} concentration. In these studies 3.5mM $Tm(DOTP)^{5-}$ with supplemented Ca^{2+} of $[0.8mM]_{free}$ was used which is similar to that used by others.[375]

The effect of perfusing hearts with lower Ca^{2+} solutions needs to be considered. Low Ca^{2+} solutions may increase intracellular Na^+, at least transiently, by facilitating forward mode NCX.[405] However, van Echteld *et al*, 1997[406] showed that perfusion of isolated rat hearts with 0mM extracellular Ca^{2+} for 30 minutes had no significant effect on intracellular Na^+. Therefore in these studies with shift reagent, it is unlikely that the reduction of extracellular Ca^{2+} to 0.8mM has significantly affected the measured Na^+ under basal conditions.

The objectives of the shift reagent study was to obtain a value for intracellular Na^+ concentrations in both WT and PLM^{3SA} hearts and whilst the above assumptions that reduction of extracellular Ca^{2+} to 0.8mM will have little effect on intracellular Na^+ in WT mouse hearts may not necessarily be true for PLM^{3SA} mouse hearts. Although there is no evidence to suggest a difference between the genotypes, it is important to be aware of reports by Cheung *et al*, that PLM may associate and regulate NCX.[202, 231, 232, 246, 247] Whilst there is no supporting evidence from other laboratories, it still remains possible that NCX function may differ between WT and PLM^{3SA} hearts. Therefore it remains a possibility that lowering extracellular Ca^{2+} to 0.8mM may have differential effects on intracellular Na^+ in the two genotypes.

6.5.3 Measurement of intracellular Na^+: shift reagent vs. TQF

Within this chapter two separate techniques have been utilised to measure intracellular Na^+: (1) the use of shift reagent and (2) TQF. Each technique provides its own unique interpretation of intracellular Na content and is discussed here.

6.5.3.1 Shift reagent

The use of shift reagent allowed the direct quantitative measurement of $[Na^+]_i$[407] in an isolated mouse heart. Many studies have reported the use of shift reagents in perfused rat hearts,[350, 393, 408-413] but little has been done in the isolated mouse heart; however the same limitations apply to both species. There are many shift reagents available for use and collectively shift reagents are considered to be expensive and biologically toxic.[268, 401, 414] Shift reagent properties differ in the degree of toxicity, the efficiency of extra- and intracellular ^{23}Na peak separation, the binding affinities for Ca^{2+} and the tolerance for additional Ca^{2+} supplementation.[379, 392, 395] Often the less toxic the shift reagent, the less peak separation is seen and fully resolved peaks are not obtained.[268] This impacts on the analysis of the separate peak integral area and subsequent calculation of $[Na^+]_i$, potentially allowing over- or under- estimation of the $[Na^+]_i$. Additionally, the reduced sensitivity of the smaller mouse coil, compared with the rat coil, make resolution of the combined ^{23}Na peak difficult prior to shift reagent extra- and intracellular ^{23}Na peak resolution. Ca^{2+} chelation by shift reagent causes additional complications with respect to LV function[358, 394] and much care was taken to select the most appropriate shift reagent for use in

these experiments and the concentration used. The "trade off" between adequate heart function during shift reagent perfusion and adequate, measurable extracellular ^{23}Na shift was complex and a compromise was found.

6.5.3.2 TQF

Alternatively, TQF technique offers a non-invasive method of measuring relative changes in $[Na^+]_i$ content[415] without the need for toxic shift reagent perfusion. Again there are many reports of TQF in perfused isolated rat hearts[381, 400-402, 416] and some even in rabbits,[417] but few studies utilise isolated mouse hearts. Among MQF techniques, TQF is the most sensitive to measuring Na nuclei experiencing quadrupolar interactions[418, 419] and allows $[Na^+]_i$ measurement at normal physiological Ca^{2+} concentrations and therefore during normal cardiac function. However, TQF represents not only the intracellular Na^+ content of the heart but also some extracellular Na^+ content as some extracellular Na^+ ions can experience the same non-averaged quadrupolar interactions. Thus the TQF signal represents both intra- and extracellular Na^+.[420]

The relative contribution of each component to the TQF signal is therefore critical when evaluating changes in intracellular Na^+ over time or during interventions of rapid pacing, ISO and ouabain perfusion. Reports using both TQF and shift reagent in isolated rat hearts have shown that $[Na^+]_e$ contributes to anywhere between 60-75% of the TQF signal[381, 400-402] with $[Na^+]_i$ corresponding to the remaining 25-40%. In these studies however, a contribution of $[Na^+]_e$ to the overall TQF signal was just 36% which is much lower than reported rat $[Na^+]_e$ contributions. However, the important fact is not necessarily the contribution of extracellular Na^+ to the overall TQF signal but whether this contribution changes during subsequent interventions, so any relative changes in the TQF signal can be assigned to changes in $[Na^+]_i$. In perfused rat hearts the TQF signal, in the absence of shift reagent, has been shown to be a reliable indicator of $[Na^+]_i$ content when the contribution from extracellular Na^+ does not appreciably vary.[402] By comparing SQ shift reagent data with TQF data, situations of constant pressure perfusion have been shown to be accompanied by constant $[Na^+]_e$ contribution.[402] Controversy exists concerning the effect of other interventions on $[Na^+]_e$, for example Tauskela *et al*,[402] have suggested that stop-flow ischemia causes collapse of the vasculature affecting cell volume and reduces extracellular Na^+ contribution to the TQF signal, therefore $[Na^+]_i$ changes are greatly underestimated. Dizon *et al*,[381] support this finding; however, Schepkin *et al*,[401]

reported that $[Na^+]_e$ TQF contribution remains unchanged with cessation of flow. The main difference between the two studies being that reperfusion was instigated in the later study which may have reversed the vascular collapse and restored $[Na^+]_e$ contribution. Ischemia is also known to be accompanied by intracellular swelling which contributes to the observed slow $[Na^+]_i$ increase rate. Changes to extracellular Na^+ are important when assessing the effect of ouabain, rapid pacing and ISO on $[Na^+]_i$ by TQF. TQF studies with ouabain at high concentrations (0.2 and 1mM) have been shown to increase TQF intracellular Na^+ content rapidly with little change in extracellular Na^+ contribution.[381, 401, 402] Isolated rat hearts studies by Jelicks *et al*,[420] investigating pacing effects on $[Na^+]_i$ by TQF showed increases in $[Na^+]_i$ in normotensive rat with little change in extracellular Na^+. However, ISO effects on $[Na^+]_i$ have been rarely studied by NMR techniques and the effect of ISO on TQF ^{23}Na signals has not been investigated. Therefore no firm conclusions can be made as to the whether there is any change to extracellular Na^+ contribution to the TQF signal, however it is unlikely.

Most importantly the sensitivity of TQF signal to intracellular Na^+ over extracellular Na^+ has been reported to be at least 10-fold[401] with one report suggesting 23-fold sensitivity[381]. Therefore it can be concluded that the measurement of any changes to $[Na^+]_i$ by TQF attenuates the effect of possible changes in $[Na^+]_e$ and if anything an underestimation of $[Na^+]_i$ will be made.[401] In the studies discussed here the TQF changes will be ascribed to changes in $[Na^+]_i$ only.

6.5.3.3 Shift reagent vs. TQF

Both of the methods for measuring $[Na^+]_i$ have their limitations. The use of shift reagents is expensive, they are considered toxic and chelate Ca^{2+} which compromises cardiac function and the extent of extracellular ^{23}Na shift. TQF measurement of $[Na^+]_i$ is not detrimental to the heart function, as can be measured throughout normal cardiac function, and is mostly representative of $[Na^+]_i$ with a small contribution from extracellular Na^+ which does not change during stability or intervention protocols. Very recent observations (not shown) investigating DQF measurements of ^{23}Na, using a special flip angle (56^o), has shown an almost unique signal corresponding to extracellular Na^+ only which does not change with ouabain or ISO. This is currently being characterised as a method for measuring extracellular Na^+ as an internal control for the use of TQF to assess $[Na^+]_i$ changes. Additionally the lack of the ability to quantify $[Na^+]_i$ without calibration by shift reagent is an issue. Therefore within these studies both

methods were utilised to gain a better understanding of $[Na^+]_i$ in both genotypes and how this was affected by ISO, rapid pacing and ouabain interventions.

6.5.4 Shift reagent estimation of basal $[Na^+]_i$ in WT and PLM^{3SA} hearts

The shift reagent, $Tm(DOTP)^{5-}$, was used to resolve intra- and extracellular ^{23}Na peaks on the SQ ^{23}Na NMR spectrum and subsequent peak integral analysis by Bruker Topspin NMR software it was estimated that the $[Na^+]_i$ in WT and PLM^{3SA} isolated mouse hearts was the same (WT: 14.4±1.9mM; PLM^{3SA}: 12.7±2.5mM). Previous literature reports for $[Na^+]_i$ vary greatly depending on species and methodology used for detection (see Table 6.2 for comprehensive list of $[Na^+]_i$ measured in cardiac muscle by a range of techniques in multiple species). Initial studies by Ellis in sheep Purkinje fibres using ion-selective electrodes determined that $[Na^+]_i$ was 9mM,[421] which was further supported by additional studies.[405, 422] Other reports of using ion-sensitive electrodes in alternative species such as rabbit and guinea pig to measure $[Na^+]_i$ ranged from 5-9mM.[423-426] Ion-sensitive electrodes are direct measurements from individual cells within an isolated tissue preparation maintained at physiological temperatures within bathing solution and use standard calibration buffers to determine the relationship between measured Na^+ activity and Na^+ concentration.[351] For each preparation the calibration constant, or activity coefficient, may vary compared with the actual intracellular activity coefficient of the tissue which may lead to under/over estimation of $[Na^+]_i$. For example when comparing ISE results with those reported by flame photometry or atomic absorption spectroscopy (AAS) estimates of $[Na^+]_i$ are often greater in the latter experimental technique. Studies in rabbit and guinea pig ventricle reported $[Na^+]_i$ >30mM[347, 427] and often studies by the same group comparing ISE and AAS in the same samples vary greatly in $[Na^+]_i$ measurements.[428] As previously discussed in Chapter 5 complications arise with flame photometry methods due to the removal of Na^+ from the extracellular compartment. Incomplete extracellular Na^+ washout or too prolonged a washout that leads to the loss of $[Na^+]_i$ via Na gradient can affect $[Na^+]_i$ estimations. In addition Na^+ measured by AAS/flame photometry may include bound Na^+ that does not necessarily participate in the dynamic Na^+ concentration in the intracellular space[351] and therefore may lead to overestimation of $[Na^+]_i$. Indeed a study by Malloy *et al*,[350] comparing $[Na^+]_i$ measured in rat heart using flame photometry and ^{23}Na NMR showed large differences in $[Na^+]_i$ (AAS: 30.7mM; ^{23}Na NMR: 6.2mM).

Conflicting reports for $[Na^+]_i$ measurements make the need for accurate reliable techniques extremely important. SBFI measurements of $[Na^+]_i$ are, in the majority, in agreement with those

reported by ion-selective electrodes and results from a variety of species range from 3-12mM.[2, 5, 6, 9, 28, 361, 428] The main concern with estimates of $[Na^+]_i$ from SBFI is that measurements are made at room temperature which may affect the dynamics of the Na^+/K^+ ATPase enzyme and may not reflect in-situ measurements of intracellular Na^+.[62] There are clearly species differences when comparing SBFI measurements of $[Na^+]_i$ with rat and mouse myocytes reporting the greatest $[Na^+]_i$ (11-12.5mM) which has been discussed by Bers *et al*, and concluded to arise from differences in Na^+ influx between the species.[3] Interestingly, there are conflicting reports of SBFI measurements in mouse myocytes from the same strain. $[Na^+]_i$ in PLM-WT and PLM-KO myocytes by SBFI have been measured by Despa *et al*,[28] and shown to be 12.5 and 12mM respectively whilst Wang *et al*,[361] have reported measurements of 7.8 and 5mM respectively which are closer to values reported in guinea pig and rabbit myocytes.[6] The results from this current NMR study are in agreement with those reported by Despa *et al*,[28] at 14.4mM in WT mouse hearts. Potentially the slighter higher reading in this study compared with SBFI measurements is the physiological state of the heart compared to the myocyte. In this study whole hearts were paced at physiological heart rate of 550bpm whereas the measurements by Despa were in quiescent myocytes. Indeed Despa went on to measure changes in $[Na^+]_i$ with pacing at 2Hz and showed increases in $[Na^+]_i$ of ~2mM after 2 minutes of pacing. 2Hz is the equivalent heart rate of 120bpm which is not physiological for a mouse heart. Additionally, although Wang *et al*, reported different baseline $[Na^+]_i$ from Despa in quiescent myocytes they did report a similar 2mM increase in Na^+ with pacing at 2Hz. The different experimental set-ups may therefore account for greater $[Na^+]_i$ observed in this NMR study.

Comparing the results from this NMR study with $[Na^+]_i$ measured in other NMR studies (although no mouse $[Na^+]_i$ has been reported) $[Na^+]_i$ in perfused hearts from other species range from 4.8 to 11.4mM[269, 350, 368, 409, 429] with lower values estimated from guinea pigs and with most rat heart measurements in the range of 9.4-11.4mM. In these studies similar Ca^{2+} chelation was encountered, as previously discussed, and additional Ca^{2+} supplemented ensuring $[Ca^{2+}]_{free}$ was 0.8-1mM. Rat hearts were paced or free running with heart rates in the physiological region of 250bpm. Compared with these reported $[Na^+]_i$ the results from this mouse heart study at 14.4mM in WT hearts are similar.

Comparison of $[Na^+]_i$ between the two genotypes WT and PLM^{3SA} show no differences in sodium measurements as previously hypothesised. It was hypothesised that unphosphorylatable PLM may increase $[Na^+]_i$ in PLM^{3SA} mouse hearts compared to WT. The lack of intracellular Na^+ differences between the genotypes is in agreement with the previous flame photometer

heart study, although the accuracy and usefulness of this is debatable (see Section 5.4.3). Previously in PLM-KO mice it was thought that the absence of PLM and increased pump function[28, 33] may result in lower $[Na^+]_i$ than WT mice due to the lack of PLM inhibition on the Na^+/K^+ ATPase, this was not the case.[28] However, the additional discovery of significantly reduced Na^+/K^+ ATPase alpha subunits in PLM-KO mice[28, 33] compared with WT was consistent with the idea that potentially the higher pump rate is offset by a lower number of Na^+/K^+ ATPase molecules resulting in normal baseline $[Na^+]_i$. With respect to PLM^{3SA} mice $[Na^+]_i$ it was previously shown in Chapter 3 that expression of both α1 and α2 Na^+/K^+ ATPase subunits in heart homogenates was unchanged, but total PLM protein expression was significantly decreased. Further data shows that pump activity measured using ruptured patch clamp techniques in resting myocytes at 35^{o}C at 25 and 50mM pipette Na^+ is the same in both genotypes (not shown). Therefore it would not be unreasonable to conclude that the changes in PLM expression in PLM^{3SA} mouse hearts offsets the presence of unphosphorylatable PLM on the pump and results in similar net pump rate in WT and PLM^{3SA} mouse and consequently $[Na^+]_i$ measurements at baseline heart rates are the same.

NB. For summary table of $[Na]_i$ measured by ISE, AAS/flame photometry, SBFI and ^{23}Na NMR in a variety of species see Table 6.2.

6.5.5 TQF measurement of $[Na^+]_i$ changes with rapid pacing

Relative changes from baseline in $[Na^+]_i$ measured by TQF showed increases in $[Na^+]_i$ in both WT and PLM^{3SA} mouse hearts with rapid pacing. Increases in stimulation frequency have been reported to increase $[Na^+]_i$ in a variety of species and preparations.[352-355] Ion-selective microelectrodes were used to measure changes in intracellular Na^+ activity by Cohen *et al*,[430] in sheep Purkinje fibres and a direct correlation between intracellular Na^+ activity and stimulation rate was observed. Langer hypothesised that increases in pacing rate causes increased Na^+ influx rate which outbalances Na^+ efflux by Na^+/K^+ ATPase until a new $[Na^+]_i$ steady state is reached.[360] These pacing induced rises in $[Na^+]_i$ are an important determinant in the force-frequency relationship.

Increases in $[Na^+]_i$ in rat and guinea pig myocytes have been reported with pacing[6] and in this study were associated with increases in contractility. However, these increases are often absent in the intact rat heart which usually display loss of contractility with increased rate.[431] Indeed, SBFI studies in Langendorff-perfused rat hearts by Maier *et al*,[306] reported a decrease in

contractility of 49% but an increase in $[Na^+]_i$ of 4mM when hearts were paced from 0 to 6Hz. Additionally, other studies in the isolated rat hearts using ^{23}Na NMR have reported similar changes in contractility and $[Na^+]_i$ with increased pacing rate (250bpm-500bpm).[356, 432, 433] However, some NMR studies have seen no change in $[Na^+]_i$ with increased pacing[434] but did see a decrease in contractility. Perhaps the changes in $[Na^+]_i$ were small and could not be resolved with this technique at this time.

It has been proposed that the changes in $[Na^+]_i$ and contractility are not only pacing rate dependent but also dependent on extracellular cation concentration.[357] Simor *et al*,[358] showed that differences in $[Ca^{2+}]_e$ affected the FFR and extent of $[Na^+]_i$ increases with increasing pacing rates. Low $[Ca^{2+}]_e$ (0.24mM) showed the smallest increases in $[Na^+]_i$ but the greatest decreases in LVDP, whereas the highest $[Ca^{2+}]_e$ (2.2mM) showed the greatest increases in $[Na^+]_i$ with the smallest decreases in LVDP. This is an important consideration when quantifying $[Na^+]_i$ using shift reagent due to the Ca^{2+} chelating nature of shift reagent. Therefore the relative changes in $[Na^+]_i$ measured by TQF were at a physiological free Ca^{2+} concentration (1.0mM) which were previously reported to increase $[Na^+]_i$ and decrease contractility with increased stimulation frequency.[358]

In Chapter 4, Section 4.4.3 a negative FFR in both WT and PLM^{3SA} mouse hearts was observed and so significant increases in $[Na^+]_i$ seen in these experiments was anticipated. The TQF increases, although significant, appear small (about 11%) however previously in mouse myocytes both Despa[28] and Wang[361] found changes in $[Na^+]_i$ of ~2mM in WT and PLM-KO myocytes when pacing from 0Hz to 2Hz over a relatively short period of time (2minutes). Changes in $[Na^+]_i$ in perfused rat hearts were of similar magnitude with Lotan *et al*,[357] measuring changes of 2.78mM and Simor *et al*,[357] measuring changes of 0.84mM (250bpm to 500bpm). Therefore extrapolating these data with the previous shift reagent $[Na^+]_i$ estimations, an increase of 11% would potentially represent a change of 1.58mM in WT hearts and 1.4mM in PLM^{3SA} hearts (500 to 800bpm).

In mouse myocytes rapid pacing has been shown to cause an increase in $[Ca^{2+}]_i$ activating NOS and producing NO which in turn phosphorylates PLM by PKCε.[177] Activation of the Na^+/K^+ ATPase pump by this route will in turn help the cell to cope with rises in $[Na^+]_i$. Therefore it was hypothesised that $\Delta[Na^+]_i$ would be greater in PLM^{3SA} mouse who carry unphosphorylatable PLM. However, no differences were seen in $\Delta[Na^+]_i$ between WT and PLM^{3SA} mouse hearts, which was in agreement with data from Na^+ flame photometry studies (however no increase from baseline was observed either). Additionally, the FFR in Chapter 4,

Section 4.4.3 showed no differences in the gradients of the negative FFR slope between genotypes supporting the similar increases in $\Delta[Na^+]_i$ seen. Potentially any differences between the genotypes may be too subtle to detect accurately with this methodology. Or stimulation of the NO pathway by pacing in myocytes is already saturated in whole hearts and contributes only to basal PLM phosphorylation and no further PLM phosphorylation is seen with rapid pacing at 800bpm.

6.5.6 TQF measurement of $[Na^+]_i$ changes with ISO

Relative changes in $[Na^+]_i$ measured by TQF showed increases in $[Na^+]_i$ in both WT and PLM^{3SA} mouse hearts with 10nM ISO perfusion. At a constant pacing rate catecholamines increase Ca^{2+} influx[423] which may increase $[Ca^{2+}]_i$, favouring forward mode NCX and potentially increasing Na^+ influx. However, the effect of catecholamines on sodium activity in cardiac tissue has been measured using ion-selective electrodes in quiescent myocytes (rabbit),[125] quiescent and active Purkinje fibres (canine and sheep)[126, 297, 435-437] and quiescent ventricular tissue (canine).[435] These studies report decreases in Na^+ activity with the application of noradrenaline or isoprenaline opposing the findings of these TQF measurements. It is possible that the opposing results in this study were due to differences in experimental set-up. Measurements made in quiescent tissue and myocytes will differ to those in active tissue due to the lack of an action potential which will affect transmembrane ionic fluxes and intracellular activities.[423] This may significantly change intracellular Na^+ activity and measurements are unlikely to be physiologically relevant. Additionally species differences and tissue choice for sodium activity measurements could contribute to differences seen with the addition of ISO. Undeniably though, the majority of studies agreed that the addition of catecholamines increased sodium efflux via the Na^+/K^+ ATPase. This was later shown to be due to PLM phosphorylation.[28, 30, 32]

Despa *et al*,[28] extensively investigated the effect of ISO in mouse myocytes from WT and PLM-KO hearts using SBFI. They showed that in quiescent myocytes $[Na^+]_i$ decreased upon addition of ISO, an effect that was absent in PLM-KO myocytes implicating the role of PLM in regulating $[Na^+]_i$. Additionally they also looked at the effect of ISO in myocytes paced at 2Hz to simulate the chronotropic response of β-adrenergic stimulation and found that $[Na^+]_i$ increased on pacing in both genotypes. However, when ISO was applied $[Na^+]_i$ decreased in WT myocytes only, returning to near resting levels.[32] Similar ISO effects were seen by Wang *et*

al,[361] when measuring $[Na^+]_i$ by SBFI in WT and PLM-KO myocytes. These are in contrast to the results seen in this TQF study which show relative intracellular Na^+ increases in both WT and PLM^{3SA} hearts. The lack of phosphorylatable PLM in PLM^{3SA} hearts may account for the increase in $[Na^+]_i$ in these hearts as Na^+ influx is potentiated by ISO[53] but is no longer accompanied by PLM phosphorylation at Ser68 so the pump is not stimulated. Na^+ influx would then outweigh Na^+ efflux, leading to intracellular Na^+ loading. However, in WT hearts an effect of ISO such as no change or a decrease in $[Na^+]_i$ (secondary to stimulation of the pump by PLM phosphorylation) may have been expected.

At the time of these studies were undertaken, cardiac function measured in the magnet was admittedly poor. While this has now been corrected, it is important to recognise that the suboptimal quality of this initial preparation may undermine the quantitative validity of the data. The studies described here therefore provide a useful characterisation of the methods and "proof of principle" but it is important to recognise that specific quantification of $[Na^+]_i$ in the different genotypes and protocols needs repeating in the recently improved set-up. Unfortunately these studies could not be repeated in time for the inclusion in this thesis.

Recognising the limitations of the data described above, it is also appropriate to consider other interpretations of the data. It is possible that differences in the models used and experimental protocols may contribute to the contrasting results obtained here with those in the literature. For example, the SBFI measurements are made at room temperature which may affect ion channel kinetics altering equilibrium $[Na^+]_i$ and $[Ca^{2+}]_i$ questioning the physiological relevance of these measurements. Additionally, the pacing rate of 2Hz used to simulate chronotropic β-adrenergic stimulation is low and may alter the balance between systolic and diastolic intervals. Since the isolated heart data was measured in hearts beating at physiological rates and temperatures perhaps these better reflect the actual *in vivo* effect of ISO. However, Wang *et al*, also looked at *in vivo* haemodynamic effects of ISO concentration response curve on isolated mouse heart and inferred decreases in $[Na^+]_i$ based on a delayed decline in LVDP after each additional concentration; an effect which was absent in KO hearts.[361] This induced ISO decline was not seen in the WT LVDP measurements in the current TQF study due to the continuous background pacing of 550bpm and a concentration of ISO low enough not to increase chronotropy further.

As discussed in Chapter 5, Section 5.5.1.2 perhaps the concentration of ISO used was too low to evoke measurable changes in WT $[Na^+]_i$ in isolated hearts and other studies that have seen effects in myocytes use greater concentrations of 1μM.[32, 361] However, Western blot data of

ISO perfused heart homogenates showed increased PLM phosphorylation at Ser68 from baseline with the concentration used in this study. In future perhaps an ISO concentration response curve in unpaced hearts will reveal differences in $[Na^+]_i$.

6.5.7 TQF measurement of $[Na^+]_i$ changes with ouabain

Relative changes in $[Na^+]_i$ measured by TQF showed increases in $[Na^+]_i$ in both WT and PLM^{3SA} mouse hearts with 50µM ouabain perfusion. Ouabain is a known inhibitor of Na^+/K^+ ATPase[330] and has been used extensively to investigate the effect of Na^+/K^+ ATPase inhibition on $[Na^+]_i$. It is well documented that ouabain has a positive inotropic effect[438-443] which has generally been accepted to be due to an increase in $[Na^+]_i$[316, 362, 363] and subsequent increases in $[Ca^{2+}]_i$ via NCX. Inhibition of the pump by ouabain has been shown in many species and tissues (rabbit auricles,[444] guinea pig hearts,[445] frog heart,[446] sheep Purkinje fibres,[364] rat hearts,[368, 400, 401] cat ventricular myocytes[447]) with the majority reporting increases in inotropy but not all show increases in $[Na^+]_i$. Indeed, it appears that at low concentrations (sub 300nM) inotropic effects can occur without changes in bulk $[Na^+]_i$[364, 445] however at high concentrations large increases in $[Na^+]_i$ are seen. This may reflect the existence of a subsarcolemmal "fuzzy space" for Na^+ as discussed in Chapter 1.

Studies using ^{23}Na NMR have reported large changes in $[Na^+]_i$ using both shift reagent and TQF methods. Van Emous measured changes in rat heart $[Na^+]_i$ with 250µM ouabain using shift reagent and saw an increase of 32% sodium concentration compared to control.[368] Various TQF studies using 1mM ouabain, showed increased changes in intracellular Na^+ signal ranging from 159-210% pre-baseline control in rat hearts.[400, 401] The study presented in this chapter used 50µM ouabain which resulted in a TQF signal increase of 53% in WT and 44% in PLM^{3SA} mouse hearts. This is similar to TQF changes reported with 250µM rather than 1mM ouabain in rat hearts, showing that TQF $[Na^+]_i$ changes are concentration dependent and the mouse, like the rat, is relatively resistant to ouabain. There are many reports of different species displaying varying degrees of sensitivity to ouabain inhibition.[71, 448] Enzyme preparations from rat hearts have been shown to have low ouabain sensitivity[449-453] further supported by studies in perfused rat hearts.[454] Mouse hearts have been shown to be similar to rat hearts with respect to ouabain sensitive alpha subunits[455] and therefore similar $[Na^+]_i$ changes may be expected. The results contrast with those seen in Chapter 5, Section 5.5.1.3 (which showed no change in intracellular Na^+ with ouabain in both genotypes) and confirms that flame photometry may not be sensitive enough to measure accurate changes in intracellular Na^+.

The lack of differences with TQF changes in WT and PLM^{3SA} were not unexpected. There is no reason to assume that a mutation in PLM would impact the ouabain binding site on the Na^+/K^+ ATPase pump. However, additionally to species differences with ouabain sensitivity, different Na^+/K^+ ATPase α subunits are known to be ouabain sensitive or resistant. Na^+/K^+ ATPase α1 subunits are known to be ouabain resistant whilst α2 subunits are ouabain sensitive.[456] Studies using SWAP mice which "swapped" the ouabain resistance to converse subunits showed that in myocytes the main effect of ouabain on Ca^{2+} transients and $[Na^+]_i$ was via the α2 subunit;[456] and that the low concentration 5μM of ouabain used increased $[Na^+]_i$ by 2mM. Protein expression studies from Chapter 3, Section 3.4.2.2 have shown that both Na^+/K^+ ATPase α1 and α2 subunit protein expression were similar in WT and PLM^{3SA}. Hence ouabain affinity for the pump binding site was most probably the same in both genotypes resulting in similar pump inhibition and consequently TQF signal changes. The previous shift reagent analysis of $[Na^+]_i$ has shown similar starting $[Na^+]_i$ values therefore similar TQF changes in WT and PLM^{3SA}, and thus $[Na^+]_i$, was not unexpected.

6.6 Summary

^{23}Na NMR provides a non-invasive technique to measure $[Na^+]_i$ in perfused beating mouse hearts. Cardiac function measurements showed depressed but stable function in both WT and PLM^{3SA} mouse hearts perfused in the magnet compared with standard Langendorff cardiac measurements. Perfusing hearts with the shift reagent, $Tm(DOTP)^{5-}$, caused extracellular Na^+ ions to resonate at a different frequency and revealed the intracellular Na^+ peak. The presence of a reference capillary of known Na^+ content enabled the $[Na^+]_i$ for each heart to be determined. It was estimated that $[Na^+]_i$ for both WT and PLM^{3SA} mouse hearts under basal pacing conditions of 550bpm were similar and in the range previously reported for rats and mice. Similar $[Na^+]_i$ values may be attributed to the changes in total PLM expression in the PLM^{3SA} mouse heart potentially normalising net pump function to that of WT hearts. TQF measurements of intracellular Na^+ showed small but significant increases in $[Na^+]_i$ in both WT and PLM^{3SA} mouse hearts with rapid pacing (800bpm) and ISO perfusion. Perfusion with ouabain increased the $[Na^+]_i$ TQF signal by approximately 50% in both genotypes suggesting successful inhibition of the Na^+/K^+ ATPase.

6.6.1 Validity of results

The results presented in this chapter were obtained from perfused hearts displaying depressed cardiac function when compared with heart function achieved on a standard Langendorff perfusion rig. Additionally in order to quantify the intracellular Na^+ concentration in these hearts, contractile function was further reduced with the perfusion of Ca^{2+} chelating shift reagent. TQF measurements offer a measure of $[Na^+]_i$ without reduction of function but could only be used to compare relative changes from baseline in these experiments.

For comparison there are relatively few NMR studies in perfused mouse hearts and those there are show only TQF measurements with ischemia or ouabain at unphysiological pacing rates. There are many rat NMR studies for comparison; however little has been shown in any species with ISO perfusion.

^{23}Na NMR is a complex method for measuring $[Na^+]_i$ in Langendorff perfused mouse hearts therefore a more reliable NMR perfusion system is required and is currently under development. When cardiac function measurements from the new NMR perfusion rig are comparable with those from a standard Langendorff rig, a greater confidence in the results will be gained.

Technique	Preparation	Temp (°C)	$[Na^+]_i$ (mM)	Ref
ISE	Sheep Purkinje Fibre	35	9	364
	Sheep Purkinje fibre	35	5-7	422
	Sheep Ventricle	34	6.4	457
	G.Pig Ventricle	37	5.4	423
	Rabbit Ventricle	36	7.5	424
	Rat Ventricle	30	12.7	8
	Rabbit Ventricle	30	7.2	8
	Chick Myocytes	36-38	8.4	426
	G.Pig Myocytes	32	6.9	425
SBFI	Rat Myocytes	RT	5	9
	Rabbit Myocytes	RT	3.8	428
	Rabbit Myocytes	RT	5.2	5
	Rat Myocytes	RT	7.8	6
	G.Pig Myocytes	RT	5.1	6
	Mouse Myocytes	RT	12.5	28
	Mouse Myocytes PLM-KO	RT	12.0	28
	Rat Myocytes	RT	11.1	2
	Rabbit Myocytes	RT	4.5	2
	Mouse Myocytes	RT	7.8	361
	Mouse Myocytes PLM-KO	RT	5.5	361
Flame Photometry	G.Pig Ventricle		36.7	347
AAS	Rabbit Papillary		32.7	427
	Rat Myocytes		10.3	458
	Perfused Rat Heart	37	20.2	349
	Perfused Rabbit Heart	37	19.3	459
	Perfused Rat Heart	37	30.7	350
^{23}Na NMR	Perfused Rat Heart	37	6.2	350
	Perfused Rat Heart	37	10	269
	Perfused Rat Heart	37	10.5	409
	Perfused Rat Heart	37	11.4	368
	Perfused Rat Heart	37	9.9	429
	Perfused Rat Heart	37	9.4	460
	Perfused G.Pig Heart	37	4.8	359
	Rat Myocytes	37	6.9	461
	Rat Myocytes		29	351
	Mouse Heart WT	37	14.4	This study
	Mouse Heart PLM^{3SA}	37	12.7	This study

Table 6.2: Values of intracellular sodium in cardiac muscle.
$[Na^+]_i$ was measured by ISE, AAS, flame photometry, SBFI or ^{23}Na NMR in a range of species. Table details method used, species and preparation, $[Na^+]_i$ and reference.

7 CHAPTER 7 –SUMMARY & GENERAL DISCUSSION

7.1 Summary of findings

The work described in this thesis investigated the role of phospholemman in the regulation of $[Na^+]_i$ by modulation of the Na^+/K^+ ATPase in the genetically modified PLM^{3SA} mouse. It was hypothesised that the inability to phosphorylate PLM in the new PLM^{3SA} mouse may cause $[Na^+]_i$ overload, contractile dysfunction and cardiac arrhythmias. The work described here focussed on the initial characterisation of the PLM^{3SA} mouse looking at both the biochemical phenotype of the heart and basal cardiac function using the isolated Langendorff perfusion model before making measurements of $[Na^+]_i$ using flame photometry and NMR methodology. Once basal heart function was determined the effects of β-adrenergic stimulation, pacing induced increases in heart rate and Na^+/K^+ ATPase inhibition by ouabain on $[Na^+]_i$ were also investigated.

Studies were mainly carried out using mice from the PLM^{3SA} colony which were compared with WT littermates. The PLM^{3SA} mouse carries an unphosphorylatable PLM protein which was created by the global mutation of the 3 PLM Ser phosphorylation sites (Ser63, Ser68 and Ser69) to Ala. Therefore, initially the inability of this mutated PLM to be phosphorylated was confirmed using Western blot analysis of heart homogenates probed with phospho-specific antibodies for each Ser residue. Evidence from Phos-tag blots using the total PLM antibody supported these findings by also showing the absence of the phosphorylation sites when comparing the same homogenates to WT heart homogenates. There did, however, appear to be the presence of additional bands in both genotypes, but whether these are additional phosphorylation sites or non-specific residual carry-over of homogenate protein would need further investigation.

The possibility that this mutated PLM would not traffick correctly to the membrane was investigated using myocyte fractionation, immunoprecipitation and confocal microscopy. The mutated PLM was located in the membrane fraction and co-immunoprecipitated with the Na^+/K^+ ATPase α1 subunit. Confocal analysis confirmed co-localisation of the α1 subunit with PLM^{3SA}. The evidence from both these studies suggests PLM^{3SA} trafficks correctly and forms a membrane bound complex with Na^+/K^+ ATPase.

The effect of the PLM mutation on protein expression of total PLM, Na^+/K^+ ATPase subunit and E-C coupling proteins was investigated. PLM expression was significantly decreased in PLM^{3SA} mouse hearts when compared to WT, however all other proteins (with the exception of total PLB) were

unaffected. PLM expression may be downregulated in order to help maintain normal pump current. Unpublished studies from our laboratory have shown using whole cell patch clamping that I_{Pump} in PLM^{3SA} is similar to currents seen in WT myocytes. This could be due to 2 reasons, either that PLM phosphorylation in WT myocytes has sufficiently decreased due to room temperature incubation prior to clamping which renders them in a state similar to unphosphorylatable PLM or that this decrease in total PLM expression has allowed PLM^{3SA} myocytes to maintain a relatively normal pump current. The stoichiometry of PLM and Na^+/K^+ ATPase α subunit is considered to be 1:1, however PLM has also been reported to form tetramers[217] and activation of PLM by PKA/PKC can lead to increased oligomerisation.[230] IP data from rat ventricular myocytes has also suggested that there is a pool of α pump subunits not associated with PLM.[62] Therefore this supports the notion that reduction of PLM expression in PLM^{3SA} hearts may help normalise the net pump current.

Characterisation studies to determine the effect of the PLM mutation on basal cardiac phenotype were undertaken investigating both ventricularly paced hearts at a constant rate of 550bpm and free-running unpaced hearts. Firstly, hearts were paced at a constant pacing rate of 550bpm in an attempt to mimic *in vivo* heart rates. At this heart rate it was clearly seen that PLM^{3SA} mouse hearts had significantly greater contractility than WT hearts. This is in keeping with the hypothesis $[Na^+]_i$ is increased in these hearts. However, unpaced studies in free-running hearts gave contrasting results with contractility in PLM^{3SA} and WT hearts showing similar values. Studies in unpaced mouse hearts are unusual but were necessary for the later ISO stimulated heart function determination. In these studies the right atrium was superfused to help maintain a physiological heart rate and reduce preparation decline over time. Unpaced PLM^{3SA} mouse hearts showed lower heart rates than WT mice but was not significant and there were no other differences in cardiac function measurements. These data were in agreement with other unpublished *in vivo* ECHO studies from our laboratory that also showed PLM^{3SA} mice have lower heart rates than WT mice but with no other differences in basal cardiac function suggesting autonomic compensation for PLM mutation.

It seems likely that the differences in contractility between *in vitro* paced and unpaced studies reflect subtle differences between the genotypes in $[Na^+]_i$ at the prevailing heart rates. Pieske *et al* (2002), noted that " the force of contraction can double with as little as 1mM increases in $[Na^+]_i$".[76] If these differences are indeed due to subtle rate-dependent changes in $[Na^+]_i$ then these effects may persist *in vivo*. However, *in vivo* studies using echocardiography or telemetry shown no differences in baseline contractility although there is a significant tendency for heart rate to be lower in PLM^{3SA} mice. *In vivo*, our unpublished data (not described here) shows profound differences in the response of the two genotypes to β-blockade and atropine suggesting *in vivo* basal changes in contractility and heart rate may be compensated by changes in background autonomic tone.

If Na^+ is indeed higher in PLM^{3SA} mice then this may manifest as increases in contractile dysfunction and arrhythmias. To address this heart rate variability analysis was used in both paced and unpaced studies. Paced studies showed both genotypes had low arrhythmia scores showing they are stable preparations with low incidence of ectopic beats. Unpaced studies had higher arrhythmia scores than paced studies; however there were no differences in arrhythmia scores between genotypes.

The force-frequency relationship is known to be strongly influenced by intracellular Na^+.[8, 285] As previously seen in small rodents[282, 290-292] both genotypes displayed a negative FFR over the range of 400-750bpm. The negative slope of the FFR may crudely reflect intracellular Na^+ load but, in these experiments, this was similar in both genotypes again suggesting that under these conditions there was no evidence for sodium overload in PLM^{3SA} hearts. In small mammals SR Ca^{2+} load and release are almost at a maximum at slow pacing rates and therefore cannot increase further with increased heart rate in spite of increasing $[Na^+]_i$ and diastolic Ca^{2+}.[462] Any differences in $[Na^+]_i$ in PLM^{3SA} hearts compared to WT may have been masked by the limit on SR Ca^{2+} load which would affect Ca^{2+} transients and contraction; however even if the SR Ca^{2+} load was rapidly maximised, increases in pacing and Na^+ load may expect to manifest as diastolic dysfunction and arrhythmias which were not seen. Additionally, although pacing has been shown to induce PLM phosphorylation in myocytes[177] this has not been shown in isolated hearts.

If lack of basal phosphorylation in WT hearts obscures differences between the genotypes, then stimulation of the β-adrenoreceptor pathway should magnify any differences. PLM^{3SA} mice should remain with the Na^+ pump unstimulated while WT mice should respond to PKA activation by phosphorylating PLM and increasing Na^+ efflux. ISO was perfused at both a low (1nM) and high (100nM) concentration and cardiac function was measured. No differences in cardiac function measurements between the 2 genotypes were observed at either ISO concentration. 1nM ISO evoked similar increases in HR, LVDP, and coronary flow accompanied by a decrease in LVEDP in both PLM^{3SA} and WT mice. 100nM ISO also caused similar changes, again with no differences between WT and PLM^{3SA} hearts. Interestingly, 100nM ISO increased contractility to the same extent as 1nM ISO; however heart rate increases were different. PKA causes the phosphorylation of many major E-C coupling proteins (L-type Ca^{2+} channels, ryanodine receptors, PLB, etc.) and they appear to play the predominant role in increasing cardiac contractility. This suggests either that the rate-induced increases in $[Na^+]_i$ contribute little quantitatively to ISO induced inotropy or, if it is important quantitatively, is not significantly influenced by whether PLM is, or is not, phosphorylated. When FFR's were generated by pacing in the presence of ISO, no differences were seen between the genotypes.

Despite the proposed role of PLM phosphorylation in limiting the rise in intracellular Na^+ during fight or flight increases in heart rate,[28] data thus far presented does not support the hypothesis that either basal Na^+ is higher in PLM^{3SA} hearts or that Na^+ increases more in response to increases in heart rate (with or without β-receptor stimulation). Basal contractility is, however, higher in PLM^{3SA} hearts – an effect that may be masked *in vivo* (by differences in autonomic tone) or at higher heart rate *in vitro*. Critical to understanding these data is an accurate determination of intracellular Na^+ under these experimental conditions.

Two different methods, flame photometry and ^{23}Na NMR, were used in an attempt to measure $[Na^+]_i$ in isolated hearts under a variety of conditions (basal, rapid pacing, ISO stimulation and ouabain). It is widely accepted that the linear range for Na^+ using the flame photometer is very narrow (0.5 to 10ppm) due to Na^+ self-absorption at higher values. Initial optimisation of the experimental protocol was carried out determining the perfusion protocol (including washout time), tissue digestion times and dilution before measuring Na^+ content in PLM^{3SA} and WT hearts. Results for intracellular Na^+ in each genotype showed that although there appears to be a greater Na^+ content in PLM^{3SA} hearts paced at 550bpm compared with WT, this is not significantly different. Previously, paced studies in isolated mouse hearts at 550bpm showed differences in contractility. A small change in intracellular Na^+ (1mM) can cause significant Ca^{2+} load[76] and therefore it is possible that these small changes do indeed reflect differences in $[Na^+]_i$ that cannot be resolved with the limited resolution of the flame photometry method.

Indeed an additional study undertaken using the flame photometer was the measurement of rubidium uptake in hearts paced at 550bpm. Rb^+ uptake was measured to gain an insight into the activity of Na^+/K^+ ATPase in both PLM^{3SA} and WT hearts. The data showed that Rb^+ uptake in both genotypes at this pacing rate was the same suggesting similar pump activity in both genotypes. This is consistent with the assumption that, under steady state conditions, Rb^+ uptake reflects Na^+ influx which should be constant in both genotypes. There was no change in Rb^+ uptake in response to ISO in both genotypes, as any possible transient changes in Rb^+ uptake were masked by the steady state influx of Na^+ by pacing at 550bpm throughout. However, it was expected that rapid pacing would increase Rb^+ uptake which was not observed and raises the possibility that flame photometry may simply lack the resolution and accuracy to reveal these differences. An intervention known to robustly change Rb^+ uptake (and $[Na^+]_i$) is ouabain and although ouabain induced significant reductions in Rb^+ uptake these represent only a 30% decline in pump function (uptake). This compares favourably with measurements in the literature for rat hearts exposed to similar concentrations of ouabain. Interestingly the same decrease in Rb^+ uptake was not accompanied by similar increases in intracellular Na^+ as no changes in Na^+ were observed with the addition of ouabain.

This highlights the likelihood that the flame photometer is not sensitive enough to accurately measure changes in Na^+. Historically intracellular Na^+ has been shown to increase with ouabain in the perfused rat heart which was not seen in this flame photometer study. Additionally using ^{23}Na NMR a 50% Na^+ increase from baseline was observed with the same concentration of ouabain and suggest that the flame photometry data is potentially unreliable.

The final series of studies undertaken in this thesis was to set up a method for measuring $[Na^+]_i$ in isolated beating mouse hearts at physiological pacing rates. ^{23}Na NMR is currently the gold standard method for measuring intracellular Na^+ in hearts under physiological conditions. This required substantial method development and validation of the modified Langendorff NMR perfusion rig, especially considering that most mouse NMR data reported in literature is at a non-physiological pacing rate of ~400bpm.[375] Contractile stability of the hearts at a physiological pacing rate of 550bpm was achieved, however at the compromise of a reduced LVDP. This reduced LVDP was seen in both genotypes so the ensuing results with regard to $[Na^+]_i$ were at least comparable. It was of note though that the previously seen significant increase in PLM^{3SA} contractility compared to WT in paced mouse hearts was reduced and was not discernible from the natural variability at these low left ventricular pressures.

By using the shift reagent $Tm(DOTP)^{5-}$ to reveal the intracellular ^{23}Na peak and peak integration software, the $[Na^+]_i$ for each genotype was determined and showed no significant differences between WT and PLM^{3SA} hearts. These results agree with the potentially unreliable flame photometer Na^+ study. There are limitations with the method and some assumptions have been made regarding the extrapolation of intracellular ^{23}Na peak from the shoulder of the larger extracellular ^{23}Na peak, cytosolic volume estimations and Na^+ visibility. Also, the chelation of Ca^{2+} by $Tm(DOTP)^{5-}$ compromises heart function which needs to be addressed in future experiments using TQF. A new perfusion rig is being developed which will hopefully allow cardiac function that is comparable with that seen on the standard Langendorff rig. Once this has been established and optimised, the shift reagent experiments will be repeated with and without TQF analysis and the data provided should give the true indications of $[Na^+]_i$ in the two genotypes.

The final study addressed $[Na^+]_i$ changes during interventions of ISO, pacing rate increases and ouabain perfusion. To remove the need for shift reagent and its Ca^{2+} chelating effects triple quantum filtering of the ^{23}Na NMR signal was developed. Firstly it was established that the TQF signal was stable over the initial 20 minute perfusion period providing a steady baseline to monitor any changes in Na^+ with each intervention. ISO and pacing significantly increased the intracellular Na^+ TQF signal by a small amount, whereas ouabain significantly increased the intracellular Na^+ TQF by

almost 50% in both genotypes. These interventions did not, however, provide the same developed pressure profiles seen previously in Chapter 4 e.g. increased contractility with ISO. Realistically, because of the poor quality of the cardiac function in these experiments, it is appropriate to consider the NMR data described here as "proof of principle" in terms of establishing the method; rather than a definitive data set describing Na^+ measurements in WT and PLM^{3SA} hearts. Again a new NMR rig may help to address these issues and give more accurate and conclusive results.

7.2 Future directions

The work described in this thesis contributes to the extensive and on-going characterisation of the PLM^{3SA} mouse and investigation into the role of PLM regulation of $[Na^+]_i$ via the Na^+/K^+ ATPase. This is only the start of the PLM^{3SA} characterisation and there is clearly more work to be done to help our understanding of this model.

The most obvious area of further development from work described in this thesis is the robust measurement of $[Na^+]_i$ in isolated hearts subjected to physiological temperatures and pacing rates. Given the limitations of the only two published studies in mouse hearts, this development would represent a very significant and useful technical advance. Accurate measurement of $[Na^+]_i$ would prove/disprove the hypothesis that interaction of Na^+/K^+ ATPase with unphosphorylatable PLM protein affects $[Na^+]_i$ sufficiently to cause Na^+ overload and subsequent contractile dysfunction. The measurement of $[Na^+]_i$ by flame photometry and ^{23}Na NMR in this thesis were clearly limited by resolution and accuracy. Flame photometry data was shown to be relatively insensitive and will not be explored further. However, ^{23}Na NMR is an area that will be of significant use in the future and requires further development. The $[Na^+]_i$ measurements made in this thesis were adequate for "proof of principle" but were in a suboptimal model and may not be representative of a normal physiological situation due to the poor cardiac function. Extensive work is therefore needed to ensure that in the future these readings are comparable. A new perfusion rig is currently under development to address these issues. The design will allow heated perfusate to reach the heart at 37°C so the heart will no longer be cannulated at room temperature. The system will now no longer be a closed system removing the problems of inertia, resonance and damping in the pressure monitoring lines and in the heart chamber itself.

It is hoped that this new rig will be more reliable and will enable robust cardiac function inside the magnet. The combination of improved Langendorff perfusion and the use of the now characterised

and refined ^{23}Na TQF measurements will provide a useful tool for studying Na^+ regulation in the future. For example measurement of $[Na^+]_i$ during FFR will be of great interest.

In this thesis the characterisation of basal cardiac phenotype of PLM^{3SA} mice was explored with the hypothesis that unphosphorylatable PLM may predispose to sodium overload, Ca^{2+} dysfunction and potential arrhythmia development. Although some Langendorff studies suggested greater intracellular Na^+ (paced and FFR) this was not seen in the Na^+ measurements. However, it is known that disease processes such as hypertrophy and heart failure raise $[Na^+]_i$[11] so a future direction for these studies would be to investigate intracellular Na^+ levels in hearts from WT and PLM^{3SA} mice that have been subjected to banding protocols to cause pressure overload and hypertrophy development. Under these conditions if PLM plays a role in regulating Na^+ in response to stress, the mutant PLM^{3SA} mouse may be expected to show increased propensity of Na^+ and Ca^{2+} overload in exacerbated disease. This could be explored further by subjecting these hearts to FFR, ISO and ouabain protocols. Allowing us a wealth of information to gain a better insight to the role PLM phosphorylation plays in regulation of $[Na^+]_i$.

Contrary to the prevailing opinion in the literature, the studies in this thesis do not provide strong evidence that PLM phosphorylation is critical to allow the myocyte to control Na^+ when heart rate is elevated (either in the presence or absence of β-stimulation). This tentative conclusion comes with the caveat that the real proof requires accurate measurement of $[Na^+]_i$ under physiological conditions of temperature and heart rate. Although this thesis provides the foundation for such studies by characterising ^{23}Na NMR and TQF measurements, the refinement of this technique is required before such definitive experiments can be undertaken.

The generation of different mouse models that have single phosphorylation site mutations would allow us to define the importance of individual phosphorylation sites on $[Na^+]_i$ regulation via the Na^+/K^+ ATPase. Finally, we hypothesise that contrary to 300 years of clinical experience with digitalis, the stimulation of the Na^+/K^+ ATPase may be beneficial in heart failure. A high throughput screen to identify small molecules that may stimulate the pump has been initiated in-house. ^{23}Na NMR will be pivotal in the assessment of the cardiac pathology and its response to these agents. The refinement of this method, as stated in this thesis, will therefore represent an important contribution to this on-going programme of studies.

7.3 Critical analysis of techniques and results in this thesis

The work in this thesis incorporates a variety of methods which will vary in their limitations. However, these limitations must be accounted for when considering the relevance and significance of any conclusions made and are discussed below.

7.3.1 Western blotting and Phos-tag gels

This technique was used in the basic phenotypic characterisation of protein expression in the PLM^{3SA} mouse heart. It relies on several factors to ensure accurate results including the equal loading of protein between heart homogenate samples, the specificity of each antibody to bind and the detection of luminescence in the linear gray-scale range.

The Western blots in this thesis were run using equal volume loading of 10% homogenates as shown in Chapter 3. Equal loading was ensured by initially checking a Coomassie blue stained gel before running the remaining gels and by staining each PVDF membrane at the end of the experiment with Coomassie blue (not shown) to ensure successful protein transfer. A protein assay was also performed and showed no variation within the samples greater than 2 standard deviations away from the mean of the group. As a final control actin and calsequestrin were run and densitometered to show that there were similar protein bands across samples and therefore equal loading. It was decided not to normalise each protein of interest by these loading control values for fear of introducing further variation in the results. The same samples were used in the Phos-tag gel experiments and equal loading was again ensured by the above methods.

For the fractionation experiment Western blots it was assumed that every myocyte isolation can produce varying cell yields dependent on animal, day, etc. Therefore these experiments were not run with quantification in mind but to simply provide an indication of PLM location.

7.3.2 Confocal microscopy

The major issue with confocal microscopy is the specificity of the antibodies for their targets and the health of the myocytes prior to paraformaldehyde fixing. Myocyte isolation, especially mouse, can be extremely difficult and some myocytes easily lose their membrane integrity. However, the need for only a few cells for successful confocal microscopy imaging allowed the imaging of an adequate

number of healthy cells. Unfortunately in the case of PLM there are very few decent antibodies for confocal microscopy. The best antibodies are the previously used phospho-antibodies which obviously cannot be used in the PLM^{3SA} mouse myocytes leaving only the use of PLM-C2 for PLM binding. Additionally the antibodies for the α subunits are not ideal for microscopy either, especially the α2 antibody. Fortunately by using high concentrations of each antibody it was confirmed that PLM co-localises with α1 subunit in both WT and PLM^{3SA} mouse myocytes. Any doubt about this result is removed by the additional findings from the co-IP experiments which again showed that PLM forms a complex with the α1 subunit.

7.3.3 Langendorff perfusion

In this thesis the Langendorff perfusion technique was used extensively in various modified forms. During the protocols, hearts were either paced or unpaced which caused some conflicting results. During paced protocols on the standard set-up contractility of PLM^{3SA} isolated hearts was increased compared to WT which was not replicated during the unpaced protocols, however these ran at 70-80% the *in vivo* physiological heart rate so cannot be directly compared.

The process of cannulation can itself pose issues because it is a stressful procedure which causes a brief period of ischaemia which can activate protein kinases and cause the phosphorylation of many proteins. As PLM is the end target of our investigations and is heavily affected by phosphorylation in order to allow accurate comparisons between WT *in vivo* environment the stability period is used to reduce the phosphorylation status of the heart proteins. The length of time of this stability period is a compromise between protein dephosphorylation and heart function deterioration over time.

Regarding FFR data the hearts were paced between a range of 400 to 750bpm, potentially if hearts had been stimulated to higher heart rates a significant difference between genotypes may have been seen, however higher heart rates were deemed unphysiological and, in the crystalloid perfused Langendorff heart, high heart rates may induce a demand ischemia which causes progressive deterioration at such high heart rates. This was based on the data from the ISO study (Chapter 4) which showed that heart rate increases with 100nM ISO reached approximately 700bpm *ex vivo*.

7.3.4 Selectivity of interventions used

Another issue was the use of appropriate concentrations of pharmacological agents and pacing rates that were used for some of the studies. For the ISO studies ideally performing a concentration response curve to ISO would have been the preferred option but severe run down of the hearts between concentrations meant that this was not possible. Therefore both low (1nM) and high (100nM) ISO concentrations were used. The results from this, especially concerning HR, allowed us to predict which concentration (10nM) to use in the subsequent flame photometer and NMR studies. However, in these studies no significant changes to $[Na^+]_i$ was observed with ISO intervention suggesting high concentrations should have been considered. Alternatively adrenaline or noradrenaline may give a more physiological response. Ouabain concentrations were limited to <1mM as it was determined that previously used literature concentrations (1-2mM) caused heart contracture. The use of 50µM ouabain should have been adequate to observe changes in $[Na^+]_i$ and was accompanied by a large increase in inotropy. In future more concentrations could be tested up to 1mM. Pacing rate was the final intervention to be decided and 800bpm was chosen even though it was outside of the range used in the FFR and which is considered physiological. Again, due to the lack of changes seen in flame photometry and NMR studies perhaps a greater duration or pacing rate could have been investigated.

7.3.5 Flame photometry

While flame photometry has been used successfully by a number of authors, in our hands, for no obvious reason, the technique was unable to resolve a Na^+ increase with ouabain. Since this is such an established and predictable response, then the failure of flame photometry to detect this suggests our method or protocol was, for some reason, unsuitable. This could be related to the narrow linear range of Na^+ or the insensitivity of the flame photometer or to systematic, but undefined, methodological problems. Since this technique is at best an approximation and unsuitable for following temporal changes, there would be little to be gained by refining this given ^{23}Na is now available.

7.3.6 NMR

The NMR technique poses many problems especially concerning successful, reliable and physiological measurements of Langendorff perfused mouse hearts. The main issues relate to temperature maintenance of perfusate to the cannula, perfusing in a closed system to prevent leakage in the magnet and external hydrostatic pressures affecting balloon measurements especially with pacing. In the absence of a different NMR perfusion rig the results gained from these studies at least are comparable between genotypes as they have been subjected to the same conditions.

The use of shift reagents to measure $[Na^+]_i$ also involves some level of compromise. The toxic nature of these compounds and their ability to chelate Ca^{2+} limits how physiologically relevant our measurements are. Too great a concentration of shift reagent causes dramatic Ca^{2+} chelation meaning hearts are effectively not beating, and too low a concentration reduces the shift of the extracellular ^{23}Na peak leaving no intracellular ^{23}Na peak to measure. 3.5mM $Tm(DOTP)^{5-}$ used in this thesis is therefore a compromise between these 2 states and highlights the importance of TQF methods which allows quantification of Na^+ changes from baseline, due to interventions, without the need for shift reagent.

7.4 Final conclusions

In conclusion, the work presented in this thesis has extensively characterised the PLM^{3SA} mouse and investigated the role of unphosphorylatable PLM modulation of Na^+/K^+ ATPase activity on $[Na^+]_i$. The increased contractile function and negative FFR are consistent with the hypothesis that PLM^{3SA} has high $[Na^+]_i$, however lack of differences of FFR gradients indicates that increases in Na^+ load with frequency are similar to WT. Unpaced studies and *in vivo* data suggest that there may be adaptive mechanisms in place in the mouse to control for the inhibition of Na^+/K^+ ATPase by unphosphorylatable PLM. Under paced and unpaced conditions PLM^{3SA} hearts have no increased propensity for cardiac arrhythmias. PLM protein expression is decreased in PLM^{3SA} hearts and may account for the similar pump current and Na^+ measurements observed in this mouse compared with WT. $[Na^+]_i$ measurements under basal physiological conditions show that there are no differences in $[Na^+]_i$ between PLM^{3SA} and WT mouse hearts and only ouabain can evoke a large significant change in intracellular Na^+, however this is similar in both genotypes. Currently there is little evidence to conclude that PLM^{3SA} hearts are Na^+ loaded.

The NMR studies within this thesis have validated TQF as a method for measuring $[Na^+]_i$ in isolated beating mouse hearts in the absence of shift reagents and this represents a significant advance in physiological measurement of $[Na^+]_i$ using ^{23}Na NMR.

However, it has to be remembered that the Na^+ measurements, especially by NMR, were made under compromised conditions and extensive work must be done on a new NMR rig enabling better cardiac function to confirm these findings. Although there was no evidence of Na^+ overload, contractile dysfunction and arrhythmias in these studies, perhaps the extent of the PLM mutation in PLM^{3SA} mice will only come to light in circumstances of disease pathology. Therefore it will be interesting to continue the investigation of this mouse during hypertrophy.

REFERENCES

1. Bers DM, Despa S. Na^+ transport in cardiac myocytes; implications for excitation-contraction coupling. *IUBMB Life*. 2009;61:215-221

2. Despa S, Islam MA, Pogwizd SM, Bers DM. Intracellular [Na^+] and Na^+ pump rate in rat and rabbit ventricular myocytes. *J Physiol*. 2002;539:133-143

3. Bers DM, Barry WH, Despa S. Intracellular Na^+ regulation in cardiac myocytes. *Cardiovasc Res*. 2003;57:897-912

4. Gray RP, McIntyre H, Sheridan DS, Fry CH. Intracellular sodium and contractile function in hypertrophied human and guinea-pig myocardium. *Pflugers Arch*. 2001;442:117-123

5. Yao A, Su Z, Nonaka A, Zubair I, Spitzer KW, Bridge JH, Muelheims G, Ross J, Jr., Barry WH. Abnormal myocyte Ca^{2+} homeostasis in rabbits with pacing-induced heart failure. *Am J Physiol*. 1998;275:H1441-1448

6. Harrison SM, McCall E, Boyett MR. The relationship between contraction and intracellular sodium in rat and guinea-pig ventricular myocytes. *J Physiol*. 1992;449:517-550

7. Levi AJ, Lee CO, Brooksby P. Properties of the fluorescent sodium indicator "SBFI" in rat and rabbit cardiac myocytes. *J Cardiovasc Electrophysiol*. 1994;5:241-257

8. Shattock MJ, Bers DM. Rat vs. Rabbit ventricle: Ca flux and intracellular Na assessed by ion-selective microelectrodes. *Am J Physiol*. 1989;256:C813-822

9. Donoso P, Mill JG, O'Neill SC, Eisner DA. Fluorescence measurements of cytoplasmic and mitochondrial sodium concentration in rat ventricular myocytes. *J Physiol*. 1992;448:493-509

10. Yao A, Su Z, Nonaka A, Zubair I, Lu L, Philipson KD, Bridge JH, Barry WH. Effects of overexpression of the Na^+-Ca^{2+} exchanger on $[Ca^{2+}]_i$ transients in murine ventricular myocytes. *Circ Res*. 1998;82:657-665

11. Despa S, Islam MA, Weber CR, Pogwizd SM, Bers DM. Intracellular Na^+ concentration is elevated in heart failure but na/k pump function is unchanged. *Circulation*. 2002;105:2543-2548

12. Pogwizd SM, Bers DM. Na/Ca exchange in heart failure: Contractile dysfunction and arrhythmogenesis. *Ann N Y Acad Sci*. 2002;976:454-465

13. Li C, Grosdidier A, Crambert G, Horisberger JD, Michielin O, Geering K. Structural and functional interaction sites between Na,K-ATPase and FXYD proteins. *J Biol Chem*. 2004;279:38895-38902

14. Geering K. Fxyd proteins: New regulators of Na-K-ATPase. *Am J Physiol Renal Physiol*. 2006;290:F241-250

15. Beguin P, Crambert G, Guennoun S, Garty H, Horisberger JD, Geering K. Chif, a member of the fxyd protein family, is a regulator of Na,K-ATPase distinct from the gamma-subunit. *EMBO J*. 2001;20:3993-4002

16. Beguin P, Crambert G, Monnet-Tschudi F, Uldry M, Horisberger JD, Garty H, Geering K. Fxyd7 is a brain-specific regulator of Na,K-ATPase α1-β isozymes. *EMBO J*. 2002;21:3264-3273

17. Beguin P, Wang X, Firsov D, Puoti A, Claeys D, Horisberger JD, Geering K. The gamma subunit is a specific component of the Na,K-ATPase and modulates its transport function. *EMBO J*. 1997;16:4250-4260

18. Therien AG, Pu HX, Karlish SJ, Blostein R. Molecular and functional studies of the gamma subunit of the sodium pump. *J Bioenerg Biomembr*. 2001;33:407-414

19. Therien AG, Blostein R. Mechanisms of sodium pump regulation. *Am J Physiol Cell Physiol*. 2000;279:C541-566

20. Presti CF, Jones LR, Lindemann JP. Isoproterenol-induced phosphorylation of a 15-kilodalton sarcolemmal protein in intact myocardium. *J Biol Chem*. 1985;260:3860-3867

21. Presti CF, Scott BT, Jones LR. Identification of an endogenous protein kinase C activity and its intrinsic 15-kilodalton substrate in purified canine cardiac sarcolemmal vesicles. *J Biol Chem*. 1985;260:13879-13889

22. Palmer CJ, Scott BT, Jones LR. Purification and complete sequence determination of the major plasma membrane substrate for camp-dependent protein kinase and protein kinase C in myocardium. *J Biol Chem*. 1991;266:11126-11130

23. Lu KP, Kemp BE, Means AR. Identification of substrate specificity determinants for the cell cycle-regulated NIMA protein kinase. *J Biol Chem*. 1994;269:6603-6607

24. Walaas O, Horn RS, Walaas SI. Inhibition of insulin-stimulated phosphorylation of the intracellular domain of phospholemman decreases insulin-dependent GLUT4 translocation in streptolysin-o-permeabilized adipocytes. *Biochem J*. 1999;343 Pt 1:151-157

25. Lindemann JP. Alpha-adrenergic stimulation of sarcolemmal protein phosphorylation and slow responses in intact myocardium. *J Biol Chem*. 1986;261:4860-4867

26. Crambert G, Fuzesi M, Garty H, Karlish S, Geering K. Phospholemman (FXYD1) associates with Na,K-ATPase and regulates its transport properties. *Proc Natl Acad Sci U S A*. 2002;99:11476-11481

27. Mahmmoud YA, Vorum H, Cornelius F. Identification of a phospholemman-like protein from shark rectal glands. Evidence for indirect regulation of Na,K-ATPase by

protein kinase C via a novel member of the FXYDγ family. *J Biol Chem*. 2000;275:35969-35977

28. Despa S, Bossuyt J, Han F, Ginsburg KS, Jia LG, Kutchai H, Tucker AL, Bers DM. Phospholemman-phosphorylation mediates the beta-adrenergic effects on Na/K pump function in cardiac myocytes. *Circ Res*. 2005;97:252-259

29. Han F, Bossuyt J, Despa S, Tucker AL, Bers DM. Phospholemman phosphorylation mediates the protein kinase C-dependent effects on Na^+/K^+ pump function in cardiac myocytes. *Circ Res*. 2006;99:1376-1383

30. Silverman BZ, Fuller W, Eaton P, Deng J, Moorman JR, Cheung JY, James AF, Shattock MJ. Serine 68 phosphorylation of phospholemman: Acute isoform-specific activation of cardiac Na/K ATPase. *Cardiovasc Res*. 2005;65:93-103

31. Berry RG. Na/K ATPase pump current is increased in ventricular myocytes isolated from phospholemman knockout mice. *J Physiol*. 2006;C171:565P

32. Despa S, Tucker AL, Bers DM. Phospholemman-mediated activation of Na/K-ATPase limits $[Na]_i$ and inotropic state during beta-adrenergic stimulation in mouse ventricular myocytes. *Circulation*. 2008;117:1849-1855

33. Bell JR, Kennington E, Fuller W, Dighe K, Donoghue P, Clark JE, Jia LG, Tucker AL, Moorman JR, Marber MS, Eaton P, Dunn MJ, Shattock MJ. Characterization of the phospholemman knockout mouse heart: Depressed left ventricular function with increased Na-K-ATPase activity. *Am J Physiol Heart Circ Physiol*. 2008;294:H613-621

34. Jia LG, Donnet C, Bogaev RC, Blatt RJ, McKinney CE, Day KH, Berr SS, Jones LR, Moorman JR, Sweadner KJ, Tucker AL. Hypertrophy, increased ejection fraction, and reduced Na-K-ATPase activity in phospholemman-deficient mice. *Am J Physiol Heart Circ Physiol*. 2005;288:H1982-1988

35. Bers DM. Cardiac excitation-contraction coupling. *Nature*. 2002;415:198-205

36. Zhou Z, Lipsius SL. Delayed rectifier potassium current (I_k) in latent atrial pacemaker cells isolated from cat right atrium. *Pflugers Arch*. 1994;426:341-347

37. Vinogradova TM, Lakatta EG. Regulation of basal and reserve cardiac pacemaker function by interactions of camp-mediated pka-dependent Ca^{2+} cycling with surface membrane channels. *J Mol Cell Cardiol*. 2009;47:456-474

38. Fry CH, Ward JP, Twist VW, Powell T. Determination of intracellular potassium ion concentration in isolated rat ventricular myocytes. *Biochem Biophys Res Commun*. 1986;137:573-578

39. Kleber AG. Resting membrane potential, extracellular potassium activity, and intracellular sodium activity during acute global ischemia in isolated perfused guinea pig hearts. *Circ Res*. 1983;52:442-450

40. Saffitz JE, Kanter HL, Green KG, Tolley TK, Beyer EC. Tissue-specific determinants of anisotropic conduction velocity in canine atrial and ventricular myocardium. *Circ Res*. 1994;74:1065-1070

41. Nerbonne JM. Studying cardiac arrhythmias in the mouse- a reasonable model for probing mechanisms? *Trends Cardiovasc Med*. 2004;14:83-93

42. Fabiato A, Fabiato F. Calcium-induced release of calcium from the sarcoplasmic reticulum of skinned cells from adult human, dog, cat, rabbit, rat, and frog hearts and from fetal and new-born rat ventricles. *Ann N Y Acad Sci*. 1978;307:491-522

43. Barry WH, Bridge JH. Intracellular calcium homeostasis in cardiac myocytes. *Circulation*. 1993;87:1806-1815

44. Callewaert G. Excitation-contraction coupling in mammalian cardiac cells. *Cardiovasc Res*. 1992;26:923-932

45. Shattock MJ. Phospholemman: Its role in normal cardiac physiology and potential as a druggable target in disease. *Curr Opin Pharmacol*. 2009;9:160-166

46. Landesberg A, Sideman S. Coupling calcium binding to troponin C and cross-bridge cycling in skinned cardiac cells. *Am J Physiol*. 1994;266:H1260-1271

47. James P, Inui M, Tada M, Chiesi M, Carafoli E. Nature and site of phospholamban regulation of the Ca^{2+} pump of sarcoplasmic reticulum. *Nature*. 1989;342:90-92

48. Lindemann JP, Jones LR, Hathaway DR, Henry BG, Watanabe AM. Beta-adrenergic stimulation of phospholamban phosphorylation and Ca^{2+}-ATPase activity in guinea pig ventricles. *J Biol Chem*. 1983;258:464-471

49. Wegener AD, Simmerman HK, Lindemann JP, Jones LR. Phospholamban phosphorylation in intact ventricles. Phosphorylation of serine 16 and threonine 17 in response to beta-adrenergic stimulation. *J Biol Chem*. 1989;264:11468-11474

50. Akabas MH. Na^{+}/Ca^{2+} exchange inhibitors: Potential drugs to mitigate the severity of ischemic injury. *Mol Pharmacol*. 2004;66:8-10

51. Blaustein MP, Lederer WJ. Sodium/calcium exchange: Its physiological implications. *Physiol Rev*. 1999;79:763-854

52. Murphy E, Eisner DA. Regulation of intracellular and mitochondrial sodium in health and disease. *Circ Res*. 2009;104:292-303

53. Bers DM, Despa S. Na/K-ATPase- an integral player in the adrenergic fight-or-flight response. *Trends Cardiovasc Med*. 2009;19:111-118

54. Saucerman JJ, McCulloch AD. Cardiac beta-adrenergic signaling: From subcellular microdomains to heart failure. *Ann N Y Acad Sci*. 2006;1080:348-361

55. Gao T, Puri TS, Gerhardstein BL, Chien AJ, Green RD, Hosey MM. Identification and subcellular localization of the subunits of L-type calcium channels and adenylyl cyclase in cardiac myocytes. *J Biol Chem*. 1997;272:19401-19407

56. Simmerman HK, Jones LR. Phospholamban: Protein structure, mechanism of action, and role in cardiac function. *Physiol Rev*. 1998;78:921-947

57. Huke S, Bers DM. Ryanodine receptor phosphorylation at serine 2030, 2808 and 2814 in rat cardiomyocytes. *Biochem Biophys Res Commun*. 2008;376:80-85

58. Kranias EG, Garvey JL, Srivastava RD, Solaro RJ. Phosphorylation and functional modifications of sarcoplasmic reticulum and myofibrils in isolated rabbit hearts stimulated with isoprenaline. *Biochem J*. 1985;226:113-121

59. Karczewski P, Bartel S, Krause EG. Differential sensitivity to isoprenaline of troponin I and phospholamban phosphorylation in isolated rat hearts. *Biochem J*. 1990;266:115-122

60. Shannon TR, Ginsburg KS, Bers DM. Potentiation of fractional sarcoplasmic reticulum calcium release by total and free intra-sarcoplasmic reticulum calcium concentration. *Biophys J*. 2000;78:334-343

61. Kentish JC, McCloskey DT, Layland J, Palmer S, Leiden JM, Martin AF, Solaro RJ. Phosphorylation of troponin I by protein kinase A accelerates relaxation and crossbridge cycle kinetics in mouse ventricular muscle. *Circ Res*. 2001;88:1059-1065

62. Pavlovic D, Fuller W, Shattock MJ. The intracellular region of FXYD1 is sufficient to regulate cardiac Na/K ATPase. *FASEB J*. 2007;21:1539-1546

63. Fuller W, Eaton P, Bell JR, Shattock MJ. Ischemia-induced phosphorylation of phospholemman directly activates rat cardiac Na/K-ATPase. *FASEB J*. 2004;18:197-199

64. Despa S, Bers DM. Functional analysis of Na^+/K^+-ATPase isoform distribution in rat ventricular myocytes. *Am J Physiol Cell Physiol*. 2007;293:C321-327

65. Silverman BZ, Warley A, Miller JI, James AF, Shattock MJ. Is there a transient rise in sub-sarcolemmal Na and activation of Na/K pump current following activation of I_{Na} in ventricular myocardium? *Cardiovasc Res*. 2003;57:1025-1034

66. Fuller W. Regulation of the cardiac sodium pump. *In review*. 2012

67. Post RL, Merritt CR, Kinsolving CR, Albright CD. Membrane adenosine triphosphatase as a participant in the active transport of sodium and potassium in the human erythrocyte. *J Biol Chem*. 1960;235:1796-1802

68. McDonough AA, Velotta JB, Schwinger RH, Philipson KD, Farley RA. The cardiac sodium pump: Structure and function. *Basic Res Cardiol*. 2002;97 Suppl 1:I19-24

69. Skou JC. The influence of some cations on an adenosine triphosphatase from peripheral nerves. *Biochim Biophys Acta*. 1957;23:394-401

70. Schwartz A. Is the cell membrane Na^+,K^+-ATPase enzyme system the pharmacological receptor for digitalis? *Circ Res*. 1976;39:1-7

71. Schwartz A, Lindenmayer GE, Allen JC. The sodium-potassium adenosine triphosphatase: Pharmacological, physiological and biochemical aspects. *Pharmacol Rev*. 1975;27:3-134

72. Verdonck F, Volders PG, Vos MA, Sipido KR. Increased Na^+ concentration and altered Na/K pump activity in hypertrophied canine ventricular cells. *Cardiovasc Res*. 2003;57:1035-1043

73. Verdonck F, Volders PG, Vos MA, Sipido KR. Intracellular Na^+ and altered Na^+ transport mechanisms in cardiac hypertrophy and failure. *J Mol Cell Cardiol*. 2003;35:5-25

74. Pike MM, Kitakaze M, Marban E. 23Na-NMR measurements of intracellular sodium in intact perfused ferret hearts during ischemia and reperfusion. *Am J Physiol*. 1990;259:H1767-1773

75. Murphy E, Perlman M, London RE, Steenbergen C. Amiloride delays the ischemia-induced rise in cytosolic free calcium. *Circ Res*. 1991;68:1250-1258

76. Pieske B, Houser SR. $[Na^+]_i$ handling in the failing human heart. *Cardiovasc Res*. 2003;57:874-886

77. Pogwizd SM, Sipido KR, Verdonck F, Bers DM. Intracellular Na in animal models of hypertrophy and heart failure: Contractile function and arrhythmogenesis. *Cardiovasc Res*. 2003;57:887-896

78. Morth JP, Pedersen BP, Toustrup-Jensen MS, Sorensen TL, Petersen J, Andersen JP, Vilsen B, Nissen P. Crystal structure of the sodium-potassium pump. *Nature*. 2007;450:1043-1049

79. Horisberger JD, Jaunin P, Good PJ, Rossier BC, Geering K. Coexpression of α1 with putative β3 subunits results in functional Na^+/K^+ pumps in xenopus oocytes. *Proc Natl Acad Sci U S A*. 1991;88:8397-8400

80. Geering K. The functional role of the β-subunit in the maturation and intracellular transport of Na,K-ATPase. *FEBS Lett*. 1991;285:189-193

81. Lingrel JB, Kuntzweiler T. Na^+,K^+-ATPase. *J Biol Chem*. 1994;269:19659-19662

82. Berry RG, Despa S, Fuller W, Bers DM, Shattock MJ. Differential distribution and regulation of mouse cardiac Na^+/K^+-ATPase α1 and α2 subunits in t-tubule and surface sarcolemmal membranes. *Cardiovasc Res*. 2007;73:92-100

83. Cornelius F, Mahmmoud YA. Functional modulation of the sodium pump: The regulatory proteins "fixit". *News Physiol Sci*. 2003;18:119-124

84. Albers RW. Biochemical aspects of active transport. *Annu Rev Biochem*. 1967;36:727-756

85. Jewell EA, Shamraj OI, Lingrel JB. Isoforms of the α subunit of Na,K-ATPase and their significance. *Acta Physiol Scand Suppl*. 1992;607:161-169

86. McDonough AA, Zhang Y, Shin V, Frank JS. Subcellular distribution of sodium pump isoform subunits in mammalian cardiac myocytes. *Am J Physiol*. 1996;270:C1221-1227

87. James PF, Grupp IL, Grupp G, Woo AL, Askew GR, Croyle ML, Walsh RA, Lingrel JB. Identification of a specific role for the Na,K-atpase α2 isoform as a regulator of calcium in the heart. *Mol Cell*. 1999;3:555-563

88. Hu YK, Eisses JF, Kaplan JH. Expression of an active Na,K-ATPase with an α-subunit lacking all 23 native cysteine residues. *J Biol Chem*. 2000;275:30734-30739

89. Crambert G, Hasler U, Beggah AT, Yu C, Modyanov NN, Horisberger JD, Lelievre L, Geering K. Transport and pharmacological properties of nine different human Na, K-ATPase isozymes. *J Biol Chem*. 2000;275:1976-1986

90. Sweadner KJ, Rael E. The FXYD gene family of small ion transport regulators or channels: cDNA sequence, protein signature sequence, and expression. *Genomics*. 2000;68:41-56

91. Kuster B, Shainskaya A, Pu HX, Goldshleger R, Blostein R, Mann M, Karlish SJ. A new variant of the γ subunit of renal Na,K-ATPase. Identification by mass spectrometry, antibody binding, and expression in cultured cells. *J Biol Chem*. 2000;275:18441-18446

92. Ismail-Beigi F, Edelman IS. The mechanism of the calorigenic action of thyroid hormone. Stimulation of Na^+ + K^+-activated adenosinetriphosphatase activity. *J Gen Physiol*. 1971;57:710-722

93. Post RL, Hegyvary C, Kume S. Activation by adenosine triphosphate in the phosphorylation kinetics of sodium and potassium ion transport adenosine triphosphatase. *J Biol Chem*. 1972;247:6530-6540

94. Clarke RJ, Humphrey PA, Lupfert C, Apell HJ, Cornelius F. Kinetic investigations of the mechanism of the rate-determining step of the Na^+,K^+-ATPase pump cycle. *Ann N Y Acad Sci*. 2003;986:159-162

95. Einholm AP, Toustrup-Jensen MS, Holm R, Andersen JP, Vilsen B. The rapid-onset dystonia parkinsonism mutation d923n of the Na^+, K^+-ATPase α3 isoform disrupts Na^+ interaction at the third Na^+ site. *J Biol Chem*. 2010;285:26245-26254

96. McGuigan JA, Blatter LA. Sodium/calcium exchange in ventricular muscle. *Experientia*. 1987;43:1140-1145

97. Blaustein MP. Sodium ions, calcium ions, blood pressure regulation, and hypertension: A reassessment and a hypothesis. *Am J Physiol*. 1977;232:C165-173

98. Philipson KD, Nishimoto AY. ATP-dependent Na^+ transport in cardiac sarcolemmal vesicles. *Biochim Biophys Acta*. 1983;733:133-141

99. Allen DG, Morris PG, Orchard CH, Pirolo JS. A nuclear magnetic resonance study of metabolism in the ferret heart during hypoxia and inhibition of glycolysis. *J Physiol*. 1985;361:185-204

100. Allen DG, Orchard CH. Myocardial contractile function during ischemia and hypoxia. *Circ Res*. 1987;60:153-168

101. Eisner DA, Elliott AC, Smith GL. The contribution of intracellular acidosis to the decline of developed pressure in ferret hearts exposed to cyanide. *J Physiol*. 1987;391:99-108

102. Smith GL, Valdeolmillos M, Eisner DA, Allen DG. Effects of rapid application of caffeine on intracellular calcium concentration in ferret papillary muscles. *J Gen Physiol*. 1988;92:351-368

103. Kupriyanov VV, Lakomkin VL, Korchazhkina OV, Steinschneider A, Kapelko VI, Saks VA. Control of cardiac energy turnover by cytoplasmic phosphates: ^{31}P-NMR study. *Am J Physiol*. 1991;261:45-53

104. Stewart LC, Deslauriers R, Kupriyanov VV. Relationships between cytosolic [ATP], [ATP]/[ADP] and ionic fluxes in the perfused rat heart: A ^{31}P, ^{23}Na and ^{87}Rb NMR study. *J Mol Cell Cardiol*. 1994;26:1377-1392

105. Collins A, Somlyo AV, Hilgemann DW. The giant cardiac membrane patch method: Stimulation of outward Na^+-Ca^{2+} exchange current by mgatp. *J Physiol*. 1992;454:27-57

106. Ewart HS, Klip A. Hormonal regulation of the Na^+-K^+-ATPase: Mechanisms underlying rapid and sustained changes in pump activity. *Am J Physiol*. 1995;269:C295-311

107. Ziegelhoffer A, Kjeldsen K, Bundgaard H, Breier A, Vrbjar N, Dzurba A. Na,K-ATPase in the myocardium: Molecular principles, functional and clinical aspects. *General physiology and biophysics*. 2000;19:9-47

108. Cabado AG, Vieytes MR, Botana LM. Inhibition of Na^+/K^+ atpase under hypertonic conditions in rat mast cells. *Life Sci*. 1998;63:1227-1237

109. Glitsch HG. Electrophysiology of the sodium-potassium-ATPase in cardiac cells. *Physiol Rev*. 2001;81:1791-1826

110. Soltoff SP, Mandel LJ. Active ion transport in the renal proximal tubule. Ionic dependence of the Na pump. *J Gen Physiol*. 1984;84:623-642

111. Gao J, Mathias RT, Cohen IS, Baldo GJ. Isoprenaline, Ca^{2+} and the Na^{+}-K^{+} pump in guinea-pig ventricular myocytes. *J Physiol*. 1992;449:689-704

112. Bielen FV, Glitsch HG, Verdonck F. Changes of the subsarcolemmal Na^{+} concentration in internally perfused cardiac cells. *Biochim Biophys Acta*. 1991;1065:269-271

113. Carmeliet E. A fuzzy subsarcolemmal space for intracellular Na^{+} in cardiac cells? *Cardiovasc Res*. 1992;26:433-442

114. Wendt-Gallitelli MF, Voigt T, Isenberg G. Microheterogeneity of subsarcolemmal sodium gradients. Electron probe microanalysis in guinea-pig ventricular myocytes. *J Physiol*. 1993;472:33-44

115. Despa S, Kockskamper J, Blatter LA, Bers DM. Na/K pump-induced $[Na]_i$ gradients in rat ventricular myocytes measured with two-photon microscopy. *Biophys J*. 2004;87:1360-1368

116. Dostanic I, Schultz Jel J, Lorenz JN, Lingrel JB. The α1 isoform of Na,K-ATPase regulates cardiac contractility and functionally interacts and co-localizes with the Na/Ca exchanger in heart. *J Biol Chem*. 2004;279:54053-54061

117. Levesque PC, Leblanc N, Hume JR. Release of calcium from guinea pig cardiac sarcoplasmic reticulum induced by sodium-calcium exchange. *Cardiovasc Res*. 1994;28:370-378

118. Levesque PC, Leblanc N, Hume JR. Role of reverse-mode Na^{+}-Ca^{2+} exchange in excitation-contraction coupling in the heart. *Ann N Y Acad Sci*. 1991;639:386-397

119. Leblanc N, Hume JR. Sodium current-induced release of calcium from cardiac sarcoplasmic reticulum. *Science*. 1990;248:372-376

120. Vites AM, Wasserstrom JA. Ca^{2+} influx via Na-Ca exchange and I_{Ca} can both trigger transient contractions in cat ventricular myocytes. *Ann N Y Acad Sci*. 1996;779:521-524

121. Winslow RL, Rice J, Jafri S, Marban E, O'Rourke B. Mechanisms of altered excitation-contraction coupling in canine tachycardia-induced heart failure, II: Model studies. *Circ Res*. 1999;84:571-586

122. O'Rourke B, Kass DA, Tomaselli GF, Kaab S, Tunin R, Marban E. Mechanisms of altered excitation-contraction coupling in canine tachycardia-induced heart failure, I: Experimental studies. *Circ Res*. 1999;84:562-570

123. Nakao M, Gadsby DC. [Na] and [K] dependence of the Na/K pump current-voltage relationship in guinea pig ventricular myocytes. *J Gen Physiol*. 1989;94:539-565

124. Han F, Tucker AL, Lingrel JB, Despa S, Bers DM. Extracellular potassium dependence of the Na^+-K^+-ATPase in cardiac myocytes: Isoform specificity and effect of phospholemman. *Am J Physiol Cell Physiol*. 2009;297:C699-705

125. Desilets M, Baumgarten CM. Isoproterenol directly stimulates the Na^+-K^+ pump in isolated cardiac myocytes. *Am J Physiol*. 1986;251:H218-225

126. Glitsch HG, Krahn T, Pusch H, Suleymanian M. Effect of isoprenaline on active Na transport in sheep cardiac purkinje fibres. *Pflugers Arch*. 1989;415:88-94

127. Dobretsov M, Hastings SL, Stimers JR. Na^+-K^+ pump cycle during β-adrenergic stimulation of adult rat cardiac myocytes. *J Physiol*. 1998;507 (Pt 2):527-539

128. Kockskamper J, Erlenkamp S, Glitsch HG. Activation of the cAMP-protein kinase A pathway facilitates Na^+ translocation by the Na^+-K^+ pump in guinea-pig ventricular myocytes. *J Physiol*. 2000;523 Pt 3:561-574

129. Bossuyt J, Despa S, Han F, Hou Z, Robia SL, Lingrel JB, Bers DM. Isoform specificity of the Na/K-ATPase association and regulation by phospholemman. *J Biol Chem*. 2009;284:26749-26757

130. Fuller W, Howie J, McLatchie LM, Weber RJ, Hastie CJ, Burness K, Pavlovic D, Shattock MJ. FXYD1 phosphorylation in vitro and in adult rat cardiac myocytes: Threonine 69 is a novel substrate for protein kinase C. *Am J Physiol Cell Physiol*. 2009;296:C1346-1355

131. Gao J, Cohen IS, Mathias RT, Baldo GJ. Regulation of the β-stimulation of the Na^+-K^+ pump current in guinea-pig ventricular myocytes by a cAMP-dependent PKA pathway. *J Physiol*. 1994;477 (Pt 3):373-380

132. Gao J, Cohen IS, Mathias RT, Baldo GJ. The inhibitory effect of beta-stimulation on the Na/K pump current in guinea pig ventricular myocytes is mediated by a cAMP-dependent PKA pathway. *Pflugers Arch*. 1998;435:479-484

133. Ishizuka N, Berlin JR. β-adrenergic stimulation does not regulate Na pump function in voltage-clamped ventricular myocytes of the rat heart. *Pflugers Arch*. 1993;424:361-363

134. Gao J, Mathias RT, Cohen IS, Shi J, Baldo GJ. The effects of β-stimulation on the Na^+-K^+ pump current-voltage relationship in guinea-pig ventricular myocytes. *J Physiol*. 1996;494 (Pt 3):697-708

135. Gao J, Wymore R, Wymore RT, Wang Y, McKinnon D, Dixon JE, Mathias RT, Cohen IS, Baldo GJ. Isoform-specific regulation of the sodium pump by α- and β-adrenergic agonists in the guinea-pig ventricle. *J Physiol*. 1999;516 (Pt 2):377-383

136. Bertorello AM, Aperia A, Walaas SI, Nairn AC, Greengard P. Phosphorylation of the catalytic subunit of Na^+,K^+-ATPase inhibits the activity of the enzyme. *Proc Natl Acad Sci U S A*. 1991;88:11359-11362

137. Fisone G, Cheng SX, Nairn AC, Czernik AJ, Hemmings HC, Jr., Hoog JO, Bertorello AM, Kaiser R, Bergman T, Jornvall H, et al. Identification of the phosphorylation site for cAMP-dependent protein kinase on Na^+,K^+-ATPase and effects of site-directed mutagenesis. *J Biol Chem*. 1994;269:9368-9373

138. Cornelius F, Logvinenko N. Functional regulation of reconstituted Na,K-ATPase by protein kinase A phosphorylation. *FEBS Lett*. 1996;380:277-280

139. Feschenko MS, Sweadner KJ. Conformation-dependent phosphorylation of Na,K-ATPase by protein kinase A and protein kinase C. *J Biol Chem*. 1994;269:30436-30444

140. Sweadner KJ, Feschenko MS. Predicted location and limited accessibility of protein kinase A phosphorylation site on Na-K-ATPase. *Am J Physiol Cell Physiol*. 2001;280:C1017-1026

141. Gao J, Mathias RT, Cohen IS, Wang Y, Sun X, Baldo GJ. Activation of PKC increases Na^+-K^+ pump current in ventricular myocytes from guinea pig heart. *Pflugers Arch*. 1999;437:643-651

142. Wang Y, Gao J, Mathias RT, Cohen IS, Sun X, Baldo GJ. α-adrenergic effects on Na^+-K^+ pump current in guinea-pig ventricular myocytes. *J Physiol*. 1998;509 (Pt 1):117-128

143. Lundmark JL, Ramasamy R, Vulliet PR, Schaefer S. Chelerythrine increases Na-K-ATPase activity and limits ischemic injury in isolated rat hearts. *Am J Physiol*. 1999;277:H999-H1006

144. Buhagiar KA, Hansen PS, Bewick NL, Rasmussen HH. Protein kinase Cε contributes to regulation of the sarcolemmal Na^+-K^+ pump. *Am J Physiol Cell Physiol*. 2001;281:C1059-1063

145. White CN, Figtree GA, Liu CC, Garcia A, Hamilton EJ, Chia KK, Rasmussen HH. Angiotensin II inhibits the Na^+-K^+ pump via PKC-dependent activation of NADPH oxidase. *Am J Physiol Cell Physiol*. 2009;296:C693-700

146. Nosek TM, Williams MF, Zeigler ST, Godt RE. Inositol trisphosphate enhances calcium release in skinned cardiac and skeletal muscle. *Am J Physiol*. 1986;250:C807-811

147. Berridge MJ. Inositol trisphosphate and diacylglycerol: Two interacting second messengers. *Annu Rev Biochem*. 1987;56:159-193

148. Berridge MJ. Inositol trisphosphate as a second messenger in signal transduction. *Ann N Y Acad Sci*. 1987;494:39-51

149. Han F, Bossuyt J, Martin JL, Despa S, Bers DM. Role of phospholemman phosphorylation sites in mediating kinase-dependent regulation of the Na^+-K^+-ATPase. *Am J Physiol Cell Physiol*.299:C1363-1369

150. Erlenkamp S, Glitsch HG, Kockskamper J. Dual regulation of cardiac Na^+-K^+ pumps and CFTR Cl^- channels by protein kinases A and C. *Pflugers Arch*. 2002;444:251-262

151. Lowndes JM, Hokin-Neaverson M, Bertics PJ. Kinetics of phosphorylation of Na^+/K^+-ATPase by protein kinase C. *Biochim Biophys Acta*. 1990;1052:143-151

152. Blanco G, Mercer RW. Isozymes of the Na-K-ATPase: Heterogeneity in structure, diversity in function. *Am J Physiol*. 1998;275:F633-650

153. Middleton JP, Khan WA, Collinsworth G, Hannun YA, Medford RM. Heterogeneity of protein kinase C-mediated rapid regulation of Na/K-ATPase in kidney epithelial cells. *J Biol Chem*. 1993;268:15958-15964

154. Vasilets LA, Fotis H, Gartner EM. Regulatory phosphorylation of the Na^+/K^+-ATPase from mammalian kidneys and xenopus oocytes by protein kinases. Characterization of the phosphorylation site for PKC. *Ann N Y Acad Sci*. 1997;834:585-587

155. Beguin P, Beggah AT, Chibalin AV, Burgener-Kairuz P, Jaisser F, Mathews PM, Rossier BC, Cotecchia S, Geering K. Phosphorylation of the Na,K-ATPase α-subunit by protein kinase A and C in vitro and in intact cells. Identification of a novel motif for PKC-mediated phosphorylation. *J Biol Chem*. 1994;269:24437-24445

156. Chibalin AV, Katz AI, Berggren PO, Bertorello AM. Receptor-mediated inhibition of renal Na^+-K^+-ATPase is associated with endocytosis of its α- and β-subunits. *Am J Physiol*. 1997;273:C1458-1465

157. Chibalin AV, Ogimoto G, Pedemonte CH, Pressley TA, Katz AI, Feraille E, Berggren PO, Bertorello AM. Dopamine-induced endocytosis of Na^+,K^+-ATPase is initiated by phosphorylation of Ser-18 in the rat α subunit and is responsible for the decreased activity in epithelial cells. *J Biol Chem*. 1999;274:1920-1927

158. Chibalin AV, Pedemonte CH, Katz AI, Feraille E, Berggren PO, Bertorello AM. Phosphorylation of the catalyic α-subunit constitutes a triggering signal for Na^+,K^+-ATPase endocytosis. *J Biol Chem*. 1998;273:8814-8819

159. Walaas SI, Czernik AJ, Olstad OK, Sletten K, Walaas O. Protein kinase C and cyclic AMP-dependent protein kinase phosphorylate phospholemman, an insulin and adrenaline-regulated membrane phosphoprotein, at specific sites in the carboxy terminal domain. *Biochem J*. 1994;304 (Pt 2):635-640

160. Shattock MJ, Matsuura H. Measurement of Na^+-K^+ pump current in isolated rabbit ventricular myocytes using the whole-cell voltage-clamp technique. Inhibition of the pump by oxidant stress. *Circ Res*. 1993;72:91-101

161. Haddock PS, Shattock MJ, Hearse DJ. Modulation of cardiac Na^+-K^+ pump current: Role of protein and nonprotein sulfhydryl redox status. *Am J Physiol*. 1995;269:H297-307

162. Figtree GA, Liu CC, Bibert S, Hamilton EJ, Garcia A, White CN, Chia KK, Cornelius F, Geering K, Rasmussen HH. Reversible oxidative modification: A key mechanism of Na^+-K^+ pump regulation. *Circ Res*. 2009;105:185-193

163. White CN, Liu CC, Garcia A, Hamilton EJ, Chia KK, Figtree GA, Rasmussen HH. Activation of camp-dependent signaling induces oxidative modification of the cardiac Na^+-K^+ pump and inhibits its activity. *J Biol Chem*. 2010;285:13712-13720

164. Bibert S, Liu CC, Figtree GA, Garcia A, Hamilton EJ, Marassi FM, Sweadner KJ, Cornelius F, Geering K, Rasmussen HH. Fxyd proteins reverse inhibition of the Na^+-K^+ pump mediated by glutathionylation of its β1 subunit. *J Biol Chem*. 2011;286:18562-18572

165. Kang DG, Kim JW, Lee J. Effects of nitric oxide synthesis inhibition on the Na,K-ATPase activity in the kidney. *Pharmacol Res*. 2000;41:121-125

166. Varela M, Herrera M, Garvin JL. Inhibition of Na-K-ATPase in thick ascending limbs by NO depends on O_2- and is diminished by a high-salt diet. *Am J Physiol Renal Physiol*. 2004;287:F224-230

167. Liang M, Knox FG. Nitric oxide reduces the molecular activity of Na^+,K^+-ATPase in opossum kidney cells. *Kidney Int*. 1999;56:627-634

168. McKee M, Scavone C, Nathanson JA. Nitric oxide, cGMP, and hormone regulation of active sodium transport. *Proc Natl Acad Sci U S A*. 1994;91:12056-12060

169. Ellis DZ, Nathanson JA, Rabe J, Sweadner KJ. Carbachol and nitric oxide inhibition of Na,K-ATPase activity in bovine ciliary processes. *Invest Ophthalmol Vis Sci*. 2001;42:2625-2631

170. Ellis DZ, Nathanson JA, Sweadner KJ. Carbachol inhibits Na^+-K^+-ATPase activity in choroid plexus via stimulation of the NO/cGMP pathway. *Am J Physiol Cell Physiol*. 2000;279:C1685-1693

171. William M, Hamilton EJ, Garcia A, Bundgaard H, Chia KK, Figtree GA, Rasmussen HH. Natriuretic peptides stimulate the cardiac sodium pump via NPR-C-coupled NOS activation. *Am J Physiol Cell Physiol*. 2008;294:C1067-1073

172. White CN, Hamilton EJ, Garcia A, Wang D, Chia KK, Figtree GA, Rasmussen HH. Opposing effects of coupled and uncoupled NOS activity on the Na^+-K^+ pump in cardiac myocytes. *Am J Physiol Cell Physiol*. 2008;294:C572-578

173. William M, Vien J, Hamilton E, Garcia A, Bundgaard H, Clarke RJ, Rasmussen HH. The nitric oxide donor sodium nitroprusside stimulates the Na^+-K^+ pump in isolated rabbit cardiac myocytes. *J Physiol*. 2005;565:815-825

174. Gupta S, McArthur C, Grady C, Ruderman NB. Role of endothelium-derived nitric oxide in stimulation of Na^+-K^+-ATPase activity by endothelin in rabbit aorta. *Am J Physiol*. 1994;266:H577-582

175. Chen SJ, Chen KH, Webb RC, Yen MH, Wu CC. Abnormal activation of Na^+-K^+ pump in aortas from rats with endotoxaemia. *Naunyn Schmiedebergs Arch Pharmacol*. 2003;368:57-62

176. Vlkovicova J, Javorkova V, Mezesova L, Pechanova O, Vrbjar N. Regulatory role of nitric oxide on the cardiac Na,K-ATPase in hypertension. *Physiological research / Academia Scientiarum Bohemoslovaca*. 2008;57 Suppl 2:S15-22

177. Pavlovic D. Pacing stimulates cardiac Na/K atpase via NO and phospholemman-dependent mechanism and protects the heart against arrhythmias. Journal of Molecular and Cellular Cardiology. 2013; S022-2828(13)00144-2 (in print)

178. Dedkova EN, Wang YG, Ji X, Blatter LA, Samarel AM, Lipsius SL. Signalling mechanisms in contraction-mediated stimulation of intracellular NO production in cat ventricular myocytes. *J Physiol*. 2007;580:327-345

179. Ping P, Takano H, Zhang J, Tang XL, Qiu Y, Li RC, Banerjee S, Dawn B, Balafonova Z, Bolli R. Isoform-selective activation of protein kinase C by nitric oxide in the heart of conscious rabbits: A signaling mechanism for both nitric oxide-induced and ischemia-induced preconditioning. *Circ Res*. 1999;84:587-604

180. Benziane B, Widegren U, Pirkmajer S, Henriksson J, Stepto NK, Chibalin AV. Effect of exercise and training on phospholemman phosphorylation in human skeletal muscle. *Am J Physiol Endocrinol Metab*.301:E456-466

181. Babes A, Fendler K. Na^+ transport, and the E_1P- E_2P conformational transition of the Na^+/K^+-ATPase. *Biophys J*. 2000;79:2557-2571

182. Segall L, Daly SE, Blostein R. Mechanistic basis for kinetic differences between the rat α1, α2, and α3 isoforms of the Na,K-ATPase. *J Biol Chem*. 2001;276:31535-31541

183. Salonikidis PS, Kirichenko SN, Tatjanenko LV, Schwarz W, Vasilets LA. Extracellular pH modulates kinetics of the Na^+,K^+-ATPase. *Biochim Biophys Acta*. 2000;1509:496-504

184. Wang WN, Wang AL, Chen L, Liu Y, Sun RY. Effects of pH on survival, phosphorus concentration, adenylate energy charge and Na^+-K^+ ATPase activities of penaeus chinensis osbeck juveniles. *Aquat Toxicol*. 2002;60:75-83

185. El-Armouche A, Wittkopper K, Fuller W, Howie J, Shattock MJ, Pavlovic D. Phospholemman-dependent regulation of the cardiac Na/K-ATPase activity is modulated by inhibitor-1 sensitive type-1 phosphatase. *FASEB J*.25:4467-4475

186. Arystarkhova E, Donnet C, Munoz-Matta A, Specht SC, Sweadner KJ. Multiplicity of expression of FXYD proteins in mammalian cells: Dynamic exchange of phospholemman and γ-subunit in response to stress. *Am J Physiol Cell Physiol*. 2007;292:C1179-1191

187. Feraille E, Doucet A. Sodium-potassium-adenosinetriphosphatase-dependent sodium transport in the kidney: Hormonal control. *Physiol Rev*. 2001;81:345-418

188. Klimes I, Howard BV, Mott DM. Sodium-potassium pump in cultured fibroblasts from obese donors; no evidence for an inherent decrease of basal or insulin-stimulated activity. *Metabolism*. 1984;33:317-322

189. Longo N. Insulin stimulates the Na^+,K^+-ATPase and the $Na^+/K^+/Cl^-$ cotransporter of human fibroblasts. *Biochim Biophys Acta*. 1996;1281:38-44

190. Longo N, Franchi-Gazzola R, Bussolati O, Dall'Asta V, Foa PP, Guidotti GG, Gazzola GC. Effect of insulin on the activity of amino acid transport systems in cultured human fibroblasts. *Biochim Biophys Acta*. 1985;844:216-223

191. Chibalin AV, Kovalenko MV, Ryder JW, Feraille E, Wallberg-Henriksson H, Zierath JR. Insulin- and glucose-induced phosphorylation of the Na^+,K^+-adenosine triphosphatase α-subunits in rat skeletal muscle. *Endocrinology*. 2001;142:3474-3482

192. Galuska D, Kotova O, Barres R, Chibalina D, Benziane B, Chibalin AV. Altered expression and insulin-induced trafficking of Na^+-K^+-ATPase in rat skeletal muscle: Effects of high-fat diet and exercise. *Am J Physiol Endocrinol Metab*. 2009;297:E38-49

193. Garty H, Karlish SJ. Role of FXYD proteins in ion transport. *Annu Rev Physiol*. 2006;68:431-459

194. Rivas E, Lew V, De Robertis E. (^3H) ouabain binding to a hydrophobic protein from electroplax membranes. *Biochim Biophys Acta*. 1972;290:419-423

195. Reeves AS, Collins JH, Schwartz A. Isolation and characterization of Na,K-ATPase proteolipid. *Biochem Biophys Res Commun*. 1980;95:1591-1598

196. Collins JH, Leszyk J. The "gamma subunit" of Na,K-ATPase: A small, amphiphilic protein with a unique amino acid sequence. *Biochemistry*. 1987;26:8665-8668

197. Forbush B, Kaplan JH, Hoffman JF. Characterization of a new photoaffinity derivative of ouabain: Labeling of the large polypeptide and of a proteolipid component of the Na,K-ATPase. *Biochemistry*. 1978;17:3667-3676

198. Therien AG, Goldshleger R, Karlish SJ, Blostein R. Tissue-specific distribution and modulatory role of the γ subunit of the Na,K-ATPase. *J Biol Chem*. 1997;272:32628-32634

199. Arystarkhova E, Wetzel RK, Asinovski NK, Sweadner KJ. The γ subunit modulates Na^+ and K^+ affinity of the renal Na,K-ATPase. *J Biol Chem*. 1999;274:33183-33185

200. Feschenko MS, Donnet C, Wetzel RK, Asinovski NK, Jones LR, Sweadner KJ. Phospholemman, a single-span membrane protein, is an accessory protein of Na,K-ATPase in cerebellum and choroid plexus. *J Neurosci*. 2003;23:2161-2169

201. Zhang XQ, Moorman JR, Ahlers BA, Carl LL, Lake DE, Song J, Mounsey JP, Tucker AL, Chan YM, Rothblum LI, Stahl RC, Carey DJ, Cheung JY. Phospholemman overexpression inhibits Na^+-K^+-ATPase in adult rat cardiac myocytes: Relevance to

decreased Na^+ pump activity in postinfarction myocytes. *J Appl Physiol*. 2006;100:212-220

202. Zhang XQ, Qureshi A, Song J, Carl LL, Tian Q, Stahl RC, Carey DJ, Rothblum LI, Cheung JY. Phospholemman modulates Na^+/Ca^{2+} exchange in adult rat cardiac myocytes. *Am J Physiol Heart Circ Physiol*. 2003;284:H225-233

203. Arystarkhova E, Donnet C, Asinovski NK, Sweadner KJ. Differential regulation of renal Na,K-ATPase by splice variants of the γ subunit. *J Biol Chem*. 2002;277:10162-10172

204. Cornelius F, Mahmmoud YA. Themes in ion pump regulation. *Ann N Y Acad Sci*. 2003;986:579-586

205. Pu HX, Cluzeaud F, Goldshleger R, Karlish SJ, Farman N, Blostein R. Functional role and immunocytochemical localization of the γ_a and γ_b forms of the Na,K-ATPase γ subunit. *J Biol Chem*. 2001;276:20370-20378

206. Pu HX, Scanzano R, Blostein R. Distinct regulatory effects of the Na,K-ATPase γ subunit. *J Biol Chem*. 2002;277:20270-20276

207. Wetzel RK, Sweadner KJ. Immunocytochemical localization of Na-K-ATPase α- and γ-subunits in rat kidney. *Am J Physiol Renal Physiol*. 2001;281:F531-545

208. Pihakaski-Maunsbach K, Vorum H, Locke EM, Garty H, Karlish SJ, Maunsbach AB. Immunocytochemical localization of Na,K-ATPase γ subunit and CHIF in inner medulla of rat kidney. *Ann N Y Acad Sci*. 2003;986:401-409

209. Crambert G, Li C, Claeys D, Geering K. FXYD3 (MAT-8), a new regulator of Na,K-ATPase. *Mol Biol Cell*. 2005;16:2363-2371

210. Garty H, Lindzen M, Scanzano R, Aizman R, Fuzesi M, Goldshleger R, Farman N, Blostein R, Karlish SJ. A functional interaction between CHIF and Na-K-ATPase: Implication for regulation by FXYD proteins. *Am J Physiol Renal Physiol*. 2002;283:F607-615

211. Shi H, Levy-Holzman R, Cluzeaud F, Farman N, Garty H. Membrane topology and immunolocalization of CHIF in kidney and intestine. *Am J Physiol Renal Physiol*. 2001;280:F505-512

212. Lubarski I, Pihakaski-Maunsbach K, Karlish SJ, Maunsbach AB, Garty H. Interaction with the Na,K-ATPase and tissue distribution of FXYD5 (related to ion channel). *J Biol Chem*. 2005;280:37717-37724

213. Kadowaki K, Sugimoto K, Yamaguchi F, Song T, Watanabe Y, Singh K, Tokuda M. Phosphohippolin expression in the rat central nervous system. *Brain Res Mol Brain Res*. 2004;125:105-112

214. Mahmmoud YA, Cramb G, Maunsbach AB, Cutler CP, Meischke L, Cornelius F. Regulation of Na,K-ATPase by PLMS, the phospholemman-like protein from shark:

Molecular cloning, sequence, expression, cellular distribution, and functional effects of plms. *J Biol Chem*. 2003;278:37427-37438

215. Wetzel RK, Sweadner KJ. Phospholemman expression in extraglomerular mesangium and afferent arteriole of the juxtaglomerular apparatus. *Am J Physiol Renal Physiol*. 2003;285:F121-129

216. Sweadner KJ, Arystarkhova E, Donnet C, Wetzel RK. Fxyd proteins as regulators of the Na,K-ATPase in the kidney. *Ann N Y Acad Sci*. 2003;986:382-387

217. Beevers AJ, Kukol A. Secondary structure, orientation, and oligomerization of phospholemman, a cardiac transmembrane protein. *Protein Sci*. 2006;15:1127-1132

218. Franzin CM, Choi J, Zhai D, Reed JC, Marassi FM. Structural studies of apoptosis and ion transport regulatory proteins in membranes. *Magn Reson Chem*. 2004;42:172-179

219. Moorman JR, Ackerman SJ, Kowdley GC, Griffin MP, Mounsey JP, Chen Z, Cala SE, O'Brian JJ, Szabo G, Jones LR. Unitary anion currents through phospholemman channel molecules. *Nature*. 1995;377:737-740

220. Bogaev RC, Jia LG, Kobayashi YM, Palmer CJ, Mounsey JP, Moorman JR, Jones LR, Tucker AL. Gene structure and expression of phospholemman in mouse. *Gene*. 2001;271:69-79

221. Chen LS, Lo CF, Numann R, Cuddy M. Characterization of the human and rat phospholemman (PLM) cDNAs and localization of the human PLM gene to chromosome 19q13.1. *Genomics*. 1997;41:435-443

222. Franzin CM, Gong XM, Thai K, Yu J, Marassi FM. NMR of membrane proteins in micelles and bilayers: The FXYD family proteins. *Methods*. 2007;41:398-408

223. Moorman JR, Jones LR. Phospholemman: A cardiac taurine channel involved in regulation of cell volume. *Adv Exp Med Biol*. 1998;442:219-228

224. Morales-Mulia M, Pasantes-Morales H, Moran J. Volume sensitive efflux of taurine in HEK293 cells overexpressing phospholemman. *Biochim Biophys Acta*. 2000;1496:252-260

225. Bell JR, Lloyd D, Curl CL, Delbridge LM, Shattock MJ. Cell volume control in phospholemman (PLM) knockout mice: Do cardiac myocytes demonstrate a regulatory volume decrease and is this influenced by deletion of PLM? *Exp Physiol*. 2009;94:330-343

226. Lindzen M, Gottschalk KE, Fuzesi M, Garty H, Karlish SJ. Structural interactions between FXYD proteins and Na^+,K^+-ATPase: α/β/FXYD subunit stoichiometry and cross-linking. *J Biol Chem*. 2006;281:5947-5955

227. Hebert H, Purhonen P, Vorum H, Thomsen K, Maunsbach AB. Three-dimensional structure of renal Na,K-ATPase from cryo-electron microscopy of two-dimensional crystals. *J Mol Biol*. 2001;314:479-494

228. Fuzesi M, Gottschalk KE, Lindzen M, Shainskaya A, Kuster B, Garty H, Karlish SJ. Covalent cross-links between the γ subunit (FXYD2) and α and β subunits of Na,K-ATPase: Modeling the α- γ interaction. *J Biol Chem*. 2005;280:18291-18301

229. Fuzesi M, Goldshleger R, Garty H, Karlish SJ. Defining the nature and sites of interaction between FXYD proteins and Na,K-ATPase. *Ann N Y Acad Sci*. 2003;986:532-533

230. Bossuyt J, Despa S, Martin JL, Bers DM. Phospholemman phosphorylation alters its fluorescence resonance energy transfer with the Na/K-ATPase pump. *J Biol Chem*. 2006;281:32765-32773

231. Ahlers BA, Zhang XQ, Moorman JR, Rothblum LI, Carl LL, Song J, Wang J, Geddis LM, Tucker AL, Mounsey JP, Cheung JY. Identification of an endogenous inhibitor of the cardiac Na^+/Ca^{2+} exchanger, phospholemman. *J Biol Chem*. 2005;280:19875-19882

232. Song J, Zhang XQ, Ahlers BA, Carl LL, Wang J, Rothblum LI, Stahl RC, Mounsey JP, Tucker AL, Moorman JR, Cheung JY. Serine 68 of phospholemman is critical in modulation of contractility, $[Ca^{2+}]_i$ transients, and Na^+/Ca^{2+} exchange in adult rat cardiac myocytes. *Am J Physiol Heart Circ Physiol*. 2005;288:H2342-2354

233. Mirza MA, Zhang XQ, Ahlers BA, Qureshi A, Carl LL, Song J, Tucker AL, Mounsey JP, Moorman JR, Rothblum LI, Zhang TS, Cheung JY. Effects of phospholemman downregulation on contractility and $[Ca^{2+}]_i$ transients in adult rat cardiac myocytes. *Am J Physiol Heart Circ Physiol*. 2004;286:H1322-1330

234. Berry RG. Regulation of cardiac Na/K ATPase by FXYD1 (phospholemman). *J. Mol. Cell. Cardiol*. 2006;40:997

235. Cornelius F, Mahmmoud YA, Christensen HR. Modulation of Na,K-ATPase by associated small transmembrane regulatory proteins and by lipids. *J Bioenerg Biomembr*. 2001;33:415-423

236. Mounsey JP, Patel MK, Mistry D, John JE, Moorman JR. Protein kinase C co-expression and the effects of halothane on rat skeletal muscle sodium channels. *Br J Pharmacol*. 1999;128:989-998

237. Rembold CM, Ripley ML, Meeks MK, Geddis LM, Kutchai HC, Marassi FM, Cheung JY, Moorman JR. Serine 68 phospholemman phosphorylation during forskolin-induced swine carotid artery relaxation. *J Vasc Res*. 2005;42:483-491

238. Dostanic I, Lorenz JN, Schultz Jel J, Grupp IL, Neumann JC, Wani MA, Lingrel JB. The α2 isoform of Na,K-ATPase mediates ouabain-induced cardiac inotropy in mice. *J Biol Chem*. 2003;278:53026-53034

239. Moseley AE, Huddleson JP, Bohanan CS, James PF, Lorenz JN, Aronow BJ, Lingrel JB. Genetic profiling reveals global changes in multiple biological pathways in the hearts of Na,K-ATPase α1 isoform haploinsufficient mice. *Cell Physiol Biochem*. 2005;15:145-158

240. Bossuyt J, Ai X, Moorman JR, Pogwizd SM, Bers DM. Expression and phosphorylation of the Na-pump regulatory subunit phospholemman in heart failure. *Circ Res*. 2005;97:558-565

241. Bibert S, Roy S, Schaer D, Horisberger JD, Geering K. Phosphorylation of phospholemman (FXYD1) by protein kinases A and C modulates distinct Na,K-ATPase isozymes. *J Biol Chem*. 2008;283:476-486

242. Wypijewski KJ, Howie J, Reilly L, Tulloch LB, Aughton KL, McLatchie LM, Shattock MJ, Calaghan SC, Fuller W. A separate pool of cardiac phospholemman that does not regulate or associate with the sodium pump: Multimers of phospholemman in ventricular muscle. *J Biol Chem*. 2013;288:13808-13820

243. Tulloch LB, Howie J, Wypijewski KJ, Wilson CR, Bernard WG, Shattock MJ, Fuller W. The inhibitory effect of phospholemman on the sodium pump requires its palmitoylation. *J Biol Chem*. 2011;286:36020-36031

244. Hall AR ML, Fuller W, Shattock MJ Nitric oxide-induced stimulation of the cardiac Na/K ATPase requires phospholemman. *J Mol Cell Cardiol*. 2007;42:S54

245. Zhou L, Burnett AL, Huang PL, Becker LC, Kuppusamy P, Kass DA, Kevin Donahue J, Proud D, Sham JS, Dawson TM, Xu KY. Lack of nitric oxide synthase depresses ion transporting enzyme function in cardiac muscle. *Biochem Biophys Res Commun*. 2002;294:1030-1035

246. Cheung JY, Rothblum LI, Moorman JR, Tucker AL, Song J, Ahlers BA, Carl LL, Wang J, Zhang XQ. Regulation of cardiac Na^+/Ca^{2+} exchanger by phospholemman. *Ann N Y Acad Sci*. 2007;1099:119-134

247. Zhang XQ, Ahlers BA, Tucker AL, Song J, Wang J, Moorman JR, Mounsey JP, Carl LL, Rothblum LI, Cheung JY. Phospholemman inhibition of the cardiac Na^+/Ca^{2+} exchanger. Role of phosphorylation. *J Biol Chem*. 2006;281:7784-7792

248. Tucker AL, Song J, Zhang XQ, Wang J, Ahlers BA, Carl LL, Mounsey JP, Moorman JR, Rothblum LI, Cheung JY. Altered contractility and $[Ca^{2+}]_i$ homeostasis in phospholemman-deficient murine myocytes: Role of Na^+/Ca^{2+} exchange. *Am J Physiol Heart Circ Physiol*. 2006;291:H2199-2209

249. Ballard C, Schaffer S. Stimulation of the Na^+/Ca^{2+} exchanger by phenylephrine, angiotensin II and endothelin 1. *J Mol Cell Cardiol*. 1996;28:11-17

250. Ballard C, Mozaffari M, Schaffer S. Signal transduction mechanism for the stimulation of the sarcolemmal Na^+-Ca^{2+} exchanger by insulin. *Mol Cell Biochem*. 1994;135:113-119

251. Main MJ, Grantham CJ, Cannell MB. Changes in subsarcolemmal sodium concentration measured by Na-Ca exchanger activity during Na-pump inhibition and β-adrenergic stimulation in guinea-pig ventricular myocytes. *Pflugers Arch*. 1997;435:112-118

252. Han X, Ferrier GR. Contribution of Na^+-Ca^{2+} exchange to stimulation of transient inward current by isoproterenol in rabbit cardiac purkinje fibers. *Circ Res*. 1995;76:664-674

253. Linck B, Qiu Z, He Z, Tong Q, Hilgemann DW, Philipson KD. Functional comparison of the three isoforms of the Na^+/Ca^{2+} exchanger (NCX1, NCX2, NCX3). *Am J Physiol*. 1998;274:C415-423

254. Ruknudin A, He S, Lederer WJ, Schulze DH. Functional differences between cardiac and renal isoforms of the rat Na^+-Ca^{2+} exchanger NCX1 expressed in xenopus oocytes. *J Physiol*. 2000;529 Pt 3:599-610

255. Schulze DH, Muqhal M, Lederer WJ, Ruknudin AM. Sodium/calcium exchanger (NCX1) macromolecular complex. *J Biol Chem*. 2003;278:28849-28855

256. Zhang YH, Hancox JC. Regulation of cardiac Na^+-Ca^{2+} exchanger activity by protein kinase phosphorylation--still a paradox? *Cell Calcium*. 2009;45:1-10

257. Pieske B, Maier LS, Piacentino V,3rd, Weisser J, Hasenfuss G, Houser S. Rate dependence of $[Na^+]_i$ and contractility in nonfailing and failing human myocardium. *Circulation*. 2002;106:447-453

258. Marsh NA, Shattock MJ. In celebration of 100 years of the isolated perfused heart - langendorff revisited. *J Physiol-London*. 1997;505P:69p-70p

259. Sutherland FJ, Hearse DJ. The isolated blood and perfusion fluid perfused heart. *Pharmacol Res*. 2000;41:613-627

260. Awad WI, Shattock MJ, Chambers DJ. Ischemic preconditioning in immature myocardium. *Circulation*. 1998;98:II206-213

261. Wang QD, Tokuno S, Valen G, Sjoquist PO, Thoren P. Cyclic fluctuations in the cardiac performance of the isolated langendorff-perfused mouse heart: Pyruvate abolishes the fluctuations and has an anti-ischaemic effect. *Acta Physiol Scand*. 2002;175:279-287

262. Sutherland FJ, Baker KE, Shattock MJ, Hearse DJ. Responses to ischaemia and reperfusion in the mouse isolated perfused heart and the phenomenon of 'contractile cycling'. *Clin Exp Pharmacol Physiol*. 2003;30:879-884

263. Mitra R, Morad M. A uniform enzymatic method for dissociation of myocytes from hearts and stomachs of vertebrates. *Am J Physiol*. 1985;249:H1056-1060

264. Bardswell SC, Cuello F, Rowland AJ, Sadayappan S, Robbins J, Gautel M, Walker JW, Kentish JC, Avkiran M. Distinct sarcomeric substrates are responsible for protein

kinase D-mediated regulation of cardiac myofilament Ca^{2+} sensitivity and cross-bridge cycling. *J Biol Chem*.285:5674-5682

265. Yin X, Cuello F, Mayr U, Hao Z, Hornshaw M, Ehler E, Avkiran M, Mayr M. Proteomics analysis of the cardiac myofilament subproteome reveals dynamic alterations in phosphatase subunit distribution. *Mol Cell Proteomics*. 2010;9:497-509

266. Everts ME, Lomo T, Clausen T. Changes in K^+, Na^+ and calcium contents during in vivo stimulation of rat skeletal muscle. *Acta Physiol Scand*. 1993;147:357-368

267. Gupta RK, Gupta P. Direct observation of resolved resonances from intracellular and extracellular Na^{-23} ions in NMR-studies of intact-cells and tissues using dysprosium(III)tripolyphosphate as paramagnetic shift-reagent. *Journal of Magnetic Resonance*. 1982;47:344-350

268. Luca Ronconi; Peter J, Sadler. Applications of heteronuclear NMR spectroscopy in biological and medicinal inorganic chemistry. *Coordination Chemistry Reviews*. 2008;252: 2239-2277

269. Jelicks LA, Gupta RK. Multinuclear NMR studies of the langendorff perfused rat heart. *J Biol Chem*. 1989;264:15230-15235

270. Askenasy N, Tassini M, Vivi A, Navon G. Intracellular volume measurement and detection of edema: Multinuclear NMR studies of intact rat hearts during normothermic ischemia. *Magn Reson Med*. 1995;33:515-520

271. Song J, Zhang XQ, Carl LL, Qureshi A, Rothblum LI, Cheung JY. Overexpression of phospholemman alters contractility and $[Ca^{2+}]_i$ transients in adult rat myocytes. *Am J Physiol Heart Circ Physiol*. 2002;283:H576-583

272. Zolk O, Marx M, Jackel E, El-Armouche A, Eschenhagen T. β-adrenergic stimulation induces cardiac ankyrin repeat protein expression: Involvement of protein kinase A and calmodulin-dependent kinase. *Cardiovasc Res*. 2003;59:563-572

273. Kinoshita E, Kinoshita-Kikuta E, Koike T. Separation and detection of large phosphoproteins using Phos-tag SDS-PAGE. *Nat Protoc*. 2009;4:1513-1521

274. Kinoshita E, Kinoshita-Kikuta E, Takiyama K, Koike T. Phosphate-binding tag, a new tool to visualize phosphorylated proteins. *Mol Cell Proteomics*. 2006;5:749-757

275. Kinoshita E, Kinoshita-Kikuta E, Matsubara M, Yamada S, Nakamura H, Shiro Y, Aoki Y, Okita K, Koike T. Separation of phosphoprotein isotypes having the same number of phosphate groups using phosphate-affinity sds-page. *Proteomics*. 2008;8:2994-3003

276. Pavlovic D, McLatchie LM, Shattock MJ. The rate of loss of t-tubules in cultured adult ventricular myocytes is species dependent. *Exp Physiol*.95:518-527

277. Mounsey JP, Lu KP, Patel MK, Chen ZH, Horne LT, John JE, 3rd, Means AR, Jones LR, Moorman JR. Modulation of xenopus oocyte-expressed phospholemman-induced

ion currents by co-expression of protein kinases. *Biochim Biophys Acta*. 1999;1451:305-318

278. Lansbery KL, Burcea LC, Mendenhall ML, Mercer RW. Cytoplasmic targeting signals mediate delivery of phospholemman to the plasma membrane. *Am J Physiol Cell Physiol*. 2006;290:C1275-1286

279. Barbieri CM, Stock AM. Universally applicable methods for monitoring response regulator aspartate phosphorylation both in vitro and in vivo using Phos-tag-based reagents. *Anal Biochem*. 2008;376:73-82

280. Wong A, Beevers AJ, Kukol A, Dupree R, Smith ME. Solid-state ^{17}O NMR spectroscopy of a phospholemman transmembrane domain protein: Implications for the limits of detecting dilute ^{17}O sites in biomaterials. *Solid State Nucl Magn Reson*. 2008;33:72-75

281. Bowditch HP. Uber die eigenthumlichkieten der reizbarkeit, welche die muskelfasem des harzens zeigen. *Ber Sachs Ges Wiss*. 1871;23:652-689

282. Bluhm WF, Kranias EG, Dillmann WH, Meyer M. Phospholamban: A major determinant of the cardiac force-frequency relationship. *Am J Physiol Heart Circ Physiol*. 2000;278:H249-255

283. Dipla K, Mattiello JA, Margulies KB, Jeevanandam V, Houser SR. The sarcoplasmic reticulum and the Na^+/Ca^{2+} exchanger both contribute to the Ca^{2+} transient of failing human ventricular myocytes. *Circ Res*. 1999;84:435-444

284. Brill DM, Wasserstrom JA. Intracellular sodium and the positive inotropic effect of veratridine and cardiac glycoside in sheep purkinje fibers. *Circ Res*. 1986;58:109-119

285. Bers DM, Christensen DM. Functional interconversion of rest decay and ryanodine effects in rabbit and rat ventricle depends on na/ca exchange. *J Mol Cell Cardiol*. 1990;22:715-723

286. Gyurko R, Kuhlencordt P, Fishman MC, Huang PL. Modulation of mouse cardiac function in vivo by eNOS and ANP. *Am J Physiol Heart Circ Physiol*. 2000;278:H971-981

287. Li P, Sur SH, Mistlberger RE, Morris M. Circadian blood pressure and heart rate rhythms in mice. *Am J Physiol*. 1999;276:R500-504

288. Langer GA. The role of sodium ion in the regulation of myocardial contractility. *J Mol Cell Cardiol*. 1970;1:203-207

289. Janssen PM, Periasamy M. Determinants of frequency-dependent contraction and relaxation of mammalian myocardium. *J Mol Cell Cardiol*. 2007;43:523-531

290. Stull LB, Leppo MK, Marban E, Janssen PM. Physiological determinants of contractile force generation and calcium handling in mouse myocardium. *J Mol Cell Cardiol*. 2002;34:1367-1376

291. Brooks WW, Apstein CS. Effect of treppe on isovolumic function in the isolated blood-perfused mouse heart. *J Mol Cell Cardiol*. 1996;28:1817-1822

292. Hoit BD, Ball N, Walsh RA. Invasive hemodynamics and force-frequency relationships in open- versus closed-chest mice. *Am J Physiol*. 1997;273:H2528-2533

293. Bers DM, Christensen DM, Nguyen TX. Can Ca entry via Na-Ca exchange directly activate cardiac muscle contraction? *J Mol Cell Cardiol*. 1988;20:405-414

294. Hasenfuss G, Pieske B. Calcium cycling in congestive heart failure. *J Mol Cell Cardiol*. 2002;34:951-969

295. Mulieri LA, Hasenfuss G, Leavitt B, Allen PD, Alpert NR. Altered myocardial force-frequency relation in human heart failure. *Circulation*. 1992;85:1743-1750

296. Palakodeti V, Oh S, Oh BH, Mao L, Hongo M, Peterson KL, Ross J, Jr. Force-frequency effect is a powerful determinant of myocardial contractility in the mouse. *Am J Physiol*. 1997;273:H1283-1290

297. Pecker MS, Im WB, Sonn JK, Lee CO. Effect of norepinephrine and cyclic AMP on intracellular sodium ion activity and contractile force in canine cardiac purkinje fibers. *Circ Res*. 1986;59:390-397

298. Langer GA. The intrinsic control of myocardial contraction--ionic factors. *N Engl J Med*. 1971;285:1065-1071

299. Endoh M. Force-frequency relationship in intact mammalian ventricular myocardium: Physiological and pathophysiological relevance. *Eur J Pharmacol*. 2004;500:73-86

300. Georgakopoulos D, Kass D. Minimal force-frequency modulation of inotropy and relaxation of in situ murine heart. *J Physiol*. 2001;534:535-545

301. Kadambi VJ, Ball N, Kranias EG, Walsh RA, Hoit BD. Modulation of force-frequency relation by phospholamban in genetically engineered mice. *Am J Physiol*. 1999;276:H2245-2250

302. Yamamoto R, Wada A, Asada Y, Yuhi T, Yanagita T, Niina H, Sumiyoshi A. Functional relation between nitric oxide and noradrenaline for the modulation of vascular tone in rat mesenteric vasculature. *Naunyn Schmiedebergs Arch Pharmacol*. 1994;349:362-366

303. Yamamoto R, Wada A, Asada Y, Yanagita T, Yuhi T, Niina H, Sumiyoshi A, Kobayashi H, Lee TJ. Nitric oxide-dependent and -independent norepinephrine release in rat mesenteric arteries. *Am J Physiol*. 1997;272:H207-210

304. Sag CM, Wadsack DP, Khabbazzadeh S, Abesser M, Grefe C, Neumann K, Opiela MK, Backs J, Olson EN, Brown JH, Neef S, Maier SK, Maier LS. Calcium/calmodulin-dependent protein kinase II contributes to cardiac arrhythmogenesis in heart failure. *Circ Heart Fail*. 2009;2:664-675

305. Minta A, Tsien RY. Fluorescent indicators for cytosolic sodium. *J Biol Chem*. 1989;264:19449-19457

306. Maier LS, Pieske B, Allen DG. Influence of stimulation frequency on $[Na^+]_i$ and contractile function in langendorff-perfused rat heart. *Am J Physiol*. 1997;273:H1246-1254

307. Lee CO, Armstrong WM. State and distribution of potassium and sodium ions in frog skeletal muscle. *J Membr Biol*. 1974;15:331-362

308. Lee CO. Electrochemical properties of Na^+- and K^+-selective glass microelectrodes. *Biophys J*. 1979;27:209-220

309. Slack C, Warner AE, Warren RL. The distribution of sodium and potassium in amphibian embryos during early development. *J Physiol*. 1973;232:297-312

310. Lundegardh H. Die quantatative spektralanalyse der elemente. *Jena*. 1929

311. Lundegardh H. *Lantbruks-Hogskol. Ann.* 1936;5

312. Domingo WR, Klyne W. A photoelectric flame photometer. *Biochem J*. 1949;45:400-408

313. Barnes RBB, J.W, Richardson, R and Hood, R.L. Flame photometry: A rapid analytical procedure. *Indust. and Engin. Chem*. 1945;17

314. Overman RR, Davis AK. The application of flame photometry to sodium and potassium determinations in biological fluids. *J Biol Chem*. 1947;168:641-649

315. Noble D. Mechanism of action of therapeutic levels of cardiac glycosides. *Cardiovasc Res*. 1980;14:495-514

316. Skou JC. The Na,K-pump. *Methods Enzymol*. 1988;156:1-25

317. Akera T, Brody TM. The role of Na^+,K^+-ATPase in the inotropic action of digitalis. *Pharmacol Rev*. 1977;29:187-220

318. Choi YR, Akera T. Kinetics studies on the interaction between ouabain and (Na^+,K^+)-ATPase. *Biochim Biophys Acta*. 1977;481:648-659

319. Ishida H, Hirota Y, Genka C, Nakazawa H, Nakaya H, Sato T. Opening of mitochondrial K_{ATP} channels attenuates the ouabain-induced calcium overload in mitochondria. *Circ Res*. 2001;89:856-858

320. Kupriyanov VV, Gruwel ML. Rubidium-87 magnetic resonance spectroscopy and imaging for analysis of mammalian K^+ transport. *NMR Biomed*. 2005;18:111-124

321. Ringer S. An investigation regarding the action of rubidium and caesium salts compared with the action of potassium salts on the ventricle of the frog's heart. *J Physiol*. 1884;4:370-386 320

322. Eisenberg HM, Suddith RL. Cerebral vessels have the capacity to transport sodium and potassium. *Science*. 1979;206:1083-1085

323. Stokes GS, Monaghan JC, Middleton AT. Erythrocyte cation fluxes in normal and hypertensive human subjects. *Clin Exp Pharmacol Physiol*. 1983;10:279-282

324. Bernstein JC, Israel Y. Active transport of Rb^{86} in human red cells and rat brain slices. *J Pharmacol Exp Ther*. 1970;174:323-329

325. Clausen T, Everts ME, Kjeldsen K. Quantification of the maximum capacity for active sodium-potassium transport in rat skeletal muscle. *J Physiol*. 1987;388:163-181

326. Kupriyanov VV, Stewart LC, Xiang B, Kwak J, Deslauriers R. Pathways of Rb^+ influx and their relation to intracellular [Na^+] in the perfused rat heart. A ^{87}Rb and ^{23}Na NMR study. *Circ Res*. 1995;76:839-851

327. Sjodin RA, Beauge LA. Strophanthidin-sensitive components of potassium and sodium movements in skeletal muscle as influenced by the internal sodium concentration. *J Gen Physiol*. 1968;52:389-407

328. Sjodin RA, Beauge LA. Coupling and selectivity of sodium and potassium transport in squid giant axons. *J Gen Physiol*. 1968;51:152-161

329. Maizels M. Effect of sodium content on sodium efflux from human red cells suspended in sodium-free media containing potassium, rubidium, caesium or lithium chloride. *J Physiol*. 1968;195:657-679

330. Skou JC. Enzymatic basis for active transport of Na^+ and K^+ across cell membrane. *Physiol Rev*. 1965;45:596-617

331. Beauge LA, Ortiz O. Rubidium, sodium and ouabain interactions on the influx of rubidium in rat red blood cells. *J Physiol*. 1970;210:519-532

332. Ponce-Hornos JE, Marquez MT, Bonazzola P. Influence of extracellular potassium on energetics of resting heart muscle. *Am J Physiol*. 1992;262:H1081-1087

333. Piwnica-Worms D, Jacob R, Shigeto N, Horres CR, Lieberman M. Na/H exchange in cultured chick heart cells: Secondary stimulation of electrogenic transport during recovery from intracellular acidosis. *J Mol Cell Cardiol*. 1986;18:1109-1116

334. Kohmoto O, Krueger JA, Barry WH. Activation of furosemide-sensitive K^+ fluxes in myocytes by ouabain and recovery from metabolic inhibition. *Am J Physiol*. 1990;259:H962-972

335. Stemmer P, Akera T. Sodium-pump activity and its inhibition by extracellular calcium in cardiac myocytes of guinea pigs. *Biochim Biophys Acta*. 1988;940:188-196

336. Kupriyanov VV, Xiang B, Sun J, Jilkina O, Kuzio B. Imaging of ischemia and infarction in blood-perfused pig hearts using ^{87}Rb MRI. *Magn Reson Med*. 2003;49:99-107

337. Anderson SE, Dickinson CZ, Liu H, Cala PM. Effects of Na-K-2Cl cotransport inhibition on myocardial Na and Ca during ischemia and reperfusion. *Am J Physiol*. 1996;270:C608-618

338. Isenring P, Jacoby SC, Chang J, Forbush B. Mutagenic mapping of the Na-K-Cl cotransporter for domains involved in ion transport and bumetanide binding. *J Gen Physiol*. 1998;112:549-558

339. Isenring P, Jacoby SC, Forbush B, 3rd. The role of transmembrane domain 2 in cation transport by the Na-K-Cl cotransporter. *Proc Natl Acad Sci U S A*. 1998;95:7179-7184

340. Isenring P, Forbush B. Ion transport and ligand binding by the Na-K-Cl cotransporter, structure-function studies. *Comp Biochem Physiol A Mol Integr Physiol*. 2001;130:487-497

341. Taouil K, Hannaert P. Evidence for the involvement of K^+ channels and K^+-Cl^- cotransport in the regulatory volume decrease of newborn rat cardiomyocytes. *Pflugers Arch*. 1999;439:56-66

342. Madhani M, Hall AR, Cuello F, Charles RL, Burgoyne JR, Fuller W, Hobbs AJ, Shattock MJ, Eaton P. Phospholemman Ser69 phosphorylation contributes to sildenafil-induced cardioprotection against reperfusion injury. *Am J Physiol Heart Circ Physiol*.299:H827-836

343. Brody TM, Akera T. Relations among Na^+,K^+-atpase activity, sodium pump activity, transmembrane sodium movement, and cardiac contractility. *Fed Proc*. 1977;36:2219-2224

344. Lee CO. 200 years of digitalis: The emerging central role of the sodium ion in the control of cardiac force. *Am J Physiol*. 1985;249:C367-378

345. Levi AJ, Boyett MR, Lee CO. The cellular actions of digitalis glycosides on the heart. *Prog Biophys Mol Biol*. 1994;62:1-54

346. Grupp I, Im WB, Lee CO, Lee SW, Pecker MS, Schwartz A. Relation of sodium pump inhibition to positive inotropy at low concentrations of ouabain in rat heart muscle. *J Physiol*. 1985;360:149-160

347. McDonald TF, MacLeod DP. Metabolism and the electrical activity of anoxic ventricular muscle. *J Physiol*. 1973;229:559-582

348. Pridjian AK, Levitsky S, Krukenkamp I, Silverman NA, Feinberg H. Developmental-changes in reperfusion injury - a comparison of intracellular cation accumulation in the newborn, neonatal, and adult heart. *J Thorac Cardiov Sur*. 1987;93:428-433

349. Pridjian AK, Levitsky S, Krukenkamp I, Silverman NA, Feinberg H. Intracellular sodium and calcium in the postischemic myocardium. *Annals of Thoracic Surgery*. 1987;43:416-419

350. Malloy CR, Buster DC, Castro MMCA, Geraldes CFGC, Jeffrey FMH, Sherry AD. Influence of global-ischemia on intracellular sodium in the perfused rat-heart. *Magnetic Resonance in Medicine*. 1990;15:33-44

351. Ivanics T, Blum H, Wroblewski K, Wang DJ, Osbakken M. Intracellular sodium in cardiomyocytes using ^{23}Na nuclear magnetic resonance. *Biochim Biophys Acta*. 1994;1221:133-144

352. Woodbury JW. Interrelationships between ion transport mechanisms and excitatory events. *Fed Proc*. 1963;22:31-35

353. Deitmer JW, Ellis D. The intracellular sodium activity of sheep heart purkinje fibres: Effects of local anaesthetics and tetrodotoxin. *J Physiol*. 1980;300:269-282

354. Conn HL, Jr., Wood JC. Sodium exchange and distribution in the isolated heart of the normal dog. *Am J Physiol*. 1959;197:631-636

355. Gadsby DC, Niedergerke R, Page S. Do intracellular concentrations of potassium or sodium regulate the strength of the heart beat? *Nature*. 1971;232:651-653

356. Elgavish GA. Shift-reagent-aided ^{23}Na NMR spectroscopy. *Invest Radiol*. 1989;24:1028-1033

357. Lotan CS, Miller SK, Simor T, Elgavish GA. Cardiac staircase and nmr-determined intracellular sodium in beating rat hearts. *Am J Physiol*. 1995;269:H332-340

358. Simor T, Lorand T, Gaszner B, Elgavish GA. The modulation of pacing-induced changes in intracellular sodium levels by extracellular Ca^{2+} in isolated perfused rat hearts. *J Mol Cell Cardiol*. 1997;29:1225-1235

359. Jelicks LA, Siri FM. Effects of hypertrophy and heart failure on $[Na^+]_i$ in pressure-overloaded guinea pig heart. *Am J Hypertens*. 1995;8:934-943

360. Langer GA. Sodium exchange in dog ventricular muscle. Relation to frequency of contraction and its possible role in the control of myocardial contractility. *J Gen Physiol*. 1967;50:1221-1239

361. Wang J, Gao E, Song J, Zhang XQ, Li J, Koch WJ, Tucker AL, Philipson KD, Chan TO, Feldman AM, Cheung JY. Phospholemman and β-adrenergic stimulation in the heart. *Am J Physiol Heart Circ Physiol*. 2010;298:H807-815

362. Akera T, Brody TM. Inotropic action of digitalis and ion transport. *Life Sci*. 1976;18:135-144

363. Akera T, Ng YC. Digitalis sensitivity of Na^+,K^+-ATPase, myocytes and the heart. *Life Sci*. 1991;48:97-106

364. Ellis D. The effects of external cations and ouabain on the intracellular sodium activity of sheep heart purkinje fibres. *J Physiol*. 1977;273:211-240

365. Deitmer JW, Ellis D. The intracellular sodium activity of cardiac purkinje fibres during inhibition and re-activation of the Na-K pump. *J Physiol*. 1978;284:241-259

366. Ellis D, Deitmer JW. The relationship between the intra- and extracellular sodium activity of sheep heart purkinje fibres during inhibition of the Na-K pump. *Pflugers Arch*. 1978;377:209-215

367. Wasserstrom JA. Changes in intracellular Na^+ during Na,K pump inhibition in sheep cardiac tissues. *J Mol Cell Cardiol*. 1992;24:1-7

368. Van Emous JG, Schreur JH, Ruigrok TJ, Van Echteld CJ. Both Na^+-K^+ ATPase and Na^+-H^+ exchanger are immediately active upon post-ischemic reperfusion in isolated rat hearts. *J Mol Cell Cardiol*. 1998;30:337-348

369. Eisner DA, Lederer WJ, Vaughan-Jones RD. The dependence of sodium pumping and tension on intracellular sodium activity in voltage-clamped sheep purkinje fibres. *J Physiol*. 1981;317:163-187

370. Rau EE, Shine KI, Langer GA. Potassium exchange and mechanical performance in anoxic mammalian myocardium. *Am J Physiol*. 1977;232:H85-94

371. Eisner DA, Lederer WJ, Vaughan-Jones RD. The effects of rubidium ions and membrane potentials on the intracellular sodium activity of sheep purkinje fibres. *J Physiol*. 1981;317:189-205

372. Sala S, Soria B. Inactivation of delayed potassium current in cultured bovine chromaffin cells. *Eur J Neurosci*. 1991;3:462-472

373. Knight RG, Nosek TM. Effects of rubidium on contractility and sodium pump activity in guinea-pig ventricle. *J Pharmacol Exp Ther*. 1981;219:573-579

374. Pike MM, Frazer JC, Dedrick DF, Ingwall JS, Allen PD, Springer CS, Jr., Smith TW. ^{23}Na and ^{39}K nuclear magnetic resonance studies of perfused rat hearts. Discrimination of intra- and extracellular ions using a shift reagent. *Biophys J*. 1985;48:159-173

375. Imahashi K, London RE, Steenbergen C, Murphy E. Male/female differences in intracellular Na^+ regulation during ischemia/reperfusion in mouse heart. *J Mol Cell Cardiol*. 2004;37:747-753

376. Babsky AM, Hekmatyar SK, Zhang H, Solomon JL, Bansal N. Application of ^{23}Na MRI to monitor chemotherapeutic response in RIF-1 tumors. *Neoplasia*. 2005;7:658-666

377. Winter PM, Seshan V, Makos JD, Sherry AD, Malloy CR, Bansal N. Quantitation of intracellular [Na^+] in vivo by using $TmDOTP^{5-}$ as an NMR shift reagent and extracellular marker. *J Appl Physiol*. 1998;85:1806-1812

378. Ren Js, a.d. ^7Li, ^6Li, ^{23}Na, ^{133}Cs multinuclear NMR studies of adducts formed with the shift reagent, $Tm\text{-}DOTP^{5-}$. *Inorg Chim Acta*. 1996;246:1-11

379. Gaszner B, Simor T, Hild G, Elgavish GA. The effects of the NMR shift-reagents $Dy(PPP)_2$, Dy(TTHA) and Tm(DOTP) on developed pressure in isolated perfused rat hearts. The role of shift-reagent calcium complexes. *Journal of Molecular and Cellular Cardiology*. 2001;33:1945-1956

380. Kohler S. Sodium magnetic resonance imaging and chemical shift imaging. *Progress in nuclear magnetic resonance imaging*. 1992;24:411-433

381. Dizon JM, Tauskela JS, Wise D, Burkhoff D, Cannon PJ, Katz J. Evaluation of triple-quantum-filtered ^{23}Na NMR in monitoring of intracellular Na content in the perfused rat heart: Comparison of intra- and extracellular transverse relaxation and spectral amplitudes. *Magn Reson Med*. 1996;35:336-345

382. Phillips WD, Looney CE, Ikeda CK. Influence of some paramagnetic ions on the magnetic resonance absorption of alcohols. *Journal of Chemical Physics*. 1957;27:1435-1436

383. Szarek WA, Dent E, Grindley TB, Baird MC. Use of paramagnetic transition-metal ions in interpretation of nuclear magnetic resonance spectra of complex alcohols and amines. *J Chem Soc Chem Comm*. 1969:953-&

384. Freymann M, Freymann R. Effet de sels paramagnetiques sur la resonance magnetique nucleaire de la pyridine et de lethanol. *Cr Hebd Acad Sci*. 1960;250:3638-3640

385. Hinckley CC. Paramagnetic shifts in solutions of cholesterol and dipyridine adduct of trisdipivalomethanatoeuropium$_3$. A shift reagent. *Journal of the American Chemical Society*. 1969;91:5160-&

386. Horrocks WD, Sipe JP. Lanthanide shift reagents - survey. *Journal of the American Chemical Society*. 1971;93:6800-&

387. Sanders JKM, Williams DH. Shift reagents in NMR-spectroscopy. *Nature*. 1972;240:385-&

388. Sanders JKM, Williams DH, Hanson SW. Paramagnetic shift reagents - nature of interactions. *Journal of the American Chemical Society*. 1972;94:5325-&

389. Springer CS, Pike MM, Balschi JA. Direct high-resolution NMR-studies of metal cation-transport across model and cell-membranes - ^{23}Na and ^{39}K NMR. *Biophysical Journal*. 1982;37:A337-A337

390. Chu SC, Pike MM, Fossel ET, Smith TW, Balschi JA, Springer CS. Aqueous shift-reagents for high-resolution cationic nuclear magnetic-resonance .3. $Dy(TTHA)^{3-}$, $Tm(TTHA)^{3-}$, and $Tm(PPP)^{27-}$. *Journal of Magnetic Resonance*. 1984;56:33-47

391. Sherry AD, Malloy CR, Jeffrey FMH, Cacheris WP, Geraldes CFGC. $Dy(DOTP)^{5-}$ - a new, stable ^{23}Na shift-reagent. *Journal of Magnetic Resonance*. 1988;76:528-533

392. Buster DC, Castro MM, Geraldes CF, Malloy CR, Sherry AD, Siemers TC. Tm(dotp)5-: A $^{23}Na^{+}$ shift agent for perfused rat hearts. *Magn Reson Med*. 1990;15:25-32

393. Kohler SJ, Perry SB, Stewart LC, Atkinson DE, Clarke K, Ingwall JS. Analysis of ^{23}Na NMR spectra from isolated perfused hearts. *Magn Reson Med*. 1991;18:15-27

394. Forester GV, Mainwood GW. Interval dependent inotropic effects in the rat myocardium and the effect of calcium. *Pflugers Arch*. 1974;352:189-196

395. Miller SK. Shift-reagent-aided ^{23}Na spectroscopy in cellular, tissue and whole-organ systems. *Biological Magnetic Resonance*. 1992;11:159-240

396. Winter PM, Bansal N. Triple-quantum-filtered ^{23}Na NMR spectroscopy of subcutaneously implanted 9L gliosarcoma in the rat in the presence of TmDOTP$^{5-1}$. *J Magn Reson*. 2001;152:70-78

397. Hubbard PS. Nonexponential nuclear magnetic relaxation by quadrupole interactions. *Journal of Chemical Physics*. 1970;53:985-&

398. Jaccard G, Wimperis S, Bodenhausen G. Multiple-quantum NMR-spectroscopy of s=3/2 spins in isotropic-phase - a new probe for multiexponential relaxation. *Journal of Chemical Physics*. 1986;85:6282-6293

399. Pekar J, Renshaw PF, Leigh JS. Selective detection of intracellular sodium by coherence-transfer NMR. *Journal of Magnetic Resonance*. 1987;72:159-161

400. Schepkin VD, Choy IO, Budinger TF, Obayashi DY, Taylor SE, DeCampli WM, Amartur SC, Young JN. Sodium TQF NMR and intracellular sodium in isolated crystalloid perfused rat heart. *Magnetic Resonance in Medicine*. 1998;39:557-563

401. Schepkin VD, Choy IO, Budinger TF. Sodium alterations in isolated rat heart during cardioplegic arrest. *J Appl Physiol*. 1996;81:2696-2702

402. Tauskela JS, Dizon JM, Whang J, Katz J. Evaluation of multiple-quantum-filtered ^{23}Na NMR in monitoring intracellular Na content in the isolated perfused rat heart in the absence of a chemical-shift reagent. *J Magn Reson*. 1997;127:115-127

403. Sutherland FJ, Shattock MJ, Baker KE, Hearse DJ. Mouse isolated perfused heart: Characteristics and cautions. *Clin Exp Pharmacol Physiol*. 2003;30:867-878

404. Askenasy N, Navon G. Continuous monitoring of intracellular volumes in isolated rat hearts during normothermic perfusion and ischemia. *J Magn Reson*. 1997;124:42-50

405. Deitmer JW, Ellis D. Changes in the intracellular sodium activity of sheep heart purkinje fibres produced by calcium and other divalent cations. *J Physiol*. 1978;277:437-453

406. Van Echteld CJ, Van Emous JG, Jansen MA, Schreur JH, Ruigrok TJ. Manipulation of intracellular sodium by extracellular divalent cations: A ^{23}Na and ^{31}P NMR study on intact rat hearts. *J Mol Cell Cardiol*. 1998;30:119-126

407. Castle AM, Macnab RM, Shulman RG. Measurement of intracellular sodium concentration and sodium transport in escherichia coli by ^{23}Na nuclear magnetic resonance. *J Biol Chem*. 1986;261:3288-3294

408. Balschi JA, Bittl JA, Springer CS, Jr., Ingwall JS. ^{31}P and ^{23}Na NMR spectroscopy of normal and ischemic rat skeletal muscle. Use of a shift reagent in vivo. *NMR Biomed*. 1990;3:47-58

409. van Echteld CJ, Kirkels JH, Eijgelshoven MH, van der Meer P, Ruigrok TJ. Intracellular sodium during ischemia and calcium-free perfusion: A ^{23}Na NMR study. *J Mol Cell Cardiol*. 1991;23:297-307

410. Pike MM, Frazer JC, Dedrick D, Ingwall JS, Allen PD, Smith TW, Springer CS. ^{23}Na and ^{39}K NMR-studies of perfused, beating, rat hearts - perfusion with shift-reagents. *Biophysical Journal*. 1984;45:A33-A33

411. Pike MM, Luo CS, Clark MD, Kirk KA, Kitakaze M, Madden MC, Cragoe EJ, Jr., Pohost GM. NMR measurements of Na^+ and cellular energy in ischemic rat heart: Role of Na^+-H^+ exchange. *Am J Physiol*. 1993;265:H2017-2026

412. Pike MM, Luo CS, Yanagida S, Hageman GR, Anderson PG. ^{23}Na and ^{31}P nuclear magnetic resonance studies of ischemia-induced ventricular fibrillation. Alterations of intracellular Na^+ and cellular energy. *Circ Res*. 1995;77:394-406

413. Ramasamy R, Liu H, Anderson S, Lundmark J, Schaefer S. Ischemic preconditioning stimulates sodium and proton transport in isolated rat hearts. *J Clin Invest*. 1995;96:1464-1472

414. Matwiyoff NA, Gasparovic C, Wenk R, Wicks JD, Rath A. ^{31}P and ^{23}Na nmr studies of the structure and lability of the sodium shift reagent, bis(tripolyphosphate)dysprosium$_3$ ($[Dy(P_3O_{10})]^{7-}$) ion, and its decomposition in the presence of rat muscle. *Magn Reson Med*. 1986;3:164-168

415. Schepkin VD, Choy IO, Budinger TF, Young JN, DeCampli WM. Multi-dose crystalloid cardioplegia preserves intracellular sodium homeostasis in myocardium. *J Mol Cell Cardiol*. 1999;31:1643-1651

416. Dizon J, Burkhoff D, Tauskela J, Whang J, Cannon P, Katz J. Metabolic inhibition in the perfused rat heart: Evidence for glycolytic requirement for normal sodium homeostasis. *Am J Physiol*. 1998;274:H1082-1089

417. Schepkin VDC, I.O; Obayashi, D.Y. Quantification of sodium TQF NMR in a neonatal rabbit heart. *Proc Intl Soc Mag Reson Med* 2000

418. Chung CW, Wimperis S. Optimum detection of spin-3/2 biexponential relaxation using multiple-quantum filtration techniques. *Journal of Magnetic Resonance*. 1990;88:440-447

419. Chung CW, Wimperis S. Measurement of spin-5/2 relaxation in biological and macromolecular systems using multiple-quantum NMR techniques. *Mol Phys*. 1992;76:47-81

420. Jelicks LA, Gupta RK. On the extracellular contribution to multiple quantum filtered ^{23}Na NMR of perfused rat heart. *Magn Reson Med*. 1993;29:130-133

421. Ellis D. The intracellular sodium ion concentration of sheep heart purkinje fibres and its relationship to external sodium [proceedings]. *J Physiol*. 1977;266:74P-75P

422. Bers DM, Ellis D. Intracellular calcium and sodium activity in sheep heart purkinje fibres. Effect of changes of external sodium and intracellular pH. *Pflugers Arch*. 1982;393:171-178

423. Wilde AA, Kleber AG. Effect of norepinephrine and heart rate on intracellular sodium activity and membrane potential in beating guinea pig ventricular muscle. *Circ Res*. 1991;68:1482-1489

424. MacLeod KT. Effects of hypoxia and metabolic inhibition on the intracellular sodium activity of mammalian ventricular muscle. *J Physiol*. 1989;416:455-468

425. Rodrigo GC, Chapman RA. The calcium paradox in isolated guinea-pig ventricular myocytes: Effects of membrane potential and intracellular sodium. *J Physiol*. 1991;434:627-645

426. Liu S, Jacob R, Piwnica-Worms D, Lieberman M. ($Na^+K^+2Cl^-$) cotransport in cultured embryonic chick heart cells. *Am J Physiol*. 1987;253:C721-730

427. Lee CO, Fozzard HA. Activities of potassium and sodium ions in rabbit heart muscle. *J Gen Physiol*. 1975;65:695-708

428. Lev AA. Determination of activity and activity coefficients of potassium and sodium ions in frog muscle fibres. *Nature*. 1964;201:1132-1134

429. Fossel ET, Hoefeler H. Observation of intracellular potassium and sodium in the heart by NMR - a major fraction of potassium is invisible. *Magnetic Resonance in Medicine*. 1986;3:534-540

430. Cohen CJ, Fozzard HA, Sheu SS. Increase in intracellular sodium ion activity during stimulation in mammalian cardiac muscle. *Circ Res*. 1982;50:651-662

431. Orchard CH, Lakatta EG. Intracellular calcium transients and developed tension in rat heart muscle. A mechanism for the negative interval-strength relationship. *J Gen Physiol*. 1985;86:637-651

432. Lotan CS, Miller SK, Simor T, Elgavish GA. Cardiac staircase and NMR-determined intracellular sodium in beating rat hearts. *American Journal of Physiology-Heart and Circulatory Physiology*. 1995;269:H332-H340

433. Simor T, Lorand T, Gaszner B, Elgavish GA. The modulation of pacing induced changes in intracellular sodium levels by extracellular Ca^{2+} in isolated perfused rat hearts. *Journal of Molecular and Cellular Cardiology*. 1997;29:1225-1235

434. Butwell NB, Ramasamy R, Sherry AD, Malloy CR. Influence of cardiac pacing on intracellular sodium in the isolated perfused rat heart. *Invest Radiol*. 1991;26:1079-1082

435. Wasserstrom JA, Schwartz DJ, Fozzard HA. Catecholamine effects on intracellular sodium activity and tension in dog heart. *Am J Physiol*. 1982;243:H670-675

436. Lee CO, Vassalle M. Modulation of intracellular Na^{+} activity and cardiac force by norepinephrine and Ca^{2+}. *Am J Physiol*. 1983;244:C110-114

437. Terris S, Wasserstrom JA, Fozzard HA. Depolarizing effects of catecholamines in quiescent sheep cardiac purkinje fibers. *Am J Physiol*. 1986;251:H1056-1061

438. Auditore JV, Murray L. Cardiac (microsomal) $Na^{+}K$ adenosinetriphosphatase and its possible relationship to the active $Na^{+}K$ transport system. *Arch Biochem Biophys*. 1962;99:372-382

439. Lee KS, Yu DH. A study of the sodium- and potassium-activated adenosinetriphosphatase activity of heart microsomal fraction. *Biochem Pharmacol*. 1963;12:1253-1264

440. Repke K, Portius HJ. On the identity of the ion-pumping-atpase in the cell membrane of the myocardium with a digitalis receptor enzyme. *Experientia*. 1963;19:452-458

441. Repke K, Est M, Portius HJ. On the cause of species differences in digitalis sensitivity. *Biochem Pharmacol*. 1965;14:1785-1802

442. Schwartz A, Laseter AH. A sodium- and potassium-stimulated adenosine triphosphatase from cardiac tissues -II. The effects of ouabain and other agents that modify enzyme activity. *Biochem Pharmacol*. 1964;13:337-348

443. Akera T, Brody TM. Inhibitory sites on sodium- and potassium-activated adenosine triphosphatase for chlorpromazine free radical and ouabain. *Mol Pharmacol*. 1970;6:557-566

444. Carslake MC, Weatherall M. Changes in the sodium, potassium and chloride of rabbit auricles treated with ouabain. *J Physiol*. 1962;163:347-361

445. Radford NB, Makos JD, Ramasamy R, Sherry AD, Malloy CR. Dissociation of intracellular sodium from contractile state in guinea-pig hearts treated with ouabain. *J Mol Cell Cardiol*. 1998;30:639-647

446. Schreiber SS. Potassium and sodium exchange in the working frog heart; effects of overwork, external concentrations of potassium and ouabain. *Am J Physiol*. 1956;185:337-347

447. Nishio M, Ruch SW, Wasserstrom JA. Positive inotropic effects of ouabain in isolated cat ventricular myocytes in sodium-free conditions. *Am J Physiol Heart Circ Physiol*. 2002;283:H2045-2053

448. Charnock JS, Dryden WF, Lauzon PA. Species difference in myocardial response to actodigin: Correlation with inhibition of myocardial Na^+ + K^+-ATPase. *Comp Biochem Physiol C*. 1980;66:153-158

449. Allen JC, Schwartz A. A possible biochemical explanation for the insensitivity of the rat to cardiac glycosides. *J Pharmacol Exp Ther*. 1969;168:42-46

450. Akera T, Larsen FS, Brody TM. The effect of ouabain on sodium- and potassium-activated adenosine triphosphatase from the hearts of several mammalian species. *J Pharmacol Exp Ther*. 1969;170:17-26

451. Tobin T, Brody TM. Rates of dissociation of enzyme-ouabain complexes and $K_{0.5}$ values in Na^+ + K^+-adenosine triphosphatase from different species. *Biochem Pharmacol*. 1972;21:1553-1560

452. Tobin T, Henderson R, Sen AK. Species and tissue differences in the rate of dissociation of ouabain from Na^++ K^+-ATPase. *Biochim Biophys Acta*. 1972;274:551-555

453. Akera T, Baskin SI, Tobin T, Brody TM. Ouabain: Temporal relationship between the inotropic effect and the in vitro binding to, and dissociation from, Na^+ + K^+- activated ATPase. *Naunyn Schmiedebergs Arch Pharmacol*. 1973;277:151-162

454. Mohammadi K, Liu L, Tian J, Kometiani P, Xie Z, Askari A. Positive inotropic effect of ouabain on isolated heart is accompanied by activation of signal pathways that link Na^+/K^+-ATPase to $ERK_{1/2}$. *J Cardiovasc Pharmacol*. 2003;41:609-614

455. Wansapura AN, Lasko V, Xie Z, Fedorova OV, Bagrov AY, Lingrel JB, Lorenz JN. Marinobufagenin enhances cardiac contractility in mice with ouabain-sensitive α1 Na^+-K^+-ATPase. *Am J Physiol Heart Circ Physiol*. 2009;296:H1833-1839

456. Despa S, Lingrel JB, Bers DM. Na^+/K^+-ATPase α2-isoform preferentially modulates Ca^{2+} transients and sarcoplasmic reticulum Ca^{2+} release in cardiac myocytes. *Cardiovasc Res*. 2012;95:480-486

457. Sheu SS, Fozzard HA. Transmembrane Na^+ and Ca^{2+} electrochemical gradients in cardiac muscle and their relationship to force development. *J Gen Physiol*. 1982;80:325-351

458. Cheung JY, Thompson IG, Bonventre JV. Effects of extracellular calcium removal and anoxia on isolated rat myocytes. *Am J Physiol*. 1982;243:C184-190

459. Pridjian AK, Levitsky S, Krukenkamp I, Silverman NA, Feinberg H. Developmental changes in reperfusion injury. A comparison of intracellular cation accumulation in the newborn, neonatal, and adult heart. *J Thorac Cardiovasc Surg*. 1987;93:428-433

460. Steenbergen C, Perlman ME, London RE, Murphy E. Mechanism of preconditioning. Ionic alterations. *Circ Res*. 1993;72:112-125

461. Wittenberg BA, Gupta RK. NMR studies of intracellular sodium ions in mammalian cardiac myocytes. *J Biol Chem*. 1985;260:2031-2034

462. Maier LS, Bers DM, Pieske B. Differences in Ca^{2+}-handling and sarcoplasmic reticulum Ca^{2+}-content in isolated rat and rabbit myocardium. *J Mol Cell Cardiol*. 2000;32:2249-2258